UNIVERSIDAD DE CÓRDOBA

Programa de doctorado: Química Fina

Título de la tesis:

Aplicación de la fotocatálisis en flujo como una nueva herramienta para el descubrimiento de nuevos fármacos

Application of photocatalysis in flow as a new tool for drug-discovery

Director: Rafael Luque Álvarez de Sotomayor

Co-director: Manuel Jesús Alcázar Vaca

Autor de la tesis: Irini Abdiaj

Fecha de depósito tesis en el Idep: 22/06/2018

TITULO: *Application of photocatalysis in flow as a new tool for drug-discovery*

AUTOR: *Irini Abdiaj*

© Edita: UCOPress. 2018
Campus de Rabanales
Ctra. Nacional IV, Km. 396 A
14071 Córdoba

https://www.uco.es/ucopress/index.php/es/
ucopress@uco.es

Doctoral thesis

Application of Photocatalysis in Flow as a New Tool for Drug-Discovery

Irini Abdiaj

Departamento de Química Orgánica

Facultad de Ciencias

Universidad de Cordoba

2018

TÍTULO DE LA TESIS:

Application of photocatalysis in flow as a new tool for drug-discovery

DOCTORANDO/A:

Ms. Irini Abdiaj

INFORME RAZONADO DEL/DE LOS DIRECTOR/ES DE LA TESIS

(se hará mención a la evolución y desarrollo de la tesis, así como a trabajos y publicaciones derivados de la misma).

Los objetivos de la tesis estaban relacionados con el uso de la fotoquímica en flujo para conseguir nuevas metodologías para crear enlaces $C(sp^2)$-$C(sp^3)$ que puedan ser aplicables al descubrimiento de nuevos fármacos.

En primer lugar, Irini estudió la forma de trasladar condiciones de reacciones fotoquímicas de batch a flujo, ya que había que conocer que aspectos serían necesarios en el caso que fuera necesario escalar algún producto en cantidades multigramo cuya síntesis original hubiera sido en ejecutada en forma tradicional y su escalado fuera no reproducible. Este paso fue conseguido con el desarrollo de la metodología necesaria para realizar reacciones de catálisis dual en flujo continuo mediante el empleo de un fotocatalizador de Iridio y un catalizador de acoplamiento cruzado de níquel. Esta parte del trabajo se publicó en *Bioorganic & Medicinal Chemistry* **2017**, *25(23)*, 6190-6196.

Una vez completado este primer paso, Irini desarrolló una nueva metodología para realizar trifuorometilaciones en flujo, usando reactivos de uso común en nuestros laboratorios, de nuevo mediante fotocatálisis con un derivado de iridio. La introducción de grupos trifluorometilo es importante en el descubrimiento de nuevos fármacos ya que este grupo confiere mejores propiedades metabólicas, así como una mejor permeabilidad membranal. De nuevo el trabajo fue recogido en una nueva publicación: *Synthesis* **2017**, *49(22)*, 4978-4985.

Su gran capacidad de aprendizaje y sus ganas por innovar le llevó a estudiar cómo se comportan los compuestos organocíncicos en presencia de luz visible. Este tipo de compuestos no habían sido descritos en reacciones fotoquímicas con anterioridad, por lo que su comportamiento en estas condiciones era totalmente desconocido. De esta forma, observó que las reacciones tipo Negishi se podían acelerar mediante el empleo de luz visible cuando se usaba un catalizador de níquel. Esta observación se desarrolló para determinar su relevancia y encontró que se podían introducir restos alquílicos de una forma sencilla mediante esta tecnología e incluso se podía usar con derivados clorados o bromados que no eran accesible mediante un acoplamiento cruzado tradicional tipo Negishi catalizado por níquel. Este descubrimiento tiene importancia, ya que la derivatización observada puede ser usada como herramienta en química médica. Este trabajo fue publicado en *Angewandte Chemie International Edition* **2018**, DOI: 10.1002/anie.201802656 y es de tal calidad que además fue seleccionado para la portada trasera de la revista.

Como esta metodología está basada en la absorción de luz visible mediante la interacción de dos metales abundantes en la naturaleza como son el zinc y el níquel, se seleccionó para estudiar la escalabilidad de las reacciones fotoquímicas en flujo. Este aspecto es muy importante ya que en algún momento del desarrollo de un programa de química médica puede ser necesaria la preparación de cantidades multigramo de compuesto y hay que asegurar que los métodos fotoquímicos nos pueden proporcionar dichas cantidades. Esta parte del trabajo la desarrolló durante una estancia en el centro que Corning tiene en Samois-sur-Seine, Francia. Durante dicha estancia trasladó las condiciones de nuestro equipo de fotoquímica en flujo marca Vapourtec al que se han desarrollado en Corning con éxito y consiguió obtener los productos finales en cantidades entre 20 a 40 gramos. Estas cantidades son perfectamente compatibles con la preparación de productos candidatos a fases clínicas, por lo que se asegura la utilidad de esta tecnología para la descubrimiento y desarrollo de nuevos fármacos. Esta parte de su trabajo aún no ha sido publicada, aunque el artículo está siendo preparado en estos momentos y se quiere enviar a la revista *Journal of Organic Chemsitry* cumpliendo con una invitación que hemos recibido de sus editores.

Siguiendo con el estudio de la fotoquímica de compuestos organocincicos, se estudiaron de nuevo las reacciones de acoplamiento tipo Negishi, pero esta vez catalizadas por paladio. El origen de este estudio está en las

limitaciones encontradas con el uso del catalizador de níquel. De nuevo su tesón consiguió demostrar que estas reacciones también se aceleran mediante irradiación de luz visible y que el origen de esa propiedad se encuentra en una interacción entre el zinc y el paladio en estado fundamental que no se había observado hasta ahora y que permite la absorción de luz azul. No sólo esa interacción es importante desde el punto de vista mecanístico, si no que tiene aplicabilidad sintética para la preparación de compuesto de difícil acceso, a través de la mejora de reactividad de los sustratos de partida. El trabajo ya está completado y nos encontramos en la fase de preparación del artículo que se quiere enviar a la revista *Journal of the American Chemical Society*. En caso de que no sea aceptada se redirigirá a otras revistas de alto índice de impacto como *Angewandte Chemie International Edition*.

Titulo: Improving the throughput of batch photochemical reactions using flow: Dual photoredox and nickel catalysis in flow for $C(sp^2)$-$C(sp^3)$ cross-coupling.
Autores: Irini Abdiaj, Jesus Alcazar
Revista: Bioorganic and Medicinal Chemistry
Indicios de Calidad (2016):
Categoría: Chemistry, Medicinal
Índice de impacto 2.930
Posición dentro de la categoría: 22/60, segundo cuartil (Q2)
Volumen 25, 2017, Paginas: 6190–6196

Titulo: Visible-Light-Induced Trifluoromethylation of Highly Functionalized Arenes and Heteroarenes in Continuous Flow
Autores: Irini Abdiaj, Cecilia Bottecchia, Timothy Noël, Jesus Alcazar
Revista: Synthesis
Indicios de Calidad (2016):
Categoría: Chemistry, Organic
Índice de impacto: 2.650
Posición dentro de la categoría: 22/59 segundo cuartil (Q2)
Volumen 49, 2017, Paginas: 4978–4985

Titulo: Visible Light-Induced Nickel-Catalyzed Negishi Cross-Coupling. By Exogenous-Photosensitizer-free Photocatalysis.
Autores: Irini Abdiaj, Alberto Fontana, M. Victoria Gomez, Antonio de La Hoz Jesus Alcazar
Revista: Angewandte Chemie

Indicios de Calidad (2016):
Categoría Chemistry Multidisciplinary
Índice de impacto 11.994
Posición dentro de la categoría: 13/166, primer cuartil (Q1)
DOI: doi:10.1002/anie.201802656

Por todo ello, se autoriza la presentación de la tesis doctoral.

Córdoba, 22 de Junio de 2018

Firma del/de los director/es

Fdo.: JESÚS ALCÁZAR Fdo.: RAFAEL LUQUE ALANÍS

Resumen de la Tesis Doctoral

En esta tesis se presentarán nuevas metodologías para la inserción de C (sp^3) en moléculas orgánicas. Hay evidencias que el aumento del carácter alifático de las moléculas organicas candidatos para futuro fármacos mejora la farmacocinética y farmacodinámica de las mismas.[i] La combinación de la química del flujo con la fotocatálisis ofrece nuevas posibilidades en el acoplamiento $C(sp^3)$ -$C(sp^2)$. Los proyectos se centran principalmente en la química heterocíclica considerando su aplicabilidad fundamental en química médica.

Las nuevas metodologías para la trifluorometilación de arenos y heteroarenos tienen una gran demanda en la industria química y farmacéutica.[ii] En el Capítulo 2 de esta tesis se describe un protocolo de flujo continuo para la inserción del resto trifluorometilo en heterociclos altamente funcionalizados. Esta metodología fotoredox se basa en el uso de trifluorometanosulfinato de sodio sólido (CF_3SO_2Na) como el agente de trifluorometilación y el complejo de iridio $[Ir\{dF(CF_3)ppy\}_2](dtbpy)]PF_6$ como catalizador fotoredox. Un conjunto de heterociclos altamente funcionalizados resultó compatible con la metodología, y se obtuvieron rendimientos de moderados a buenos dentro de los 30 minutos del tiempo de residencia. Este proyecto se realizó en colaboración con la Universidad de Tecnología de Eindhoven y el proyecto se finalizó con una publicación en *Synthesis 2017, 49, 4978-4985.*

En el Capítulo 3, se describe la transferencia de una reacción fotoredox en batch al flujo. La catálisis combinada de Ni/Ir proporciona una metodología de condición leve muy interesante para el acoplamiento cruzado $C(sp^3)$ -$C(sp^2)$.[iii] Sin embargo, las condiciones de reacción en batch limitan su aplicabilidad a la producción a pequeña escala. Este nuevo procedimiento de flujo mejora claramente la escalabilidad de la reacción del lote anterior por el tamaño del reactor y la reducción del tiempo de operación, y permite la preparación de compuestos interesantes para el descubrimiento de fármacos en cantidades de varios estadios. Los resultados de este proyecto se han publicado en *Bioorg. Medicina. Chem. 2017, 25, 6190-6196.*

La reacción de Negishi es una metodología versátil y tolerante a grupos funcionales que permite el acoplamiento cruzado de reactivos de organocincicos con diferentes haluros de arilo.[iv] Teniendo en cuenta nuestra experiencia en la preparación de soluciones claras de soluciones de organocincicos en condiciones de flujo continuo, decidimos estudiar su comportamiento bajo irradiación de luz. Sorprendentemente, observamos que la reactividad de estos reactivos organometálicos bajo irradiación de luz visible es altamente mejorada. Estudiamos esta nueva versión de la reacción de acoplamiento

cruzado de Negishi usando níquel (Capítulo 4) y paladio (Capítulo 5) como catalizadores. La reacción de Negishi catalizada por Ni y luz (Capítulo 4) permitió el acoplamiento cruzado de diferentes reactivos de alquil-zinc, que no sería posible usar como socios de acoplamiento cruzado. El alcance del haluro de arilo se amplió aún más a bromo y derivados de cloro, poco descritos en la reacción tradicional de Ni Negishi. El método proporciona acceso a nuevos derivados con valor potencial en química médica. Los estudios mecanísticos sugieren que el complejo formado entre Ni y Zn es el que absorbe la luz visible sin la necesidad de un fotosensibilizador exógeno. Como la reacción se lleva a cabo en flujo, la escalabilidad directa se logra fácilmente. Este capítulo se refiere a nuestro artículo publicado *Angew. Chem Int. Ed. 2018, DOI: 10.1002 / anie.201802656.* Además, el trabajo se destacará como contraportada de la edición correspondiente.

El origen de la exploración de la reacción de Pd Photoinduced Negishi (Capítulo 5) estaba en la limitación de la metodología anterior para el acoplamiento cruzado de derivados de haluro más desactivados o organocincicos problemáticos como los reactivos de Reformatsky. Incluso en este caso, la reacción fue claramente acelerada por la irradiación de la luz. Se obtuvo una reacción de amplio alcance y las grandes diferencias en conversión entre reacciones irradiadas y reacciones sin irradiación probaron que la luz es esencial para obtener esta transformación. Incluso en este caso, los estudios mecanísticos mostraron que la presencia de Pd y Zn en la misma solución cambió la absorción de Pd en la región visible. Además, la investigación de RMN sugiere que el paso que se acelera es la adición oxidativa. La reacción ha sido ampliamente estudiada y este trabajo será presentado próximamente en el *Journal of the American Chemical Society.*

Junto con este último trabajo, para probar la aplicabilidad de estas nuevas metodologías no solo en el descubrimiento de fármacos sino también en el proceso de desarrollo de fármacos, seleccionamos la reacción de Negishi inducida por luz y catalizada por Ni para escalarla en una escala piloto de producción. Este proyecto se describe en el Capítulo 6 y fue posible gracias a la colaboración con Corning Inc. que nos permitió utilizar su Corning G1 5-modules Photoreactor. La ampliación progresó con éxito proporcionando 20-40 gramos de productos finales puros. Además, el monitoreo en línea de RMN demostró ser esencial para analizar el primer paso de esta reacción, la formación de reactivos de organozinc. Este trabajo se presentará pronto en el *Journal of Organic Chemistry* gracias a una invitación de la revista a nuestro equipo.

Estas nuevas y sencillas metodologías para insertar motivos alifáticos en moléculas orgánicas proporcionan nuevas herramientas para los químicos sintéticos. Las metodologías son simples de ejecutar y la química de flujo permite una reproducibilidad y escalabilidad. La fotocatálisis ofrece condiciones de reacción suaves con una amplia

tolerancia de grupos para diferentes compuestos heterocíclicos, compuestos clave en la química médica. Además, la combinación de fotocatálisis con catálisis de metales de transición sin el uso de fotosensibilizador exógeno abre nuevas vías dentro de este campo. Estos hallazgos no solo permiten nuevos patrones de reactividad para moléculas de intereses de baja reactividad, sino que también han creado nuevos conocimientos sobre la interacción del metal y la absorción de la luz visible. Como se informó en los capítulos anteriores de esta tesis, hay pruebas claras de que la reactividad de dos metales de transición, como el Ni y el Pd, se puede mejorar mediante la interacción con Zn bajo irradiación con luz visible. Aunque se requieren futuras investigaciones mecanicistas para elucidar y caracterizar todos los intermedios de estas interacciones bimetálicas, el potencial de este enfoque es obvio. Cambia la forma en que los químicos sintéticos utilizan los catalizadores de metales de transición y permite nuevos patrones de química a través de la irradiación de la luz. Realmente creemos que todavía hay más interacción bimetálica para explorar y descubrir que puede abrir nuevas puertas al químico sintético para acceder a la química desafiante.

Bibliografía

[i] Walsh, B. Escape from Flatland. *J. Evol. Biol.* **2007**, 20(1), 36–38.

[ii] (a) Müller, K.; Faeh, C.; Diederich, F. Fluorine in Pharmaceuticals: Looking beyond Intuition. *Science*. **2007**,*317* (5846), 1881-1886; (b) Hagmann, W. K. The Many Roles for Fluorine in Medicinal Chemistry. *J. Med. Chem*., **2008**, *51* (15), 4359–4369; (c) Swallow, S. Fluorine in Medicinal Chemistry. *Prog. Med. Chem.* **2015**, *54*, 65–133.

[iii] Zuo, Z.; Ahneman, D. T.; Chu, L.; Terrett, J. A.; Doyle, A. G.; MacMillan, D. W. C. Merging Photoredox with Nickel Catalysis: Coupling of -Carboxyl Sp3-Carbons with Aryl Halides. *Science.* **2014**, *345* (6195), 437–440.

[iv] (a) Metal-Catalyzed Cross-Coupling Reactions, 2nd ed. (Eds.: A. de Meijere, F. Diederich), **2004**, Wiley-VCH, Weinheim; (b) Johansson Seechurn, C. C. C.; Kitching, M. O.; Colacot, T. J.; Snieckus, V. Palladium-Catalyzed Cross-Coupling: A Historical Contextual Perspective to the 2010 Nobel Prize. *Angew. Chem. Int. Ed*. **2012**, 51 (21), 5062–5085; (c) Cantillo, D.; Kappe, C. O. Immobilized Transition Metals as Catalysts for Cross-Couplings in Continuous Flow - A Critical Assessment of the Reaction Mechanism and Metal Leaching. *ChemCatChem* **2015**, *6* (12), 3286–3305; (d) Noël, T.; Buchwald, S. L. Cross-Coupling in Flow. *Chem. Soc. Rev.* **2011**, *40* (10), 5010.

The work described in this thesis has been carried out within the Chemical Technologies group in Janssen R&D, Toledo, Spain. The research was financially supported by the European Union's Horizon 2020 research and innovation program under the Marie Sklodowska-Curie grant agreement No. 641861.

Aknowledgments

Time flies and now I am at the end of my PhD studies. I feel extremely lucky to be a Marie Sklodowska-Curie fellow and complete my PhD research in Janssen R&D basic research center in collaboration with the University of Cordoba. First of all, I want to thank the European Commission for the funding and the two directors of this thesis; my university tutor Prof. Rafael Luque for his supervision as director of this thesis and Dr. Jesus Alcazar as co-director and direct supervisor of the work.

I have always loved science and research, but for a girl coming for a country in development, doing a PhD in a scientific breakingthrough research center such as Janssen, was a dream highly impossible to be achieved.

Thank you, Jesus, for making my dream come true. I still remember that flight back after my interview, where I thought this would be too much for me and I could never believe I would ever be part of this team. But you trusted in me and you did it more and more times (sometimes even more than what I do it for myself). We started this journey with little ideas on how the future would be like and I think we are finishing it in glory and with the best achievements we could imagine, not only work-type but even personal ones. It is amazing the ability that you have to create a work environment with people who are so different but that connect so well between them thanks to your support, your advices and your knowledge. I must confess that I was a little bit scared that you were not an academic when we started but, now I can shout loudly that I was superlucky to have you as my supervisor. You are the best professor I could ever imagine and I am so proud that I had the opportunity to learn and grow with you. Please, never forget that you will always be the grandfather of my Vapourtecs so take care of them when I will not be here.

Many thanks to mi Hucki, mi hermanona y mi jefa in these three years. You were my example to follow, what I wanted to be as a grown-up flow chemist and my reference point in my everyday life in Toledo. I feel privileged to have learned from your German work ethic and your Spanish culture in enjoying life.

A team can be very successful with a supercritical personality inside. And this is what we learned when you joined our group, Mateo. Thank you for being a big brother for me and being there every time, I needed you. Synthesis 3, con la jefa, MB1 y el pequeño foton was the best place in Janssen where learning and having fun was perfectly combined and transformed in successful results.

Thanks to mi Maria de Castellon that was there for every doubt I had in writing this thesis. She always had an answer and a solution for my problems. Her maturity and wise words helped me in the biggest drawbacks I had in the last steps of this journey. Even though, we have spent just a few months working together, we connected immediately and became good friends. Thanks to Nicola, my first official intern, even though with time I had to be more focused in my thesis and left you under the supervision of Jesus. I was so happy when I met you, first because you were my first intern and then because you are Italian, my second hometown. It is a pleasure to work with you and I feel lucky for that.

A big thank goes for all the people in Janssen and our director Javier Fernandez that allowed me to be part of this team. You were my everyday life and I felt honored to work in an environment with such high qualified scientists. Many thanks to my new colleagues of Synthesis 2, Ignacio, Jose Cid, Carlos, Encarna, Alcira and Nacho. It was very hard for me to leave Synthesis 3 after spending most of my PhD there but the way you accepted us in your lab made me feel directly comfortable and I really enjoyed and learned a lot in these months in Synthesis 2. Thank you, Alberto. Analysis would not survive without you. In these three years I was really amazed how you could manage to maintain under control all the analytic machines. Without your help, insights about the photo-induced nickel Negishi mechanism would not have been possible. Many thanks for that! Thanks to Jose Manuel for all the support in the characterization of products and identification of the stereochemistry. I really like to hear you when you talk about your traveling around the world. Thank you, Antonio Gomez for preparing all the contracts when I went to Rivendell and then in France. Thanks to Hector and Polonio for all the help with the chemicals.

I want to express my strong gratitude to all the Photo4Future members. This innovative project gave me the opportunity to learn from the most outstanding scientists in the field of flow chemistry and photochemistry. Thank you, Tim, for creating this group and bringing together such brilliant minds. Especially, I feel privileged to have had the chance to be working under your supervision. Thanks to all the principal investigators Prof. Dorota Koziej, Prof. Kirsten Zeitler, Dr. Patrick Jean, Prof. Samuel Marre, Prof. Simon Kuhn, Dr. Laszlo Kocsis, for coordinating the research. Thank you, Clemens, for your supervision and great advices during my secondment in Corning. And, also many thanks to Esther for organizing all our meetings. Thanks to all the Photo4Future fellows, Dario, Cecilia, Weiyi, XiaoJing, Laura, Prasaanth, Stella, Anca and Philipp, for sharing great ideas in our meetings and spending nice time together.

My research would not have been complete without the collaboration with Prof. Antonio de la Hoz, Dr. Maria Victoria Gomez and Jose Miguel Mateo. Thank you for your

great work in the NMR investigation. I felt home every time I came to work in the University of Ciudad Real.

Of course, I cannot forget my first Spanish family, my first Citius colleagues with whom I shared my afternoons and my evenings in the afterwork life in Toledo. Thank you, Pablo, for teaching me always the difference between '*ser*' and '*estar*'; Jose Angel the biggest guy I have ever met; Dani, the NMR guy; Adri for always making jokes and Fabio and Gabriela the best couple in the world. Thank you all for all the laughs and the tears I have shared with you. It was amazing to know you all.

And thanks to the other Citius generations for sharing nice lunch breaks and this experiences together.

Other great colleagues and friends, that I cannot forget to thank and mention are Novalix colleagues. We shared great experiences together not only at work but even outside. Thank you to mi Anita for our Sunday breakfasts that made me feel home when I was most missing my Sunday's family times. You knew immediately how to become a close and confident friend when you were here in Toledo.

Natalia, even though, I have never met you personally, your help was essential for drawing my Angewandte cover and my thesis cover. Thank you, a lot for your time and your availability.

Thank you Colm, for helping me editing this thesis and especially for our nice talks during our interesting English classes.

Thank you, Alina, for all the help in the paperwork I had to prepare for the university. Your help was essential to me.

My achievements in career and personal life would not have been the same if my family wouldn't have supported me in every step of life. Who I am now, is because of their great work on me. Thank you, Mom and Dad, and my lovely little brother Bledi. You are my life.

Last but not least, I want to thank my best friend in life, the one who always knows how to cheer me up and make things look easier, my Ildo. In my hardest times your love was the motor that helped me to move on and succeed. Thank you for everything.

Table of Contents

Chapter 1

General introduction

Introduction into the importance of C(sp^3) in medicinal chemistry; flow chemistry in drug-discovery and flow photocatalysis

1.1 Importance of C(sp^3) in medicinal chemistry

It takes approximately 12.5 years to bring a drug-molecule into market and the success rate from target discovery to FDA approval are quite low. This long cycle time associated with high costs, due to failure of the chemical leads to turn into final marketed drugs, has become a key problem to address. The pharmaceutical industry is currently involved in a continuous change that emphasized the importance of the strategic role of the medicinal chemist to bring innovation into medicinal chemistry.

Since Lipinski's seminal paper[5] introducing the rule of 5, medicinal chemists have become increasingly aware of the value of the physical properties of potential drug candidates. These properties are used as key elements in ADMET (Absorption, Distribution, Metabolism, Excretion and Toxicity) prediction models. An increasing number of literature suggests that ADMET properties are related with molecular complexity.[6]

Lovering and coworkers defined the saturation as key descriptor for the molecular complexity.[7] They reported a series of data suggesting that saturation allows the preparation of architecturally more complex molecules resulting in the exploration of more chemical space, without increasing significantly the MW. The saturation of a molecule [$F(sp^3)$] is measured from its (sp^3) character (Equation 1.1).

$$F(sp^3) = \frac{Number\ of\ C(sp^3)}{Total\ C\ number}$$

Equation 1.1: Saturation of a molecule

In their study, they demonstrated that there was a trend carried out through all the stages from discovery to drug development where each phase had a higher F(sp^3). The average F(sp^3) he measured was 0.36 for drug discovery compounds and increased to 0.47 for marketed drugs, 31% increase of the saturation of the molecule (Figure 1.1).

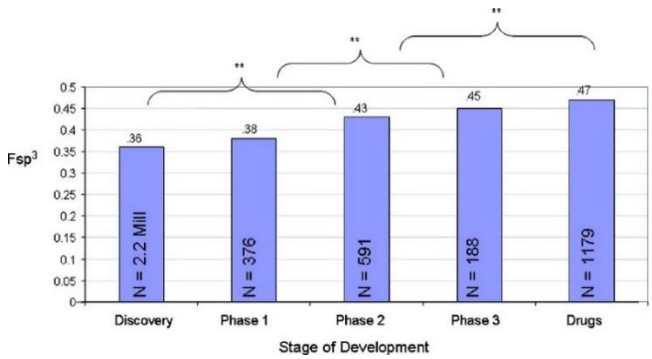

*Figure 1.1: F(sp^3) for compounds in different stages of development. **P value <0.001.[7]*

Moreover, the complexity metrics was correlated with both solubility and melting point. For a drug to be absorbed it has to be soluble and permeable. High aqueous solubility provides high free concentration of the compound to permeate the biological membranes. Low aqueous solubility can result in low absorption even though permeability is good.[5,8] The study revealed that there is a strong correlation between the F(sp^3) and solubility. As can be seen in Figure 1.2 the average of F(sp^3) increases linearly with log(S).

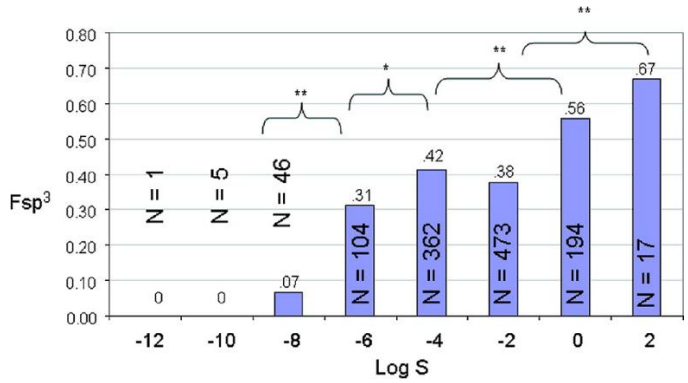

*Figure 1.2: F(sp^3) as a function of log(S). *P value <0.01. **P value <0.001.[3]*

The solubility of an organic compound is closely related to its melting point.[9] Breaking up the crystal lattice is the first step in the dissolution process. A correlation between melting point and F(sp^3) was also observed from the researchers. The average of F(sp^3) is found to decrease with increasing melting point (Figure 1.3). This may be since molecules with a lower F(sp^3) are more easily involved in π-interactions, forming stronger crystal interactions. As saturation increases the molecules tend to have lower melting points due to the disruption of the planarity and symmetry.[10]

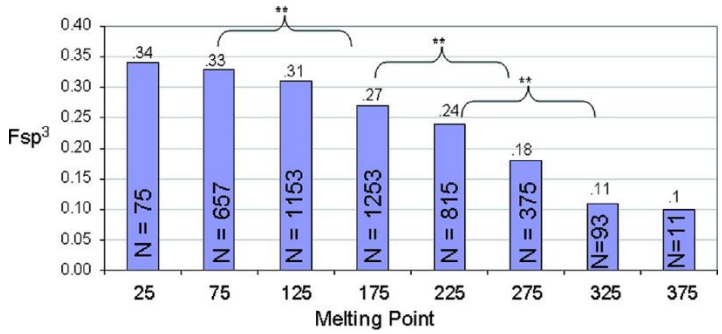

*Figure 1.3: Fsp³ as a function of melting point. *P value <0.001.[3]*

These results clearly suggest that increasing the F(sp^3) at early stages in drug discovery leads to molecules with improved ADMET profile accelerating the entire drug development process.

1.1.1 Cross-coupling reaction for C(sp^3)-C(sp^2) bond formation

Transition metal cross-coupling reagents have emerged as a powerful synthetic tool for C-C bond construction. Since its discovery, synthetic chemists have broadly used it to assemble complex molecular frameworks of interests in total synthesis of natural products, medicinal chemistry, and industrial process development as well as chemical biology, materials and nanotechnologies.[11] The development has reached a level of sophistication that allows for a wide range of coupling partners to be combined efficiently. The importance of this general class of reactions was recognized by the awarding of the Nobel Prize in chemistry to Richard Heck, Ei-ichi Negishi and Akira Suzuki for "palladium catalyzed cross-coupling in organic synthesis". Traditionally, transition metal catalyzed cross coupling reactions for the coupling of alkyl-organometalics proceed through 3 consecutive steps: oxidative addition; transmetalation and reductive elimination (Figure 1.4).

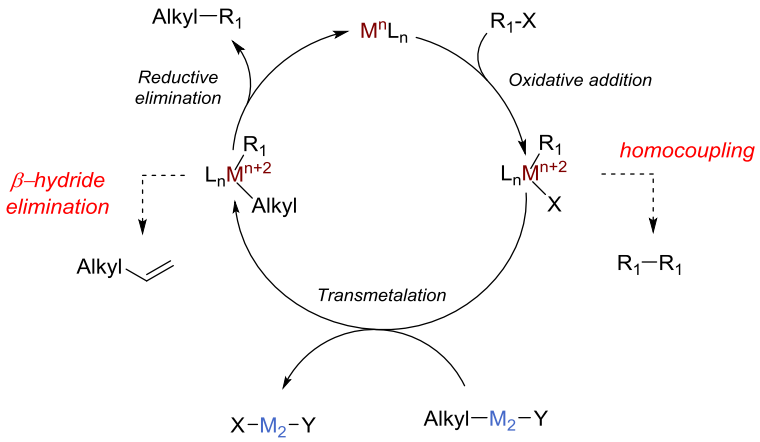

Figure 1.4: C(sp^3) cross coupling with alkyl-organometallics

Historically, transition metal catalysis reactions have been mainly focused in C(sp^2)-C(sp^2) cross-coupling. C(sp^3) cross coupling reactions have been less reported probably due to several serious problems, making its use in medicinal chemistry more limited related to the C(sp^2) cross coupling. These issues, include generally the stability problems of C(sp^3) organometallics, necessity to perform organometallics inline without purification as they are air sensitive and often slow transmetalation step.[11b] Oxidative addition for (sp) or (sp^2) is faster in comparison with the (sp^3) ones. Slow oxidative addition, leads to the formation of homocoupling products. Additionally, moderate

reductive elimination can compete with β-hydride elimination, leading to more byside products.

The metal catalyzed cross coupling reactions of (sp^3)-organometallics can be categorized in 5 types: 1) Negishi protocol, using alkylzinc reagents; 2) Suzuki-Miyaura protocol, using alkyl boronates; 3) Kumada protocol, using alkylmagnesium reagents; 4) Stille protocol, using alkyltin reagents and 5) Hiyama protocol, using alkylsilicon derivatives.

The alkyl zinc reagents have good ability to go to transmetalation step due to the presence of an empty low-lying *p* orbital of zinc. Consequently, nickel and palladium catalyzed cross-coupling reactions of alkylzinc reagents with aryl[11b,12], acyl[12] or alkyl halides[13] have proved to be a powerful tool in organic synthesis.

Organoboron compounds have been reported as an alternative due to their thermal stability in comparison with the organozinc reagents.[14] The broad functional group tolerance of these organometallic reagents especially compared to Negishi and Kumada reaction was an added value to this protocol.[12,14a] However, although organoboron compounds are highly electrophilic, the organic groups on boron are weakly nucleophilic, limiting the applicability of this protocol.[15]

The Kumada coupling was the first cross-coupling reaction described with Ni or Pd catalysts. The organomagnesium reagents are used as coupling partners with alkyl, vinyl or aryl halides.[16] However, the modest functional group tolerance of these reagents in comparison with boron and zinc reagents limits their use in organic synthesis.

Stille protocol with organotin reagents is a versatile method for C-C bond forming. Aryl and alkenyltin reagents are commonly used as coupling partner while alkyl transfer is practically limited to the methyl group using $SnMe_4$.[17] Longer alkyltin reagents have low reactivity and alkyl transfer capability. Moreover, due to the toxicity of tin reagents and their low polarity, Stille reactions are frequently substituted by Negishi and Suzuki couplings.

Alkylsilicones have several advantages in comparison with other alkyl metals such as: low toxicity; high stability to air and moisture and easy handling in reaction preparation. Hiyama first reported the cross-coupling reaction with alkylsilicon reaction in 1988[18], however their use in synthetic chemistry is still limited.[19] The strong C-Si bond requires higher temperatures for the activation of organosilicon reagent for successful transmetalation. Normally, additives such as a base of fluorine ions are used for the silane activation. The hard activation conditions combined with the broad commercial availability of boronates, brings the Hiyama reaction as a second choice after Suzuki-Miyaura protocol.

The alternative of metal cross coupling reactions for C(sp^3) insertion is the direct C-H activation through radicalic pathways. Radical chemistry is highly reactive chemistry with low selectivity. New technologies such as flow chemistry may help to control its overreactivity.[20]

1.2 Flow chemistry in drug discovery

While for decades, in the petrochemical and bulk chemical industry continuous plants exist and proved to be the most economical ones, pharma industry still relies on multipurpose batch or semi batch reactors. Only recently continuous process technology has become a major focus of drug development in the pharmaceutical industry.[21] As the goal in this phase is the preparation of the active principle ingredient (API) in the most efficient and faster way it has been more straightforward to see the benefits of continuous process. Compared to batch, flow chemistry offers various advantages such as:

- Implementation of new chemistry not readily available to scale up in batch mode (electrochemistry, photochemistry, microwave heating)
- Opportunity for improved purity and selectivity
- Readily accessible extreme conditions such as high and low temperatures and high pressures
- Safer execution of hazardous chemistry
- Decreased environmental impact
- Possibility for automation and inline or online monitoring

However, medicinal chemists have been trained using batch chemistry and most laboratories are set up for conducting experiments in batch mode and changing these conditions in drug discovery has required some more time than in drug development. Nevertheless, in the latest years, considering the need for a medicinal chemistry innovation, flow chemistry is gaining ground even in discovery labs. The preparation of diverse sets of compounds instead of a single one, makes direct comparison between both technologies not possible and has reattracted many medicinal chemists to explore the advantages of continuous processing in small scale. Reaction optimization is key element to obtain reliable results in shorter times. In flow, the reaction time, and concentration are modulated by the solvent and reagents flow rates. These parameters can be screened rapidly in real time in flow without the need for the set-up of individual batch reactions. Inline and online analytics permit fast feedback optimization accelerating the entire synthetic process. Moreover, direct scalability in a faster and reproducible way enables connections between drug discovery and drug development, avoiding further optimization towards the next steps of a drug development and

therefore reducing time, costs and chemical waste of the entire process that brings a new molecule in the market.[21c]

1.2.1 Practical considerations for flow reactions

There are fundamental differences between batch and flow systems in terms of stoichiometry, concentration, production time, and yield.[22] Stoichiometry in batch processes is defined by the concentration of chemical reagents and their volumetric ratio. In flow it is defined from the concentration of the reagents and the ration of their flow rates. For instance, the substrate concentration in a batch reaction decreases over time and is uniformly distributed in the flask. In a flow reaction, the concentration of the starting materials decreases along the reactor reaching a minimum at its end. If ideal plug-flow behavior is assumed the length dependency leads to a constant concentration of the substrate and product under steady-state conditions.

In batch production, the reaction time is determined by how long the batch reactor is held at certain conditions to reach full conversion. In flow conditions the residence time is determined by the volume of the reactor and the bulk flow rates. The reaction time or better-defined residence time for continuous processes can be varied either via changing the flow rates (v) or the volume of the flow reactor (V) (Equation 1.2).

$$t_R = \frac{V}{v}$$

Equation 1.2: Residence time measurment

The key steps for accurate residence time are the precise initiation and termination of the reaction. Initiation starts when the reagents are mixed together or when physical activation such as heating or irradiation.

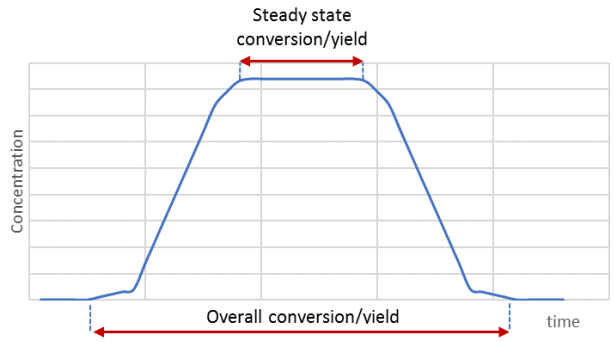

Figure 1.5: Difference between steady state conversion/yield and overall conversion/yield

The residence time is very important for the overall conversion/yield of the reaction especially when the reaction volume is significantly smaller than the reactor volume. Overall conversion/yield means that the entire reaction mixture was collected and analyzed, while the conversion/yield under steady state conditions reflects the value under stable conditions (Figure 1.5).

In the following subchapter several examples supporting the advantages of flow chemistry are introduced. These selected transformations are relevant to drug discovery as they are commonly used in medicinal chemistry settings.

1.2.2 Enabling difficult chemistry

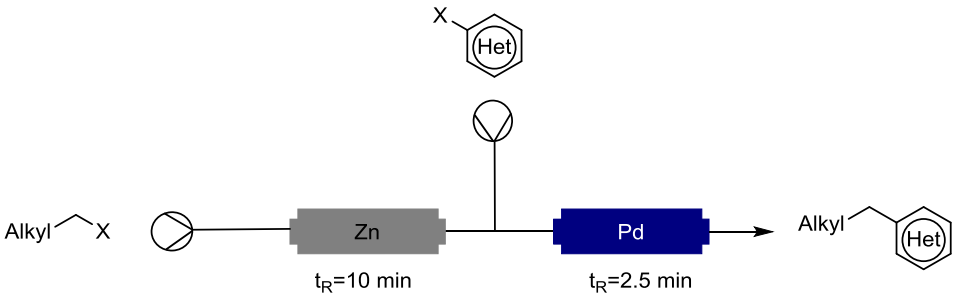

Figure 1.6: Continuous synthesis of organozinc coupled with Negishi reaction

The Negishi coupling is broadly applicable in medicinal chemistry whereby the transmetalation of organozinc reagents to a palladium or nickel catalyst allows for the coupling to a wide range of unsaturated halides increasing the (sp^3) character of biological molecules. Organozinc reagents can be prepared by oxidative addition to zinc metal, transmetalation and iodide/ boron zinc exchange. However, problems of reproducibility and handling of these sensitive species limits the applications of the Negishi reaction in comparison with other cross coupling reactions. In 2014, a continuous flow formation of organozinc reagents using an activated packed bed of metallic zinc was reported and subsequently the organozinc halide was used in Negishi cross-coupling using another packed-bed reactor of Pd catalyst.[23,39] The authors demonstrated that high and reproducible titers of organozinc solution can be obtained in time when well activated Zn column is used. The scope includes a variety of alkyl halides readily converted in organozinc reagent and then coupled with aryl halides. The two-column system demonstrated to be tolerant to many functional groups including those of high interests in medicinal chemistry perspective such as azetidines. Moreover, this protocol is environmentally friendly as it allows the chemist to reuse the metal column several times reducing the metal waste (Figure 1.6).

1.2.3 Safer chemistry

Carbon monoxide (CO) is a colorless, odorless and tasteless gas which is extremely toxic. This hazardous gas is an important reagent for the insertion of carbonylic groups into organic molecules through metal catalysis. Flow chemistry has been used as a safe and efficient tool for catalytic carbonylation reactions using gaseous CO. The Ley's group has reported a palladium catalyzed carbonylation using a tube in tube reactor for the gas loading in combination with a coil reactor.[24] The initial set up suffered from the precipitation of Pd in the tube in tube reactor, and therefore the researchers made some further modifications. First of all, the reagents got mixed with a second liquid stream containing the gas dissolved before entering the reactor and the black palladium precipitation issues were solved by changing the solvent system (DMF/Toluene). High conversions for several aryl halides were obtained at 100 °C at a pressurized system 6.9 bars within 37.5 minutes using $Pd(OAc)_2$/ XantPhos, Et_3N and MeOH (Figure 1.7). Less reactive aryl bromide required higher pressure (15 bars), dioxane as solvent and hydrazine to facilitate Pd(II) reduction.

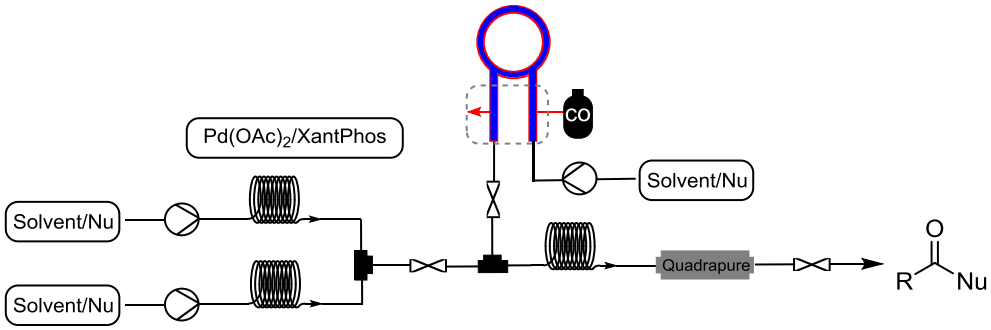

Figure 1.7: General Flow approach for Pd-catalyzed carbonlylation

1.2.4 Improved selectivity

The reduction of esters to aldehydes with DIBAL-H is an attractive approach. However, in practice the reaction is limited due to uncontrolled overreactivity leading to the primary alcohol.[25] Various groups reported that DIBAL-H performs better in flow than in batch.[26] Jamison's group reported an inline quenching of the reaction to avoid overreactivity.[26b] They observed that mixing efficiency was key element to control the reactivity. Therefore T-mixers performed much better than Y-mixers because of the poorer mixing energy of these last ones. The authors also noticed that with higher flow rates the conversion as well increased. This is again related to the mixing. In high flow rates, more energy is put into the system, stimulating better mixing. Temperature influenced both batch and flow reactions but while in -42 °C in batch the alcohol was the major product, in flow at the same temperature its presence was not identified (Figure 1.8).

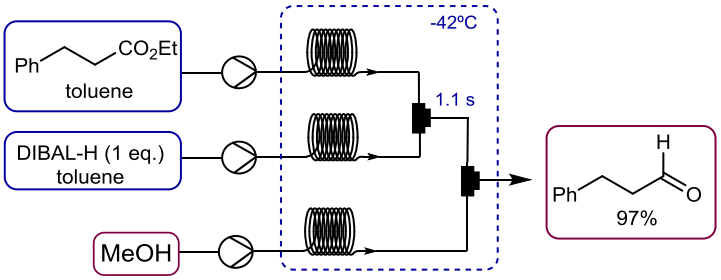

Figure 1.8: Selective Flow Reduction of Esters using DIBAL-H

1.3 Flow photocatalysis

As mentioned in the Subchapter 1.2 implementing new chemistries not readily available to scale up in batch mode such as photochemistry and electrochemistry is one of the big advantages of flow chemistry. Herein, we want to highlight the importance of flow photocatalysis as it is the core topic of the present dissertation.

Photochemical reactions are light driven chemical reactions. Light activation of organic molecules facilitates reaction's pathways that are otherwise difficult to reach by thermochemical or electrochemical activation. There are two fundamental ways to excite organic molecules; they include direct and indirect excitation. Direct excitations can be realized through absorption of photons by an organic molecule. The limitation of this method is related with the presence of a chromophore in the organic molecule which absorbs the light efficiently. Limited reactivity of these compounds can be overcome by indirect excitation. Hereby, incident light is absorbed by a catalyst or sensitizer and the electrons or energy are transferred to an acceptor molecule than can be substrate of a chemical transformation. The latter is an attractive method for organic chemists, due to the fact that these reactions are driven by visible light of which starting materials and products generally do not absorb. Moreover, it opens the potential to use solar light as an infinite green energy source.[27]

The molecules involved in the light absorption process in photochemical reactions are called photocatalysts of photosensitizers. A photocatalyst is an organic molecule that has the ability to undergo a redox reaction in the excited state and a subsequent turnover step enables participation in light driven catalytic redox cycles. Most of the photoredox catalytic reactions follow a reductive or oxidative redox cycle (Figure 1.9). Both catalytic cycles are categorized by the primary direction of the electron transfer to the excited state catalyst cat*. In an oxidative quenching cycle, the excited state cat* is quenched by donating an electron either to substrate or an oxidant present in the reaction mixture. In a reductive quenching cycle, cat* is quenched by accepting an electron from the substrate or a reductant. The catalyst turnover step involves reduction

of the oxidized [cat]·+ in the oxidative cycle and oxidation of the reduced catalyst [cat]·- in the reductive cycle. In either case, the substrate, an external redox active reagent, or an intermediate may be responsible for the catalyst turnover.

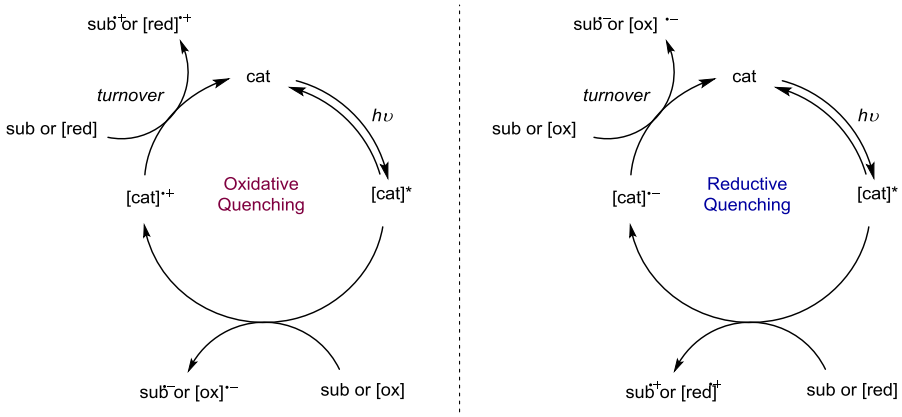

Figure 1.9: Oxidative and Reductive quenching cycle in photoredox catalysis

Photocatalysis in general relies on efficient irradiation of the reaction mixture. Therefore, starting materials, products, photosensitizers and photocatalysts can all act as filters reducing the light intensity available for the rest of the reaction mixture. Consequently, a homogeneous energy distribution inside a photoreactor is crucial to obtain high yields and high selectivity. According to the Lambeert-Beer Law (Equation 1.3) the light attenuation is dependent on the molar attenuation coefficient of the molecule (ε), the concentration of the molecule (*c*) and the pathlength of the reactor. Therefore, depending on the reactor type, the irradiation distribution will not be uniform due to these absorption effects.

$$\mathrm{A} = \log_{10} T = \log_{10} \frac{I_0}{I} = \varepsilon c l$$

Equation 1.3: Lambeert-Beer Law

To keep the irradiation distribution uniform and thus maximize the efficiency of photochemical reactors microflow technology can be used. In microflow reactors, the large surface to volume ratio ensures increased irradiation efficiency of the entire reaction mixture. This results in intensified chemistry and reproducibility of results.[28]

Even though, the absorption of photons is crucial for photochemical reactions,[29] not all the incident photons are absorbed for the conversion of starting material in product. The quantum yield (*f*) is an important parameter to describe the efficiency of photochemical reactions (Equation 1.4).

$$\varphi = \frac{number\ of\ molecules\ of\ product\ formed}{number\ of\ photons\ absorbed\ from\ the\ reaction\ media}$$

Equation 1.4: Quantum yield measurement

The quantum yield, typically varies from 0 to 1 for nonchain mechanisms.[30] Quantum yields above 1 indicate that chain photoredox reactions occur.[31] In such chain reactions, photoabsorption leads to the generation of a radical or photo-initiator which is subsequently propagated until termination occurs. The quantum yield can be determined by measuring the photon flux of the set up and subsequently carrying out the reaction in the same set up.[32] Photon flux is the number of photons emitted per unit of time. It is important to understand that not every emitted photon will end up in the photoreactor. By using reflectors or minimized reactor set ups the photon flux can be improved. The group of Loubiere has compared the photo flux of a batch reactor and a flow reactor.[33] The batch reactor received a photon flux of 7.4×10^{-6} einstein/s, while the microreactor had a photon flux of 4.1×10^{-6} einstein/s. However, this value needs divided by the reactor volume to obtain the absorbed photon flux density. For the microreactor, 5.02 einstein/(m^3s) was observed, while the batch reactor only had 0.033 einstein/(m^3s). This 150-fold higher absorbed photon flux density explains clearly why photochemical reactions can be substantially accelerated in flow reactors. The photon flux strongly affects the intrinsic reaction rate of photochemical processes; the higher the photon flux, the faster the reaction will be completed.

1.3.1 Practical examples

Stephenson *et al*. have transferred several of their batch radical reactions to continuous flow.[34] The flow reactor consisted of commercial capillary PFA tubing (I.D.= 750 µm) which was irradiated blue LEDs (5.88W, λ =447.5nm) While the large-scale batch reaction required more than 48 h with low conversion, the flow reaction could be completed in 1 minute furnishing the target compound in 91% of yield (Figure 1.10).

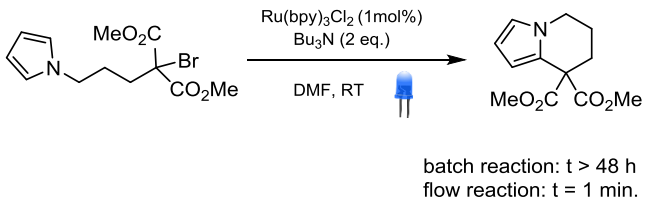

Figure 1.10: Photocatalytic radical pyrrole functionalization

Seeberger and coworkers reported a photocatalytic system to reduce a carbon-chlorine bond in a-chlorophenyl acetates in a continuous flow reactor using 1mol% of $Ru(bpy)_3Cl_2$.[35] The microreactor consisted of FEP tubing (I.D.= 750 µm; V= 4.7mL) around

two metal cylinders. The reactor was irradiated with two face-to-face aligned white LED lamps (17 W). In flow the reaction was completed in 30 minutes with 82% of yield of target compound compared to 24 hours in batch. Notably, the hydrolysis of the Vilsmeier-Haack intermediate forming the formate ester as a byproduct in 14% of yield in batch, in flow system was avoided, increasing the selectivity and efficiency of the reaction (Figure 1.11).

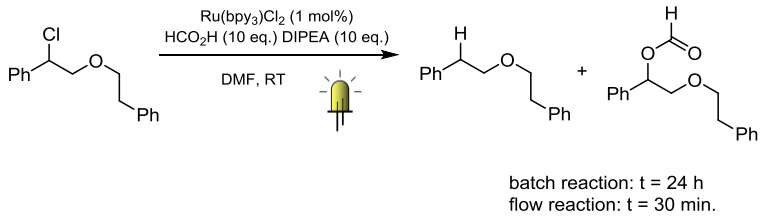

Figure 1.11: Photocatalytic reduction of carbon-chlorine

The Noël group used PFA tubing (I.D.= 500 µm) around a large diameter syringe coated with aluminum film to increase the photon flux as photo-flow reactor set up. They reported the $Ru(bpy)_3$ catalyzed trifluoromethylation of five membered ring heterocycles using gaseous CF_3I as trifluoromethylating source.[36] Full conversion was achieved in several minutes in flow (8-16 min.) compared to hours of irradiation in batch (Figure 1.12). This acceleration was attributed to increased irradiation in flow and increased gas-liquid mass transfer due to the segmented flow regime. Moreover, the improved efficiency of the reactor allowed to reduce the catalyst loading to 0.05mol%.

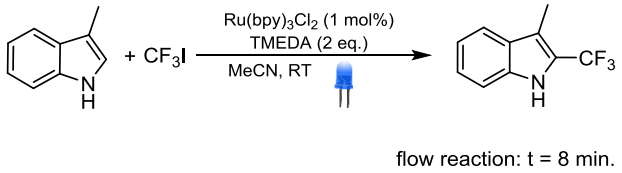

Figure 1.12: Rapid trifluoromethylation of 5-membered ring heterocycles

The same group, reported lately, a novel reactor concept which combines continuous microreactor technology with the concept of luminescent solar concentration (LSCs). A classical LSC device is made by dispersing a luminophore in a waveguide which can be made out of polymeric materials or glass.[37,64] Light can penetrate the surface of the waveguide where it is absorbed by the luminophore. The re-emitted light is guided and concentrated by total internal reflection toward the edge of the device where a photovoltaic cell is attached. The Noël group adapted this principle to continuous flow synthesis by building a chip-based reactor made out of PDMS doped with fluorescent dye Lumogen F red 305. This dye absorbs visible light from 400-600 nm and re-emits the

light at 600-700 nm, which perfectly overlap with the absorption spectra of methylene blue. They studied the singlet oxygen cycloaddition to 9-10 diphenylanthracene using sunlight. The experiment showed that this reactor is significantly more efficient that a non dopped one (Figure 1.13). However, this promising finding still need to be explored to broader range of wavelength to access more powerful catalysts.

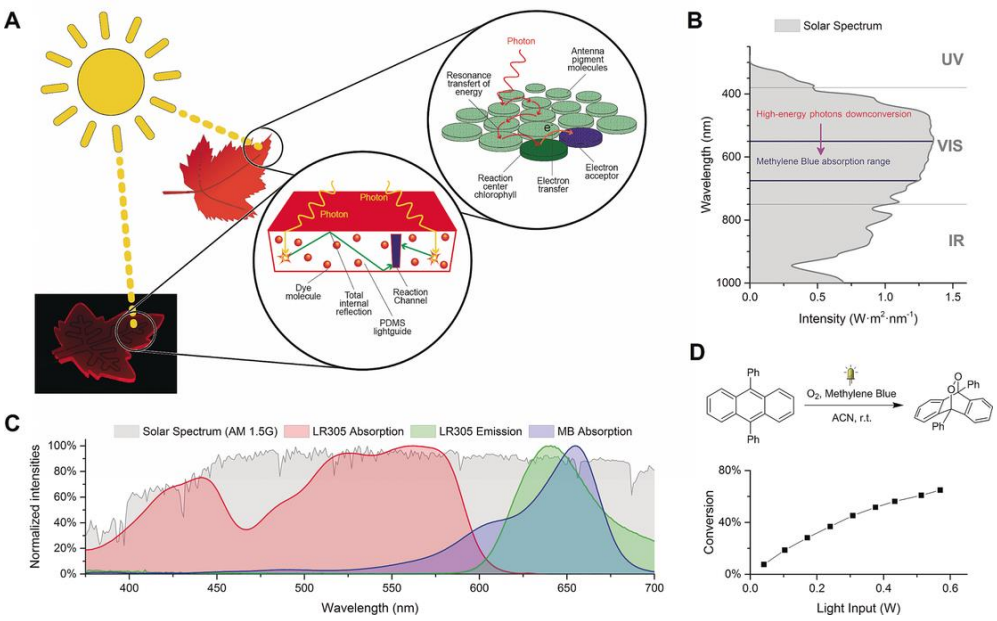

Figure 1.13: Working principles of LSC-PM[64]

Despite the proved efficiency of all the homemade photoreactors, nowadays, the market offers a wide variety of commercially available flow photoreactors (Figure 1.14). They are made with FEP tubing or high-quality glass or falling film modules irradiated with different light sources and the final selection should rely on the need of the final user.

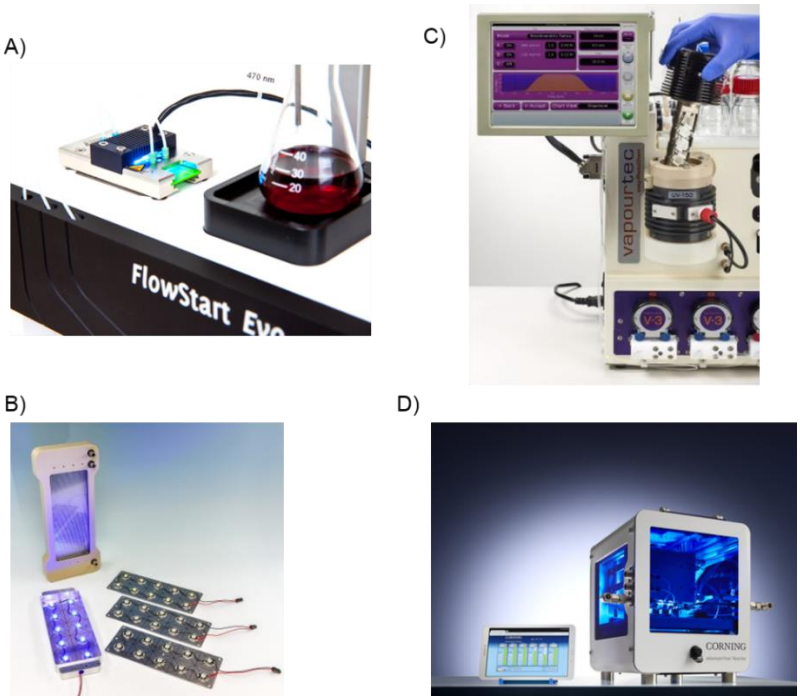

Figure 1.14: Commercial available photoreactors: A) Futurechemistry photoreactor; B) Fraunhofer photoreactor; C) Vapourtec photoreactor; D) Corning Lab photoreactor

1.3.2 Scalability

Increasing the productivity of photochemical reactions to industrial scale has proven to be an important challenge for chemists and chemical engineers. Due to the Lambert−Beer limitation of photon transport, scalability and reproducibility has been problematic even on a laboratory scale. In fact, advantages of photochemical syntheses observed on a small scale cannot be fully transferred on a larger scale when using a classical batch reactor technology. Consequently, the implementation of photochemical transformations in the pharmaceutical and fine-chemical industry has been severely limited. Flow technologies have been embraced by the scientific community as an ideal solution to scale up photochemistry.[38]

Essentially two strategies can be distinguished to scale-up photochemistry with photoflowreactors: (1) longer operation times and increasing the throughput by increasing the flow rates and (2) numbering-up.

The first strategy is the most popular one on a laboratory scale as it is simple and straightforward to do. Reaction conditions are often optimized using only small amounts of starting materials in a microreactor. The same device can be subsequently used,

without reoptimization of the reaction conditions, to produce the desired amount of material by continuous introduction of starting materials. Higher throughputs can be achieved by increasing the volume of the reactor and flow rates while keeping the residence time constant. In flow photoreactors, reaction times are usually reduced from hours to the minutes. This provides an important increase in productivity compared to batch technology. With this strategy, typically several milligrams to hundreds of grams can be prepared in a reasonable time frame. This is often enough to prepare enough material for the initial stages of a drug discovery process or to screen the properties of new materials.

More material can be prepared by placing several flow reactors in parallel. This strategy is called numbering-up and there are two different approaches, i.e. internal and external numbering-up. External numbering-up is achieved by placing several microreactors along with their pumping system and process control in parallel. So, the entire microreactor setup is copied several times until the desired amount of product can be reached. This is a reliable way of scaling up since individual reactor failure will not influence the throughput of the other reactors. However, this is a very costly strategy as typically the most expensive parts of any microreactor setup are the pumps and the process control. In contrast, internal numbering is more economically accessible as only the reactor itself is numbered-up while the process control and pumping system is shared. Commercially available examples of internal numbering-up for photoreactors are the falling film microreactor[39] microcapillary films[40] and the Corning Advanced-Flow G1 Photo Reactor.[41]

1.4 Outline and scope of this thesis

In this thesis the development of new methodologies for the insertion of $C(sp^3)$ in organic molecules will be discussed. Combination of flow chemistry with photocatalysis opens new pathways in $C(sp^3)$-$C(sp^2)$ coupling. The projects are mainly focused in heterocycle chemistry considering their applicability fundamental in medicinal chemistry.

Novel methodologies for the trifluoromethylation of arenes and heteroarenes are in high demand in the chemical and pharmaceutical industry. In ***Chapter 2*** a continuous flow protocol for the insertion of the trifluoromethyl moiety into highly functionalized heterocycles is discussed. This photoredox methodology relies on the use of solid sodium trifluoromethanesulfinate (CF_3SO_2Na) as the trifluoromethylating agent and the iridium complex $[Ir\{dF(CF_3)\ ppy\}_2](dtbpy)]PF_6$ as the photoredox catalyst. A diverse set of highly functionalized heterocycles proved compatible with the methodology, and moderate to good yields were obtained within 30 minutes of residence time. This project was done in collaboration with the University of Technology of Eindhoven and the project was finalized with a publication in *Synthesis 2017, 49, 4978-4985.*

In ***Chapter 3*** the transfer of a batch photoredox reaction into flow is described. The combined Ni/Ir catalysis provides very interesting mild condition methodology for $C(sp^3)$-$C(sp^2)$ cross coupling. However, batch reaction conditions limit its applicability, to small scale production. This new flow procedure clearly improves the scalability of the previous batch reaction by the reactor's size and operating time reduction, and allows the preparation of interesting compounds for drug discovery in multigram amounts. The results of this project are published in *Bioorg. Med. Chem. 2017, 25, 6190-6196.*

Negishi reaction is a versatile functional group tolerant methodology that allows the cross-coupling of organozinc reagents with different aryl halides. Considering our experience in preparing clear solutions of organozinc reagent under continuous flow conditions, we decided to study their behavior under light irradiation. Surprisingly, we observed that the reactivity of these organometallic reagents under visible light irradiation is highly enhanced. We studied this new version of Negishi cross-coupling reaction using nickel (***Chapter 4***) and palladium (***Chapter 5***) as catalysts. The Ni-photo induced Negishi reaction (***Chapter 4***) enabled the cross-coupling of different alkylic-zinc reagents, otherwise not possible to be used as cross coupling partners. The aryl halide scope was further broadened to bromo and chloro derivatives, poorly described in traditional Ni Negishi reaction. The method provides access to new derivatives with potential value in medicinal chemistry. Mechanistic studies suggest that the complex formed between Ni and Zn is the one which absorbs the visible light without the need of an exogenous photosensitizer. As the reaction is carried out in flow, direct scalability

is easily achieved. This chapter refers to our published article *Angew. Chem Int. Ed. 2018, DOI: 10.1002/anie.201802656*. Moreover, it will be highlighted as back cover of the corresponding issue.

The origin of the exploration of Pd Photoinduced Negishi (***Chapter 5***) reaction was in the limitation of the previous methodology for the cross coupling of more disactivated halide derivatives or problematic organozinc reagents such as Reformatsky reagents. Even in this case, the reaction was clearly accelerated by the light irradiation. Broad scope reaction was obtained and big differences light no light proved that light is essential to obtain this transformation. Even in this case, the mechanistic studies showed that the presence of Pd and Zn in the same solution shifted the absorption of Pd into visible reagion. Moreover, the NMR investigation suggests that the step which is accelerated is the oxidative addition. The reaction has been broadly studied and this work will be submitted soon at *Journal of the American Chemical Society*.

In conjunction to the latter work, to prove the applicability of these new methodologies not only in drug discovery but even in drug development process we selected the Ni photo-induced Negishi reaction to scale it up in pilot-production scale. This project is described in ***Chapter 6*** and it was possible thanks to the collaboration with Corning Inc. that allowed us to use their Corning G1 5-modules Photoreactor. The scale up proceeded successfully providing 20-40 grams of pure final products. Moreover, inline NMR monitoring proved to be essential in analyzing the first step of this reaction, the formation of organozinc reagents. This work will be soon submitted in *Journal of Organic Chemistry* by fulfilling an invitation of the journal to the team.

Bibliography

[5] Lipinski, C. A.; Lombardo, F.; Dominy, B. W.; Feeney, P. J. Experimental and Computational Approaches to Estimate Solubility and Permeability in Drug Discovery and Develop Ment Settings. *Adv. Drug Deliv. Rev.* **1997**, *23*, 3–25.

[6] (a) Gleeson, M. P. Generation of a Set of Simple, Interpretable ADMET Rules of Thumb. *J. Med. Chem.* **2008**, *51* (4), 817–834; (b) Leeson, P. D.; Springthorpe, B. The Influence of Drug-like Concepts on Decision-Making in Medicinal Chemistry. *Nat. Rev. Drug Discov.* **2007**, *6* (11), 881–890; Hughes, J. D.; Blagg, J.; Price, D. A.; Bailey, S.; DeCrescenzo, G. A.; Devraj, R. V.; (c) Ellsworth, E.; Fobian, Y. M.; Gibbs, M. E.; Gilles, R. W.; et al. Physiochemical Drug Properties Associated with in Vivo Toxicological Outcomes. *Bioorganic Med. Chem. Lett.* **2008**, *18* (17), 4872–4875; Yang, Y.; Engkvist, O.; Llinàs, A.; (d) Chen, H. Beyond Size, Ionization State, and Lipophilicity: Influence of Molecular Topology on Absorption, Distribution, Metabolism, Excretion, and Toxicity for Druglike Compounds. *J. Med. Chem.* **2012**, *55* (8), 3667–3677.

[7] Walsh, B. Escape from Flatland. *J. Evol. Biol.* **2007**, 20(1), 36–38.

[8] (a) Ran, Y.; Yalkowsky, S. H. Prediction of Drug Solubility by the General Solubility Equation (GSE). *J. Chem. Inf. Comput. Sci.* **2001**, *41* (2), 354–357; (b) Delaney, J. S. ESOL: Estimating Aqueous Solubility Directly from Molecular Structure. *J. Chem. Inf. Comput. Sci.* **2004**, *44* (3), 1000–1005.

[9] (a) Ran, Y.; He, Y.; Yang, G.; Johnson, J. L. H.; Yalkowsky, S. H. Estimation of Aqueous Solubility of Organic Compounds by Using the General Solubility Equation. *Chemosphere* **2002**, *48* (5), 487–509; (b) Sanghvi, T.; Jain, N.; Yang, G.; Yalkowsky, S. Estimation of Aqueous Solubility By The General Solubility Equation (GSE) The Easy Way. *QSAR Comb. Sci.* **2003**, *22* (2), 258–262; (c) Johnson, S. R.; Chen, X. Q.; Murphy, D.; Gudmundsson, O. A Computational Model for the Prediction of Aqueous Solubility That Includes Crystal Packing, Intrinsic Solubility, and Ionization Effects. *Mol. Pharm.* **2007**, *4* (4), 513–523.

[10] Ishikawa, M.; Hashimoto, Y. Improvement in Aqueous Solubility in Small Molecule Drug Discovery Programs by Disruption of Molecular Planarity and Symmetry. *J. Med. Chem.* **2011**, *54* (6), 1539–1554.

[11] (a) Jana, R.; Pathak, T. P.; Sigman, M. S. Advances in Transition Metal (Pd, Ni, Fe)-Catalyzed Cross-Coupling Reactions Using Alkyl-Organometallics as Reaction Partners. *Chem. Rev.* **2011**, *111* (3), 1417–1492; (b) Negishi, E. I. Historical Background of Organopalladium Chemistry. *J. Am. Chem. Soc.,* **2003**, 125 (3), 850–850.

[12] Knochel, P.; Singer, R. D. Preparation and Reactions of Polyfunctional Organozinc Reagents in Organic Synthesis. *Chem. Rev.* **1993**, *93* (6), 2117–2188.

[13] Terao, J.; Kambe, N. Transition Metal-Catalyzed C-C Bond Formation Reactions Using Alkyl Halides. *Bull. Chem. Soc. Jpn.* **2006**, *79* (5), 663–672.

[14] (a) Miyaura, N. Cross-coupling reactions: A practical guide, **2002**, Berlin: Springer; (b) Suzuki, A. Recent Advances in the Cross-Coupling Reactions of Organoboron Derivatives with Organic Electrophiles, 1995–1998. *J. Organomet. Chem.* **1999**, *576* (1–2), 147–168.

[15] Onak, T. Organoborane Chemistry, **2012**, (1st ed.) Burlington: Elsevier Science.

[16] (a) Metal-catalyzed cross-coupling reactions **2006,** (2nd ed.), Weinheim: Wiley-VCH; (b) Càrdenas, D. J. Advances in Functional-Group-Tolerant Metal-Catalyzed Alkyl-Alkyl Cross-Coupling Reactions. *Angew. Chem. Int. Ed.* **2003**, *42* (4), 384–387; (c) Seyferth, D. The Grignard Reagents. *Organometallics*, **2009**, 28 (6), 1598–1605

[17] Milstein, D.; Stille, J. K. Palladium-Catalyzed Coupling of Tetraorganotin Compounds with Aryl and Benzyl Halides. Synthetic Utility and Mechanism. *J. Am. Chem. Soc.* **1979**, *101* (17), 4992–4998.

[18] Hatanaka, Y.; Hiyama, T. Pentacoordinate Organosilicate as an Alkylating Reagent: Palladium Catalyzed Methylation of Aryl Halides. *Tetrahedron Lett.* **1988**, *29* (1), 97–98.

[19] (a) Hiyama, T.; Hatanaka, Y. Palladium-Catalyzed Cross-Coupling Reaction of Organometalloids through Activation with Fluoride Ion. *Pure Appl. Chem.* **1994**, *66* (7), 1471–1478; (b) Denmark, S. E.; Regens, C. S. Palladium-Catalyzed Cross-Coupling Reactions of Organosilanols and Their Salts: Practical Alternatives to Boron- and Tin-Based Methods. *Acc. Chem. Res.,* **2008**, *41* (11), 1486–1499*;* (c) Spivey, A.; Gripton, C.; Hannah, J. Recent Advances in Group 14 Cross-Coupling: Si and Ge-Based Alternatives to the Stille Reaction. *Curr. Org. Synth.* **2004**, *1* (3), 211–226.

[20] (a) Chatgilialoglu, C., & Studer, A. Encyclopedia of radicals in chemistry, biology, and materials, **2012**, (1st ed.). Chichester, West Sussex: John Wiley & Sons; (b) Ley, S. V. On Being Green: Can Flow Chemistry Help? *Chem. Rec.* **2012**, *12* (4), 378–390; (c) Gilmore, K.; Seeberger, P. H. Continuous Flow Photochemistry. *Chem. Rec.* **2014**, *14* (3), 410–418; (d) Wirth, T. Flow Chemistry: Enabling Technology in Drug Discovery and Process Research. *ChemSusChem*. **2012**, 5, 215–216.

[21] (a) Malet-Sanz, L.; Susanne, F. Continuous Flow Synthesis. a Pharma Perspective. *J. Med. Chem.* **2012**, 55 (9), 4062–4098; (b) Poechlauer, P.; Colberg, J.; Fisher, E.; Jansen, M.; Johnson, M. D.; Koenig, S. G.; Lawler, M.; Laporte, T.; Manley, J.; Martin, B.; et al. Pharmaceutical Roundtable Study Demonstrates the Value of Continuous Manufacturing in the Design of Greener Processes. *Org. Process Res. Dev.* **2013**, *17* (12), 1472–1478; (c) Jimenez-Gonzalez, C.; Poechlauer, P.; Broxterman, Q. B.; Yang, B. S.; Am Ende, D.; Baird, J.; Bertsch, C.; Hannah, R. E.; Dell'Orco, P.; Noorman, H.; et al. Key Green Engineering Research Areas for Sustainable Manufacturing: A Perspective from Pharmaceutical and Fine Chemicals Manufacturers. *Org. Process Res. Dev.* **2011**, *15* (4), 900–911; (d) Baxendale, I. R.; Braatz, R. D.; Hodnett, B. K.; Jensen, K. F.; Johnson, M. D.; Sharratt, P.; Sherlock, J. P.; Florence, A. J. Achieving Continuous Manufacturing: Technologies and Approaches for Synthesis, Workup, and Isolation of Drug Substance May 20–21, 2014 Continuous Manufacturing Symposium. *J. Pharm. Sci.*, **2015**, 104, 781–791.

[22] (a) Plutschack, M. B.; Pieber, B.; Gilmore, K.; Seeberger, P. H. The Hitchhiker's Guide to Flow Chemistry. *Chem. Rev*. **2017**,117, 11796–11893; (b) Wegner, J.; Ceylan, S.; Kirschning, A. Ten Key Issues in Modern Flow Chemistry. *Chem. Commun.* **2011**, *47* (16), 4583.

[23] Alonso, N.; Miller, L. Z.; De M. Muñoz, J.; Alcázar, J.; McQuade, D. T. Continuous Synthesis of Organozinc Halides Coupled to Negishi Reactions. *Adv. Synth. Catal.* **2014**, *356* (18), 3737–3741.

[24] Gross, U.; Koos, P.; O'brien, M.; Polyzos, A.; Ley, S. V. A General Continuous Flow Method for Palladium Catalysed Carbonylation Reactions Using Single and Multiple Tube-in-Tube Gas-Liquid Microreactors. *Eur. J. Org. Chem.* **2014**, *2014* (29), 6418–6430.

[25] (a) Haycock-Lewandowski, S. J.; Wilder, A.; Åhman, J. Development of a Bulk Enabling Route to Maraviroc (UK-427,857), a CCR-5 Receptor Antagonist. *Org. Process Res. Dev.* **2008**, *12* (6), 1094–1103; (b) Haycock-Lewandowski, S. J.; Wilder, A.; Åhman, J. Development of a Bulk Enabling Route to Maraviroc (UK-427,857), a CCR-5 Receptor Antagonist. *Org. Process Res. Dev.* **2008**, *12* (6), 1094–1103.

[26] (a) Ducry, L.; Roberge, D. M. Dibal-H Reduction of Methyl Butyrate into Butyraldehyde Using Microreactors. *Org. Process Res. Dev.* **2008**, *12* (2), 163–167; (b) Webb, D.; Jamison, T. F. Diisobutylaluminum Hydride Reductions Revitalized: A Fast, Robust, and Selective Continuous Flow System for Aldehyde Synthesis. *Org. Lett.* **2012**, *14* (2), 568–571; (c) Carter, C. F.; Lange, H.; Sakai, D.; Baxendale, I. R.; Ley, S. V. Diastereoselective Chain-Elongation Reactions Using Microreactors for Applications in Complex Molecule Assembly. *Chem. Eur. J.* **2011**, *17* (12), 3398–3405; (d) Yoshida, M.; Otaka, H.; Doi, T. An Efficient Partial Reduction of α,β-Unsaturated Esters Using DIBAL-H in Flow. *Eur. J. Org. Chem.* **2014**, *2014* (27), 6010–6016.

[27] (a) Tucker, J. W.; Stephenson, C. R. J. Shining Light on Photoredox Catalysis: Theory and Synthetic Applications. *J. Org. Chem.* **2012**, *77* (4), 1617–1622; (b) Schultz, D. M.; Yoon, T. P. Solar Synthesis: Prospects in Visible Light Photocatalysis. Science, **2014**, *343* (6174), 123917; (c) Shaw, M. H.; Twilton, J.; MacMillan, D. W. C. Photoredox Catalysis in Organic Chemistry. *J. Org. Chem.* **2016**, *81* (16), 6898–6926; (d) Hopkinson, M. N.; Sahoo, B.; Li, J.-L.; Glorius, F. Dual Catalysis Sees the Light: Combining Photoredox with Organo-, Acid, and Transition-Metal Catalysis. *Chem. Eur. J.* **2014**, *20* (14), 3874–3886; (e) Hoffmann, N. Homogeneous Photocatalytic Reactions with Organometallic and Coordination Compounds-Perspectives for Sustainable Chemistry. *ChemSusChem*. **2012**, 5 (2), 352–371; (f) Albini, A.; Fagnoni, M.; Mella, M. Environment-Friendly Organic Synthesis. The Photochemical Approach. *Pure Appl. Chem.* **2000**, *72* (7), 1321–1326.

[28] Su, Y.; Straathof, N. J. W.; Hessel, V.; Noël, T. Photochemical Transformations Accelerated in Continuous-Flow Reactors: Basic Concepts and Applications. *Chem. Eur. J*. **2014**, 20 (34), 10562–10589.

[29] Cambié, D.; Bottecchia, C.; Straathof, N. J. W.; Hessel, V.; Noël, T. Applications of Continuous-Flow Photochemistry in Organic Synthesis, Material Science, and Water Treatment. *Chem. Rev*. **2016**, 116, 17, 10276–10341.

[30] Studer, A.; Curran, D. P. Catalysis of Radical Reactions: A Radical Chemistry Perspective. *Angew. Chem. Int. Ed*. **2016**, 55(1), 58–102.

[31] (a) Majek, M.; Filace, F.; Von Wangelin, A. J. On the Mechanism of Photocatalytic Reactions with Eosin Y. *Beilstein J. Org. Chem.* **2014**, *10*, 981–989; (b) Karkas, M. D.; Matsuura, B. S.; Stephenson, C. R. J. Enchained by Visible Light-Mediated Photoredox Catalysis. *Science.* **2015**, *349* (6254), 1285–1286.

[32] Ziegenbalg, D.; Wriedt, B.; Kreisel, G.; Kralisch, D. Investigation of Photon Fluxes within Microstructured Photoreactors Revealing Great Optimization Potentials. *Chem. Eng. Technol.* **2016**, *39* (1), 123–134.

[33] Aillet, T.; Loubiere, K.; Dechy-Cabaret, O.; Prat, L. Accurate Measurement of the Photon Flux Received inside Two Continuous Flow Microphotoreactors by Actinometry. *Int. J. Chem. React. Eng.* **2014**, *12* (1).

[34] Tucker, J. W.; Zhang, Y.; Jamison, T. F.; Stephenson, C. R. J. Visible-Light Photoredox Catalysis in Flow. *Angew. Chem. Int. Ed.* **2012**, *51* (17), 4144–4147.

[35] Bou-Hamdan, F. R.; Seeberger, P. H. Visible-Light-Mediated Photochemistry: Accelerating Ru(Bpy)32+-Catalyzed Reactions in Continuous Flow. *Chem. Sci.* **2012**, *3* (5), 1612.

[36] Straathof, N. J. W.; Gemoets, H. P. L.; Wang, X.; Schouten, J. C.; Hessel, V.; Noël, T. Rapid Trifluoromethylation and Perfluoroalkylation of Five-Membered Heterocycles by Photoredox Catalysis in Continuous Flow. *ChemSusChem* **2014**, *7* (6), 1612–1617.

[37] Cambie, D.; Zhao, F.; Hessel, V.; Debije, M. G.; Noël, T. A Leaf-Inspired Luminescent Solar Concentrator for Energy-Efficient Continuous-Flow Photochemistry. *Angew. Chem. Int. Ed.* **2017**, *56* (4), 1050–1054.

[38] (a) Coyle, E. E.; Oelgemöller, M. Micro-Photochemistry: Photochemistry in Microstructured Reactors. The New Photochemistry of the Future? *Photochem. Photobiol. Sci.* **2008**, *7* (11), 1313; (b) Oelgemoller, M.; Shvydkive, O. Recent Advances in Mircoflow Photochemistry. *Molecules* **2011**, *16* (9), 7522–7550; (c) Elliott, L. D.; Knowles, J. P.; Koovits, P. J.; Maskill, K. G.; Ralph, M. J.; Lejeune, G.; Edwards, L. J.; Robinson, R. I.; Clemens, I. R.; Cox, B.; et al. Batch versus Flow Photochemistry: A Revealing Comparison of Yield and Productivity. *Chem. Eur. J.* **2014**, *20* (46), 15226–15232.

[39] Jähnisch, K.; Dingerdissen, U. Photochemical Generation and [4+2]-Cycloaddition of Singlet Oxygen in a Falling-Film Microreactor. *Chem. Eng. Technol.* **2005**, *28* (4), 426–427.

[40] (a) Elvira, K. S.; Wootton, R. C. R.; Reis, N. M.; Mackley, M. R.; DeMello, A. J. Through-Wall Mass Transport as a Modality for Safe Generation of Singlet Oxygen in Continuous Flows. *ACS Sustain. Chem. Eng.* **2013**, *1* (2), 209–213; Reis, N. M.; Li Puma, G. A Novel Microfluidic Approach for Extremely Fast and Efficient Photochemical Transformations in Fluoropolymer Microcapillary Films. *Chem. Commun.* **2015**, *51* (40), 8414–8417.

[41] Elgue, Sébastien and Aillet, Tristan and Loubiere, Karine and Conté, Annelyse and Dechy-Cabaret, Odile and Prat, Laurent E. and Horn, Clement R. and Lobet, Olivier and Vallon, Sophie Flow photochemistry: a meso-scale reactor for industrial applications. *Chimica Oggi*, **2015**, *33* (5). 58-62.

Chapter 2

Visible-Light-Induced Trifluoromethylation of Highly Functionalized Arenes and Heteroarenes in Continuous Flow

This chapter is based on:

Abdiaj, I., Bottecchia, C., Alcazar, J. & Noël, T. Visible-Light-Induced Trifluoromethylation of Highly Functionalized Arenes and Heteroarenes in Continuous Flow. *Synth.* **49,** 4978–4985 (2017).

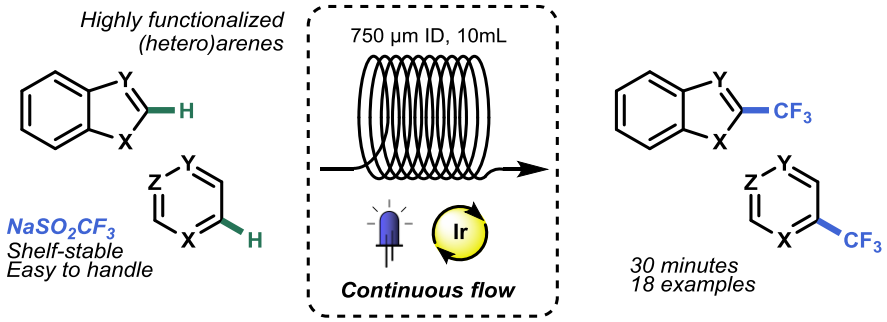

2.1 Introduction on trifluoromethylations

Although organo fluorine groups are very scarce in nature,[1] nowadays 20-25% of modern drugs contain at least one fluorine atom.[2] The introduction of fluorine or a trifluoromethyl group has been shown to significantly enhance the metabolic stability of organic molecules due to the unfavourable energetic cost of breaking a C-F (116 kcal/mol) relative to that of C–H (99 kcal/mol) in the enzymatic metabolism of a drug by cytochrome P450.[3] Trifluoromethylations of organic molecules have been of increasing importance to medicinal chemistry over the past few decades due to the properties of the trifluoromethyl group.[4] A very interesting example is reported in the lead optimization of Ezetimib (Figure 2.1).[5] The electron withdrawing nature of the fluorine substituent deactivates the aromatic ring towards metabolic pathways. These structural modifications led to a second-generation drug which was found to be 400 times more potent, requiring lower doses due to improved metabolic stability in vivo.

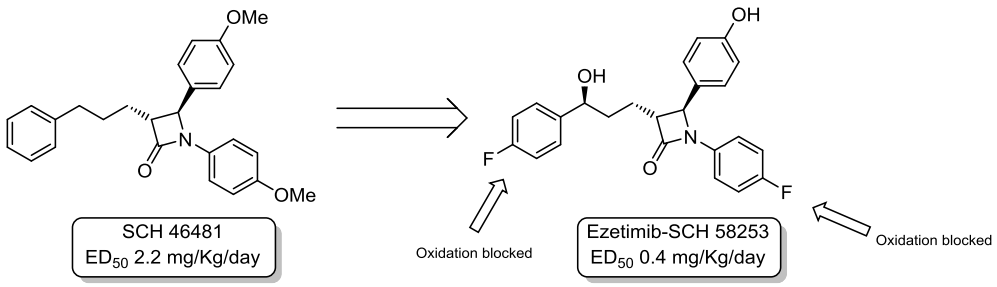

Figure 2.1: SAR optomization of Ezetimib

Moreover, of all halogens, fluorine has the highest electron density while occupying the least amount of volume.[6] This means that fluorine can alter the electron distribution of a molecule translated into a clear impact on pKa and therefore on the bioavalability of a drug molecule.[7] The pKa of an ionizable center in a drug molecule changes the lipophilicity profile (because of the pH dependence of the distribution coefficient, D), which influences solubility, permeability, and protein binding. Hydrogen atoms which are situated in alfa versus the fluorine atom are generally more acidic as the electronegativity is directed towards the fluorine atom. This effect has a direct impact on binding affinity of the fluorinated compound. Fluorine is often used to influence permeability by way of modulation of lipophilicity, association with pendent H-bond donors, or reduction of amine basicity. Most orally administered drugs have log P values, a common measure of lipophilicity of between 1 and 5.86 The log P of a neutral molecule is typically increased upon the addition of an aryl or vinyl fluorine but, conversely, often decreases with alkyl fluorination.[8] Monofluorination of a terminal alkyl methyl group

typically leads to a larger reduction in lipophilicity than trifluorination, while difluorination is predicted to have a similar effect on log P as monofluorination. These effects are primarily due to the participation of arylfluorines in resonance electron donation and the large dipole associated with carbon–fluorine bonds in fluoroalkanes.[8] However, a high lipophilicity typically results in a reduced solubility and a number of other undesirable properties for a compound. Therefore, the right balance between a required lipophilicity and a certain minimal overall polarity of the molecule is one of the recurring challenges for medicinal chemists.

Considering all the benefits that a fluorine can import to a drug candidate, novel methodologies for the fluorination and trifluoromethylation of arenes and heteroarenes are in high demand in the chemical and pharmaceutical industry today.[5,1c,9] The initially reported trifluoromethylation protocols relied on transition-metal-catalysed cross-coupling methods, but suffered from the need for prefunctionalized substrates and stoichiometric amounts of metal salts.[10] More recently, several strategies reported in the literature demonstrated the utility of photocatalytic protocols for the trifluoromethylation of alkenes, thiols, heterocycles, and arenes.[11] The most commonly used trifluoromethyl sources include expensive Togni and Umemoto's reagents, unstable triflyl chloride (CF_3SO_2Cl), gaseous CF_3I, and readily available trifluoroacetic anhydride.[11e,12] In addition, the Langlois reagent (CF_3SO_2Na) can be regarded as an easy-to-handle, inexpensive, and solid trifluoromethylating agent, capable of generating CF_3 radicals in the presence of a strong oxidant (e.g., t- BuOOH).[13] In 2011, Baran disclosed the direct trifluoromethylation of heterocycles using t-BuOOH as a sole oxidant (Figure 2.2). This method was operationally simple but still the use of over stoichiometric amounts of peroxides raised concerns regarding operational safety.

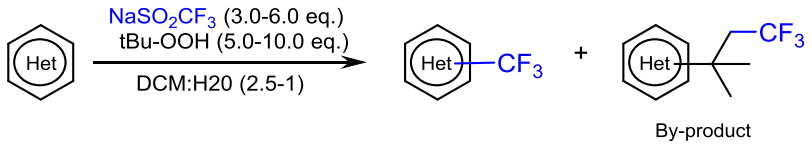

Figure 2.2:Baran's trifluoromethylation of heterocycles

As part of our interest in developing an efficient and safe continuous flow protocol to enable new tools for drug discovey[14], we envisioned a photocatalytic strategy for the trifluoromethylation of a variety of highly functionalized heteroarenes, which are of interest in medicinal chemistry.[11a,11b] Such substrates are often ignored in many reports, since these compounds are known to be highly challenging and thus low yielding. To develop a practical and widely applicable methodology, we opted to use the stable, inexpensive, and solid Langlois reagent (CF_3SO_2Na) as a trifluoromethyl source combined with an iridium catalyst that uses the light energy to release the CF_3 radical.

2.2 Optimization of the conditions

We commenced our investigations by performing luminescence quenching studies, which allowed us to rapidly select the optimal photocatalyst for our transformation.[15] Among the photocatalysts tested, the luminescence of both *fac*-Ir(ppy)$_3$ and [Ir{dF(CF$_3$)ppy}$_2$](dtbpy)]PF$_6$ was significantly quenched by increasing equivalents of CF_3SO_2Na, as depicted in Figure 2.3. This suggests that the excited state of both photocatalysts can be reductively quenched by the Langlois reagent, thus generating a CF_3 radical. In particular, a high luminescence quenching percentage of 58% was obtained for [Ir{dF(CF$_3$)ppy}$_2$](dtbpy)]PF$_6$ in the presence of 300 equivalents of the Langlois reagent, while 2500 equivalents of CF_3SO_2Na were needed to obtain a quenching percentage of only 44% in the case of *fac*-Ir(ppy)$_3$ (Figure 2.3). The higher quenching efficiency observed with [Ir{dF(CF$_3$)ppy}$_2$](dtbpy)]PF$_6$ is consistent with the higher excited state reduction potential reported for this catalyst compared to fac-Ir(ppy)$_3$ [1.21 V vs 0.31 V, respectively; both values reported versus the saturated calomel-electrode (SCE).[16] As reported by Glorius and co-workers, a quenching percentage larger than 25% should be considered as significant and relevant for photocatalytic reaction purposes.[15a] Therefore, we selected [Ir{dF(CF$_3$)ppy}$_2$](dtbpy)]PF$_6$ as the photocatalyst for our further investigations.

The photoflow reactor consisted of a Vapourtec UV-150 photoreactor equipped with a 10mL capillary reactor (I.D. 750 µm), which was subjected to 450 nm irradiation (54 blue LEDs; 24 W).

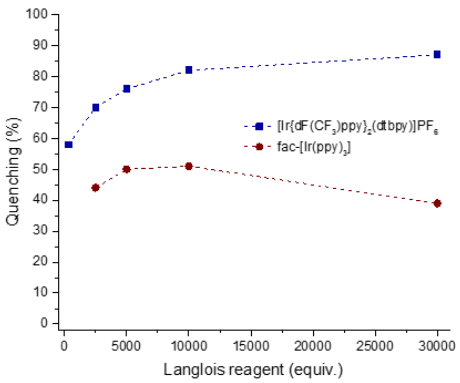

Figure 2.3: Luminescence quenching percentage of [Ir{dF(CF$_3$)ppy}$_2$](dtbpy)]PF$_6$ and fac-Ir(ppy)$_3$ in the presence of increasing amounts of Langlois reagent

Table 2.1: Optimization of Reaction Conditions for the Trifluoromethylation of Caffeine in Continuous Flow[a]

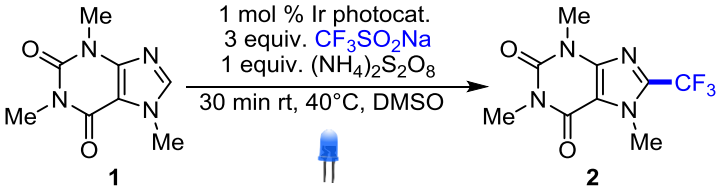

Entry	Changes from optimized conditions a	LC-MS Yield (%)
1	20 min residence time, no oxidant	5
2	no oxidant, CF_3SO_2Na (1.5 equiv)	12
3	1 eq $(NH_4)_2S_2O_8$, 1.5 eq CF_3SO_2Na	48
4	1 eq, Diacetoxyiodobenzene 1.5 eq CF_3SO_2Na	32b
5	none	54 (45b)
6	*fac*-Ir(ppy)$_3$ as photocatalyst	38
7	60 °C	50
8	no light	6
9	light, no [Ir{dFCF$_3$(ppy)}$_2$](dtbpy)]PF$_6$	-
10	365 nm LEDs	46

[a]**Reaction conditions**: caffeine (0.2 mmol), [Ir{dF(CF$_3$)ppy}$_2$](dtbpy)]PF$_6$ (1 mol%), CF_3SO_2Na (3 equiv), $(NH_4)_2S_2O_8$ (1 equiv), DMSO (2 mL; 0.1 M). Reactions performed in a commercially available Vapourtec UV-150 photoreactor, irradiation with 450 nm blue LEDs, 30 min residence time. [b] Isolated yield.

DMSO was chosen as a suitable solvent, ensuring high solubility of the densely functionalized substrates and thus avoiding the occurrence of microreactor clogging. At 40 °C, unsatisfactory yields were observed in flow for the trifluoromethylated caffeine (Table 2.1, entries 1 and 2). We rationalized that the addition of an oxidant might assist the re-aromatization of the radical intermediate to the final product. Indeed, in the presence of $(NH_4)_2S_2O_8$ (1 equiv.) as an oxidant, an improved LC-MS yield of 48% was obtained (Table 2.1, entry 3). Next, diacetoxyiodobenzene was tested as the oxidant, but this resulted in a lower 32% isolated yield (Table 2.1, entry 4). Increasing the amount of Langlois reagent to three equivalents further boosted the LC-MS yield to 54% (Table 2.1, entry 5) (45% isolated yield). Notably, under the same reaction conditions, the reaction with *fac*- Ir(ppy)$_3$ gave 38% yield (Table 2.1, entry 6), thus confirming the choice of the photocatalyst based on the luminescence quenching studies. Increasing the reaction temperature to 60 °C did not lead to a further improvement of the reaction yield (Table 2.1, entry 7). Control experiments revealed the photocatalytic nature of our protocol, as little to no product was observed in the absence of either light or photocatalyst (Table 2.1, entries 8 and 9). Finally, irradiation of the reaction mixture with

a 365 nm UV lamp resulted in 46% of the target compound been attributed to the UV-tailing absorption of the iridium photocatalyst (Table 2.1, entry 10). Nevertheless, it should be noted that, especially for the synthesis of densely functionalized drug candidates, irradiation with low-energy blue light is preferred over higher-energy ultraviolet light, to minimize the occurrence of side reactions and compound degradation.[17]

2.3 Trifluoromethylation of heterocycles

With the optimized reaction conditions in hand, our photocatalytic trifluoromethylation strategy was evaluated on a wide range of heteroarenes and arenes, as well as benzofused heterocycles (Figure 2.4). We focused our attention specifically on halogen-bearing substrates, which are of high value for drug discovery programs. In these programs, such functionalized substrates are key building blocks for the very popular cross-coupling methods, which allow the construction of carbon–carbon or carbon–heteroatom bonds.[18]

3-Methyl and 2-methylindole derivatives **4** and **5** were obtained in satisfactory yields, 62% and 69%, respectively (Figure 2.4). Notably, the presence of an iodo substituent on the indole was well tolerated yielding the two possible regioisomers **6** and **7**; C2/C3 respectively, in ratio 1:1. We then explored our transformation on a series of benzimidazole derivatives. Unlike indoles, benzimidazoles showed higher reactivity for the C4 and C6 positions on the aromatic ring.[19] For example, (trifluoromethyl)benzimidazole was obtained in 50% yield as a separable mixture of **8** and **9** C4/C6 respectively (3:2) isomers; the 2-bromo trifluoromethyl derivatives **10** and **11** were obtained in 52% yield (C4/C6, 3:2, separable mixture). Interestingly, 5-chlorobenzimidazole showed different selectivity, and was trifluoromethylated at positions C4 and C7 (**12**/**13**, 45%; C4:C7 2:1), probably due to the electronic and steric effect of the chlorine atom. Notably, the possibility to easily separate the regioisomers obtained for compounds **6** to **13** renders our strategy advantageous for the simultaneous synthesis of fluorinated analogues relevant for medicinal chemistry SAR studies. Next, we tested pyridone and pyrimidone, which are frequently used scaffolds in the synthesis of novel active pharmaceutical ingredients (APIs).[20] Trifluoromethylated pyrimidone **14** and bromopyridone **15** were obtained in good to excellent yields 80% and 60%, respectively (Figure 2.4). We further investigated the reactivity of pyridine, obtaining trifluoromethylated pyridine derivatives **17**, **18**, and **19** in modest yields, 40%, 35%, and 53%, respectively. Furthermore, phenylpyrazole could be trifluoromethylated on the phenyl substituent giving product **20** in 28% yield. Conversely, the tetrahydropyran-substituted 4-aminopyrazole derivative **21** was trifluoromethylated at position C5 on the pyrazole ring and isolated in a reasonable 45% yield. 3-Bromo-2,5-dimethylpyridine was successfully trifluoromethylated, giving **22** in 38% yield. Finally,

we explored the scope of our methodology with regard to inactivated arene substrates. Trifluoromethylated mesitylene and iodomesitylene **23** and **24** were obtained in good to excellent yields (53% and 80%, respectively). Trifluoromethylation of unactivated arenes is a particularly challenging transformation, often requiring long reaction times (18–24h), and has so far rarely been reported in photoredox-based protocols.[11i,21] Therefore, we were pleased to observe significant product formation in our system within only 30 minutes of reaction time. The main reason for the remarkable acceleration of the reaction rate observed in our protocol lies in the improved irradiation of the reaction mixture obtained in the microflow reactor. [17,22]

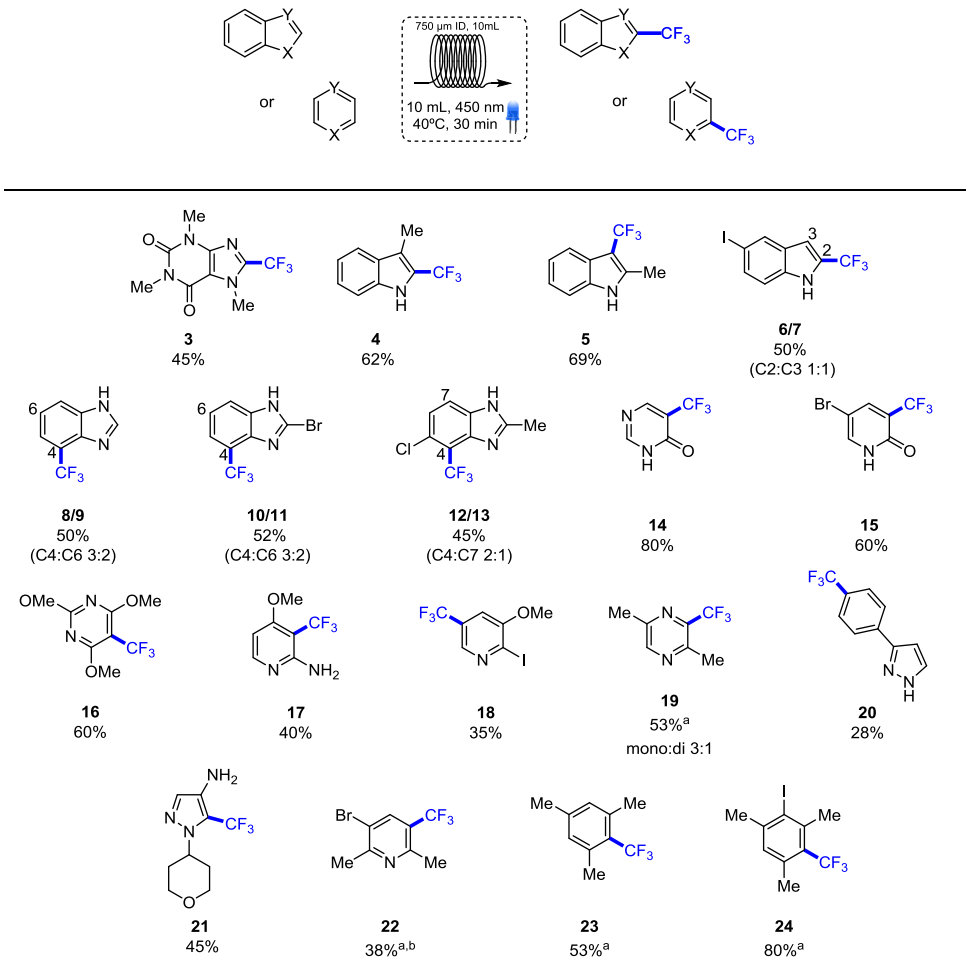

Figure 2.4: Scope of the trifluoromethylation of heteroarenes, benzofused heterocycles, and arenes. **Reaction conditions**: substrate (0.5 mmol), $[Ir\{dF(CF_3)ppy\}_2](dtbpy)]PF_6$ (1 mol%), CF_3SO_2Na (3 equiv), $(NH_4)_2S_2O_8$ (1 equiv), DMSO (2 mL, 0.1 M). Reactions performed in a Vapourtec UV-150 photoreactor, irradiation with 450 nm blue LEDs, 30 min residence time, isolated yields. [a] Yield determined by LC-MS. [b] Regioselectivity determined by ^1H NMR analysis of the crude reaction mixture.

2.4 Scale up of the reaction

A serious problem limiting the photochemical transformation in larger scale is the inefficient irradiation of the reaction mixture in batch system. Passing from batch systems to continuous flow systems this issue is elegantly avoided. The large surface-volume ratio assures efficient irradiation of the entire solution. To showcase the potential of microreactors in photochemistry in terms of productivity, we performed a scale-up experiment on bromopyridone.[22b,23]

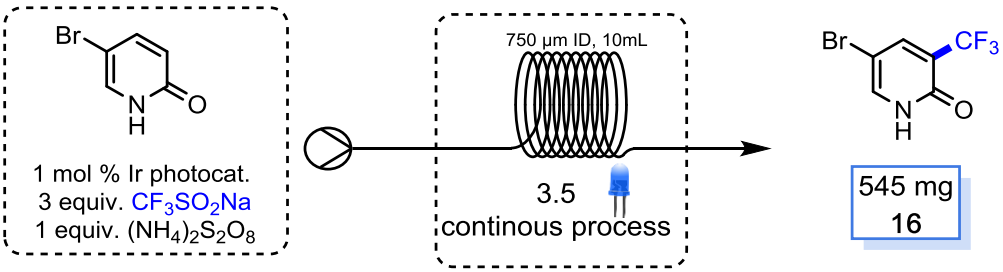

Figure 2.5: Scale up of bromopyridone

We prepared the solution of the starting materials following general procedure and using the equipment pumps the Vapourtec UV-150 photoreactor was continuously run for 3.5 hours without any intervention. The conversion of the starting material in product remained constant in time and at the end of the experiment we could afford 545 mg of purified trifluoromethylated derivative **16** (56%).

2.5 Possible reaction mechanism

A proposed mechanism for the trifluoromethylation reaction is depicted in Figure 2.6. Despite the fact that no in depth mechanistic studies were conducted, we can hypothesize that the first step involved in our photocatalytic trifluoromethylation would be the reductive quenching of the excited state of $[Ir\{dF(CF_3)ppy\}_2](dtbpy)]PF_6$ by the Langlois reagent, thus generating the trifluoromethyl radical. This can be based on the evidence that the Langlois reagent quenches the emission of $[Ir\{dF(CF_3)ppy\}_2](dtbpy)]PF_6$. Subsequent trapping of the trifluoromethyl radical by the substrate would generate the radical intermediate **A** that upon oxidation with persulfate **B** and deprotonation would generate the final product.

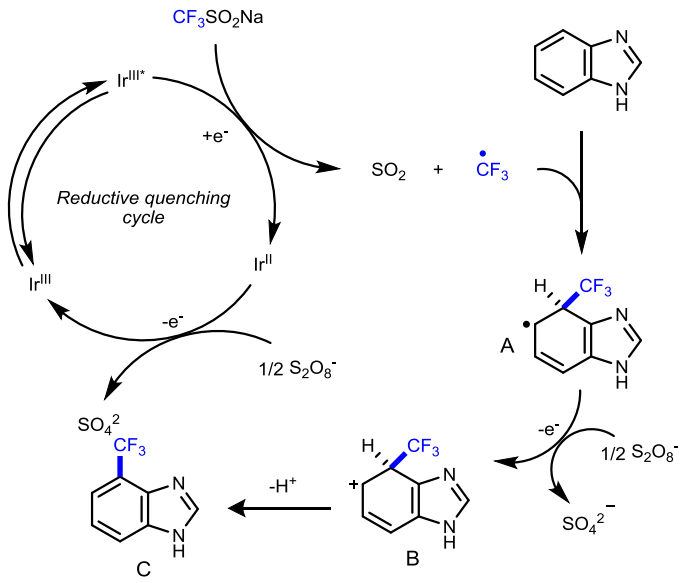

Figure 2.6: Proposed reaction mechanism

2.6 Conclusions

Fluorinated compounds are key compounds in the pharmaceutical industry. In structure–activity relationship (SAR) studies, the introduction of fluorine atoms can greatly impact the electronic properties, acidity, and lipophilicity of drug candidates. These effects are due to the high electronegativity of the fluorine atom, to its relatively small radius and to the less polarizable nature of C–F bonds compared to C–H bonds. The replacement of methyl groups with their trifluoromethyl counterparts represents a conservative substitution in terms of steric hindrance, while constituting a valuable strategy to block potential metabolically labile sites in drug candidates, prolonging their half-life and metabolic stability. Nevertheless, there are limited methodologies described in literature to insert fluorinated motifs in highly functionalised arenes and heteroarenes.

Reported in this chapter is a new continuous-flow strategy for trifluoromethylation of arenes, heteroarenes, and benzofused heterocycles. This photoredox methodology relies on the use of solid sodium trifluoromethanesulfinate (CF_3SO_2Na) as the trifluoromethylating agent and the iridium complex $[Ir\{dF(CF_3)ppy\}_2](dtbpy)]PF_6$ as the photoredox catalyst. A variety of substrates of high interest in drug discovery programs were trifluoromethylated with good to excellent yields. Moreover, bromo, chloro-, and iodo-containing substrates were well tolerated, thus demonstrating the compatibility of our methodology with cross-coupling methods. Process intensification in a microflow reactor afforded reduced reaction times (30 minutes residence time) and high

productivity. This methodology provides mild and easy to handle reaction conditions for the preparation of trifluoromethylated key intermediates in medicinal chemistry programmes.

2.7 Experimental part

General information

The UPLC (Ultra Performance Liquid Chromatography) measurement was performed using an Acquity® IClass UPLC® (Waters) system comprising a sampler organizer, a binary pump with degasser, a column oven, a diode-array detector (DAD), and a column as specified below. The MS detector (Waters, SQD or QTOF) was configured with an ESCI dual ionization source (electrospray combined with atmospheric pressure chemical ionization). Nitrogen was used as the nebulizer gas. The source temperature was maintained at 140 °C. Data acquisition was performed with MassLynx-Openlynx software. For IClass-SQD, reversed phase UPLC was carried out on an RRHD Eclipse Plus-C18 (1.8 µm, 2.1 × 50 mm) from Agilent, with a flow rate of 1.0 mL/min, at 50 °C. The gradient conditions used were: 95% A (0.5 g/L ammonium acetate solution +5% acetonitrile), 5% B (acetonitrile), to 40% A, 60% B in 1.2 min, to 5% A, 95% B in 0.6 min, held for 0.2 min. Injection volume 1.0 µL. Low-resolution ESI mass spectra (single quadrupole, SQD detector) were acquired by scanning from 100 to 1000 in 0.1 s using an interchannel delay of 0.08 s. The capillary needle voltage was 3 kV. The cone voltage was 25 V for positive ionization mode and 30 V for negative ionization mode. For IClass-QTOF, reversed phase UPLC was carried out on a BEH-C18 (1.7 µm, 2.1 × 50 mm) from Waters, with a flow rate of 1.0 mL/min, at 50 °C. The gradient conditions used are: 95% A (0.5 g/L ammonium acetate solution +5% acetonitrile), 5% B (acetonitrile), to 40% A, 60% B in 1.2 min, to 5% A, 95% B in 0.6 min, held for 0.2 min. Injection volume 1.0 µL. High-resolution ESI mass spectra were recorded on a Xevo G2-S QTOF mass spectrometer (Waters) configured with an electrospray ionization source, maintained at 140 °C, using nitrogen as the nebulizer gas, argon as collision gas, and Lockmass device for mass calibration using leucine-enkephalin as standard substance. Spectra were acquired either in positive or in negative ionization mode, by scanning from 50 to 1200 Da in 0.1 s. In positive mode the capillary needle voltage was 0.25 kV and the cone voltage was 25 V. In negative mode the capillary needle voltage was 2.0 kV and the cone voltage was 25 V.

GC measurements were performed using a 6890 Series gas chromatograph (Agilent Technologies) system comprising a 7683 Series injector and auto sampler, J&W HP-5MS column (20 m × 0.18 mm, 0.18 µm) from Agilent Technologies coupled to a 5973N MSD mass selective detector (single quadrupole, Agilent Technologies). The MS detector was configured with an electronic impact ionization source/chemical ionization source (EI/CI). EI low-resolution mass spectra were acquired by scanning from 50 to 550 at a rate of 5.51 scan/s per second. The source temperature was maintained at 230 °C. Helium was used as the nebulizer gas. Data acquisition was performed with Chemstation-Open Action software. TLC was carried out on silica gel 60 F254 plates

(Merck), using reagent grade solvents. Unless otherwise specified, reagents were obtained from commercial sources and used without further purification. The reactions were carried out in a Vapourtec photoreactor UV-150 fixed on an E-series Vapourtec equipment. ^{1}H NMR spectra were recorded on Bruker DPX-400 or Bruker AV-500 spectrometers with standard pulse sequences, operating at 400 MHz and 500 MHz, respectively. Chemical shifts (δ) are reported in parts per million (ppm) downfield from tetramethylsilane (TMS), which was used as an internal standard. ^{13}C NMR spectra were recorded on the same spectrometers operating at 101 MHz and 126 MHz, respectively. ^{19}F NMR spectra were recorded on the Bruker AV-500 spectrometer operating at 471 MHz. All microfluidic fittings were purchased from IDEX Health and Science. The syringes were connected to the capillary using ¼-28 flat-bottom flangeless fittings. A syringe pump (Fusion- 200 Classic) equipped with 5 or 10 mL syringes was used to feed liquid reagents through a high purity perfluoroalkoxyalkane (PFA) capillary tubing (I.D. 0.750 mm) to a Tefzel® tee mixer (I.D. 0.5 mm). The melting points were measured on DSC equipment (Mettler 823 Toledo; method: 30–300 °C, 10 °C/min).

Luminescence quenching studies

All samples used in the luminescence quenching studies were prepared under oxygen free conditions according to the procedure reported by Glorius and co-workers.[110] The quencher $NaSO_2CF_3$ and the photocatalysts to be screened were weighed into vials, dissolved separately in acetonitrile and degassed by freeze-pump-thaw. For each measurement, the appropriate amount of the solution of photocatalyst and quencher were added to a cuvette and diluted to 1 mL with degassed acetonitrile. We conducted our investigation with a photocatalyst concentration of 10 µM. The structures of the photocatalysts employed in this study are represented in Figure 2.7.

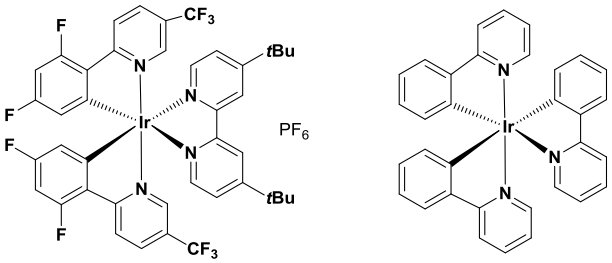

$(Ir[dF(CF_3)ppy]_2(dtbpy))PF_6$
Photocatalyst (1)

fac-$Ir(ppy)_3$
Photocatalyst (2)

Figure 2.7: Structures of the photocatalyst screened for the luminescence quenching experiments

The luminescence emission spectrum of each photocatalyst was measured multiple times (three different samples were prepared and measured each twice) and an average

was taken as the standard reference spectrum. Solutions of increasing concentrations of quencher (CF_3SO_2Na) were prepared in acetonitrile and tested. The concentrations employed are the following:

- 25 mM, corresponding to 2500 equivalents of quencher relative to the photocatalyst;
- 50 mM, corresponding to 5000 equivalents of quencher relative to the photocatalyst;
- 100 mM, corresponding to 10000 equivalents of quencher relative to the photocatalyst.
- 300 mM, corresponding to 30000 equivalents of quencher relative to the photocatalyst.

As depicted below, the luminescence of both photocatalysts was quenched by increasing equivalents of CF_3SO_2Na. However, a quenching percentage of 58% was obtained for $[Ir\{dF(CF_3)ppy_2\](dtbpy)]PF_6$ (1) in presence of 300 eq of Langlois reagent, while 2500 eq were necessary to observe a quenching percentage of 44% for fac-$Ir(ppy)_3$ (2). Therefore, we selected $[Ir\{dF(CF_3)ppy\}_2](dtbpy)]PF_6$ (1) as the best photocatalyst for our reaction. Moreover, after further optimization in continuous flow of the reaction protocol, we further analyzed the quenching efficiency of $[Ir\{dF(CF_3)ppy\}_2](dtbpy)]PF_6$ (1) in the reaction conditions. Specifically, a 10µM solution of $[Ir\{dF(CF_3)ppy\}_2](dtbpy)]PF_6$ was quenched with a 0.3 mM solution of Langlois. This concentration of quencher corresponds to 300 equivalents compared to the photocatalyst and reflects the ratio used in the optimized reaction conditions. The results obtained are represented in Figure 2.8 (purple line).

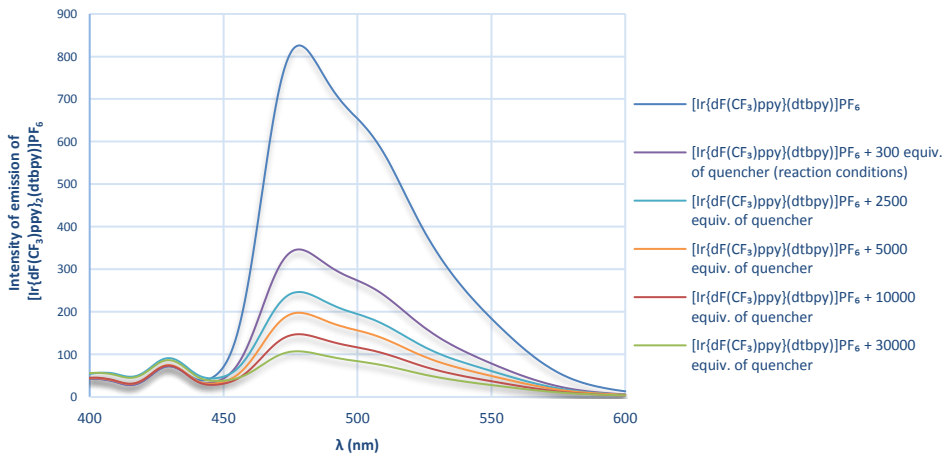

Figure 2.8: Luminescence quenching of Photocatalyst 1

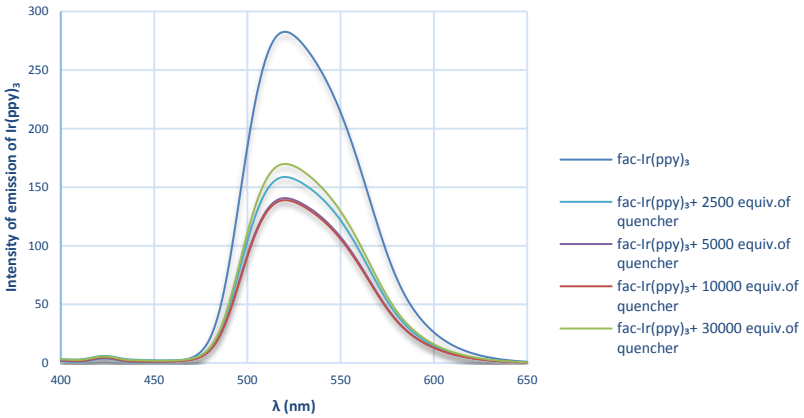

Figure 2.9: Luminescence quenching of Photocatalyst 2

Trifluoromethylation general procedure:

In an oven-dried vial equipped with a magnetic stirrer and a PTFE septum, $[Ir\{dF(CF_3)ppy\}_2](dtbpy)]PF_6$ (5.6 mg, 1 mol%) was added to a mixture of the substrate (0.5 mmol, 1 equiv), CF_3SO_2Na (1.5 mmol, 3 equiv), and $(NH_4)_2S_2O_8$ (0.5 mmol, 1 equiv) in DMSO (5 mL). The solution was pumped into the Vapourtec photoreactor (FEP tube, 0.75 mm I.D., 10 mL) and the liquid flowrate was set at 0.33 mL/min (30 min residence time). The reactor was irradiated with 54 blue LEDs (450 nm, total power 24 W). The reaction mixture collected from the outlet was diluted with H_2O and extracted with Et_2O (3×). The combined organic layers were washed with brine, dried over $MgSO_4$, and concentrated in vacuo. The crude was then pre-adsorbed onto silica, dried in vacuo, and purified by flash chromatography to yield the trifluoromethylated product.

Product's characterization

*1,3,7-Trimethyl-8-(trifluoromethyl)-7H-purine-2,6-dione (**3**)* [13a]

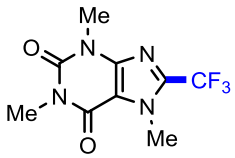

3

The product was prepared according to the general procedure and was purified by flash chromatography (silica gel, Heptane/Ethyl acetate, 75/25); this afforded the desired product as a white solid. Yield: 59 mg (45%).

^{1}H NMR (500 MHz, $CDCl_3$): δ = 4.14–4.19 (m, 3 H), 3.60 (s, 3 H), 3.42 (s, 3 H).
^{13}C NMR (101 MHz, $CDCl_3$): δ = 155.5, 151.3, 146.5, 138.9, 119.5, 109.6, 33.2, 29.9, 28.2.
^{19}F NMR (471 MHz, $CDCl_3$): δ = –62.37 (s).
HRMS (ESI): m/z $[M + H]^+$ calcd for $C_9H_9F_3N_4O_2$: 263.0749; found: 263.0742.
Melting point: 130.9 °C.

*3-Methyl-2-(trifluoromethyl)-1H-indole (**4**)*[24]

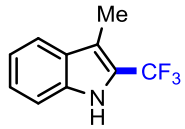

4

The product was prepared according to the general procedure and was purified by flash chromatography (silica gel, Heptane:Ethyl acetate, 80:20); this afforded the desired product as a white amorphous solid. Yield: 61.8 mg (62%).

^{1}H NMR (400 MHz, $CDCl_3$): δ = 8.18 (br s, 1 H), 7.64 (d, J = 8.1 Hz, 1 H), 7.37–7.41 (m, 1 H), 7.29–7.35 (m, 1 H), 7.15–7.23 (m, 1 H), 2.45 (q, J = 1.8 Hz, 3 H).
^{13}C NMR (101 MHz, $CDCl_3$): δ = 135.2, 128.1, 124.8, 124.6, 121.6, 122.2, 120.1, 114.1, 8.4.
^{19}F NMR (471 MHz, $CDCl_3$): δ = –58.65 (s).
HRMS (ESI): m/z $[M + H]^+$ calcd for $C_{10}H_8F_3N$: 200.0680; found: 200.0683.

*2-Methyl-3-(trifluoromethyl)-1H-indole (**5**)*[11f]

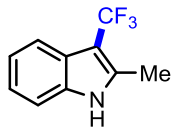

5

The product was prepared according to the general procedure and was purified by flash chromatography (silica gel, Heptane:Ethyl acetate, 80:20); this afforded the desired product as a white solid. Yield: 68.7 mg (69%).

^{1}H NMR (500 MHz, $CDCl_3$): δ = 8.18 (br s, 1 H), 7.67 (br d, J = 7.5 Hz, 1 H), 7.24–7.32 (m, 1 H), 7.09–7.22 (m, 2 H), 2.49 (s, 3 H).
^{13}C NMR (101 MHz, $CDCl_3$): δ = 133.9, 121.8, 121.3, 120.2, 119.1, 117.3, 113.7, 110.7, 99.3, 12.4.
^{19}F NMR (471 MHz, $CDCl_3$): δ = –54.63 (s).
HRMS (ESI): m/z $[M + H]^+$ calcd for $C_{10}H_8F_3N$: 200.0680; found: 200.0686.
Melting point: 147.5 °C.

*5-Iodo-3-(trifluoromethyl)-1H-indole (**6**)*

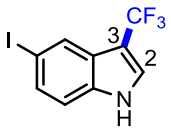

6

The product was prepared according to the general procedure and was purified by flash chromatography (silica gel, Heptane:Ethyl acetate, 90:10); this afforded the desired product as a transparent oil. Yield: 39 mg (25%).

^{1}H NMR (400 MHz, $CDCl_3$): δ = 8.47 (br s, 1 H), 8.10 (s, 1 H), 7.56 (dd, J = 8.6, 1.6 Hz, 1 H), 7.51 (dd, J = 2.7, 1.3 Hz, 1 H), 7.23 (s, 1 H).
^{13}C NMR (101 MHz, $CDCl_3$): δ = 138.0, 134.9, 132.2, 128.4, 125.1, 125.0, 124.2, 113.5, 85.2.
^{19}F NMR (471 MHz, $CDCl_3$): δ = –57.37 (s).
HRMS (ESI): m/z $[M – H]^-$ calcd for $C_9H_5F_3IN$: 309.9345; found: 309.9368.

*5-Iodo-2-(trifluoromethyl)-1H-indole (**7**)*

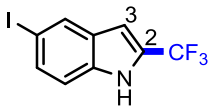

7

The product was prepared according to the general procedure and was purified by flash chromatography (silica gel, Heptane:Ethyl acetate, 80:20); this afforded the desired product as a transparent oil. Yield: 39 mg (25%).

^{1}H NMR (500 MHz, $CDCl_3$): δ = 8.52 (br s, 1 H), 8.03 (s, 1 H), 7.58 (d, J = 10.4 Hz, 1 H), 7.22 (d, J = 8.4 Hz, 1 H), 6.85 (s, 1 H).
^{13}C NMR (101 MHz, $CDCl_3$): δ = 135.2, 133.2, 130.9, 129.1, 126.7, 126.4, 121.9, 113.7, 103.4, 84.5.

^{19}F NMR (471 MHz, $CDCl_3$): δ = –60.73 (s).
HRMS (ESI): m/z [M – H]$^-$ calcd for $C_9H_5F_3IN$: 309.9345; found: 309.9368.

*4-(Trifluoromethyl)benzimidazole (**8**)*[19]

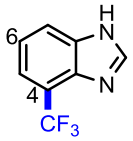

8

The product was prepared according to the general procedure and was purified by flash chromatography (silica gel, Heptane:Ethyl acetate, 80:20); this afforded the desired product as a white amorphous solid. Yield: 27 mg (29%).

^{1}H NMR (500 MHz, CD_3OD): δ = 8.20 (s, 1 H), 7.63–7.88 (br s, 1 H), 7.48 (br d, J = 7.2 Hz, 1 H), 7.31 (t, J = 7.8 Hz, 1 H).
^{13}C NMR (126 MHz, CD_3OD): δ = 164.1, 143.0, 133.2, 125.2, 123.1, 100.0, 99.8.
^{19}F NMR (471 MHz, CD_3OD): δ = –64.21 (s).
HRMS (ESI): m/z [M – H]$^-$ calcd for $C_8H_5F_3N_2$: 185.0331; found: 185.0337.

*6-(Trifluoromethyl) benzimidazole (**9**)*

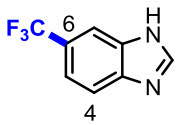

9

The product was prepared according to the general procedure and was purified by flash chromatography (silica gel, Heptane:Ethyl acetate, 80:20); this afforded the desired product as a yellow oil. Yield: 19 mg (20%).

^{1}H NMR (400 MHz, $CDCl_3$): δ = 8.25 (s, 1 H), 7.99 (s, 1 H), 7.74 (d, J = 8.6 Hz, 1 H), 7.57 (d, J = 8.6 Hz, 1 H).
^{13}C NMR (101 MHz, $CDCl_3$): δ = 142.6, 128.7, 126.0, 125.7, 125.4, 123.3, 120.1.
^{19}F NMR (471 MHz, $CDCl_3$): δ = –62.20 (s).
HRMS (ESI): m/z [M – H]$^-$ calcd for $C_8H_5F_3N_2$: 185.0331; found: 185.0337.

*2-Bromo-4-(trifluoromethyl) benzimidazole (**10**)*

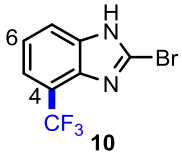

10

The product was prepared according to the general procedure and was purified by flash chromatography (silica gel, Heptane: Ethyl acetate, in gradient from 100/0 to 50:50); this afforded the desired product as a white solid. Yield: 40.2 mg (30%)

^{1}H NMR (400 MHz, CD_3OD): δ = 7.85 (s, 1 H), 7.68 (d, J = 8.6 Hz, 1 H), 7.55 (d, J = 8.6 Hz, 1 H).
^{13}C NMR (101 MHz, CD_3OD): δ = 140.8, 131.2, 130.1, 126.2, 122.2, 120.8, 115.7, 113.7.
^{19}F NMR (471 MHz, CD_3OD): δ = –62.40 (s).
HRMS (ESI): m/z $[M - H]^-$ calcd for $C_8H_4BrF_3N_2$: 262.9436; found: 262.9434.
Melting point: 214.7 °C.

*2-Bromo-6-(trifluoromethyl)-1H-benzimidazole (**11**)*

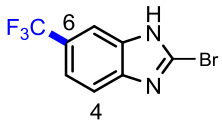

11

The product was prepared according to the general procedure and was purified by flash chromatography (silica gel, Heptane:Ethyl acetate, gradient 100:0 to 50:50); this afforded the desired product as a white solid. Yield: 26.7 mg (20%);

^{1}H NMR (400 MHz, $CDCl_3$): δ = 8.25 (s, 1 H), 7.99 (s, 1 H), 7.74 (d, J = 8.6 Hz, 1 H), 7.57 (d, J = 8.6 Hz, 1 H).
^{13}C NMR (101 MHz, $CDCl_3$): δ = 142.6, 128.7, 126.0, 125.7, 125.4, 123.3, 120.1.
^{19}F NMR (471 MHz, $CDCl_3$): δ = –62.20 (s).
HRMS (ESI): m/z $[M - H]^-$ calcd for $C_8H_4BrF_3N_2$: 262.9436; found: 262.9434.
Melting point: 216.7 °C.

*5-Chloro-2-methyl-7-(trifluoromethyl)-1H-benzimidazole (**12**)*

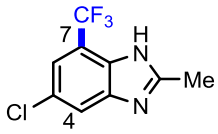

12

The product was prepared according to the general procedure and was purified by flash chromatography (silica gel, heptane–Ethyl acetate, 80:20); this afforded the desired product as a white amorphous solid. Yield: 23.8 mg (20%).

^{1}H NMR (400 MHz, $CDCl_3$): δ = 9.48 (br s, 1 H), 7.82 (br s, 1 H), 7.47 (s, 1 H), 2.68 (s, 3 H).
^{13}C NMR (101 MHz, CD_3OD): δ = 157.3, 128.1, 126.1, 123.4, 120.7, 105.2, 14.3.
^{19}F NMR (471 MHz, CD_3OD): δ = –62.87 (s).
HRMS (ESI): m/z $[M - H]^-$ calcd for $C_9H_6ClF_3N_2$: 233.0098; found: 233.0108.

*5-Chloro-2-methyl-4-(trifluoromethyl)-1H-benzimidazole (**13**)*

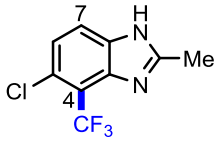

13

The product was prepared according to the general procedure and was purified by flash chromatography (silica gel, Heptane:Ethyl acetate, 80:20); this afforded the desired product as a white amorphous solid. Yield: 35.2 mg (30%).

^{1}H NMR (500 MHz, $CDCl_3$): δ = 9.50 (br s, 1 H), 7.74 (d, J = 8.4 Hz, 1 H), 7.34 (d, J = 8.4 Hz, 1 H), 2.66 (s, 3 H).
^{13}C NMR (126 MHz, $CDCl_3$): δ = 153.3, 143.5, 131.9, 127.0, 125.1, 122.9, 15.3.
^{19}F NMR (471 MHz, $CDCl_3$): δ = –57.09 (s).
HRMS (ESI): m/z $[M - H]^-$ calcd for $C_9H_6ClF_3N_2$: 233.0098; found: 233.0108.

*5-(Trifluoromethyl) pyrimidin-4(3H)-one (**14**)*

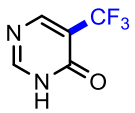

14

The product was prepared according to the general procedure, after which the solvent was evaporated in a Genevac turboevaporator overnight. The rests were taken up with CH_2Cl_2 and the solvent was evaporated; the product was purified by flash chromatography (silica gel, MeOH–NH_4OH, 9:1/CH_2Cl_2, 0–10%); this afforded the desired product as a yellow oil. Yield: 65.9 mg (80%).

^{1}H NMR (400 MHz, DMSO-d_6): δ = 8.44 (s, 1 H), 8.40 (s, 1 H)
^{13}C NMR (126 MHz, $CDCl_3$): δ = 154.7, 152.1, 129.7, 121.9
^{19}F NMR (471 MHz, $CDCl_3$): δ = –65.35 (s).
HRMS (ESI): m/z [M – H]$^-$ calcd for $C_5H_3F_3N_2O$: 163.0124; found: 163.0129.

*5-Bromo-3-(trifluoromethyl)-1H-pyridin-2-one (**15**)*[25]

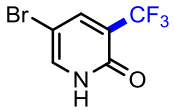

15

The product was prepared according to the general procedure and was purified by flash chromatography (silica gel, Heptane: Ethyl acetate, 50:50); this afforded the desired product as a yellow solid. Yield: 72.6 mg (60%).

^{1}H NMR (500 MHz, $CDCl_3$): δ = 12.52–14.24 (m, 1 H), 7.92 (d, J = 2.0 Hz, 1 H), 7.76 (d, J = 2.3 Hz, 1 H).
^{13}C NMR (126 MHz, $CDCl_3$): δ = 160.0, 143.8, 139.4, 121.5, 121.9, 97.7.
^{19}F NMR (471 MHz, $CDCl_3$): δ = –65.98.
HRMS (ESI): m/z [M – H]$^-$ calcd for $C_6H_3BrF_3NO$: 239.9277; found: 239.9272.
Melting point: 213.3 °C.

*2,4,6-Trimethoxy-5-(trifluoromethyl)pyrimidine (**16**)*

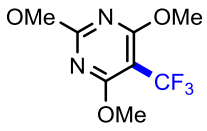

16

The product was prepared according to the general procedure and was purified by flash chromatography (silica gel, Heptane:Ethyl acetate, 80:20); this afforded the desired product as a pink solid. Yield: 71.4 mg (60%).

^{1}H NMR (500 MHz, $CDCl_3$): δ = 4.03 (s, 6 H), 4.01 (s, 3 H).
^{13}C NMR (101 MHz, $CDCl_3$): δ = 169.8, 165.0, 123.5, 89.3, 55.1, 55.0.
^{19}F NMR (471 MHz, $CDCl_3$): δ = –55.97 (s).
Melting point: 123.6 °C.

*4-Methoxy-3-(trifluoromethyl) pyridin-2-amine (**17**)*

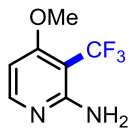

17

The product was prepared according to the general procedure and was purified by flash chromatography (silica gel, Heptane: Ethyl acetate, 40:60); this afforded the desired product as a yellow solid. Yield: 38.5 mg (40%).

^{1}H NMR (400 MHz, $CDCl_3$): δ = 8.07 (d, J = 5.8 Hz, 1 H), 6.31 (dd, J = 5.9, 0.8 Hz, 1 H), 5.00–5.20 (m, 2 H), 3.88 (s, 3 H).
^{13}C NMR (101 MHz, $CDCl_3$): δ = 166.3, 156.6, 152.8, 124.9, 98.3, 56.1.
^{19}F NMR (471 MHz, $CDCl_3$): δ = –55.42 (s).
HRMS (ESI): m/z $[M - H]^-$ calcd for $C_7H_7F_3N_2O$: 191.0437; found: 191.0423.
Melting point: 213.4 °C.

*2-Iodo-3-methoxy-5-(trifluoromethyl) pyridine (**18**)*[10b]

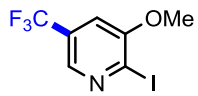

18

The product was prepared according to the general procedure and was purified by flash chromatography (silica gel, Pentane: Diethyl ether, 90:10); this afforded the desired product as a transparent oil. Yield: 52.9 mg (35%).

^{1}H NMR (400 MHz, $CDCl_3$): δ = 7.59 (d, J = 8.6 Hz, 1 H), 7.05 (d, J = 8.6 Hz, 1 H), 3.98 (s, 3 H).
^{13}C NMR (101 MHz, $CDCl_3$): δ = 157.4, 140.4, 134.2, 121.0, 116.1, 111.7, 56.7.
^{19}F NMR (471 MHz, $CDCl_3$): δ = –66.70.
HRMS (ESI): m/z $[M + H]^+$ calcd for $C_7H_5F_3INO$: 303.9488; found: 303.9492.

*2,5-Dimethyl-3-(trifluoromethyl) pyrazine (**19**)*

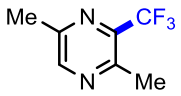

19

The product was prepared according to the general procedure. The organic layer was evaporated and the crude was analyzed by LC-MS; yield: 53%.

LC-MS: R_T= 0.90; 53%.

*3-[4-(Trifluoromethyl) phenyl]-1H-pyrazole (**20**)*

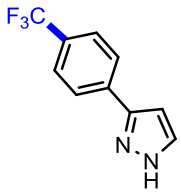

20

The product was prepared according to the general procedure and was purified by flash chromatography (silica gel, Heptane: Ethyl acetate, 40:60); this afforded the desired product as a transparent oil. Yield: 29.7 mg (28%).

^{1}H NMR (400 MHz, $CDCl_3$): δ = 7.90 (d, J = 8.1 Hz, 2 H), 7.65–7.70 (m, 1 H), 7.62–7.74 (m, 2 H), 6.70 (d, J = 2.3 Hz, 1 H).
^{13}C NMR (101 MHz, $CDCl_3$): δ = 136.0, 131.8, 129.5, 129.0, 128.8, 126.0, 125.7, 124.6, 122.6, 103.3.
^{19}F NMR (471 MHz, $CDCl_3$): δ = –62.58 (s).
HRMS (ESI): m/z $[M - H]^-$ calcd for $C_{10}H_7F_3N_2$: 211.0488; found: 211.0486.

*1-Tetrahydropyran-4-yl-5-(trifluoromethyl) pyrazol-4-amine (**21**)*

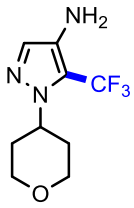

21

The product was prepared according to the general procedure and was purified by flash chromatography (silica gel, Heptane: Ethyl acetate, 50:50); this afforded the desired product as a dark yellow oil. Yield: 52.9 mg (45%).

^{1}H NMR (400 MHz, $CDCl_3$): δ = 7.16 (s, 1 H), 4.24 (tt, J = 11.5, 4.0 Hz, 1 H), 4.10 (dd, J = 11.8, 4.6 Hz, 2 H), 3.50 (td, J = 12.2, 2.0 Hz, 2 H), 3.28–3.42 (m, 2 H), 2.26 (qd, J = 12.4, 4.6 Hz, 2 H), 1.78–1.92 (m, 2 H).
^{13}C NMR (101 MHz, $CDCl_3$): δ = 130.8, 130.0, 121.8, 114.9, 67.1, 57.0, 32.9.
^{19}F NMR (471 MHz, $CDCl_3$): δ = –56.70 (s).
HRMS (ESI): m/z $[M - H]^-$ calcd for $C_9H_{12}F_3N_3O$: 234.2859; found: 234.2855.

*3-Bromo-2,6-dimethyl-5-(trifluoromethyl) pyridine (**22**)*

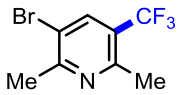

22

The product was prepared according to the general procedure. The organic layer was evaporated and the crude was analyzed by LC-MS; yield: 38%.

^{1}H NMR (400 MHz, $CDCl_3$): δ = 7.97 (s, 1 H), 2.68 (s, 3 H), 2.62–2.64 (m, 3 H).
^{19}F NMR (471 MHz, $CDCl_3$): δ = –62.23.

*1,3,5-Trimethyl-2-(trifluoromethyl) benzene (**23**)*

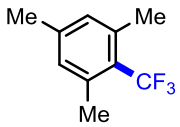

23

The product was prepared according to the general procedure. The organic layer was evaporated and the crude was analyzed by LC-MS and GCMS; yield: 53%.

LC-MS: R_T= 1.61; 30%.
GC-MS: R_T= 2.54; mass found: 188.0.

*2-Iodo-1,3,5-trimethyl-4-(trifluoromethyl) benzene (**24**)*

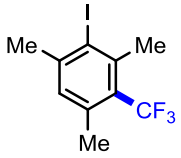

24

The product was prepared according to the general procedure. The organic layer was evaporated and the crude was analyzed by LC-MS; yield: 80%.

LC-MS: R_T= 1.81; 65%.
GC-MS: R_T= 3.53; mass found: 313.9.

Bibliography

[1] (a) Müller, K.; Faeh, C.; Diederich, F. Fluorine in Pharmaceuticals: Looking beyond Intuition. *Science*. **2007**,*317* (5846), 1881-1886; (b) Hagmann, W. K. The Many Roles for Fluorine in Medicinal Chemistry. *J. Med. Chem*., **2008**, *51* (15), 4359–4369; (c) Swallow, S. Fluorine in Medicinal Chemistry. *Prog. Med. Chem.* **2015**, *54*, 65–133.

[2] G. K. S. Prakash, F. W. Fluorine: the new kingpin of drug discovery. *Chim. Oggi* **2012**, *30*, 30–36.

[3] (a) Ortiz de Montellano, P. R. Cytochrome P450: Structure, mechanism, and biochemistry. **2015**, Cham: Springer; (b) Pauling, L. The Nature of the Chemical Bond. IV. The Energy of Single Bonds and the Relative Electronegativity of Atoms. *J. Am. Chem. Soc.* **1932**, *54* (9), 3570–3582.

[4] (a) Zhou, Y.; Wang, J.; Gu, Z.; Wang, S.; Zhu, W.; Acenã, J. L.; Soloshonok, V. A.; Izawa, K.; Liu, H. Next Generation of Fluorine-Containing Pharmaceuticals, Compounds Currently in Phase II-III Clinical Trials of Major Pharmaceutical Companies: New Structural Trends and Therapeutic Areas. *Chem. Rev*. **2016**, *116* (2), 422–518; (b) Gutekunst, W. R.; Baran, P. S. C-H Functionalisation in Organic Synthesis. *Chem. Soc. Rev.* **2011**, *40* (4), 1976–199; (c) Champagne, P. A.; Desroches, J.; Hamel, J. D.; Vandamme, M.; Paquin, J. F. Monofluorination of Organic Compounds: 10 Years of Innovation. *Chem. Rev*. **2015**, *115* (17), 9073–9174.

[5] Stuart B. Rosenblum*, Tram Huynh, Adriano Afonso, Harry R. Davis, Nathan Yumibe, John W. Clader, and D. A. B. Discovery of 1-(4-Fluorophenyl)-(3R)-[3-(4-Fluorophenyl)-(3S)-Hydroxypropyl]-(4S)-(4-Hydroxyphenyl)-2-Azetidinone (SCH 58235): A Designed, Potent, Orally Active Inhibitor of Cholesterol Absorption. *J. Med. Chem.* **1998**, *41* (6), 973–980.

[6] Cavallo, G.; Metrangolo, P.; Milani, R.; Pilati, T.; Priimagi, A.; Resnati, G.; Terraneo, G. The Halogen Bond. *Chem. Rev*. **2016**, *116* (4), 2478–2601.

[7] Van Niel, M. B.; Collins, I.; Beer, M. S.; Broughton, H. B.; Cheng, S. K. F.; Goodacre, S. C.; Heald, A.; Locker, K. L.; MacLeod, A. M.; Morrison, D.; et al. Fluorination of 3-(3-(Piperidin-1-Yl)propyl)indoles and 3-(3-(Piperazin- 1-Yl)propyl)indoles Gives Selective Human 5-HT(1D) Receptor Ligands with Improved Pharmacokinetic Profiles. *J. Med. Chem.* **1999**, *42* (12), 2087–2104.

[8] (a) Gillis, E. P.; Eastman, K. J.; Hill, M. D.; Donnelly, D. J.; Meanwell, N. A. Applications of Fluorine in Medicinal Chemistry. *J. Med. Chem.* **2015**, *58* (21), 8315–8359; (b) Smart, B. E. Fluorine Substituent Effects (on Bioactivity). *J. Fluor. Chem*. **2001**, 109, 3–11; (c) Huchet, Q. A.; Kuhn, B.; Wagner, B.; Fischer, H.; Kansy, M.; Zimmerli, D.; Carreira, E. M.; Müller, K. On the Polarity of Partially Fluorinated Methyl Groups. *J. Fluor. Chem.* **2013**, *152*, 119–128.

[9] Yerien, D. E.; Bonesi, S.; Postigo, A. Fluorination Methods in Drug Discovery. *Org. Biomol. Chem.* **2016**, *14* (36), 8398–8427.

[10] (a) Barata-Vallejo, S.; Postigo, A. (Me3Si)3SiH-Mediated Intermolecular Radical Perfluoroalkylation Reactions of Olefins in Water. *J. Org. Chem.* **2010**, *75* (18), 6141–6148; (b) Huiban, M.; Tredwell, M.; Mizuta, S.; Wan, Z.; Zhang, X.; Collier, T. L.; Gouverneur, V.; Passchier, J. A Broadly Applicable [18F] Trifluoromethylation of Aryl and Heteroaryl Iodides for PET Imaging. *Nat. Chem.* **2013**, *5* (11), 941–944; (c) Tomashenko, O. A.; Grushin, V. V. Aromatic Trifluoromethylation with Metal Complexes. *Chem. Rev*. **2011**,*111* (8) pp 4475–4521

[11] (a) Straathof, N. J. W.; Cramer, S. E.; Hessel, V.; Noël, T. Practical Photocatalytic Trifluoromethylation and Hydrotrifluoromethylation of Styrenes in Batch and Flow. *Angew.*

Chem. Int. Ed. **2016**, *55* (50), 15549–15553; (b) Bottecchia, C.; Wei, X. J.; Kuijpers, K. P. L.; Hessel, V.; Noël, T. Visible Light-Induced Trifluoromethylation and Perfluoroalkylation of Cysteine Residues in Batch and Continuous Flow. *J. Org. Chem.* **2016**, *81* (16), 7301–7307; (c) Lefebvre, Q.; Hoffmann, N.; Rueping, M. Photoorganocatalysed and Visible Light Photoredox Catalysed Trifluoromethylation of Olefins and (Hetero)aromatics in Batch and Continuous Flow. *Chem. Commun.* **2016**, *52* (12), 2493–2496; (d) Chatterjee, T.; Iqbal, N.; You, Y.; Cho, E. J. Controlled Fluoroalkylation Reactions by Visible-Light Photoredox Catalysis. *Acc. Chem. Res.* **2016**, *49* (10), 2284–2294; (e) Beatty, J. W.; Douglas, J. J.; Cole, K. P.; Stephenson, C. R. J. A Scalable and Operationally Simple Radical Trifluoromethylation. *Nat. Commun.* **2015**, *10* (6), 7919; (f) Straathof, N. J. W.; Gemoets, H. P. L.; Wang, X.; Schouten, J. C.; Hessel, V.; Noël, T. Rapid Trifluoromethylation and Perfluoroalkylation of Five-Membered Heterocycles by Photoredox Catalysis in Continuous Flow. *ChemSusChem* **2014**, *7* (6), 1612–1617; (g) Prier, C. K.; Rankic, D. A.; MacMillan, D. W. C. Visible Light Photoredox Catalysis with Transition Metal Complexes: Applications in Organic Synthesis. *Chem. Rev.* **2013**, *113* (7), 5322–5363; (h) Nagib, D. A.; Macmillan, D. W. C. Trifluoromethylation of Arenes and Heteroarenes by Means of Photoredox Catalysis. *Nature* **2011**, *480* (7376), 224–228; (i) Cui, L.; Matusaki, Y.; Tada, N.; Miura, T.; Uno, B.; Itoh, A. Metal-Free Direct C-H Perfluoroalkylation of Arenes and Heteroarenes Using a Photoredox Organocatalyst. *Adv. Synth. Catal.* **2013**, *355* (11–12), 2203–2207; (j) Iqbal, N.; Choi, S.; Kim, E.; Cho, E. J. Trifluoromethylation of Alkenes by Visible Light Photoredox Catalysis. *J. Org. Chem.* **2012**, *77* (24), 11383–11387.

[12] (a) Pan, X.; Xia, H.; Wu, J. Recent Advances in Photoinduced Trifluoromethylation and Difluoroalkylation. *Org. Chem. Front.* **2016**, *3* (9), 1163–1185; (b) Barata-Vallejo, S.; Lantano, B.; Postigo, A. Recent Advances in Trifluoromethylation Reactions with Electrophilic Trifluoromethylating Reagents. *Chem. Eur. J.* **2014**, *20* (51), 16806–16829.

[13] (a) Ji, Y.; Brueckl, T.; Baxter, R. D.; Fujiwara, Y.; Seiple, I. B.; Su, S.; Blackmond, D. G.; Baran, P. S. Innate C-H Trifluoromethylation of Heterocycles. *Proc. Natl. Acad. Sci. U. S. A.* **2011**, *108* (35), 14411–14415; (b) Wang, D.; Deng, G.-J.; Chen, S.; Gong, H. Catalyst-Free Direct C–H Trifluoromethylation of Arenes in Water–acetonitrile. *Green Chem.* **2016**, *18* (22), 5967–5970; (c) Langlois, B. R.; Billard, T.; Mulatier, J. C.; Yezeguelian, C. A New Preparation of Trifluoromethanesulfinate Salts. *J. Fluor. Chem.* **2007**, *128* (7), 851–856; (d) Langlois, B. R.; Billard, T.; Mulatier, J. C.; Yezeguelian, C. A New Preparation of Trifluoromethanesulfinate Salts. *J. Fluor. Chem.* **2007**, *128* (7), 851–856; (d) Tordeux, M.; Langlois, B.; Wakselman, C. Reactions of Bromotrifluoromethane and Related Halides. 8. Condensations with Dithionite and Hydroxymethanesulfinate Salts. *J. Org. Chem.* **1989**, *54* (10), 2452–2453; (f) Lefebvre, Q. Toward Sustainable Trifluoromethylation Reactions: Sodium Triflinate under the Spotlight. *Synlett* **2017**, *28* (1), 19–23.

[14] (a) Huck, L.; Berton, M.; de la Hoz, A.; Díaz-Ortiz, A.; Alcázar, J. Reformatsky and Blaise Reactions in Flow as a Tool for Drug Discovery. One Pot Diversity Oriented Synthesis of Valuable Intermediates and Heterocycles. *Green Chem.* **2017**, *19* (6), 1420–1424; (b) Wirth, T. Flow Chemistry: Enabling Technology in Drug Discovery and Process Research. *ChemSusChem*. **2012**, *5*, 215–216; (c) Galloway, W. R. J. D.; Isidro-Llobet, A.; Spring, D. R. Diversity-Oriented Synthesis as a Tool for the Discovery of Novel Biologically Active Small Molecules. *Nat. Comm*. **2010**, *1*, 80.

[15] (a) Hopkinson, M. N.; Gómez-Suárez, A.; Teders, M.; Sahoo, B.; Glorius, F. Accelerated Discovery in Photocatalysis Using a Mechanism-Based Screening Method. *Angew. Chem. Int.*

Ed. **2016**, *55* (13), 4361–4366; (b) Teders, M.; Gómez-Suárez, A.; Pitzer, L.; Hopkinson, M. N.; Glorius, F. Diverse Visible-Light-Promoted Functionalizations of Benzotriazoles Inspired by Mechanism-Based Luminescence Screening. *Angew. Chem. Int. Ed.* **2017**, *56* (3), 902–906; (c) Demissie, T. B.; Hansen, J. H. Synergy between Experimental and Computational Approaches to Homogeneous Photoredox Catalysis. *Dalt. Trans.* **2016**, *45* (27), 10878–10882.

[16] Teegardin, K.; Day, J. I.; Chan, J.; Weaver, J. Advances in Photocatalysis: A Microreview of Visible Light Mediated Ruthenium and Iridium Catalyzed Organic Transformations. *Org. Process Res. Dev.,* **2016***, 20* (7), 1156–1163.

[17] Cambié, D.; Bottecchia, C.; Straathof, N. J. W.; Hessel, V.; Noël, T. Applications of Continuous-Flow Photochemistry in Organic Synthesis, Material Science, and Water Treatment. *Chem. Rev*. **2016**, 117, 10276–10341.

[18] (a) Brown, D. G.; Boström, J. Analysis of Past and Present Synthetic Methodologies on Medicinal Chemistry: Where Have All the New Reactions Gone? *J. Med. Chem.* **2016**, *59* (10), 4443–4458; (b) Alonso, N.; Juan de, M. M.; Egle, B.; Vrijdag, J. L.; De Borggraeve, W. M.; de la Hoz, A.; Díaz-Ortiz, A.; Alcázar, J. First Example of a Continuous-Flow Carbonylation Reaction Using Aryl Formates as CO Precursors. *J. Flow Chem.* **2014**, *4* (3), 105–109; (c) Alonso, N.; Miller, L. Z.; De M. Muñoz, J.; Alcázar, J.; McQuade, D. T. Continuous Synthesis of Organozinc Halides Coupled to Negishi Reactions. *Adv. Synth. Catal.* **2014**, *356* (18), 3737–3741; (d) De M. Muñoz, J.; Alcázar, J.; De La Hoz, A.; Díaz-Ortiz, A. Cross-Coupling in Flow Using Supported Catalysts: Mild, Clean, Efficient and Sustainable Suzuki-Miyaura Coupling in a Single Pass. *Adv. Synth. Catal.* **2012**, *354* (18), 3456–3460; (e) Noël, T.; Musacchio, A. J. Suzuki-Miyaura Cross-Coupling of Heteroaryl Halides and Arylboronic Acids in Continuous Flow. *Org. Lett.* **2011**, *13* (19), 5180–5183; (f) Cooper, T. W. J.; Campbell, I. B.; MacDonald, S. J. F. Factors Determining the Selection of Organic Reactions by Medicinal Chemists and the Use of These Reactions in Arrays (Small Focused Libraries). *Angew. Chem. Inter. Ed.* **2010**, 49 (44), 8082–8091.

[19] Gao, G.-L.; Yang, C.; Xia, W.; Usachev, B. I.; Meanwell, N. A.; Daniels, S.; Tohid, S. F. M.; Velanguparackel, W.; Westwell, A. D.; Filler, R.; et al. Selective C–H Trifluoromethylation of Benzimidazoles through Photoredox Catalysis. *Chem. Commun.* **2017**, *53* (6), 118–1044.

[20] Linghu, X.; Wong, N.; Jost, V.; Fantasia, S.; Sowell, C. G.; Gosselin, F. Kumada-Corriu Heteroaryl Cross-Coupling for Synthesis of a Pharmaceutical Intermediate: Comparison of Batch Versus Continuous Reaction Modes. *Org. Process Res. Dev.* **2017**, *21* (9), 1320–1325.

[21] Li, L.; Mu, X.; Liu, W.; Wang, Y.; Mi, Z.; Li, C. J. Simple and Clean Photoinduced Aromatic Trifluoromethylation Reaction. *J. Am. Chem. Soc.* **2016**, *138* (18), 5809–5812.

[22] (a) Tucker, J. W.; Zhang, Y.; Jamison, T. F.; Stephenson, C. R. J. Visible-Light Photoredox Catalysis in Flow. *Angew. Chem. Int. Ed.* **2012**, *51* (17), 4144–4147; (b) Elliott, L. D.; Knowles, J. P.; Koovits, P. J.; Maskill, K. G.; Ralph, M. J.; Lejeune, G.; Edwards, L. J.; Robinson, R. I.; Clemens, I. R.; Cox, B.; et al. Batch versus Flow Photochemistry: A Revealing Comparison of Yield and Productivity. *Chem. Eur. J.* **2014**, *20* (46), 15226–15232; (c) Knowles, J. P.; Elliott, L. D.; Booker-Milburn, K. I. Flow Photochemistry: Old Light through New Windows. *Beilstein, J. Org. Chem.* **2012***, 8,* 2025–2052*;* (d) Noël, T. Photochemical processes in continuous-flow reactors: From engineering principles to chemical applications. **2017**, New Jersey: World Scientific.

[23] (a) Elliott, L. D.; Berry, M.; Harji, B.; Klauber, D.; Leonard, J.; Booker-Milburn, K. I. A Small-Footprint, High-Capacity Flow Reactor for UV Photochemical Synthesis on the Kilogram Scale. *Org. Process Res. Dev.* **2016**, *20* (10), 1806–1811; (b) Abdiaj, I.; Alcázar, J. Improving the Throughput of Batch Photochemical Reactions Using Flow: Dual Photoredox and Nickel Catalysis in Flow for C(sp2)C(sp3) Cross-Coupling. *Bioorganic Med. Chem.* **2017**, *25* (23), 6190–6196; (c) Su, Y.; Kuijpers, K.; Hessel, V.; Noël, T. A Convenient Numbering-up Strategy for the Scale-up of Gas–liquid Photoredox Catalysis in Flow. *React. Chem. Eng.* **2016**, *1* (1), 73–81.

[24] Pitre, S. P.; McTiernan, C. D.; Ismaili, H.; Scaiano, J. C. Metal-Free Photocatalytic Radical Trifluoromethylation Utilizing Methylene Blue and Visible Light Irradiation. *ACS Catal.* **2014**, *4* (8), 2530–2535.

[25] Gleave, R. J.; Beswick, P. J.; Brown, A. J.; Giblin, G. M. P.; Haslam, C. P.; Livermore, D.; Moses, A.; Nicholson, N. H.; Page, L. W.; Slingsby, B.; et al. 2-Amino-5-Aryl-Pyridines as Selective CB2 Agonists: Synthesis and Investigation of Structure-Activity Relationships. *Bioorg. Med. Chem. Lett.* **2009**, *19* (23), 6578–6581.

Chapter 3

Improving the throughput of batch photochemical reactions using flow: Dual photoredox and nickel catalysis in flow for C(sp^2)-C(sp^3) cross-coupling

This chapter is based on:

Abdiaj, I. & Alcázar, J. Improving the throughput of batch photochemical reactions using flow: Dual photoredox and nickel catalysis in flow for C(sp^2)-C(sp^3) cross-coupling. *Bioorganic Med. Chem.* **25,** 6190–6196 (2017).

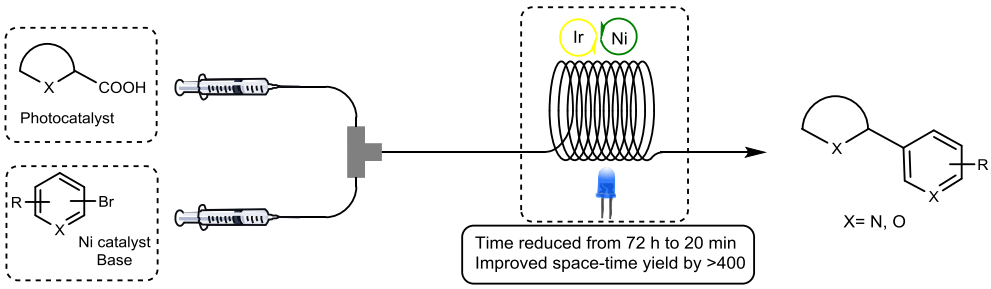

3.1 Introduction

As mentioned in the general introduction (Chapter 1), light has long been recognized as a valuable tool for performing efficient organic reactions. It allows access to complex molecules using photon as a traceless reagent which adds energy to a chemical system without generating waste in the process.[1] In the last few decades, visible light photoredox catalysis has emerged as a powerful strategy for organic synthesis, since organic or organometallic photoredox catalyst are able to transfer light into chemical energy having both oxidant and reductant species in the reaction.[2]

Considering these properties, in recent years many research groups have been focused on combining photoredox catalysis with other catalytic systems. In this way both oxidant and reductant species can be used as turnover of the interdependent catalytic cycles moduling the oxidation states of the transient intermediates. The intercycle dependence can prevent the generation of excess quantities of highly reactive intermediates, assuring better selecivity and less byproducts.

In this regard a new dual catalytic method which has recently emerged is the combination of photoredox catalysis with transition metal catalysis. Organic chemistry has been revolutionized since the discovery of metal-mediated cross coupling technologies.[3] In most cases, transition metal-catalyzed reactions proceed through a series of two electron redox event (M^n to M^{n+2}).[3] However, recent publications have demonstrated that combining photoredox catalysis with transition metal catalysis can enable single electron modulation of redox state. Photoredox catalysts can modulate the oxidation state of transition metal catalysts by direct single electron transfer between the catalysts, oxidative/reductive generation of a radical partner which can intercept the transition metal or oxidative/reductive generation of a radical species that can undergo SET with the metal catalyst. In all cases, by moduling the oxidation state, the active metal catalyst is regenerated thereby enables catalytic turnover.[2a,4]

In 2014, MacMillan *et. al.* described a sinergistic merge of visible light photoredox catalysis with nickel catalysis for C(sp^2)-C(sp^3) bond formation.[5] They selected a decarboxylative approach using the long-lived photo excited state $*Ir^{III}$ of $Ir[dF(CF_3)ppy]_2(dtbbpy)PF_6$ that generates a carboxyl radical which, upon loss of CO_2, produces the alfa-amino radical and the corresponding Ir^{II} species (Figure 3.1). Simultaneously with this photoredox cycle, the nickel catalytic cycle starts with the oxidative addition generating Ni^{II} intermediates that intercepts the amino radical forming Ni^{III} transient species which through reductive elimination build the C-C bond and thereby expelling the desired product. The Ni^{III} intermediate get converted into Ni^{I} intermediate which through a SET process captures an e^- from Ir^{II} species and in a concomitant way both catalytic cycles are completed.

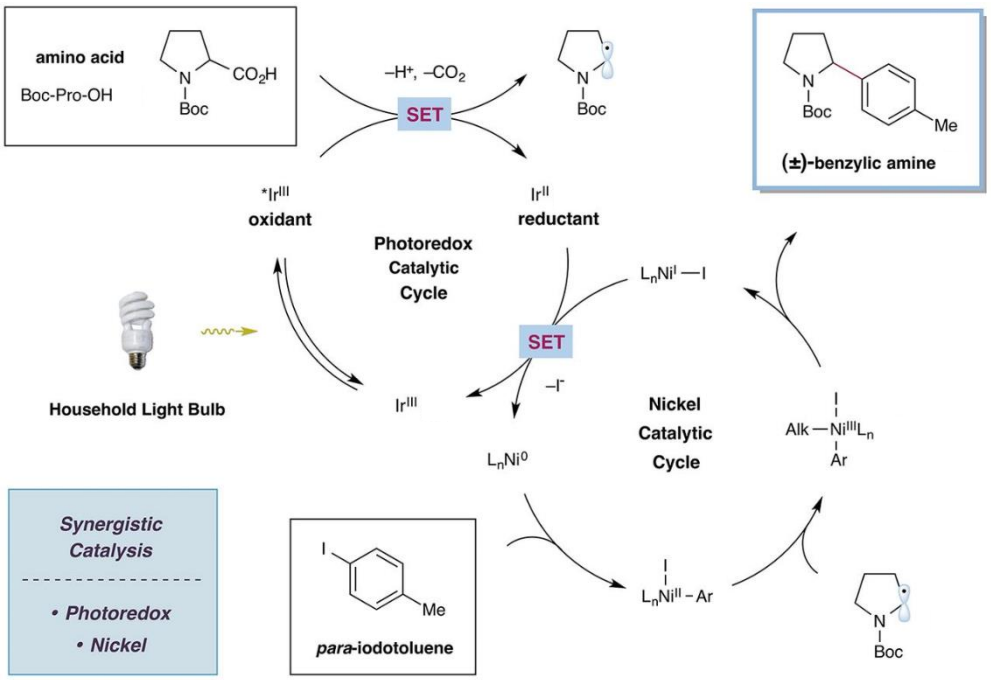

Figure 3.1: Photoredox-nickel catalyzed decarboxylative arylation: proposed mechanistic pathway presented by MacMillan et. al.

Considering the interest of cyclic amines in medicinal chemistry[6], this protocol is of high importance for drug discovery purposes. This reaction increases the prevalence of sp^3 carbons in drug compounds allowing medicinal chemists to access new chemical space with improved phisicochemical properties.[7] However, the scalability of photochemical processes is limited by the attenuation effect of photon transfer (Lambert-Beer Law). We thought that the combination of photoredox catalysis with continuous flow technologies would be the key element to overcome these issues. The use of continuous flow reactors ensures uniform irradiation of the narrow channels where the mixture is flowing.[8] Moreover, it provides an efficient heat transfer, good control of reaction temperature and enhanced mass transfer[9], making procedures more reproducible and scalable. Furthermore, flow chemistry has been identified as a very interesting sustainable alternative in chemical research and production.[10]

With the afore mentioned data in our hands and taking into acount our experience in flow chemistry, we have deduced that the transfer from batch to flow of the decarboxylative coupling of aminoacids with aryl halides described by MacMillan and coworkers would be of high importance for production and drug discovery purposes. In this regard we focused our efforts in finding a suitable flow protocol that would give applicability to the chemisrty in drug discovery.

3.2 Exploration of a suitable combination of reagents for the flow protocol

Lately, Stephenson and coworkers, reported the translation of a batch protocol to flow in order to get kilograms of the desired product.[11] In this case direct transfer to flow was possible, as all the components were soluble and he was using a mono-catalytic system. This is not suitable in MacMillan's dual catalysis because of the solubility issues in the reaction media. Considering the complexity of these catalytic cycles, in flow it is hard to match both cycles in short times. In batch dual catalytic reactions you do not have to deal with this problem due to the long reaction's time.

Nevertheless, the first example of dual catalytic system in flow was reported by Ley and coworkers.[12] They reported a new activation mode for boronic esters to increase the solubility of the starting materials in comparison with trifluoroborate salts used in he corresponding batch protocols. Following this approach, a series of benzylboronates were coupled with several bromoarenes.

In our case, the first challenge we had to deal with to obtain an effective flow protocol was to identify a suitable combination base-solvent that would avoid a potential blockage of the reactor. In the reference article[5], Cs_2CO_3 ,insoluble salt in organic sovents, is used as base. In order to speed up the finding of a suitable organic base, in a solvent where all the reagents were soluble, we started with a parallel batch screening of different bases under non optimal conditions using a handmade photoreactor irradiatied with a CFL bulb (Power 9W). With this approach, differences in performance among all possible combinations would be more sensitive and would help in the identification of the most promising one.[13] Control reactions using the base and the solvent described in batch were also included in the set to provide an appropriate comparison. (Table 3.1, entries 1 and 2). Among all the organic bases tested, 1,5-diazabiciclo [5.4.0] undec-5-ene (DBU) was found as the most promising one (Table 3.1, entry 4). A combination of this base with photocatalyst **2** provided a comparative result as in the one obtained with cesium carbonate. Nevertheless, using DBU with the original photocatalyst gives much lower conversion, suggesting that the base is not only involved in the deprotonation of the carboxylic acid, but also in the coordination of the photocatalyst.

Table 3.1: Initial screening in batch

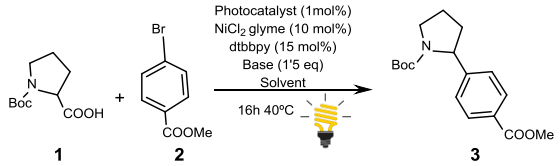

1 2 3

Entry	Base	Solvent	Photocatalyst	Conv.[a](%)
1	Cs_2CO_3	DMF	1	8
2	Cs_2CO_3	DMF	2	4
3	DBU	DMF	1	Traces
4	DBU	DMF	2	6
5	DMAP	DMF	2	0
6	MTBD	DMF	2	3
7	TEA	DMF	2	0
8	Lutidine	DMF	2	Traces
9	BTPP	DMF	2	0
10	DBU	DMSO	2	Traces
11	DBU	THF	2	24[b]
12	DBU	DMA	2	12
13	DBU	ACN	2	2[b]
14	DBU	Acetone	2	12[b]
15	DBU	Toluene	2	13[b]
16	DBU	Isopropanol	2	0
17	DBU	EtOAc	2	22[b]
18	DBU	$(MeO)_2CO$	2	0

[a] % of product measured by LC-MS. [b] Precipitation of side products.

Once the appropriate base and photocatalyst were identified, solvent screening was performed (Table 3.1, entries 10–12). THF, acetone, toluene and ethyl acetate were found to provide good conversion to product (Table 3.1, entries 11, 14, 15 and 17), but precipitation of insoluble material was observed, most probably the corresponding HBr salt of the base, preventing their potential use in flow. On the other hand, dimethylacetamide (DMA) managed to solubilize all the reagents and byproducts of the reaction and it also provided good conversion in product (Table 3.1, entry 12) making it the solvent of choice for our flow protocol.

3.3 Optimization of reaction conditions in flow

The parallel batch screening provided the best combination of base (DBU), solvent (DMA) and photocatalyst **2** suitable for the flow protocol. The following step was optimizing reaction conditions modulating the different flow parameters (Table 3.2). For this second step of optimization, the commercially available UV-150 photoreactor from Vapourtec was used.[14] This system is ideally suited for exploratory studies as it can

be operated at various temperatures via active heating or cooling. As the reaction in batch proceeded in 72 h, the initial attempt was to perform the reaction at 40 °C with a relatively long residence time for a flow reactor (Table 3.2, entry 1). The conversion achieved was a promising starting point as it was higher than the one observed in batch at the same temperature in overnight reaction (Table 3.1, entry 12). With higher temperature, 60 °C, full conversion was observed but the crude reaction mixture was dirty and only 40% of isolated product was obtained (Table 3.2, entry 2). In order to control overreaction products, we started to combine different reaction times with different temperatures in order to improve the outcome. Finally, the best isolated yield was achieved at 60 °C and 20 min residence time (Table 3.2, entry 4).

Table 3.2: Optimization of the conditions in flow

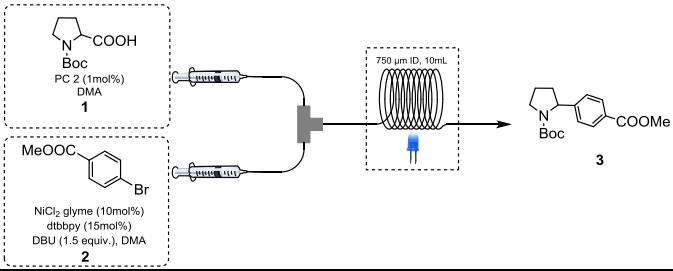

Entry	Temp. (°C)	Time (min.)	Conv.[a] (%)
1	40	33	40
2	60	33	100 (40)[b]
3	60	10	42
4	60	20	100 (74)[b]
5	75	10	47
6	80	5	40
7	60	20	2[c]
8	60	20	4[d]
9	60	20	0[e]
10	60	20	4[f]

[a]Conversion of 2a by LC-MS. [b]Isolated yield. [c]Test Reaction without light irradiation. [d]Test reaction without photocatalyst. [e]Test reaction without Nickel catalyst. [f]Test reaction without 4,4′-Di-tert-butyl-2,2′-dipyridyl (dtbby).

To prove that the reaction required the combination of both catalytic cycles, several blind experiments were performed (Table 3.2, entries 7–10). Running the reaction in the dark provided very low conversion (entry 7). A similar outcome was achieved when the photocatalyst was removed (entry 8). In both examples, a dirty crude reaction was observed. The presence of the nickel catalyst was key for the outcome of the reaction. When the reaction was run in the absence of nickel catalyst, no conversion of starting materials in product was observed (entry 9). For this reason, it was decided to run it in

two separated lines, so that no transformations would take place in the initial solution before entering the photochemical reactor. Finally, the presence of 4,4'-Di-tert-butyl-2,2'-dipyridyl (dtbbpy) as nickel ligand was also important for the reaction outcome (entry 10).

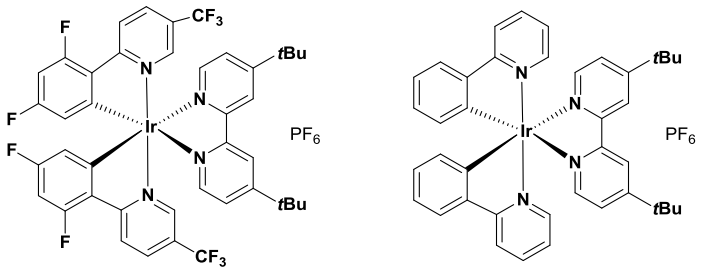

$(Ir[dF(CF_3)ppy]_2(dtbpy))PF_6$
Photocatalyst (1)

$(Ir(ppy)_2(dtbpy))PF_6$
Photocatalyst (2)

Figure 3.2: Photocatalysts screened in reaction optimization

3.4 Exploration of substrate scope

Modulating the properties of cyclic amines is a key element in finding good clinical candidates.[6] Therefore, substrate scope was explored, focusing on aromatic substituents and heterocycles of potential interest for drug discovery (Figure 3.3). The results shown in this table are the most optimal found after testing different conditions. Many aryl bromides function effectively, including those that contain functional groups as diverse as, esters, ketones, nitriles, trifluoromethyl groups, and chlorides (**3** to **8**, 32 to 74% yield). Heteroaromatics, in the form of differentially substituted bromopyridines and bromopyperazine are also efficient coupling partners (**9** to **12**, 30 to 45% yield). Not only monocyclic heterocycles but even bicyclic ones provided the desired products **13** and **14** (56% and 37% yield each). thereby demonstrating the value of the protocol for medicinal chemistry. These reactions are typically complete in 20 to 30 minutes. Only the π- exceeding compound **13** required longer residence time of 40 minutes.

Next, we investigated the nature of the carboxylic acid coupling partner. Benzopiperadines derivatives have shown to be biologically active cores with antitumoral[15] and antithrombotic[16] activity. Therefore, further functionalization will be of great interest for medicinal chemists. Product **15** was obtained in very good yield (71%) in only one step, providing new series of hits to be tried in this regard. Stereochemistry can be modulated by such substitution. Enantiopure aminoacid (2S,4R)-1-(tert-Butoxycarbonyl)-4-hydroxypyrrolidine-2-carboxylic acid, showed to

maintain its chirality giving as main product the trans one, compound **17** in a ratio 3:1 with the cis one **18**. Not only aminoacids but even α-oxicarboxylic acids can function as proficient coupling partners, producing a-arylated ethers in moderate yield over a single step (**19**, 42% yield).

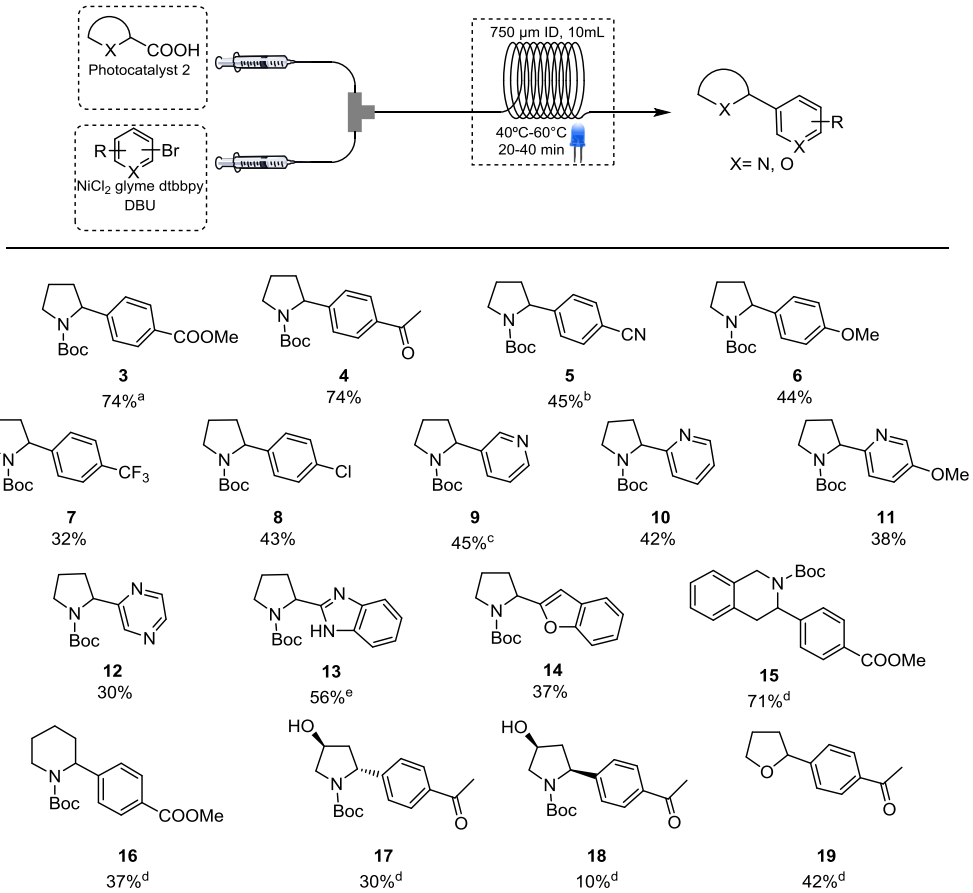

Figure 3.3: Scope of the reaction

General conditions: ArX (0.2 mmol), RCOOH (1.5 eq.), DBU (1.5 eq.), $Ir(ppy)_2(dtbbpy)^{3+}$ (1 mol%), $NiCl_2$ glyme(10 mol%), dtbbpy (15 mol%), t_R = 30 min, T = 60 °C LED = 450 nm.[a] t_R = 20 min, T = 60 °C;[b] t_R = 20 min, T = 40 °C;[c] t_R = 30 min, T = 40 °C.[d] RCOOH (3 eq.), DBU (3 eq.);[e] t_R = 40 min, T = 60 °C.

3.5 Determination of stereochemistry of the compounds **17** and **18** by 2D-NMR experiments

The stereochemistry of the compounds **17** and **18** was determined by bidimensional NMR analysis.[17] First of all, HSQC (heteronuclear single quantum coherence or heteronuclear single quantum correlation) analysis was performed to both conformers. HSQC detects correlations between nuclei of two different types which are separated by one bond. This method gives one peak per pair of coupled nuclei, whose two coordinates are the chemical shifts of the two coupled atoms.[18] In this way we have the correlation carbon-proton in the molecule. Primary and tertiary carbon atoms are highlighted in blue and secondary carbon atoms in red. After determining to which carbon corresponds each proton we performed a COSY (correlation spectroscopy) experiment.[17] COSY is a homonuclear bidimensional NMR experiment which is used to identify spins which are coupled to each other. We focused our attention in the protons of the methylene group C_4 to see how these protons were coupled with the protons H_{26} and H_{23}. For the conformer **17** in COSY, we observe the coupling of H_{26} with H_{24} and H_{25} and by the other hand H_{23} is coupled only with H_{24}. The same coupling is observed even with the conformer **18** considering that with COSY experiment we only observe the coupling of closed protons with each other but not their location in space. To see how they are located in space we performed a NOESY experiment. In NOESY experiments, the nuclear Overhauser cross relaxation between nuclear spins during the mixing period is used to establish the correlations. The spectrum obtained is similar to COSY, with diagonal peaks and cross peaks, however the cross peaks connect resonances from nuclei that are spatially close rather than those that are through-bond coupled to each other. In the case of conformer **17** we observed a strong correlation of proton H_{26} with H_{25}. The proton H_{23} gives correlation with both H_{24} and H_{25} but the strongest is the one with H_{24}. This correlation made us deduce that the first conformer is the conformer **17**. For the conformer **18**, H_{26} is correlated with H_{25} and there is no correlation with H_{24}. H_{23} by the other hand, has strong correlation with H_{25} and less correlation with H_{24}. These results confirmed us that the conformer is the cis one.

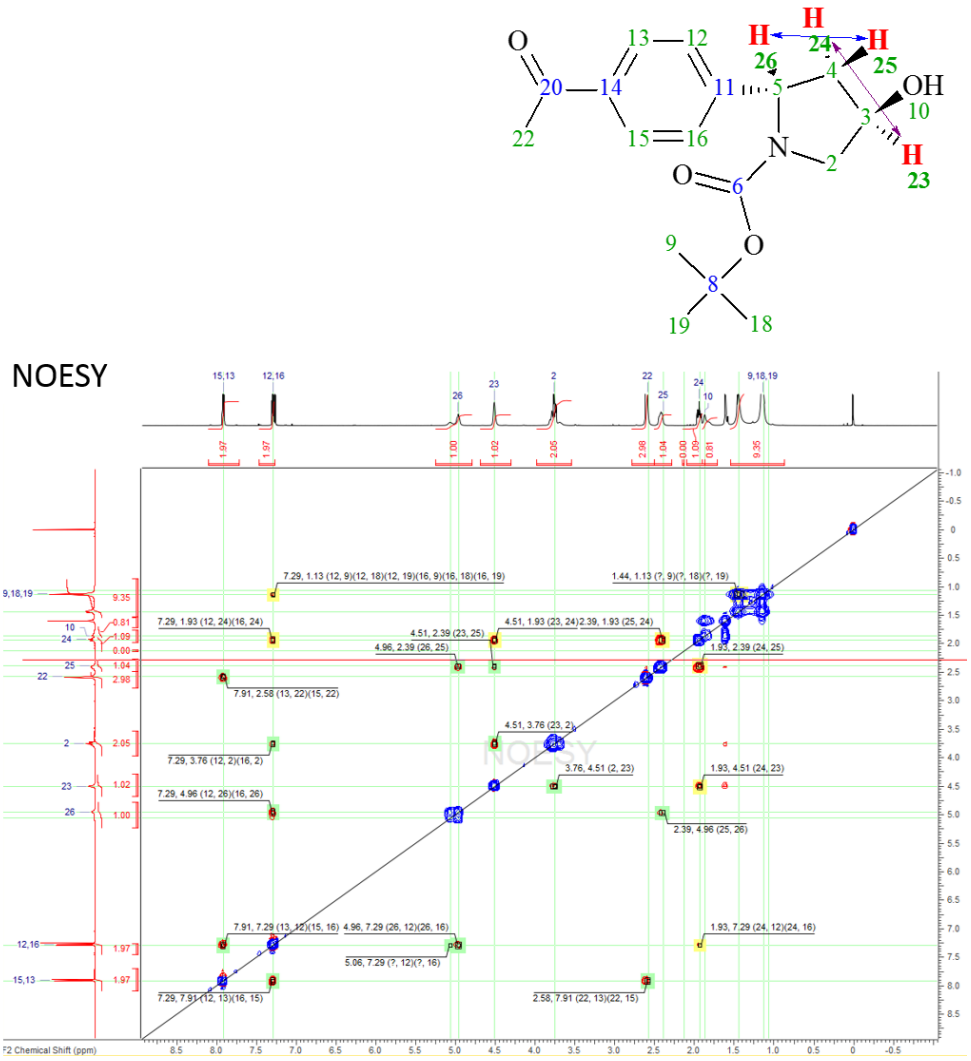

*Figure 3.3.4: NOESY experiment of conformer **17**.*

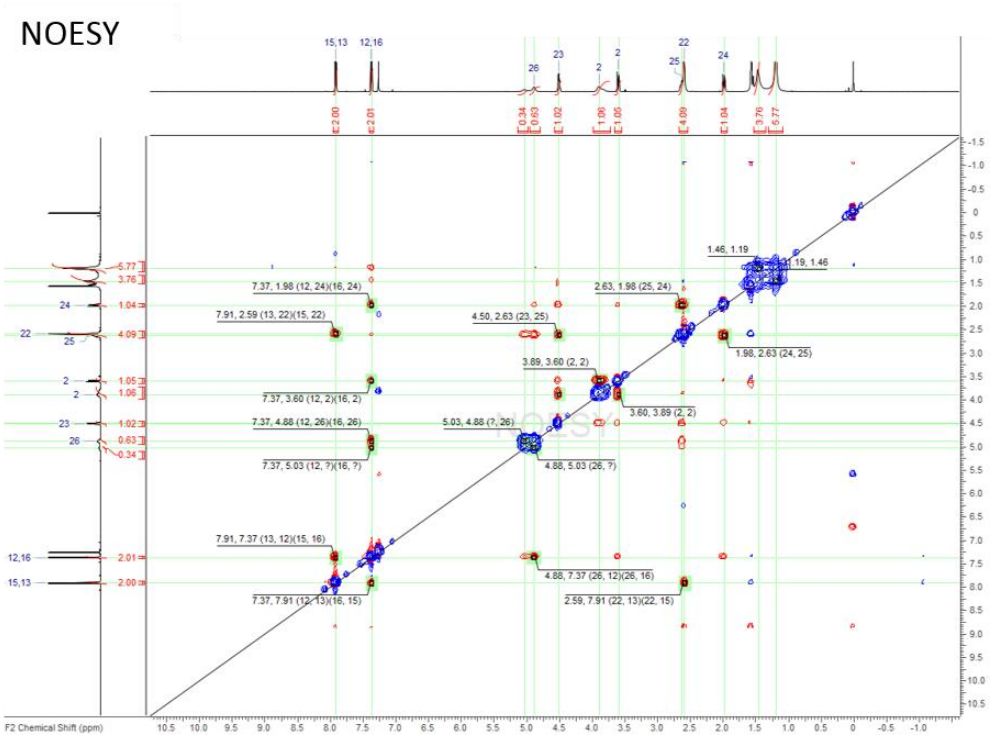

*Figure 3.3.5: NOESY experiment of conformer **18**.*

3.6 Scale up

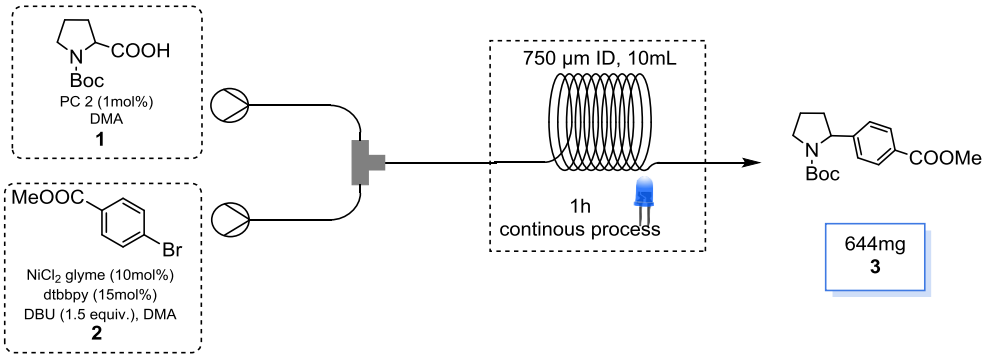

Figure 3.6: Scale up in continuous flow process

The next step in proving the value of this flow protocol in drug discovery processes was the scaling up of the reaction (Figure 3.6). Thus, the reaction was run for 1h continuously in the machine and the resulting outcome was compared with the one reported in batch.[5] Even though the isolated yield in flow was confirmed and was still lower than the one described in batch, 644 mg of **3** as a white solid were isolated. Considering the time necessary to obtain it, this quantity is more than enough material to support drug-discovery processes. The lower yield was balanced by the reduced time and increased concentration. These combined effects provided 430 times better space-time yield[10a,19] than the one calculated for the batch protocol, clearly demonstrating the improved efficacy of the flow procedure (Table 3.3).

Table 3.3: Comparison batch versus flow

	Flow	**Batch[a]**
Yield	74%	90%
Reaction Time	20 min	72 h
Product Throughput	644 mg/h	109 mg/72 h
[2]	0.1M	0.02M
Space-time Yield[b]	64.4 mg/h·mL	0.15 mg/h·mL

[a]Results from reference 10. [b]Calculated according to references 4d and 14.

3.7 Conclusions

Herein, a stepwise procedure to translate photochemical batch reactions with insoluble reagents in flow is described. Due to the high potential of the dual catalytic protocol presented by MacMillan and coworkers for replacing thermal catalytic cross-coupling, we developed homogeneous conditions to transfer this light mediated coupling protocol to continuous flow. Combination of DBU and Photocatalyst **2** were crucial to obtain productivity. With this homogeneous system we moved to flow using a two-feed

approach and a coil reactor irradiated with 450nm blue Leds. Slightly elevated temperatures were beneficial to the continuous coupling procedure reducing the residence time from 72 h to 20-40 minutes. The continuous process and time reduction allows the scalability of the reaction to reach amounts of compound that could be difficult to achieve in batch. The optimized protocol increases significantly the amount of product produced per reactor volume, clearly showed in the space-time yield value. This is translated in a more sustainable protocol with mild reaction conditions for challenging $C(sp^2)$-$C(sp^3)$ cross-coupling. The reaction has a broad scope that perfectly fits the requirements for drug discovery in terms of functionalized aryl groups and heterocycles as well as cyclic amines. The new flow protocol is a promising tool for drug discovery to increase $C(sp^3)$ motifs in bioactive molecules.

3.8 Experimental session

General information

GC measurements were performed using a 6890 Series Gas Chromatograph (Agilent Technologies) system comprising a 7683 Series injector and autosampler, J&W HP-5MS column (20 m 0.18 mm, 0.18 lm) from Agilent Technologies coupled to a 5973N MSD Mass Selective Detector (single quadrupole, Agilent Technologies). The MS detector was configured with an electronic impact ionization source/chemical ionization source (EI/CI). EI lowresolution mass spectra were acquired by scanning from 50 to 550 at a rate of 5.5 scan/s. The source temperature was maintained at 230 °C. Helium was used as the nebulizer gas. Data acquisition was performed with Chemstation-Open Action software. Thin layer chromatography (TLC) was carried out on silica gel 60 F254 plates (Merck) using reagent grade solvents. Unless otherwise specified, reagents were obtained from commercial sources and used without further purification. The reactions were carried out in a Vapourtec photoreactor UV-150 fixed on a E-series Vapourtec equipment. 1 H NMR spectra were recorded on Bruker DPX-400 or Bruker AV-500 spectrometers with standard pulse sequences, operating at 400 MHz and 500 MHz respectively. Chemical shifts (d) are reported in parts per million (ppm) downfield from tetramethylsilane (TMS), which was used as an internal standard.

Dual photoredox-nickel catalysis for decarboxylative arylation.

General procedure A for the decarboxylative Arylation (Arene's scope):

Two different solutions for feeds A and B were separately prepared in 2 mL vial equipped with a Teflon septum and magnetic stir bar. Feed A: $[Ir(dtbbpy)(ppy)_2][PF_6]$ (0.0002 mmol, 0.01 equiv) and Boc-Pro-OH (0.3 mmol, 1.5 equiv) in 1 mL of DMA; Feed B: $NiCl_2$ glyme (0.02 mmol, 0.1 equiv), 4,40 -di-tert-butyl-2,20 - bipyridyl (0.03 mmol, 0.15 equiv), the corresponding aromatic halides (0.20 mmol, 1.0 equiv), DBU (0.3 mmol, 1.5 equiv) in 1 mL of DMA. The two solutions were degassed by bubbling nitrogen stream for 20 min. Feeds A and B were injected simultaneously into the photoreactor, mixed in a T-mixer, and passed through a 10 mL residence time coil (0.75 mm I.D., 4 m length, FEP tube) irradiated with blue LED 450 nm and heated at the indicated temperature. The reaction mixture collected from the output was diluted with saturated aqueous $NaHCO_3$ solution, extracted with Et_2O (3 x 10 mL). The combined organic extracts were washed with water and brine, dried over $MgSO_4$ and concentrated in vacuo. Purification of the crude product by flash chromatography on silica gel using as eluent heptane/ethyl acetate afforded the desired product.

General procedure B for the decarboxylative Arylation (Carboxylic Acid's scope):

Two different solutions for feeds A and B were separately prepared in 2 mL vial equipped with a Teflon septum and magnetic stir bar. Feed A: $[Ir(dtbbpy)(ppy)_2][PF_6]$ (0.0002 mmol, 0.01 equiv) and the correspondent carboxylic acid (0.6 mmol, 3 equiv) in 1 mL of DMA; Feed B: $NiCl_2$ glyme (0.02 mmol, 0.1 equiv), 4,40 -ditert-butyl-2,20 -bipyridyl (0.03 mmol, 0.15 equiv), the corresponding aromatic halides (0.20 mmol, 1.0 equiv), DBU (0.6 mmol, 3 equiv) in 1 mL of DMA. The two solutions were degassed by bubbling nitrogen stream for 20 min. Feeds A and B were injected simultaneously into the photoreactor, mixed in a T-mixer, and passed through a 10 mL residence time coil (0.75 mm I.D., 4 m length, FEP tube) irradiated with blue LED 450 nm and heated at the indicated temperature. The reaction mixture collected from the output was diluted with saturated aqueous $NaHCO_3$ solution, extracted with Et_2O (3 x 10 mL). The combined organic extracts were washed with water and brine, dried over $MgSO_4$ and concentrated in vacuo. Purification of the crude product by flash chromatography on silica gel using as eluent heptane/ethyl acetate afforded the desired product.

Product's characterization

*tert-Butyl 2-(4-methoxycarbonylphenyl) pyrrolidine-1- carboxylate (**3**)*

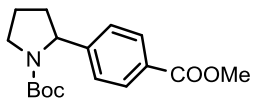

3

The product was prepared according to general procedure A; t_R = 20 min, T = 60 °C. Yield:45 mg (74%)

^{1}H NMR (500 MHz, $CDCl_3$): δ= 7.90 (d, J = 10.0 Hz, 2 H), 7.29 (d, J = 5.0 Hz, 2 H), 4.67 and 5.06 (2brs, 1 H rotamer) 3.91 (s, 3 H), 3.51–3.70 (m, 2 H), 2.37–2.34 (m, 1 H), 1.77–1.96 (m, 3 H), 1.46 (s, 3 H), 1.17 (br s, 6 H)

^{13}C NMR (126 MHz, $CDCl_3$) rotameric mixture, resonances for minor rotamer are enclosed in parenthesis (): δ= 166.9, 154.3, 150.6 (149.5), (129.7) 129.6, 128.5, 125.4, 79.4, 61.2 (60.6),51.9, (47.4) 47.1, 35.91 (34.7), (28.4) 28.1, (23.6) 23.2;

HRMS(ESI): m/z calcd. for $C_{17}H_{23}NO_4$: 305.1627; found: 328.1531 [$(M+Na)^+$].

*tert-Butyl 2-(4-acetylphenyl) pyrrolidine-1-carboxylate (**4**)*

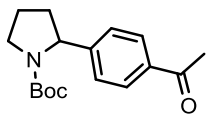

4

The product was prepared according to general procedure A; t_R = 30 min, T = 60 °C. Yield: 43 mg (74%).

^{1}H NMR (400 MHz, $CDCl_3$): δ = 7.91 (br d, J = 8.09 Hz, 2 H), 7.21 (d, J = 8.09 Hz, 2 H), 4.82 and 5.06 (2 br s, 1 H rotamer), 3.65–3.52 (m, 2 H), 2.60–2.58 (m, 3 H), 2.36–2.32 (m, 1 H), 1.75– 1.98 (m, 2 H), 1.40–1.52 (m, 3 H), 1.18 (br s, 6 H).
^{13}C NMR (101 MHz, $CDCl_3$) rotameric mixture, resonances for minor rotamer are enclosed in parenthesis (): δ = 197.8, 154.4, 150.8, 135.7, (128.6) 128.4, 125.6 (125.2), 79.5, 61.2 (60.7), (47.5) 47.2, 35.9, (28.4) 28.2, 26.6, (23.7) 23.3.
HRMS(ESI): m/z calcd. for $C_{17}H_{23}NO_3$:289.1677, found: 312.1579 [$(M+Na)^+$].

*tert-Butyl 2-(4-cyanophenyl) pyrrolidine-1-carboxylate (**5**)*

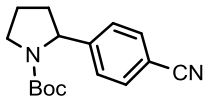

5

The product was prepared according to general procedure A; t_R = 20 min, T = 40 °C. Yield: 24.5 mg (45%).

^{1}H NMR (500 MHz, $CDCl_3$): δ= 7.60 (d, J = 8.09 Hz, 2 H), 7.28 (d, J = 8.38 Hz, 2 H), 4.72–5.09 (m, 1 H), 3.52–3.73 (m, 2 H), 2.36 (br d, J = 6.65 Hz, 1 H), 1.89 (br d, J = 6.07 Hz, 2 H), 1.78 (br dd, J = 11.70, 5.64 Hz, 1 H), 1.41–1.53 (m, 3 H), 1.18 (br s, 6 H).
^{13}C NMR (126 MHz, $CDCl_3$) rotameric mixture, resonances for minor rotamer are enclosed in parenthesis (): δ= 150.8, 134.3, 132.2, 126.2, 118.9, 110.5, 79.8, 61.2 (60.7), (47.5) 47.2, 35.9 (34.7), (28.5) 28.2, (23.7) 23.3.
HRMS(ESI): m/z calcd. for $C_{16}H_{20}N_2O_2$: 272.1524, found: 295.1424 [$(M+Na)^+$].

*tert-Butyl 2-(4-methoxyphenyl) pyrrolidine-1-carboxylate (**6**)*

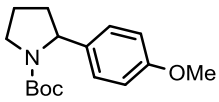

6

The product was prepared according to general procedure A; t_R = 30 min, T = 60 °C. Yield: 49 mg (44%).

^{1}H NMR (500 MHz, $CDCl_3$): δ= 7.08 (d, J = 7.5 Hz, 2 H), 6.83 (d, J = 8.5 Hz, 2 H), 4.69 and 4.90 (2brs, 1 H rotamer), 3.79 (s, 3 H), 3.54–3.65 (m, 2 H), 2.28 (br, 1 H), 1.72–1.98 (m, 3 H), 1.46 (s, 3 H), 1.20 (br s, 6 H);

^{13}C NMR (126 MHz, $CDCl_3$) rotameric mixture, resonances for minor rotamer are enclosed in parenthesis (): δ= 158.2, 154.6, 137.3, 126.6, (113.8) 113.5, 79.1, 60.8, 55.3, (47.3) 47.0, 36.1 (34.9), (28.6) 28.2, (23.5) 23.5.
HRMS(ESI): m/z calcd. for $C_{17}H_{23}NO_3$: 289.1677, found: 312.1705 [$(M+Na)^+$].

*tert-Butyl 2-[4-(trifluoromethyl) phenyl] pyrrolidine-1- carboxylate (**7**)*

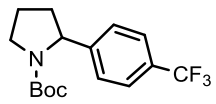

7

The product was prepared according to general procedure A; t_R = 30 min, T = 60 °C. Yield: 21 mg (32%).

^{1}H NMR (400 MHz, $CDCl_3$): δ= 7.56 (d, J = 8.1 Hz, 2H), 7.28 (d, J = 8.1 Hz, 2H), 4.81 (br s, 1H), 3.64 (br s, 2H), 2.34 (br s, 1H), 1.86–1.93 (m, 2H), 1.80 (br dd, J = 11.4, 5.4 Hz, 1H), 1.46 (br s, 3H), 1.18 ppm (br s, 6H).
^{13}C NMR (126 MHz, $CDCl_3$) rotameric mixture, resonances for minor rotamer are enclosed in parenthesis (): δ= 149.3, 128.9, 125.8, (125.4), 125.1, 79.6, 61.1 (60.5), (47.5) 47.2, 36.0 (34.8), 28.6, 28.1, (23.6) 23.2.
HRMS (ESI): m/z calcd. for $C_{16}H_{20}F_3NO_2$: 315.3354, found: 338.1324 [$(M+Na)^+$].

*tert-Butyl 2-(4-chlorophenyl) pyrrolidine-1-carboxylate (**8**)*

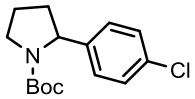

8

The product was prepared according to general procedure A; t_R = 30 min, T = 60 °C. Yield: 24 mg (43%).

^{1}H NMR (400 MHz, CDCl3): δ= 7.24–7.27 (m, 2H), 7.10 (d, J = 8.3 Hz, 2H), 4.66 and 4.97 (2brs, 1H rotamer), 3.61 (br s, 2H), 2.18–2.38 (m, 1H), 1.82–1.94 (m, 2H), 1.70–1.81 (m, 1H), 1.45 (br s, 3H), 1.20 ppm (br s, 6H).
^{13}C NMR (126 MHz, $CDCl_3$) rotameric mixture, resonances for minor rotamer are enclosed in parenthesis (): δ= 154.5, 143.8, 132.1, (128.5), 128.2, 126.9, 79.4, 60.8 (60.2), (47.4) 47.1, 36.0 (34.9), 29.7 (29.37), (28.5) 28.2, (23.6) 23.2 ppm.
HRMS (ESI): m/z calcd. for $C_{15}H_{20}ClNO_2$: 281.1182, found: 304.1081 [$(M+Na)^+$].

*tert-Butyl 2-(3-pyridyl) pyrrolidine-1-carboxylate (**9**)*

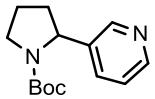

9

The product was prepared according to general procedure A; t_R = 30 min, T = 40 °C. Yield: 24 mg (45%).

^{1}H NMR (400 MHz, $CDCl_3$): δ= 8.47 (s, 2H), 7.49 (br d, J = 7.9 Hz, 1H), 7.23 (dd, J = 7.6, 5.1 Hz, 1H), 4.78 and 4.96 (2 br s, 1H rotamer), 3.63 (br s, 2H), 1.73–1.99 (m, 3H), 1.20 (br s, 6H).
^{13}C NMR (126 MHz, $CDCl_3$) rotameric mixture, resonances for minor rotamer are enclosed in parenthesis (): d ppm 154.3, 148.2 (147.7), 132.9 (133.1), 123.1, 100.1, 79.7, 59.0 (58.7), 47.2, 35.9 (34.5), (28.6) 28.3, (23.7) 23.3
HRMS (ESI): m/z calcd. for $C_{14}H_{20}N_2O_2$: 248.1524, found: 249.1607 [$(M+H)^+$].

*tert-Butyl 2-(2-pyridyl) pyrrolidine-1-carboxylate (**10**)*

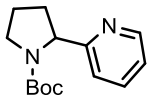

10

The product was prepared according to general procedure A; t_R = 30 min, T = 60 °C. Yield: 21 mg (42%).

^{1}H NMR (400 MHz, $CDCl_3$): δ = 8.53 (br d, J = 4.4 Hz, 1H), 7.63 (br t, J = 7.6 Hz, 1H), 7.09–7.20 (m, 2H), 4.87 (br d, J = 3.5 Hz, 1H), 3.54–3.69 (m, 2H), 2.30–2.45 (m, 1H), 1.98–2.10 (m, 1H), 1.84–1.93 (m, 2H), 1.42–1.50 (m, 3H), 1.20 ppm (s, 6H).
^{13}C NMR (126 MHz, CDCl3): δ = 163.8, 154.5, (149.3) 149.0, (136.4) 136.2, 121.4, (120.1) 119.7, 79.3, 63.0 (62.2), (47.4) 47.1, 34.3 (33.0), (28.5) 28.2, (23.8) 23.2.
HRMS (ESI): m/z calcd. for $C_{14}H_{20}N_2O_2$: 248.1524, found: 271.1432 [$(M+Na)^+$].

*tert-Butyl 2-(5-methoxy-2-pyridyl) pyrrolidine-1-carboxylate (**11**)*

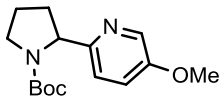

11

The product was prepared according to general procedure A; t_R = 30 min, T = 60 °C. Yield: 21 mg (38%).

^{1}H NMR (400 MHz, $CDCl_3$): δ = 8.24 (s, 1H), 7.01–7.21 (m, 2H), 4.68–5.14 (m, 1H), 3.80–3.96 (m, 3H), 3.49–3.72 (m, 2H), 2.25–2.44 (m, 1H), 1.82–2.11 (m, 3H), 1.76 (br s, 1H), 1.39– 1.56 (m, 3H), 1.15–1.31 ppm (m, 6H).
^{13}C NMR (126 MHz, $CDCl_3$) rotameric mixture, resonances for minor rotamer are enclosed in parenthesis (): δ = 155.8, 154.7, 154.2, (136.9) 136.3, 121.0 (120.6), 120.0, 79.4, 62.0 (61.4), 55.6, (47.7) 47.0, 34.3 (33.0), (28.7) 28.0, (24.0) 23.1 ppm.
HRMS (ESI): m/z calcd. for $C_{14}H_{20}N_2O_2$: 278.1630, found: 301.1538 [$(M+Na)^+$].

*tert-Butyl 2-pyrazin-2-ylpyrrolidine-1-carboxylate (**12**)*

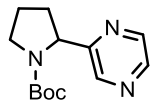

12

The product was prepared according to general procedure A; t_R = 30 min, T = 40 °C. Yield: 15 mg (30%).

^{1}H NMR (400 MHz, $CDCl_3$): δ = 8.50 (br s, 2H), 8.44 (br s, 1H), 4.84 and 5.08 (2 br s, 1H rotamer), 3.65 (br d, J = 5.1 Hz, 2H), 2.29–2.49 (m, 1H), 1.98–2.11 (m, 2H), 1.93 (br d, J = 6.0 Hz, 1H), 1.45 (br s, 3H), 1.21 ppm (s, 6H).
^{13}C NMR (126 MHz, $CDCl_3$) rotameric mixture, resonances for minor rotamer are enclosed in parenthesis (): δ= 158.9 (158.0), (154.7) 154.1, (144.0) 143.8, (142.9) 142.8, 79.8, 60.9 (60.3), (47.4) 47.1, 34.1 (32.8), (28.5) 28.2, (24.0) 23.5.
HRMS (ESI): m/z calcd. for $C_{13}H_{19}N_3O_2$: 249.1477, found: 272.1378 [$(M+Na)^+$].

*tert-Butyl 2-(1H-benzimidazol-2-yl) pyrrolidine-1-carboxylate (**13**)*

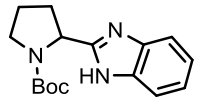

13

The product was prepared according to general procedure A; t_R = 40 min, T = 60 °C. Yield: 21 mg (57%).

^{1}H NMR (400 MHz, $CDCl_3$): δ = 10.36–10.85 (m, 1 H), 7.60–7.87 (m, 1 H), 7.37–7.46 (m, 1 H), 7.19–7.25 (m, 2 H), 5.13 (br d, J = 5.78 Hz, 1 H), 3.41 (br s, 2 H), 3.08 (br s, 1 H) 2.20 (br s, 2 H), 2.01 (br s, 2 H), 1.51 (br s, 9 H).
^{13}C NMR (101 MHz, $CDCl_3$): δ = 156.6, (154.9), 133.9, 122.8 (121.8), 119.5, 110.9, 80.7, 54.7, 47.4, 28.1, 28.5 (31.9), 24.9.
HRMS(ESI): m/z mass calcd. for $C_{16}H_{21}N_3O_2$: 287.1633, found: 288.1713 [$(M+H)^+$].

tert-Butyl 2-(*benzofuran-2-yl) pyrrolidine-1-carboxylate (**14**)*

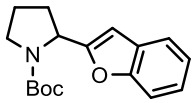

14

The product was prepared according to general procedure A; t_R = 30 min, T = 60 °C. Yield: 21 mg (37%).

^{1}H NMR (400 MHz, $CDCl_3$): δ = 7.45–7.53 (m, 1 H),7.41 (d, J = 7.63 Hz, 1 H),7.17–7.27 (m, 2 H) 6.41–6.53 (m, 1 H),4.97 (br s, 1 H),3.61 (br s, 1 H), 3.49 (br d, J = 5.55 Hz, 1 H), 2.09–2.28 (m, 2 H), 2.05 (br d, J = 6.01 Hz, 1 H),1.87–2.01 (m, 1 H), 1.51– 1.62 (m, 1 H), 1.47 (br d, J = 6.94 Hz, 3 H), 1.32 (br s, 6 H).
^{13}C NMR (126 MHz, $CDCl_3$) rotameric mixture, resonances for minor rotamer are enclosed in parenthesis (): δ = 154.4, 128.4, 123.7 (122.5), (120.6) 102.4, 79.7, 55.3 (54.9), (46.9) 46.2, 32.2 (31.2), 29.7, (28.6) 28.1, (24.1) 23.3.
HRMS (ESI): m/z calcd. for $C_{17}H_{21}NO_3$: 287.1521, found: 310.1420 [$(M+Na)^+$].

*tert-Butyl 3-(4-methoxycarbonylphenyl)-3,4-dihydro-1Hisoquinoline-2-carboxylate (**15**)*

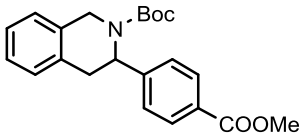

15

The product was prepared according to general procedure B; t_R = 30 min, T = 60 °C. Yield: 59 mg (71%).

^{1}H NMR (400 MHz, $CDCl_3$): δ= 8.60 (dd, J = 5.1, 0.7 Hz, 1H), 7.88 (d, J = 8.3 Hz, 2H), 7.17 (br d, J = 8.1 Hz, 4H), 7.13–7.20 (m, 1H), 7.09 (br d, J = 6.9 Hz, 1H), 4.81 (br d, J = 16.0 Hz, 1H), 4.41 (br s, 1H), 3.87 (s, 3H), 3.32 (br dd, J = 15.6, 5.4 Hz, 1H), 3.06 (br s, 1H), 1.29–1.48 ppm (m, 9H).
^{13}C NMR (126 MHz, $CDCl_3$): δ= 183.9, 166.9, 155.1, 129.6, 128.7, (127.5) 126.7, 125.6, 100.0, 80.3, 52.0, 44.2, 28.4.
HRMS (ESI): m/z calcd. for $C_{14}H_{20}N_2O_2$: 367.1783, found: 390.1679 [$(M+Na)^+$].

*tert-Butyl 2-(4-methoxycarbonylphenyl) piperidine-1- carboxylate (**16**)*

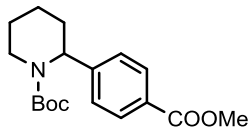

16

The product was prepared according to general procedure B; t_R = 30 min, T = 60 °C. Yield: 24 mg (37%).

^{1}H NMR (400 MHz, $CDCl_3$): δ= 7.98–8.04 (m, 2H), 7.27–7.32 (m, 2H), 5.40–5.47 (m, 1H), 4.03–4.13 (m, 1H), 3.91 (s, 3H), 2.71–2.82 (m, 1H), 2.26–2.34 (m, 1H), 1.87– 1.97 (m, 1H), 1.47–1.69 (m, 4H), 1.45 ppm (s, 9H).
^{13}C NMR (101 MHz, $CDCl_3$): δ= 167.0, 155.6, 146.3, 129.9, 128.4, 126.5, 79.8, 53.5, 52.1, 40.3, 28.4, 28.3, 25.3 ppm.
HRMS (ESI): m/z calcd. for $C_{14}H_{20}N_2O_2$: 367.1783, found: 390.1679 [$(M+Na)^+$].

*tert-Butyl 2-(4-acetylphenyl)-4-hydroxy-pyrrolidine-1- carboxylate (**17**)*

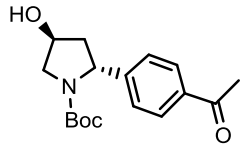

17

The product was prepared according to general procedure B; t_R = 30 min, T = 40 °C. Yield: 18 mg (30%).

^{1}H NMR (400 MHz, $CDCl_3$): δ= 7.91 (d, J = 8.3 Hz, 2H), 7.37 (d, J = 8.1 Hz, 2H), 4.80–5.18 (m, 1H), 4.42–4.59 (m, 1H), 3.88 (br s, 1H), 3.60 (dd, J = 11.8, 3.2 Hz, 1H), 2.59 (s, 3H), 1.98 (dt, J = 13.3, 4.1 Hz, 1H), 1.47 (br s, 3H), 1.19 ppm (br s, 6H).
^{13}C NMR (101 MHz, $CDCl_3$): δ= 197.7, 154.7, 150.4, 135.9, (128.8) 128.6, 125.7 (125.5), 80.0, 69.6, 60.1, 55.9, 45.1, (28.4) 28.1, 26.6 ppm.
HRMS (ESI): m/z calcd. for $C_{14}H_{20}N_2O_2$: 305.1627, found: 328.1527 [$(M+Na)^+$].

*tert-Butyl 2-(4-acetylphenyl)-4-hydroxy-pyrrolidine-1- carboxylate (**18**)*

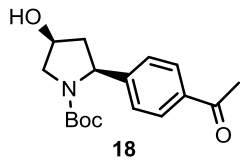

18

The product was prepared according to general procedure B; t_R = 30 min, T = 40 °C. Yield: 6 mg (10%).

^{1}H NMR (400 MHz, $CDCl_3$): δ= 7.91 (d, J = 8.3 Hz, 2H), 7.29 (d, J = 8.1 Hz, 3H), 4.86–5.25 (m, 1H), 4.51 (br s, 1H), 3.66–4.09 (m, 2H), 2.60 (s, 3H), 2.42 (br dd, J = 12.7, 6.7 Hz, 1H), 1.93 (ddd, J = 13.4, 8.8, 4.4 Hz, 1H), 1.84 (br s, 1H), 1.44 (br s, 2H), 1.14 ppm (br s, 6H);
^{13}C NMR (101 MHz, $CDCl_3$): δ= 197.7, 154.7, 150.4, 135.9, (128.8) 128.6, 125.7 (125.5), 79.9, 69.7, 60.0, 55.9, 45.1, (28.43) 28.1, 26.6 ppm.
HRMS (ESI): m/z calcd. for $C_{14}H_{20}N_2O_2$: 305.1627, found: 328.1527 [$(M+Na)^+$].

*1-(4-Tetrahydrofuran-2-ylphenyl) ethanone (**19**)*

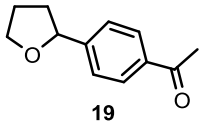

19

The product was prepared according to general procedure B; t_R = 30 min, T = 60 °C. Yield: 13 mg (34%).

^{1}H NMR (400 MHz, $CDCl_3$): δ= 7.93 (d, J = 8.3 Hz, 2H), 7.43 (s, 2H), 4.92–4.99 (m, 1H), 4.05–4.16 (m, 1H), 3.93–4.00 (m, 1H), 2.60 (s, 3H), 2.33–2.42 (m, 1H), 1.97–2.06 (m, 2H), 1.73– 1.83 ppm (m, 1H).
^{13}C NMR (126 MHz, $CDCl_3$): δ= 153.1, 150.3, 128.5, 128.3, 126.4, 125.6, 80.1, 69.5, 68.9, 37.5, 34.7, 26.9, 26.0, 25.0.
HRMS (ESI): m/z calcd. for $C_{12}H_{14}O_2$: 190.0993, found: 213.0965 [$(M+Na)^+$].

Bibliography

[1] Albini, Angelo. Photochemistry: Past, Present and Future. **2016**, Springer.

[2] (a) Prier, C. K.; Rankic, D. A.; MacMillan, D. W. C. Visible Light Photoredox Catalysis with Transition Metal Complexes: Applications in Organic Synthesis. *Chem. Rev.* **2013**, *113* (7), 5322–5363; (b) Romero, N. A.; Nicewicz, D. A. Organic Photoredox Catalysis. *Chem. Rev*. **2016**, *116* (17), 10075–10166.

[3] (a) Johansson Seechurn, C. C. C.; Kitching, M. O.; Colacot, T. J.; Snieckus, V. Palladium-Catalyzed Cross-Coupling: A Historical Contextual Perspective to the 2010 Nobel Prize. *Angew. Chem. Int. Ed*. **2012**, *51* (21), 5062–5085; (b) Nicolaou, K. C.; Bulger, P. G.; Sarlah, D. Palladium-Catalyzed Cross-Coupling Reactions in Total Synthesis. *Angew. Chem. Int. Ed*. **2005**, *44* (29), 4442–4489.

[4] Shaw, M. H.; Twilton, J.; MacMillan, D. W. C. Photoredox Catalysis in Organic Chemistry. *J. Org. Chem.* **2016**, *81* (16), 6898–6926.

[5] Zuo, Z.; Ahneman, D. T.; Chu, L.; Terrett, J. A.; Doyle, A. G.; MacMillan, D. W. C. Merging Photoredox with Nickel Catalysis: Coupling of -Carboxyl Sp3-Carbons with Aryl Halides. *Science.* **2014**, *345* (6195), 437–440.

[6] Morgenthaler, M.; Schweizer, E.; Hoffmann-Röder, A.; Benini, F.; Martin, R. E.; Jaeschke, G.; Wagner, B.; Fischer, H.; Bendels, S.; Zimmerli, D.; et al. Predicting and Tuning Physicochemical Properties in Lead Optimization: Amine Basicities. *ChemMedChem*. **2007**, *2* (8), 1100–1115.

[7] (a) Tsukamoto, T. Tough Times for Medicinal Chemists: Are We to Blame? *ACS Med. Chem. Lett.*, **2013**, *4* (4), 369–370; (b) Walters, W. P.; Green, J.; Weiss, J. R.; Murcko, M. A. What Do Medicinal Chemists Actually Make? A 50-Year Retrospective. *J. Med. Chem.* **2011**, *54* (19), 6405–6416.

[8] (a) Knowles, J. P.; Elliott, L. D.; Booker-Milburn, K. I. Flow Photochemistry: Old Light through New Windows. *Beilstein J. Org. Chem*. **2012**, 8, 2025–2052; (b) Cambié, D.; Bottecchia, C.; Straathof, N. J. W.; Hessel, V.; Noël, T. Applications of Continuous-Flow Photochemistry in Organic Synthesis, Material Science, and Water Treatment. *Chem. Rev*. **2016**, 117, 10276–10341; (c) Su, Y.; Straathof, N. J. W.; Hessel, V.; Noël, T. Photochemical Transformations Accelerated in Continuous-Flow Reactors: Basic Concepts and Applications. *Chem. Eur. J*. **2014**, 20 (34), 10562–10589; (d) Noël Timothy. Organometallic Flow Chemistry. **2016**, Springer.

[9] (a) Malet-Sanz, L.; Susanne, F. Continuous Flow Synthesis. a Pharma Perspective. *J. Med. Chem*. **2012**, *55* (9), 4062–4098; (b) Rasheed, M.; Wirth, T. Intelligent Microflow: Development of Self-Optimizing Reaction Systems. *Angew. Chem. Int. Ed.* **2011**, *50* (2), 357–358; Wegner, J.; Ceylan, S.; Kirschning, A. Ten Key Issues in Modern Flow Chemistry. *Chem. Commun.* **2011**, *47* (16), 4583.

[10] (a) Newman, S. G.; Jensen, K. F. The Role of Flow in Green Chemistry and Engineering. *Green Chem.* **2013**, *15* (6), 1456; (b) Wiles, C.; Watts, P. Continuous Flow Reactors: A Perspective. *Green Chem.* **2012**, *14* (1), 38–54; (c) Ley, S. V. On Being Green: Can Flow Chemistry Help? *Chem. Rec.* **2012**, *12* (4), 378–390.

[11] Beatty, J. W.; Douglas, J. J.; Miller, R.; McAtee, R. C.; Cole, K. P.; Stephenson, C. R. J. Photochemical Perfluoroalkylation with Pyridine N-Oxides: Mechanistic Insights and Performance on a Kilogram Scale. *Chem* **2016**, *1* (3), 456–472.

[12] Lima, F.; Kabeshov, M. A.; Tran, D. N.; Battilocchio, C.; Sedelmeier, J.; Sedelmeier, G.; Schenkel, B.; Ley, S. V. Visible Light Activation of Boronic Esters Enables Efficient Photoredox C(Sp2)–C(Sp3) Cross-Couplings in Flow. *Angew. Chem. Int. Ed.* **2016**, *55* (45), 14085–14089.

[13] (a) Alcázar, J.; Diels, G.; Schoentjes, B. Reproducibility across Microwave Instruments: First Example of Genuine Parallel Scale up of Compounds under Microwave Irradiation. *QSAR Comb. Sci.* **2004**, *23* (10), 906–910; (b) Alcázar, J. Reproducibility across Microwave Instruments: Preparation of a Set of 24 Compounds on a Multiwell Plate under Temperature-Controlled Conditions. *J. Comb. Chem.* **2005**, *7* (3), 353–355.

[14] For Further Information about Instrument Used Visit the Web: <www.Vapourtec.Com>.

[15] Zhang, X.; Zhang, J.; Zhang, L.; Feng, J.; Xu, Y.; Yuan, Y.; Fang, H.; Xu, W. Design, Synthesis and Biological Evaluation of Novel 1,2,3,4- Tetrahydroisoquinoline-3-Carboxylic Acid Derivatives as Aminopeptidase N/CD13 Inhibitors. *Bioorganic Med. Chem.* **2011**, *19* (20), 6015–6025.

[16] Wang;, H. L. P. M. Z. P. 2-Substituted (S)-2-(3,3-Dimethyl-1-Oxo-10,10a-Dihydroimidazo[1,5-b]Isoquinolin-2(1H,3H,5H)-Yl)Acetic Acids: Conformational Prediction, Synthesis, Anti-Thrombotic and Vasodilative Evaluation. *Bioorg. Med. Chem.* **2011**, *19* (2), 871–882.

[17] Claridge, Timothy D. W. High-Resolution NMR Techniques in Organic Chemistry. **2016**, Elsevier Science.

[18] (a) Bodenhausen, G.; Ruben, D. J. Natural Abundance Nitrogen-15 NMR by Enhanced Heteronuclear Spectroscopy. *Chem. Phys. Lett.* **1980**, *69* (1), 185–189; (b) Chevelkov, V.; Chen, Z.; Bermel, W.; Reif, B. Resolution Enhancement in MAS Solid-State NMR by Application of 13C Homonuclear Scalar Decoupling during Acquisition. *J. Magn. Reson.* **2005**, *172* (1), 56–62.

[19] Löwe, H.; Hessel, V.; Löb, P.; Hubbard, S. Addition of Secondary Amines to α,β-Unsaturated Carbonyl Compounds and Nitriles by Using Microstructured Reactors. *Org. Process Res. Dev.* **2006**, *10* (6), 1144–1152.

Chapter 4

Visible-Light-Induced Nickel-Catalyzed Negishi Cross-Couplings by Exogenous Photosensitizer-Free Photocatalysis

This chapter is based on:

Abdiaj, I., Fontana, A., Gomez, M. V., De la Hoz, A., Alcazar, J. Visible Light-Induced Nickel-Catalyzed Negishi Cross-Coupling. By Exogenous-Photosensitizer-free Photocatalysis. *Angew. Chem. Int. Ed.* (2018). doi:10.1002/anie.201802656

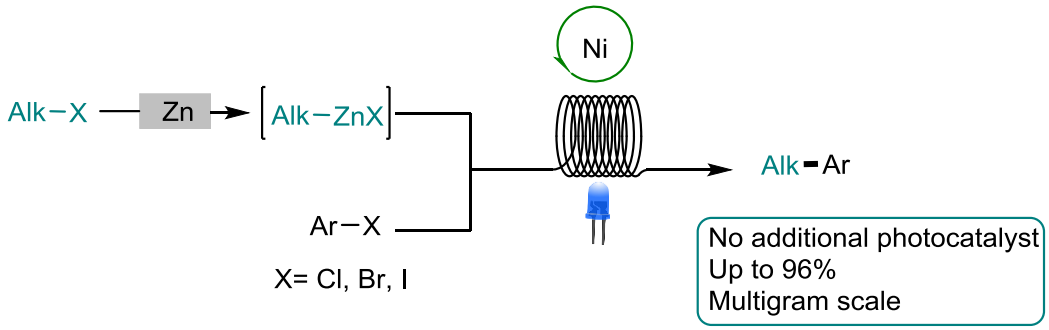

4.1 Introduction on transition metal catalysis

The development of transition-metal-mediated cross-coupling chemistry for carbon–carbon bond formation has changed the way in which organic synthesis is carried out. These transformations allow the substitution of an aryl, vinyl and alkyl halide/pseudo halide by a nucleophile in the presence of a transition metal catalyst. Usually the mechanism of cross-coupling reactions is described in 3 steps: 1. oxidative addition of an electrophilic carbon-heteroatom bond into the low valent transition metal 2. transmetalation or displacement of a heteroatom leaving group by the nucleophilic partner, and 3. reductive elimination to form the new C-C bond (Figure 4.1).

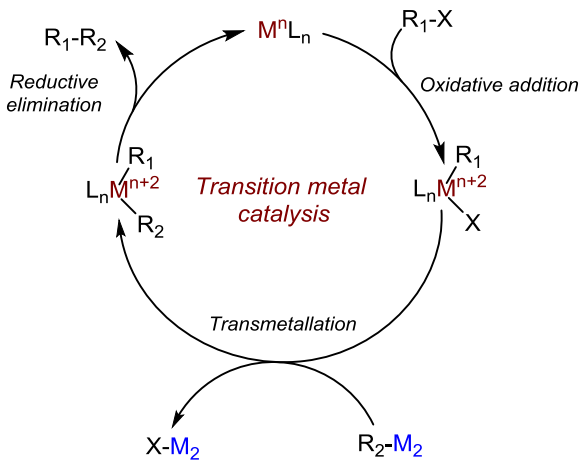

Figure 4.1: General mechanism for transition metal catalysis

Most commonly these reactions involve the formation of a carbon-carbon bond utilizing a range of different carbon nucleophiles such as aryl, vinyl and alkyl derivatives of magnesium (Kumada-Corriu), boron (Suzuki-Miyaura), zinc (Negishi), silicon (Hiyama), tin (Stille-Migita-Kosugi).[1] C-C bond formation methods have impacted the chemical industry, especially useful in the pharmaceutical one for the synthesis of biologically active molecules.[1b,2] Therefore, considering the scientific and societal impact, the Nobel prize in chemistry in 2010 was awarded to professor Negishi, professor Suzuki and Professor Heck for palladium catalyzed cross-couplings.

In Negishi type cross-coupling, simultaneously with the Pd variants, was reported even the use of Ni-complexes. Ni-catalyzed variants have demonstrated to be quite powerful on broad substrate types. Moreover, nickel is more cost effective and more abundant in nature. Nickel metal cost roughly $1.20/mol, whereas palladium is precious metal which demands a significantly higher price of $1500/mol.[3] Thus, unless a process is viable with very low levels of Pd, or very high levels of Ni are required, a Ni catalyzed approach would be preferred on cost bases.

In 2001, the Yang group reported Pd-catalyzed cross-coupling reactions of arene and vinyl sulfonates with organozinc to produce 4-substituted coumarines.[4] Switching from Pd to Ni resulted in the coupling of organozinc reagents with vinyl phosphates and a new serie of 4-substituted were obtained. Substrates with basic nitrogen substituents have showed no reactivity in Pd catalyzed Negishi in general. The Knochel group reported in a Ni-catalyzedprotocol for aminoalkylations of arenes.[5] The alkylzinc reagent was prepared in situ using as precursors the corresponding lithium salt of amino alkyl Grignard treated with $ZnBr_2$. Subsequently, $Ni(acac)_2$/DPEPhos-catalyzed cross-coupling with an aryl or a heteroaryl (pseudo)halides introduced the aminoalkyl moiety into the arene system.

In 2009, Terao group developed a Ni-catalyzed regioselective three-component coupling of alkyl halides, arylalkynes, or enynes with R–M (M = MgX', ZnX').[6] Mechanistically, it was proposed that $Ni(acac)_2$ reacts with R-M to generate the zero valent complex (**a**) that further reacts with R-M to form the nickelate complex (**b**). This nickelate complex acts as an active electron-transfer reagent. Electron transfer from (**b**) to the alkyl halide results in the formation of an alkyl radical, along with the concomitant generation of the nickel(I) complex (**c**), the resulting alkyl radical adds to the terminal carbon of the arylalkynes to yield the vinyl radical intermediate (**d**). The combination of (**c**) with (**d**) affords the vinyl-Ni-R intermediate (**e**), which then undergoes reductive elimination to afford the three-component coupling product along with (**a**) to complete the catalytic cycle and afford the product (Figure 4.2).

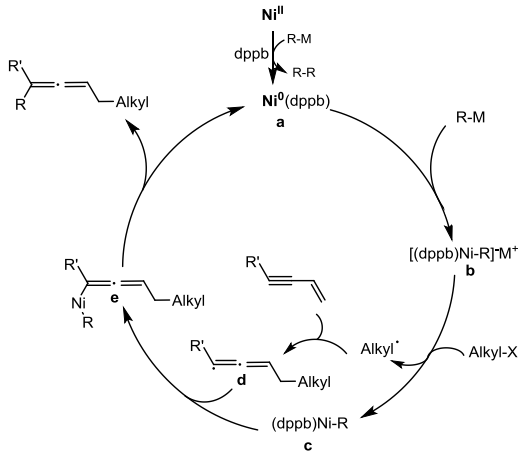

Figure 4.2: Nickel catalyzed three-component coupling

Despite all these advances the coupling of $C(sp^3)$ still remains challenging. In the last five years, with the advent of dual catalysis, metallophotoredox catalysis has opened new avenues to C-C bond formation.[7] Nickel has proved to be the catalyst of choice of most

metallophotoredox reactions. The early transition metal Ni can be found in 0, +2, as well as +1 and +3 oxidation states making it more nucleophilic and able to engage SET and radical capture mechanism.[3,8]

The first example of photoredox catalysis combined with transition metal catalysis was reported by Osawa in 2007.[9] He reported that the efficiency of Pd catalyzed Sonogashira reaction was significantly increased by the presence of the [Ru(bpy)]$(PF_6)_2$ and visible light. Nevertheless, only 4 years later, the role of the catalyst was elucidated as a result of the work of Sanford and coworkers in a seminal report. In the aforementioned report, they describe directed C-H arylations using aryl diazonium salts as coupling partners in a dual photoredox Pd catalysis under CFL bulb irradiation (Figure 4.3).[10]

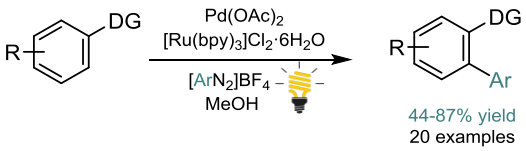

Figure 4.3: Sanford Photoredox Pd-catalyzed C-H arylation

The number of cross-coupling protocols that have been developed based on this finding has increased significantly in the last fifteen years demonstrating its broad applicability and versatility.

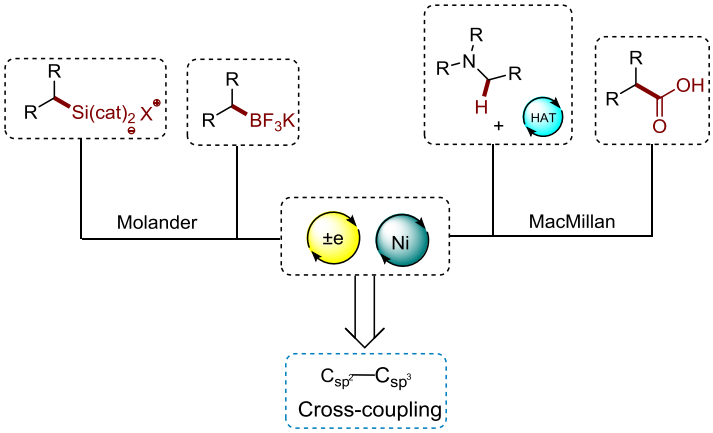

Figure 4.4: Radical coupling precursors in dual catalysis

Molander, for example, uses trifluoroborates salts as radical precursors in dual Ruthenium-Nickel catalysis for the coupling of benzylic[11], secondary alkyl[12], alfa alkoxy[13] and alfa amino radicals[14] (Figure 4.4). Moreover, to further broad the scope of the reaction with primary and secondary unstabilized radicals the same group reported in a second article the use of silicates as radical precursors.[15] The silicate derivatives undergo oxidation and generation of the C-centered radical without the need of a base or even mildly acidic conditions. As such, unprotected amines, can be incorporated directly using ammonium silicate precursors in this cross-coupling protocol. MacMillan by the other

hand uses carboxylic acid as radical precursors[16] or combines metallophotoredox catalysis with hydrogen atom transfer (HAT) processes for direct C-H activation[17] (Figure 4.4).

However, in the aforementioned examples the photocatalysts used are based on rare metals, such as ruthenium or iridium, rendering these procedures less sustainable and less suitable in terms of scalability.

In 2016, Baran and co-workers reported the use of organozinc derivatives in combination with light for C(sp^3)-C(sp^2) couplings but, as reported by the authors, the reaction is a purely thermal process, and light did not add value to the reaction.[18] Beyond this article, there are no other reports on the use of organozinc reagents in a photochemical reaction to date. Considering the lack of knowledge on the behaviour of these intermediates in photochemical processes and given our experience in organozinc chemistry,[19] we decided to explore the use of these reagents in dual catalysis as a replacement of other, previously reported organometallic reagents.[20]

4.2 Optimization of the conditions

Initially, we selected methyl 4-bromobenzoate (**2**) and benzylzinc bromide (**1**) as coupling partners, and conducted the reaction in the presence of 1 mol% of an iridium photocatalyst and 10 mol% of a nickel cross-coupling catalyst in a batch setup. We obtained clear evidence for the formation of the expected product in the crude mixture. In parallel we tried different nickel catalysts, Ni^0 precursors and Ni^{II} but the best result was obtained with nickel chloride glyme using 4,4'-Di-tert-butyl-2,2'-dipyridyl (dtbbpy) as ligand (Table 4.1).

Table 4.1: Screening of Nickel catalysts. Parallel batch reactions.

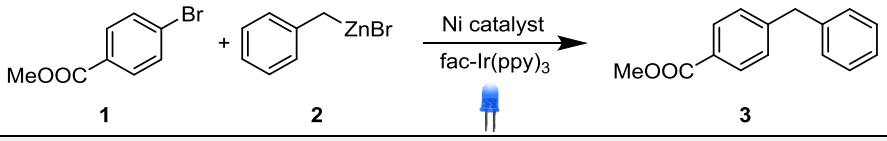

1 **2** **3**

Entry	Nickel catalyst	Conversion(%)
1	$NiCl_2$ glyme + dtbbpy	65
2	Ni(cod) + dtbbpy	58
3	Ni(cod)	26
4	Ni(acac)	34

Reaction conditions: The reactions were run in parallel in batch in a 24 vials Lumidox photoreactor preparing 1 mL of reaction mixture for each vial; methyl 4-bromobenzoate (1 eq., 0.1 mmol); benzylzinc bromide (2 eq., 0.2 mmol); $NiCl_2$ glyme (0.1 eq., 0.01 mmol); dtbbpy (0.03 eq., 0.003 mmol); fac-Ir(ppy)$_3$ (0.01 eq., 0.001 mmol).

Photochemical reactions are often enhanced by flow designs,[21] and we therefore decided to apply this technology to further optimize this finding. Taking into account the solubility issues of $NiCl_2$ solvents such as dimethylformamide (DMF), dimethylsulfoxide (DMSO) and dimethylacetamide (DMA) were added as additives to THF to avoid clogging of the reactor. In an equivalent mixture THF/DMF (Table 4.2, entry 1) the conversion in P decreases to 45%. Decreasing the percentage of the DMF in the mixture to 10% full conversion was achieved (Table 4.2, entry 3). Changing DMF with DMSO the conversion decreases to 65% and with DMA the reaction is completely blocked (Table 4.2, entry 4 and 5). (Table 4.2; entry 3). As anticipated, with the right solvent mixture a higher conversion was achieved in flow than in the batch process.

Table 4.2: Transfer of the conditions from batch to flow. Solvent screening.

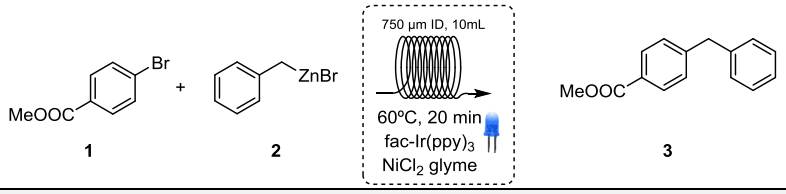

Entry	Solvent	Conversion (%)
1	THF/DMF (5/5)	45
2	THF/DMF (8/2)	60
3	THF/DMF (9/1)	100
4	THF/DMSO (9/1)	65
5	THF/DMA (9/1)	0

Reaction conditions: Methyl 4-bromobenzoate (1 eq., 0.2 mmol); benzylzinc bromide (2 eq., 0.4 mmol); $NiCl_2$ glyme (0.1 eq., 0.04 mmol); dtbbpy (0.3 eq., 0.06 mmol); fac-Ir(ppy)$_3$ (0.01 eq., 0.002 mmol)

Afterwards, control reactions were carried out to determine whether this process was driven by temperature or light. To our surprise, while irradiation was essential for the reaction (Table 4.3, entry 3), the use of a photocatalyst was not (entry 2). A temperature of 60 °C was required to achieve full conversion (entry 4). Even in the flow procedure $NiCl_2$ glyme (1) confirmed the results of the batch experiments, giving better conversion than Ni(COD) (2) (Table 4.3, entries 4 and 5). The percentage of nickel catalyst was reduced to 2% maintaining full conversion in P (Table 4.3, entry 9) Furthermore, we tried to reduce the organozinc equivalents to lower than 2 however this attempt was not successful (Table 4.3, entries 11 and 12). These optimization experiments were carried out with the commercial available benzyl zinc bromide.

The use of our flow procedure for the formation of the organozinc derivative,[19b] instead of the commercially available reagent, also led to full conversion; however, in the absence of light, the conversion was still 78% (Table 4.3, entry 14), implying that the

thermally driven process is much more significant for our zincate reagent than for the commercial one.

Table 4.3: Optimization of the conditions

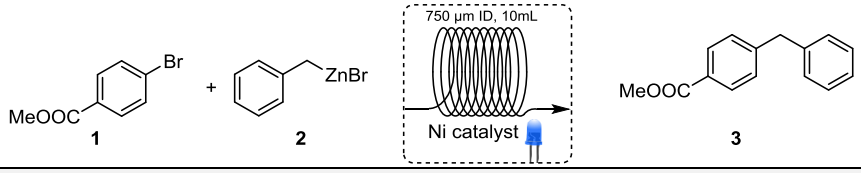

Entry	Time (min)	Temp. (°C)	Ni Catalyst*	Ir Catalyst	Irradiation	Equiv. R-Zn	Conv. (%)
1	20	40	(1) 10 mol%	1 mol%	On	2	64
2	20	40	(1) 10 mol%	-	On	2	75
3	20	40	(1) 10 mol%	1 mol%	Off	2	4
4	20	60	(1) 10 mol%	-	On	2	100
5	20	60	(2) 10 mol%	-	On	2	40
6	10	60	(1) 10 mol%	-	On	2	80
7	15	60	(1) 10 mol%	-	On	2	100
8	20	60	(1) 5 mol%	-	On	2	100
9	20	60	(1) 2 mol%	-	On	2	100
10	20	60	(1) 1 mol%	-	On	2	70
11	20	60	(1) 2 mol%	-	On	1.7	
12	20	60	(1) 2 mol%	-	On	1.5	
13	20	60	(1) 2 mol%	-	On	2[a]	100
14	20	60	(1) 2 mol%	-	Off	2[a]	78

*(1) = $NiCl_2$ glyme+dtbbpy; (2) = $Ni(COD)_2$+dtbbpy
Reaction conditions: Methyl 4-bromobenzoate (1 eq., 0.2 mmol); benzylzinc bromide (2 eq., 0.4 mmol); Nickel catalyst (0.02 eq., 0.004 mmol); dtbbpy (0.03 eq., 0.006 mmol).

Therefore, to reduce the effect of the thermal component of the reaction, we selected 4-bromoanisole as the coupling partner, a substrate that has not been used in nickel-catalyzed Negishi couplings. With the commercially available reagent, no reaction was observed (Table 4.4, entry 1). Nevertheless, by applying our flow process to generate the zincate, a conversion of 53% was achieved at a catalyst loading of 2% (Table 4.4, entry 4), and full conversion was observed when the catalyst loading was increased to 5% (Table 4.4, entry 5). The same reaction conditions in the absence of light provided the compound with 55% conversion (Table 4.4, entry 6).

Table 4.4: 4-Bromo anisole as a less reactive substrate

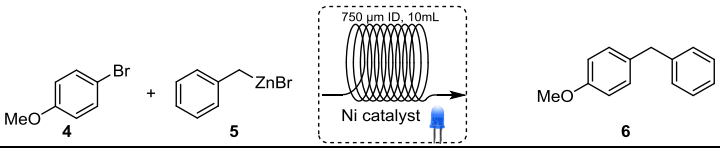

Entry	Time (min)	Temp. (°C)	Irradiation (nm)	Nickel catalyst*	Conv. (%)
1**	20	60	450	(1) 0.02 eq.	0
2	20	40	450	(1) 0.05 eq.	30
3	20	40	off	(1) 0.05 eq.	0
4	20	60	450	(1) 0.02 eq	53
5	20	60	450	(1) 0.05 eq.	100
6	20	60	off	(1) 0.05 eq.	55

*(1)= $NiCl_2$ glyme; (2)= $Ni(COD)_2$
**commercial zincate
Reaction conditions: 4-bromoanisole (1 eq., 0.2 mmol); benzylzinc bromide (2 eq., 0.4 mmol); NiCl2 glyme (0.02 eq., 0.004 mmol); dtbbpy (0.03 eq., 0.006 mmol).

Even though the difference in conversion between the purely thermal Negishi coupling and the new light-driven reaction was only 45%, we considered it sufficient to follow the conversion in flow at different time points both in the presence and absence of light (Figure 4.5). The experiment was performed in a closed system using a Vapourtec photoreactor modifying the flow rates in continuous, as soon as steady state was achieved. The outcoming solution was collected and analysed. The results are presented in Figure 4.5 and they confirm our initial statement that the reaction is accelerated in the presence of light and that this acceleration is particularly marked at the beginning of the reaction.

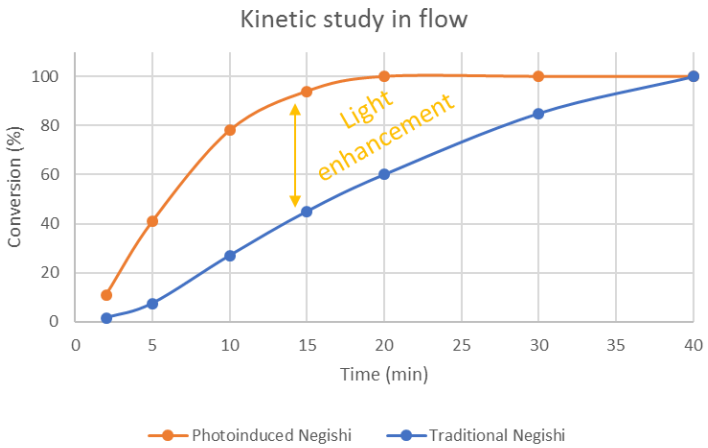

Figure 4.5: Kinetic study of the reaction in flow

4.3 Exploration of the scope of the reaction

Based on the findings outlined above, the scope of the reaction was further explored by varying both substrates (Figure 4.7). A wide range of organozinc reagents were synthetized in flow as cross-coupling partners of the halo-derivatives (Figure 4.6). Benzyl bromide analogues functionalized with ester group, trifluoromethyl group in ortho and meta, trifluoromethoxy group and nitrile group were prepared (**5**-**11**) in soultions of 0.3 M to 0.45 M in THF. 4-iodo tetrahydropyrane and cyclopentylmethyl iodide also formed the corresponding organozinc reagents **12** and **13** in 0.4 M solutions in THF.

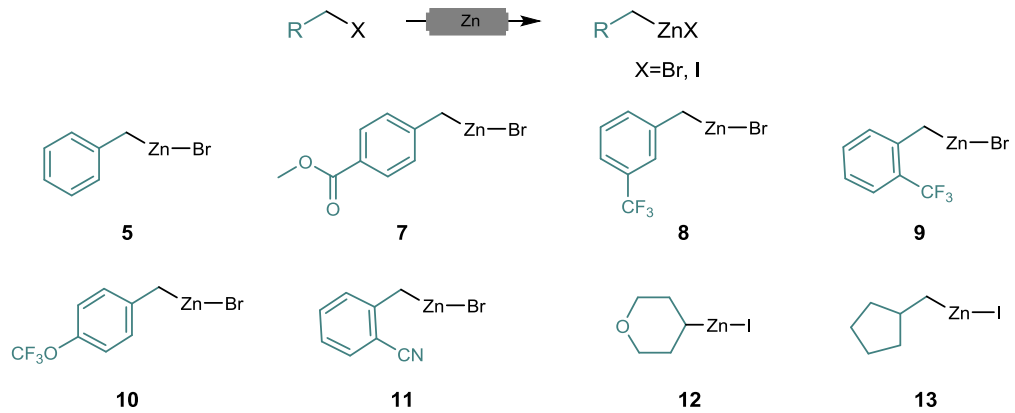

Figure 4.6: Organozinc reagents prepared in flow

Our study, regarding the haloarene partner, was focused mainly on bromo and chloroarenes as they are rarely used in nickel-catalyzed Negishi cross-couplings.[22] To obtain comparable results, the reactions were performed under the same conditions either in the presence or absence of light.

Compounds with electron-withdrawing groups required only 2 mol% of the nickel catalyst. 4-bromo anisole, not described in literature in nickel Negishi cross-couplings before, provided 96% of product **6** with light irradiation and the conversion decreased to 55% when light was turned off. Light irradiation had a particularly strong effect on the reaction when strongly electron-donating groups were present in the molecule, such as in compounds **16** and **18**, where the conversion significantly increased in the presence of light (70% and 44% isolated yield each). Iodine derivatives were also suitable substrates but a strongly electron-donating group, such as a free amino group, was required to observe significant differences between the light-irradiated and thermal reactions (e.g., compound **26**, 93% yield). The methodology proved to be compatible with different functional group such as esters, ketones, nitriles, trifluoromethyl and trifluoromethoxy group, fluorine and amines. The Boc protection group, also was well tolerated. It is interesting to notice that the steric effect of ortho substituents

trifluoromethyl group **17** and nitrile group **25** in the benzyl zinc analogues did not affect reaction and afforded the product in 80% and 53% respectively. This procedure is also applicable to different alkylzinc reagents beyond benzyl analogues, either freshly prepared or commercially available, to generate compounds such as **14**, **15**, and **20** (67% to 90% yield).

It is important to highlight the fact that chloroarenes participate in this reaction as these coupling partners have only rarely been described in literature in this context.[23] The synthesis of compound **27** clearly illustrates the value of the new method as irradiation with light was key to generate the desired product in good yield (70%) from the chloroarene. Not only chloroarenes but as well chloro heterocycles were used as coupling partners. The difference light/no light with chloroderivatives is higher. This is in line with the low reactivity of these coupling partners in traditional Negishi reaction. Increasing the challenge of the reaction, increases the value of the light irradiation. A clear example is compound **31** that is a 3-chloropyridine, very unreactive cross-coupling partner, and was possible to increase its reactivity only in the presence of light (54%). Fluorinated 2-chloropyridine also provided the product **29** in high yield (93%) and the fluorine was well tolerated.

To demonstrate the value of this method in a medicinal chemistry setting, compounds **33** and **34** were prepared, which are based on the chlorotriazolopyridine core that has previously been described in a series of compounds with activity as positive allosteric modulators of the metabotropic glutamate receptor 2. This core has never been used in Negishi cross-coupling reactions.[24] Both reactions clearly benefited from light irradiation, and the products were obtained in good to excellent yields, whereas little or no conversion was observed in the absence of light. This finding will be key to introduce C(sp^3)- enriched motifs, which are important to improve various physicochemical parameters such as the solubility.[25]

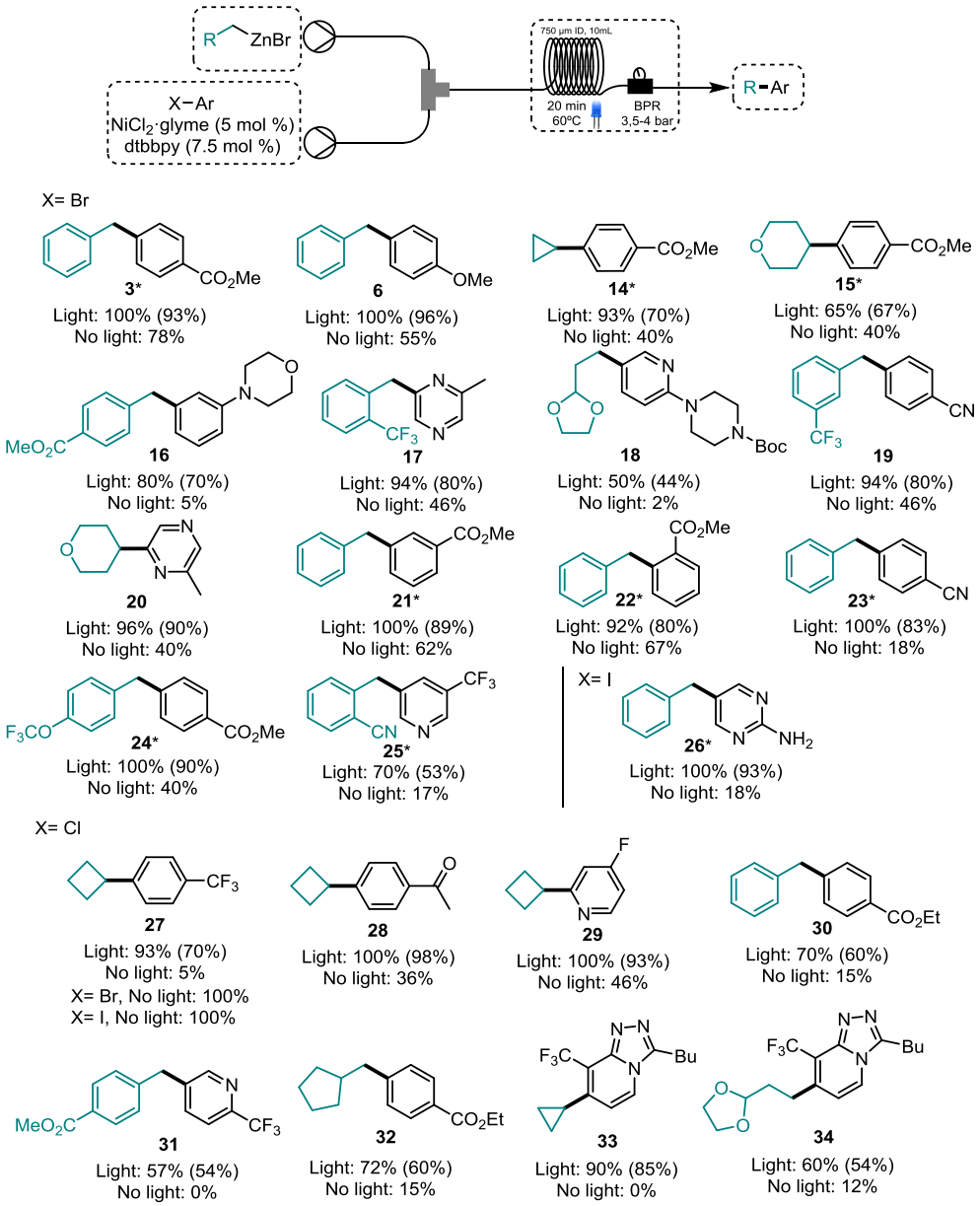

Figure 4.7: Scope of the light-induced nickel-catalyzed Negishi coupling in respect to the organozinc and haloarene coupling partners. Conversions determined by liquid chromatography. Yields of isolated products given in parentheses. a) With 2 mol% of catalyst and 3 mol% of ligand dtbbpy.

4.4 Scale up

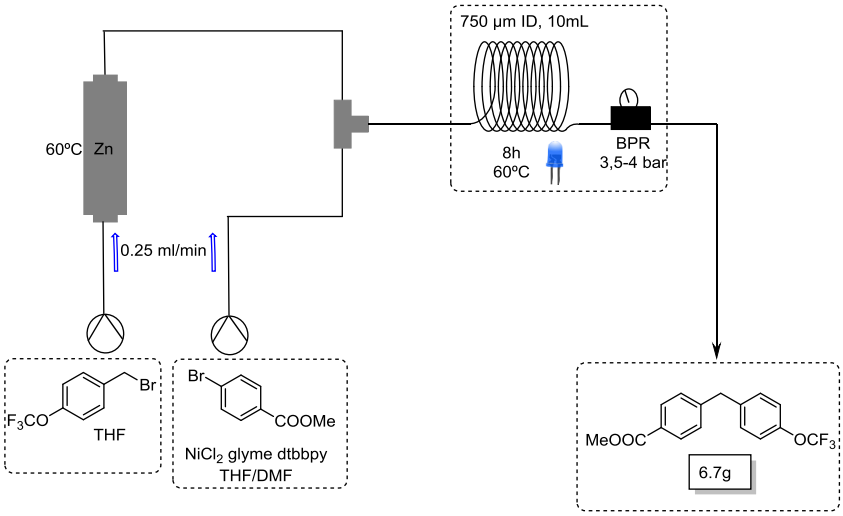

Figure 4.8: General scheme for the scale up set up.

The preparation of compound **16** was selected to demonstrate the scalability of this method. The organozinc reagent was prepared in flow, and the exiting stream was connected to a second solution stream containing the haloarene and the catalytic complex before entering the photoreactor (Figure 4.8). This process was run continuously for 8 h and compared with the same reaction in batch by sampling at different timepoints (Figure 4.9A). The flow protocol provided 6.7 g of the desired product upon isolation (93% yield), with a productivity of 800 mg/h. In contrast, in the traditional Negishi batch protocol, the product was only isolated in 39% yield. Considering the reaction times and reaction volumes, the space/time yields[26] were calculated; these clearly support the new flow process (Figure 4.9B).

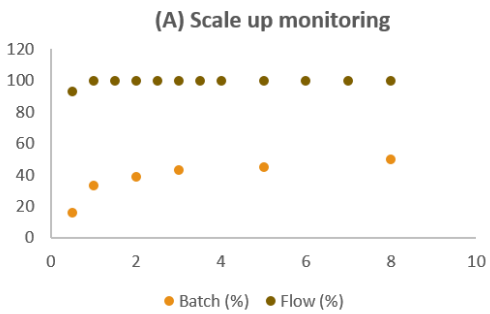

(B) Flow/Batch Comparison	Flow	Batch
Yield	93	39
Time	20 min	8 h
Throughput	800 mg/h	7.7 mg/h
Space-time Yield	40.4 mg/h·ml	1.7 mg/h·ml

Figure 4.9: (A) Monitoring of the conversion of starting material in product in time during the run in both batch and flow reactions; (B) Flow/Batch comparison.

4.5 Mechanistic investigation

4.5.1 Absorbance studies

Regarding the mechanism of the reaction, it is important to note that visible-light-induced transition-metal-catalyzed transformations are known in literature and have been recently reviewed.[27] Metals used for such reactions include cobalt, iron, copper, palladium, gold, and platinum. However, the use of nickel has not been described for this chemistry. To clarify the impact of light irradiation on the reaction, we initially recorded UV/Vis spectra for each component of the reaction and different mixtures. We only observed a broad band in the visible region when the catalytic complex was mixed with the organozinc reagent (Figure 4.10D).

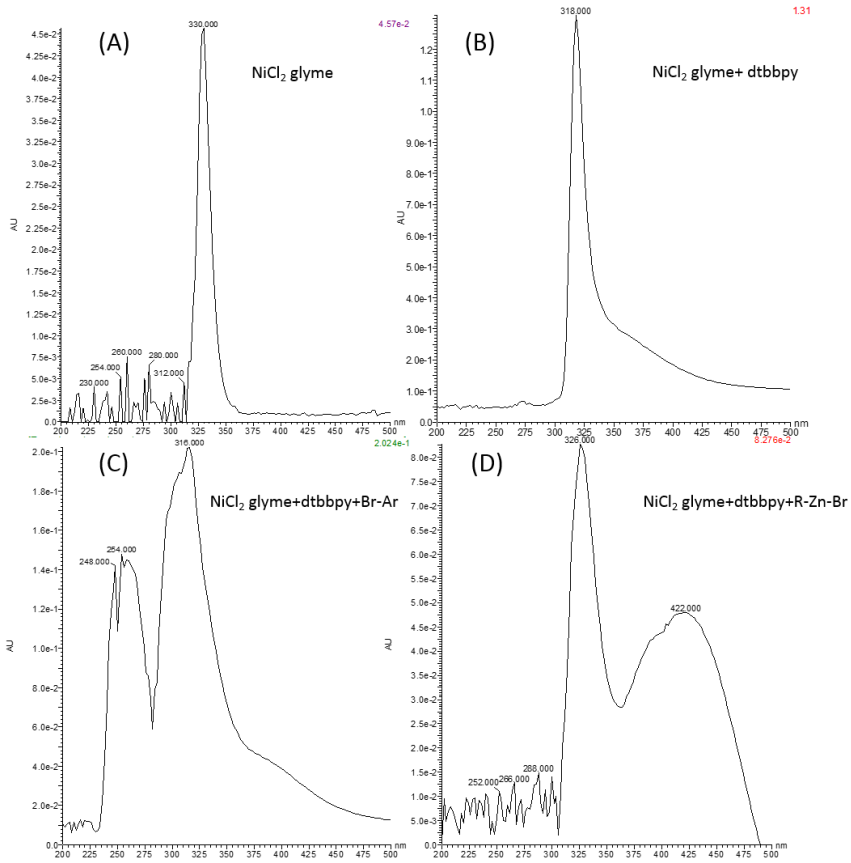

Figure 4.10: UV-visible absorbance spectra

To further study this absorbance, an injected sample was monitored for 20 min (Figure 4.11). The absorption in the visible region was observed 4 min after injection and remained stable through the duration of the study. A similar experiment was run with Ni^0 (Figure 4.11 right). When Ni^{II} ($NiCl_2$), was replaced by Ni^0 ($Ni(COD)_2$), there was no

absorption in the visible region, which demonstrates the need for nickel(II) species for light absorption. Considering the spectra shown in Figure 4.10, we studied the generation of compound **5** under irradiation at different wavelengths to determine the effect on the reaction outcome. The best conversion was achieved when the reaction mixture was irradiated at λ=450 nm (blue light). Lower conversions were achieved when the reaction was irradiated at either λ=365 nm (black light) or λ=520 nm (green light) (Table 4.5). These results are consistent with the absorption spectra.

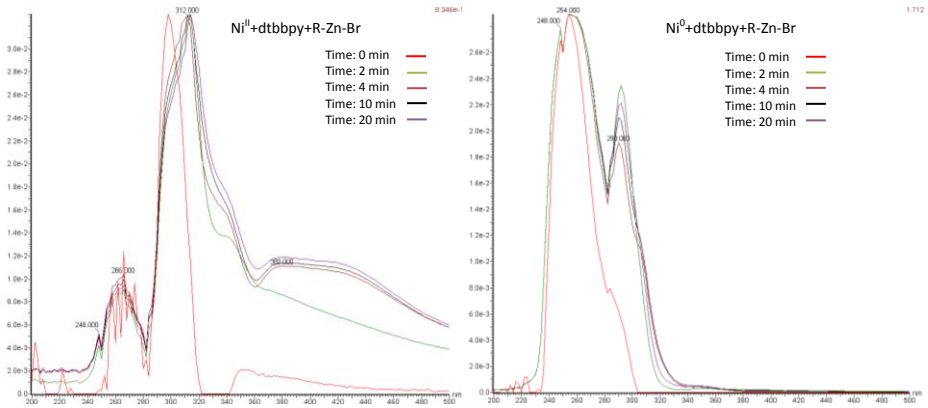

Figure 4.11: Absorption spectra of mixtures of Nickel complexes with the organozinc reagent. Evolution of absorption recorded over 20 minutes.

Table 4.5: Effect of the light source

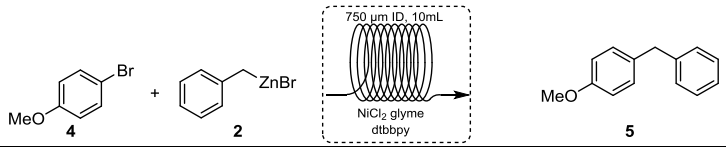

λ (nm)	dark	365	450	525
Conv. (%)	55	73	100	85

4.5.2 Radicalic reactions

Single electron transfer (SET) processes and radical formation play key roles in dual-catalytic light-induced reactions. In this respect, different reactions were carried out to detect such radicals. With TEMPO and methyl acrylate (Table 4.6, entries 3 and 6) the formation of the product was reduced, thereby obtaining the corresponding adducts P2 and P3. We can observe the same result with and without light reaction (Table 4.6, entries 4 and 7). In the absence of nickel, the TEMPO adduct was also observed (Table 4.6, entry 5). Using diphenylethylene as a radical trap (Table 4.6, entries 8 and 9) we do not observe any reactivity with the organozinc or methyl 4-bromobenzoate. In

summary, with TEMPO and methyl acrylate the reaction was quenched as a result of the reactivity of the zincate and with phenyl ethylene no trapping was observed.

Table 4.6: Radical trap reactions

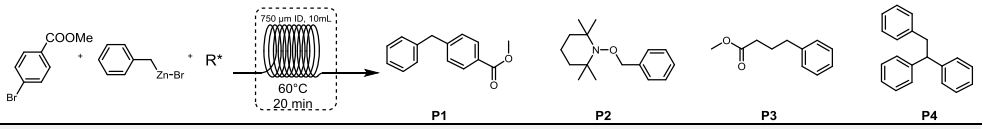

Entry	Reaction conditions	P1	P2	P3	P4
1	With light irradiation	√	×	×	×
2	Without light irradiation	√	×	×	×
3	With light + TEMPO	√	√	×	×
4	Without light + TEMPO	√	√	×	×
5	With light without Nickel catalyst + TEMPO	×	√	×	×
6	With light + Methyl acrylate	√	×	√	×
7	Without light + methyl acrylate	√	×	√	×
8	With light + diphenylethylene	√	×	×	×
9	Without light + diphenylethylene	√	×	×	×

Rearrangements of radical probes, also known as radical clocks, cannot be used in the reaction discussed here as radicals had been detected during the organozinc formation in batch.[28] To check if flow chemistry could provide a different result than that observed in batch, 6-iodohexen-1-ene **35** was prepared. This substrate was flowed to the zinc column to obtain the organozinc **36** and the solution obtained was quenched immediately with I_2 (Figure 4.12). The solvent was evaporated and the residue was analysed by NMR. In the NMR spectra of the crude presented in Figure 4.13, we observed signals of the cyclized product **38** (red circle) and linear product **37** (blue circle). The use of a flow process did not make any difference in this respect.

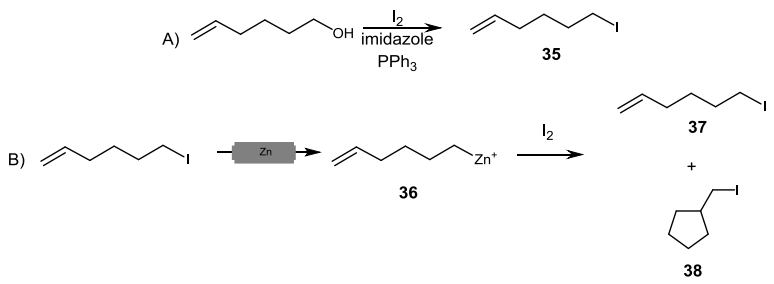

Figure 4.12: (A) Synthesis of iodohexane; (B) Formation of hex-5-enyl(iodo)zinc and quenching with iodine

None of these assays provided suitable data to support the presence of radicals during the coupling process although the absence of radicals cannot be ruled out.

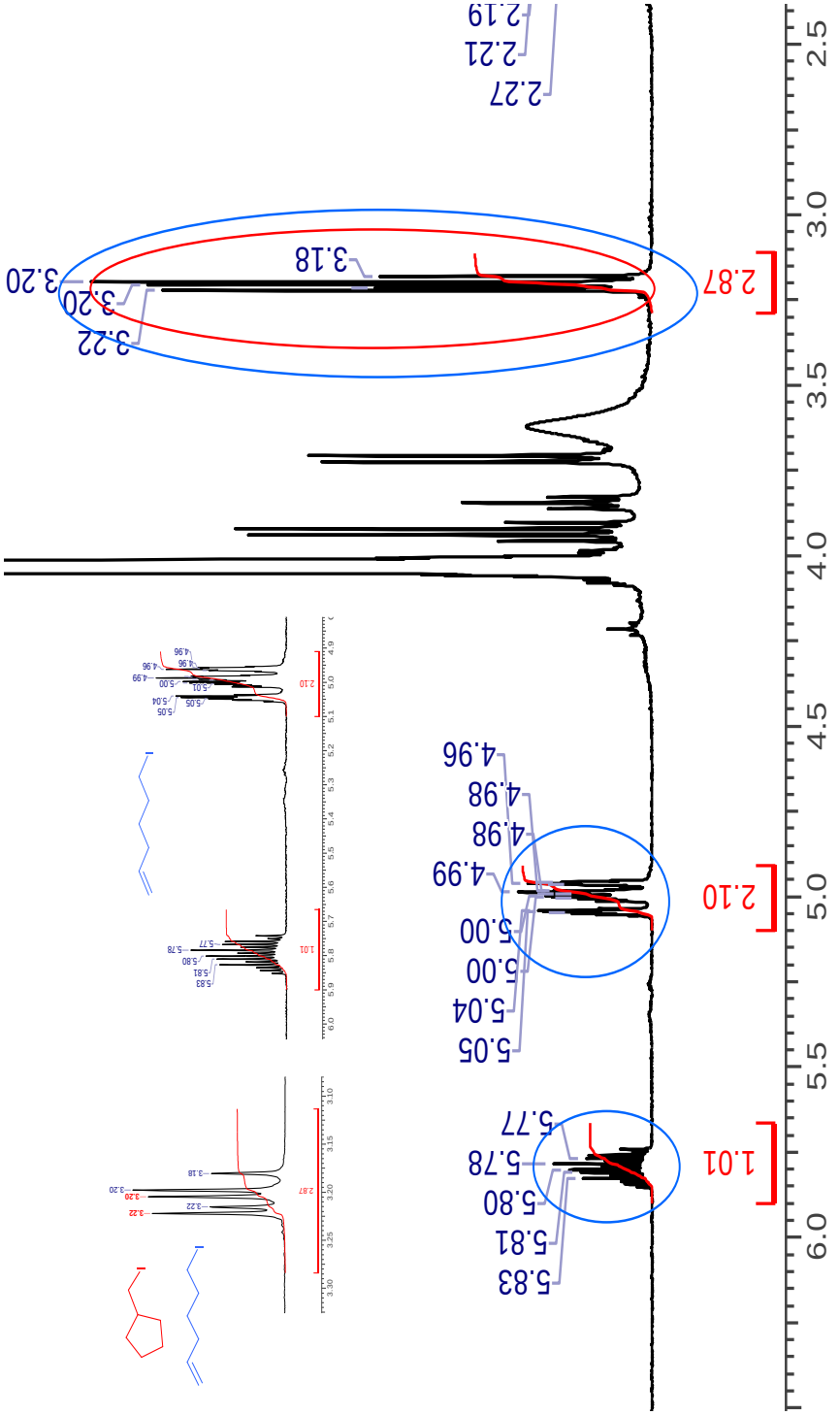

Figure 4.13: Spectra of the crude of the reaction: red circles correspond to the cyclic product; blue circles correspond to the linear product

4.5.3 NMR investigation

With the aim of shedding additional light on the mechanism of the reaction, NMR spectroscopy was employed as an analytical tool given its potential to elucidate molecular structures. The aim was to study the reaction generating compound **17** by following the signal of the trifluoromethyl group close to the reactive site by ^{19}F-NMR spectroscopy. The laser diode-based illumination device previously reported by the the group of Dr. Victoria Gomez Almargo and Prof. Antonio de La Hoz in the University of Castilla La Mancha[29] was used to activate the reaction mixture in a 5 mm NMR tube for in situ NMR monitoring.[30] The reaction mixtures were freshly prepared and transferred quickly to the 5 mm NMR tube to record the ^{19}F-NMR spectrum.

We started our investigation with the monitoring of the ^{19}F-NMR spectra of 2-(trifluoromethyl) benzyl zinc bromide (Figure 4.14). The peak corresponding to 2-(trifluoromethyl) benzyl zinc bromide is at -63.03 ppm. It is important to note that experiments in the NMR with the light probe on the top were not performed under inert atmosphere due to technical limitations. In this way, oxidation of the zincate to alcohol in the presence of oxygen[31] and subsequent second oxidation to aldehyde in the presence of Ni^{II} [32] was observed as secondary reaction, decreasing the availability of organozinc derivative to produce the target Negishi product. Due to moisture and air we can observe the presence of (2-(trifluoromethyl) phenyl) methanol (-60.30 ppm) and 1,2-bis(2 (trifluoromethyl)phenyl)ethane (-60.17 ppm).

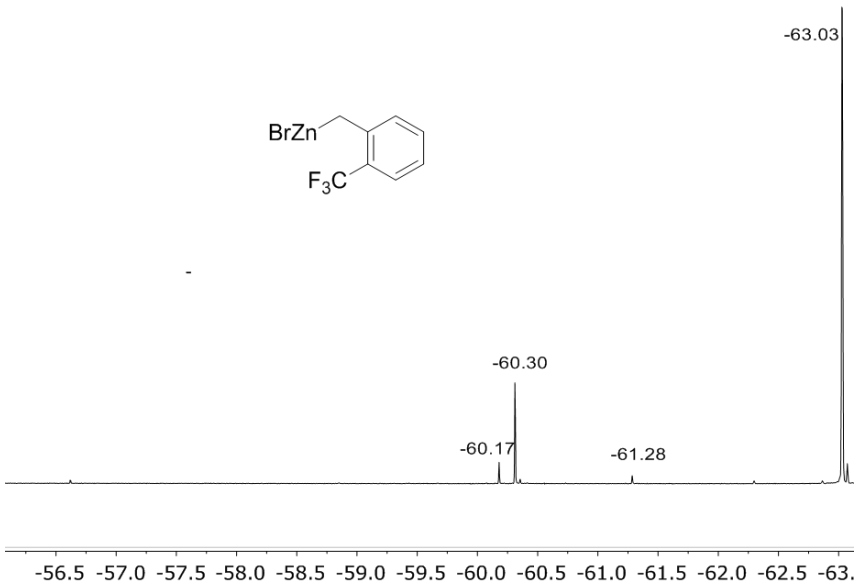

Figure 4.14: ^{19}F NMR spectrum of a freshly prepared zincate by continuous flow: (-60.17 ppm) corresponds to 1,2-bis(2-(trifluoromethyl) phenyl) ethane; (-60.30 ppm) corresponds to (2-(trifluoromethyl)phenyl) methanol. (-61.28 ppm) could not be identified; (-63.03 ppm) corresponds to the zincate derivative (2-(trifluoromethyl)benzyl) zinc(II) bromide.

To detect by NMR the photoabsorbing species in the blue region, we rapidly added equimolar amounts of a zincate derivative and the nickel complex in a NMR tube. The green solution of nickel complex was transformed immediately into a dark red solution. The same red colour was observed in the UV-visible absorption experiments when absorbance in the visible region was detected. Rapidly, the ^{19}F-NMR spectrum of the red solution was measured and the presence of a new peak at -61 ppm was observed (Figure 4.15). This new signal is deshielded and appears approximately 2 ppm downfield from the signal of the original zincate, indicating a reduction in the electron density of this reagent. The recording of consecutive NMR experiments showed that the peak increased over time and remained constant after 10 min of monitoring time. At this point, the light was switched on and the signal intensity started to decrease quickly (10-20 min), what illustrated that the consumption of this compound is clearly accelerated by light (Figure 4.16). In parallel the signal corresponding to dimer **40** clearly increased, following the same pattern.

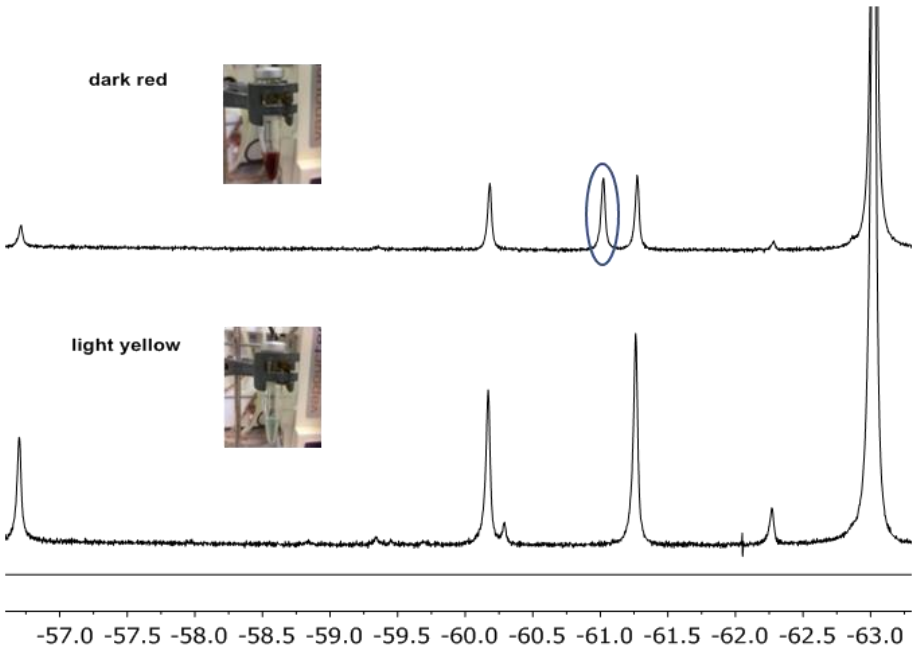

Figure 4.15: Top: ^{19}F-NMR spectrum after a quick addition of the zincate derivative over the Nickel complex. The solution turned a dark red color. Bottom: ^{19}F-NMR spectrum of the reaction mixture within time and after light irradiation. The peak at -61 ppm has disappeared and the reaction media lost its dark red color.

The dimerization of organozinc reagents from the reduction of Ni^{II} precatalyst in Ni^{0} as a first step in forming the real catalytic complex is broadly reported in literature.[6,22,23,33] One example is described in Figure 4.2. Taking into account these reports, the new peak at -61 ppm, was assigned to a complex formed when the nickel catalyst and the

organozinc compound were mixed, but its structure could not be assigned due to its short lifetime. The results from this experiment demonstrate that this step is clearly accelerated in the presence of light. Similar accelerated conversions of Pd^{II} into Pd^{0} have been observed in light-induced Heck reactions.[34]

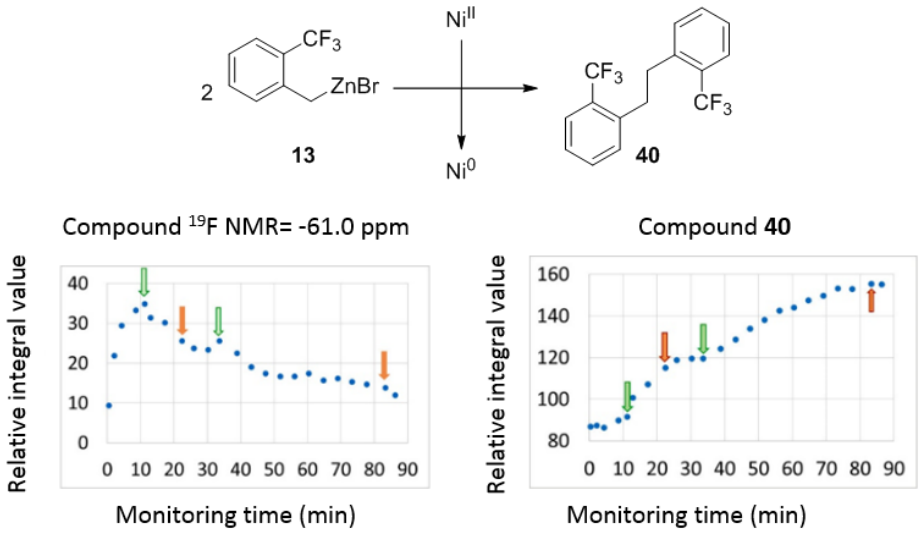

Figure 4.16: Effect of light on the degradation of an intermediate signal and in the acceleration of the formation of dimer 40. Green arrows mark when the light was turned on and orange arrows when the light was turned off.

In a second experiment, the standard reaction was performed by adding all the components at the required concentrations to a NMR tube (Figure 4.17). In the spectra (Figure 4.17A) of the no-light reaction we can observe the following signals: peak 1 (-56.63 ppm) corresponds to 2-(trifluoromethyl) benzaldehyde; peak 2 (-60.17 ppm) corresponds to 1,2-bis(2-(trifluoromethyl) phenyl) ethane; peak 3 (-60.30 ppm) corresponds to (2-(trifluoromethyl) phenyl) methanol; peak 4 (-61.28 ppm) could not be identified; peak 5 (-63.03 ppm) corresponds to the zincate derivative (2-(trifluoromethyl)benzyl) zinc(II) bromide. The NMR peak corresponding to the reaction product **17** (-60.12 ppm) is not shown up as it is not present at the initial moments of the reaction. Only after the light is switched on, we clearly see product formation increasing rapidly in time. (Figure 4.17B). We observe also that in the final moments of the reactions peak **3** disappears. The evolution of the resonance peak of the product was then followed. At the beginning of the reaction, with the light turned off, the peak of the product was increasing very slowly. When the light is turned on the slope of the curve significantly changes indicating that the quantity of the product in the reaction mixture is increasing rapidly. The correlation of the relative integral value of the product's peak 7 in time is represented in Figure 4.18.

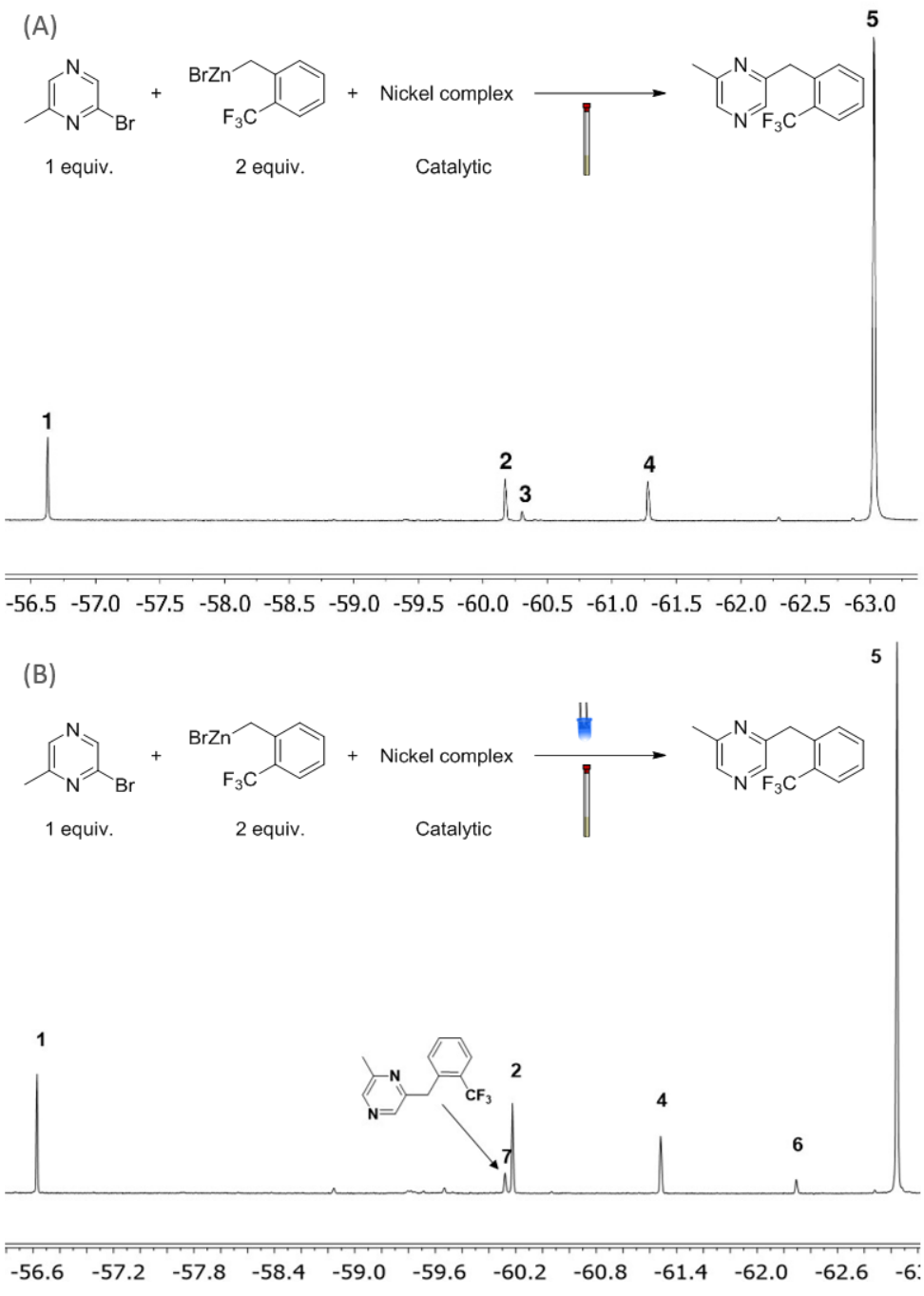

*Figure 4.17: (A)[19]F-NMR spectrum of the initial moments of the reaction for the synthesis of compound **17**: (B) [19]F-NMR spectrum of the kinetic experiment for the synthesis of compound **17.** All NMR peaks were referenced to ethyl trifluoroacetate as internal standard (-76.38 ppm).*

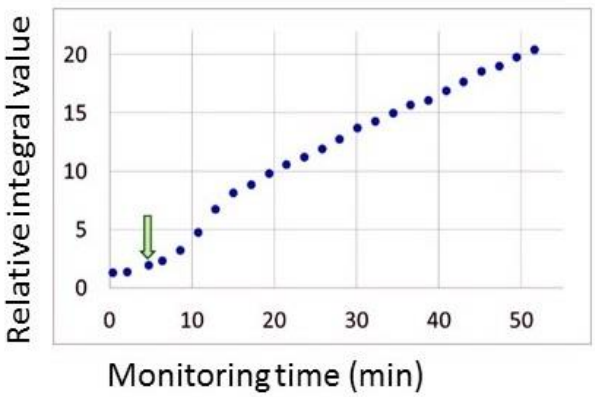

Figure 4.18: Evolution of the integral of product signal 7 over time. A clear increased is observed when the light was switched on (indicated with the green arrow), indicating the catalytic cycle is accelerated in the presence of light.

4.6 Proposed mechanism

The data obtained from these experiments are consistent with light acceleration of the overall reaction. In January 2017, MacMillan and coworkers reported a photosensitized, energy transfer mediated organometallic catalysis through exited nickel(II). Using the well-known iridium photocatalyst as an antenna for absorption of visible light, the energy transfer occurs and produces electronically exited nickel (II) species. This high energy state of the nickel catalyst promotes the reductive elimination, accelerating the reaction (Figure 4.19).

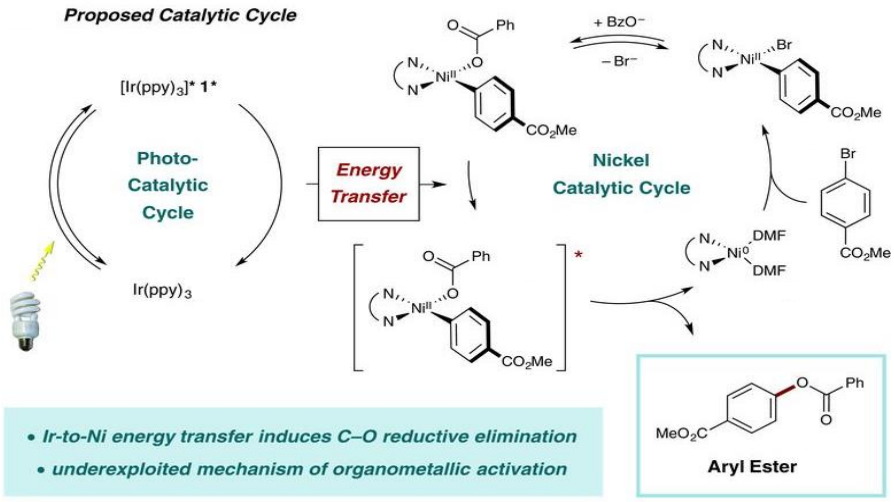

Figure 4.19: MacMillan proposed energy transfer Ni catalytic cycle

In our case, the UV/Vis spectra shown in Figure 4.10 may indicate that the strongly absorbing chromophore for the energy transfer is created in situ. The experiments suggest that direct visible light absorption is obtained when Ni and Zn are in the same solution. The disappearance of the complex formed between the two metals, when the reduction of the Ni^{II} to the Ni^{0} complex with concomitant oxidation of the zincate to the dimer **40**, is proved to be accelerated by light. Moreover, the NMR experiments showed that the product formation also is accelerated when the reaction mixture is irradiation. Therefore, we suggest that when Ni and Zn are coordinated during the transmetallation step of the catalytic cycle, we could have a second absorbing chromophore that could bring Ni(II) into electronically excited state and accelerate the reductive elimination step expelling the product (Figure 4.20). Nevertheless, further work will be required to unveil the species formed and to fully elucidate the mechanism.

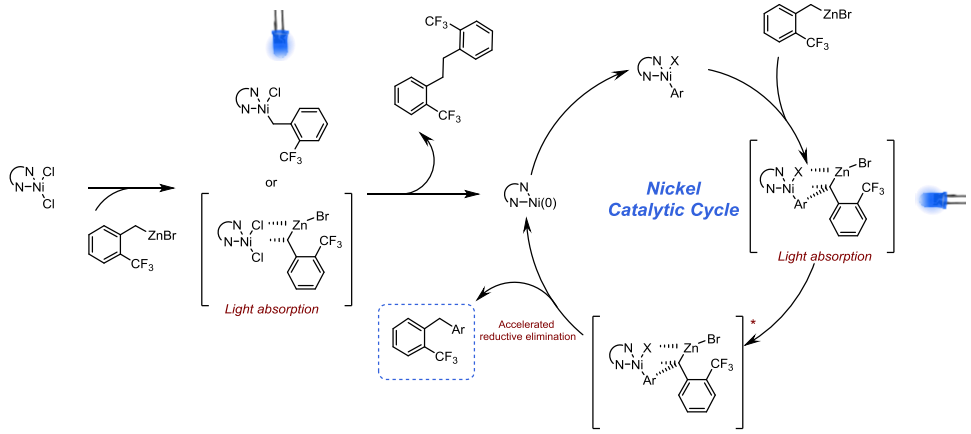

Figure 4.20: Proposed reaction mechanism

4.7 Conclusion

In conclusion, nickel-catalyzed Negishi cross-couplings can be accelerated by visible-light irradiation. This can be considered as a new photocatalytic process involving two naturally abundant metals. The use of freshly prepared organozinc derivatives in a flow process is key for the success of the reaction. The scope of the reaction is broader than that of the traditional batch Negishi and dual-catalytic reactions, especially with regard to aryl chlorides. The catalyst loading can be reduced to only 2 mol% nickel. This method provides access to new derivatives with potential value in medicinal chemistry. As the reaction is carried out in flow, direct scalability is easily achieved, and the overall approach is superior to that of the batch protocols.

Even though further work will be required to understand the mechanism in more detail, it seems that two steps of the reaction are accelerated upon light irradiation, namely

the formation of the catalyst and the catalytic cycle itself. We believe that the current findings provide new insight into photocatalysis and open new avenues within this field.

4.8 Experimental part

General information

GC measurements were performed using a 6890 Series Gas Chromatograph (Agilent Technologies) system comprising a 7683 Series injector and auto sampler, J&W HP-5MS column (20 m x 0.18 mm, 0.18 µm) from Agilent Technologies coupled to a 5973N MSD Mass Selective Detector (single quadrupole, Agilent Technologies). The MS detector was configured with an electronic impact ionization source/chemical ionization source (EI/CI). EI low-resolution mass spectra were acquired by scanning from 50 to 550 at a rate of 14.29 scan/s. The source temperature was maintained at 230 °C. Helium was used as the nebulizer gas. Data acquisition was performed with Chemstation-Open Action software. Thin layer chromatography (TLC) was carried out on silica gel 60 F254 plates (Merck) using reagent grade solvents. Unless otherwise specified, reagents were obtained from commercial sources and used without further purification. The reactions were carried out in a Vapourtec photoreactor UV-150 fixed on an E-series Vapourtec equipment. ^{1}H NMR spectra were recorded on Bruker DPX-400 or Bruker AV-500 spectrometers with standard pulse sequences, operating at 400 MHz and 500 MHz respectively. Chemical shifts are reported in parts per million (ppm) downfield from tetramethylsilane (TMS), which was used as an internal standard. All microfluidic fittings were purchased from IDEX Health and Science. The syringes were connected to the capillary using ¼-28 flat-bottom flangeless fittings. The peristaltic pumps of the Vapourtec system were used to feed liquid reagents through a high purity perfluoroalkoxyalkane (PFA) capillary tubing (I.D. = 0.75 mm) to a Tefzel® tee mixer (I.D. = 0.5 mm).

Preparation of the organozinc compounds in flow:

Activation of the Zn column:

A solution 1.0 M trimethylchlorosilane (TMSCl) and 0.24 M 1-bromo-2-chloroethane was prepared under nitrogen (N_2) atmosphere in a dried flask by dissolving 1.25 mL of TMSCl and 0.2 mL of 1-bromo-2-chloroethane in 10 mL of dried tetrahydrofuran (THF). 5 mL of this solution were passed through the Omnifit (column 100x10 mm) containing Zn (12 g) using the Vapourtec E-series system at 40 °C and 1mL/min flow rate.

General Procedure (1):

A solution of the correspondent halo derivative (1 mmol) 0.5 M in THF was passed through the column containing activated Zn using the Vapourtec E-series system at 40 °C and flow rate of 0.5 mL/min. The outcoming solution of the organozinc compound was collected in a closed flask under nitrogen (N_2) atmosphere.

Titration:

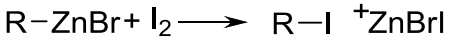

Figure 4.21: Titration reaction

Titration with I_2 was used to determine approximatively the concentration of the organozinc solution obtained. A known quantity (25 mg-30 mg approx.) of I_2 is weighted and dissolved in 0.5 mL of dry THF in a closed vial under N_2 atmosphere. The solution of the organozinc compound was added dropwise until the I_2 solution became transparent. The volume of organozinc used to titrate the I_2 was used to calculate the molarity (Equation 4.1).

$$[RZnBr](M) = \frac{W\ iodine\ (mg)}{MW\ iodine\left(\frac{mg}{mmol}\right) * V\ RZnBr\ (ml)}$$

Equation 4.1: Calculation of the molarity of the organozinc compound (W ≡ weight; MW ≡ molecular weight; V ≡ volume).

General procedure (2) for Photo Induced Nickel Negishi cross-coupling

A solution of Bromoarene (1 eq. 0.5 mmol), $NiCl_2$ glyme (0.05 eq., 0.025 mmol); dtbbpy (0.075 eq., 0.038 mmol) in THF/DMF 9/1 was mixed using a T-mixer with the corresponding solution of R-Zn prepared following General Procedure 1 in a Vapourtec UV-150 Photoreactor at 0.250 mL/min each line (t_R = 20 min; coil volume = 10 mL) at 60 °C irradiating with 450 nm blue LEDs. Due to the pressure generated in the system a variable back pressure regulator was used at the outlet of the photoreactor to maintain a stable pressure of 3.5-4 bars. The out coming solution was diluted with ethyl acetate and added to a separatory funnel containing 150 mL of ammonium chloride saturated aqueous solution.* The layers were separated and the aqueous layer was extracted with ethyl acetate (3 x 15 mL). The combined organic extracts were washed with brine, dried ($MgSO_4$) and concentrated in vacuo. Purification was carried out using flash column chromatography (silica, Ethyl acetate in Heptane) to obtain the product.

*For low boiling point compounds extraction was done with diethyl ether instead of ethyl acetate and the purification in pentane/ethyl acetate instead of heptane/ethyl acetate.

Rearrangements of radical probes

Synthesis of iodohexane and preparation of the organozinc in flow (

Figure 4.12)

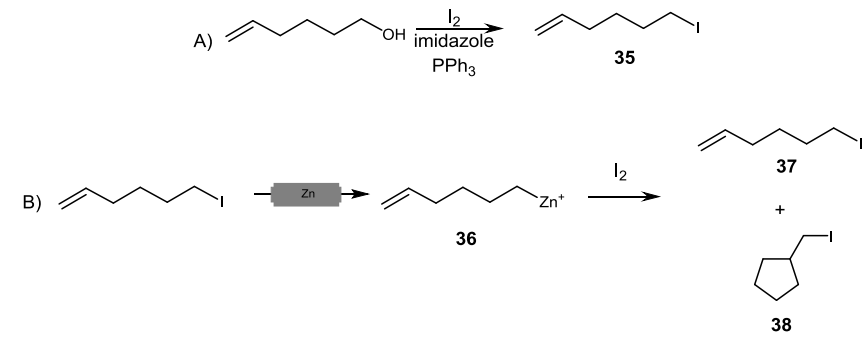

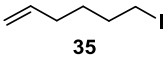

6-iodohex-1-ene

A) Preparation of **35**: I_2 (1.2 eq.; 12 mmol) was added portionwise to a solution of 5-hexen-1-ol (1 eq.; 10 mmol), imidazole (1.5 eq.; 15 mmol) and triphenyl phosphine (PPh_3) (1.2 eq.; 12 mmol) in THF (18 mL) at 0 °C (ice bath). The mixture was stirred for 1 h. at rt. The excess of I_2 was quenched with a solution 10% $Na_2S_2O_3$ in water. The mixture was extracted with ethyl acetate, the organic layer was separated, dried (Na_2SO_4), filtered and the solvent evaporated. The residue was purified by column chromatography (Silica, Pentane 100%). Desired fractions were collected and the solvent evaporated to obtain **36** as a transparent liquid (67% yield).

^{1}H NMR ($CDCl_3$, 500 MHz): δ = 5.79 (ddt, J = 17.0, 10.2, 6.6 Hz, 1H), 4.94-5.05 (m, 2H), 3.19 (t, J = 7.1 Hz, 2H), 2.03-2.13 (m, 2H), 1.84 (dt, J = 14.8, 7.2 Hz, 2H), 1.47-1.56 ppm (m, 2H)

B) **35** was passed through the zinc column following General procedure 1 to obtain the organozinc solution **36** that was collected over iodine in order to provide the mixture of both iodo compounds **37** and **38** (ratio 5:1).

Influence of the light irradiation

Two solutions: the first one of 4-bromoanisole, $NiCl_2$ glyme and dtbbpy in THF and DMF (9/1); the second one of benzyl bromide zincate were prepared and were passed through a Vapourtec photoreactor UV-150 irradiating with 450 nm LEDs in a 10 mL coil using different flow rates and analyzing the sample at the stationary state by LCMS:

- Flow rate 2.5 mL/min residence time 2 min: 11% P

- Flow rate 1 mL/min residence time 5 min: 41% P
- Flow rate 0.5 mL/min residence time 10 min: 78% P
- Flow rate 0.175 mL/min residence time 15 min: 94% P
- Flow rate 0.25 mL/min residence time 20 min: 100% P
- Flow rate 0.165 mL/min residence time 30 min: 100% P
- Flow rate 0.125 mL/min residence time 40 min: 100% P

The same experiment was repeated without light irradiation:

- Flow rate 2.5 mL/min residence time 2 min: 1.5% P
- Flow rate 1 mL/min residence time 5 min: 7.5% P
- Flow rate 0.5 mL/min residence time 10 min: 27% P
- Flow rate 0.175 mL/min residence time 15 min: 45% P
- Flow rate 0.25 mL/min residence time 20 min: 55% P
- Flow rate 0.165 mL/min residence time 30 min: 85% P
- Flow rate 0.125 mL/min residence time 40 min: 100% P

UV-Vis absorbtion spectra studies

The UV-visible measurement was performed using an HP 1100 (Agilent Technologies, Waldbronn, Germany) system containing a photo-diode array detector (DAD). UV range from 200 to 500 nm with 2 nm interval was acquired using MassLynx v4.1 software (Waters®, Milford, MA, USA). Solutions 0.001 M of the desired substrates were prepared in mixture THF/DMF (4/1) and samples were manually injected through an external syringe into the DAD detector.

^{19}F-NMR experiments

General procedure for the in situ irradiation NMR spectroscopy experiments

^{19}F NMR experiments were carried out in a 11.7 T narrow-bore Oxford Instrument magnet (500 MHz ^{1}H Larmor frequency and 470.2 ppm ^{19}F Larmor frequency) INOVA NMR spectrometer (Oxford, Agilent). The light source used to illuminate the inside of a 5 mm NMR tube was described previously by the University of Castilla La Mancha. It consisted of a laser diode emitting at 450 nm, operating at 1.6 W output power. The optical power was lowered to the desired power by using a potentiometer (Thorlabs LDC240C) that regulates the current through the diode. A photometer was used to monitor the desired power from the light beam coming out of a 1 mm optical fiber (Thorlabs FT1000EMT). The sample was irradiated continuously with 600 mW of optical power. A temperature controller ensured no variation of the output light power.

Scale up procedure

Flow procedure: A solution (A) of 4-(trifluoromethoxy) benzyl bromide (37.2 mmol; 2 eq.) in 74.4 mL of THF was pumped through a column containing activated zinc at 0.250 mL/min T= 40 °C. The outcome solution was combined with a solution (B) of methyl 4-bromobenzoate (1 eq., 18.6 mmol), $NiCl_2$ glyme (0.02 eq., 0.37 mmol); dtbbpy (0.03 eq., 0.59 mmol) in 59.52 mL of THF and 14.88 mL of DMF in a Vapourtec UV-150 Photoreactor at 0.250 mL/min each line (RT= 20 min; coil volume= 10 mL) at 60 °C irradiating with 450 nm blue LEDs. Due to the pressure generated in the system a variable back pressure regulator was used at the outlet of the photoreactor to maintain a stable pressure of 3.5-4 bars. The reaction was diluted with ethyl acetate and added to a separatory funnel containing 150 mL of ammonium chloride saturated aqueous solution.

The layers were separated and the aqueous layer was extracted with ethyl acetate (3 x 150 mL). The combined organic extracts were washed with brine, dried ($MgSO_4$) and concentrated in vacuo.

Purification by flash column chromatography (silica, Ethyl acetane:Heptane 0:100 to 20:80) to obtain the product as a transparent liquid (6.7 g, 93% of isolated yield).

Batch procedure: The same reaction was run in batch and the conversion was monitored in time during 8 h. To a solution of methyl 4-bromobenzoate (1 eq. 1 mmol), $NiCl_2$ glyme (0.02 eq., 0.02 mmol); dtbbpy (0.03 eq., 0.03 mmol) in 4.8 mL of THF and 1.2 mL of DMF 4-(trifluoromethoxy) benzyl zinc bromide solution (0.33 M; 2 eq., 2 mmol) was added and was reacted in batch in 8 h 60 °C without light irradiation. The solution was analysed by GCMS every 30 minutes. The reaction was diluted with ethyl acetate and added to a separatory funnel containing 25 mL of water. The layers were separated and the aqueous layer was extracted with ethyl acetate (3 x 25 mL). The combined organic extracts were washed with brine, dried ($MgSO_4$) and concentrated in vacuo. Purification by flash column chromatography (silica, Ethyl acetate:Heptane 0:100 to 20:80) to obtain the product as a transparent liquid (62 mg, 39% of isolated yield).

Product's characterization

*Benzylzinc bromide (**5**)*

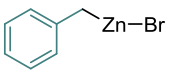

5

Prepared following General procedure 1; **Titration**: 0.45 M.

*[(4-Methoxycarbonylphenyl)methyl]zinc bromide (**7**)*

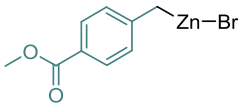

7

Prepared following General procedure 1; **Titration**: 0.36 M.

*3-Trifluoromethylbenzylzinc bromide (**8**)*

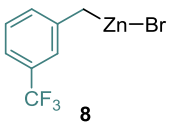

8

Prepared following General Procedure 1; **Titration**: 0.3 M.

*2-Trifluoromethylbenzylzinc bromide (**9**)*

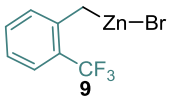

9

Prepared following General procedure 1; **Titration**: 0.33 M.

*4-Trifluoromethoxybenzylzinc bromide (**10**)*

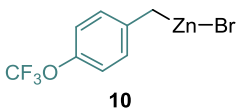

10

Prepared following General procedure 1; **Titration**: 0.39 M

*2-Cyanobenzylzinc bromide (**11**)*

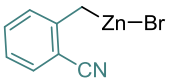

11

Prepared following General procedure 1; **Titration**: 0.35 M.

*Iodo(tetrahydropyran-4-yl) zinc (**12**)*

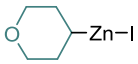

12

Prepared following General procedure 1; **Titration**: 0.4 M.

*Cyclopentylmethylzinc iodide (**13**)*

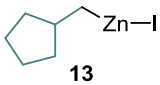

13

Prepared following General procedure 1; **Titration**: 0.4 M.

*Methyl 4-benzylbenzoate (**3**)*

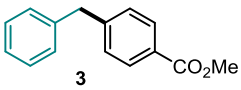

3

Prepared following the general procedure 2 on 0.5 mmol scale with methyl 4-bromobenzoate (1 eq., 0.5 mmol); benzylzinc bromide (**5**) (2 eq., 1 mmol); $NiCl_2$ glyme (0.02 eq., 0.01 mmol); dtbbpy (0.03 eq., 0.015 mmol). Purification by flash chromatography ethyl acetate/ heptane: 20/80 to afford the product as a transparent liquid. Yield:105 mg; 93%.

^{1}H NMR ($CDCl_3$, 500 MHz): δ = 7.90 (s, 1H), 7.88 (dt, J = 7.0, 1.7 Hz, 1H), 7.32-7.40 (m, 2H), 7.25-7.32 (m, 2H), 7.15-7.23 (m, 3H), 4.00-4.05 (m, 2H), 3.83-3.94 ppm (m, 3H).
^{13}C NMR ($CDCl_3$, 126 MHz): δ = 167.2, 141.5, 140.5, 133.6, 130.4, 130.1, 128.9, 128.6, 128.6, 127.5, 126.3, 52.1, 41.7 ppm.
HRMS (ESI-TOF): m/z calculated for $C_{15}H_{15}O_2$ $[M+H]^+$: 227.0993. Found 227.0904.

*1-benzyl-4-methoxybenzene (**6**)*

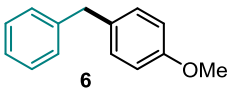

6

Prepared following the general procedure 2 on 0.5 mmol scale with 4-bromoanisole (1 eq., 0.5 mmol); benzylzinc bromide (**5**) (2 eq., 1 mmol); $NiCl_2$ glyme (0.05 eq., 0.025 mmol); dtbbpy (0.075 eq., 0.0375 mmol). Purification by flash chromatography ethyl acetate/pentane: 20/80 to afford the product as a transparent liquid. Yield: 99 mg, 96%.

^{1}H NMR ($CDCl_3$, 400 MHz): δ = 7.23-7.33 (m, 3H), 7.14-7.21 (m, 3H), 7.10 (d, J = 8.8 Hz, 2H), 6.83 (d, J = 8.8 Hz, 2H), 3.92 (s, 2H), 3.78 ppm (s, 3H).
^{13}C NMR ($CDCl_3$, 101MHz): δ = 158.0, 141.6, 133.3, 129.9, 128.8, 128.4, 126.0, 113.9, 55.3, 41.0 ppm.
GC-MS (ESI): m/z calculated for $C_{14}H_{14}O$: 198.1044. Found 198.0.

*Methyl 4-cyclopropylbenzoate (**14**)*

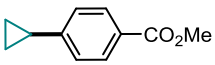

14

Prepared following the general procedure 2 on 0.5 mmol scale with Methyl 4-bromobenzoate (1 eq., 0.5 mmol); cyclopropylzinc bromide (2 eq., 1 mmol); $NiCl_2$ glyme (0.02 eq., 0.01 mmol); dtbbpy (0.03 eq., 0.015 mmol). Purification by flash chromatography ethyl acetate/pentane: 20/80 to afford the product as a transparent liquid. Yield: 60 mg, 70%.

^{1}H NMR ($CDCl_3$, 400 MHz): δ = 7.89-7.94 (m, 2H), 7.06-7.13 (m, 2H), 3.86-3.90 (m, 3H), 1.87-1.99 (m, 1H), 1.00-1.10 (m, 2H), 0.71-0.79 ppm (m, 2H).
^{13}C NMR ($CDCl_3$, 101 MHz): δ = 167.1, 150.0, 129.6, 127.2, 125.3, 51.9, 15.7, 10.2 ppm.
GC-MS (ESI): m/z calculated $C_{11}H_{12}O_2$: 176.0837. Found 176.0.

*Methyl 4-tetrahydropyran-4-ylbenzoate (**15**)*

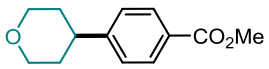

15

Prepared following the general procedure 2 on 0.5 mmol scale with 4-methyl bromo benzoato (1 eq., 0.5 mmol); iodo(tetrahydropyran-4-yl) zinc (**12**) (2 eq., 1 mmol); $NiCl_2$

glyme (0.02 eq., 0.01 mmol); dtbbpy (0.03 eq., 0.015 mmol). Purification by flash chromatography ethyl acetate/heptane: 20/80 to afford the product as a white solid. Yield: 74 mg, 67%.

^{1}H NMR ($CDCl_3$, 400 MHz): δ = 7.75-8.07 (m, 2H), 7.29 (d, J = 8.1 Hz, 2H), 4.05-4.14 (m, 2H), 3.91 (s, 3H), 3.54 (td, J = 11.6, 2.8 Hz, 2H), 2.82 (tt, J = 11.4, 4.4 Hz, 1H), 1.73-1.90 ppm (m, 4H).
^{13}C NMR ($CDCl_3$, 101 MHz): δ = 166.7, 151.1, 129.9, 128.2, 126.8, 68.2, 52.0, 41.7, 33.6 ppm.
GC-MS (ESI): m/z calculated for $C_{13}H_{16}O_3$: 220.1. Found 220.0.
Melting Point: 70.36 °C.

*Methyl 4-[(3-morpholinophenyl) methyl] benzoate (**16**)*

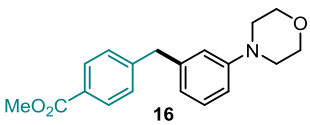

16

Prepared following the general procedure 2 on 0.5 mmol scale with 4-(3-bromophenyl) morpholine (1 eq., 0.5 mmol); [(4-methoxycarbonylphenyl) methyl] zinc bromide (**7**) (2 eq., 1 mmol); $NiCl_2$ glyme (0.05 eq., 0.025 mmol); dtbbpy (0.075 eq., 0.0375 mmol). Purification by flash chromatography ethyl acetate/heptane: 20/80 to afford the product as a sticky yellow solid. Yield: 100 mg, 70%.

^{1}H NMR ($CDCl_3$, 400 MHz): δ = 7.95 (d, J = 8.3 Hz, 2H), 7.24-7.27 (m, 2H), 7.20 (t, J = 7.9 Hz, 1H), 6.75-6.80 (m, 1H), 6.71 (br d, J = 3.0 Hz, 2H), 3.99 (s, 2H), 3.90 (s, 3H), 3.81-3.86 (m, 4H), 3.10-3.15 ppm (m, 4H).
^{13}C NMR ($CDCl_3$, 101 MHz): δ = 191.6, 167.1, 146.5, 141.1, 130.2, 129.8, 129.5, 128.9, 128.1, 116.5, 113.9, 66.9, 52.6, 52.0, 49.4, 49.4, 42.2 ppm.
HRMS (ESI-TOF): m/z calculated for $C_{19}H_{22}NO_3$ $[M+H]^+$: 312.1521. Found 312.1525.

*2-methyl-6-[[2-(trifluoromethyl) phenyl] methyl] pyrazine (**17**)*

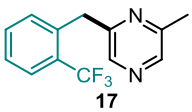

17

Prepared following the general procedure 2 on 0.5 mmol scale with 2-bromo-6-methylpyrazine (1 eq., 0.5 mmol); 2-trifluoromethylbenzylzinc bromide (**9**) (2 eq., 1

mmol); $NiCl_2$ glyme (0.05 eq., 0.025 mmol); dtbbpy (0.075 eq., 0.0375 mmol). Purification by flash chromatography ethyl acetate/heptane: 25/85 to afford the product as a transparent oil. Yield: 100 mg, 80%.

^{1}H NMR ($CDCl_3$, 500 MHz): δ = 8.30 (s, 1H), 8.11 (s, 1H), 7.69 (d, J = 7.8 Hz, 1H), 7.45-7.53 (m, 1H), 7.30-7.41 (m, 2H), 4.34 (s, 2H), 2.55 ppm (s, 3H).
^{13}C NMR ($CDCl_3$, 126 MHz): δ = 154.1, 153.1, 142.2, 141.5, 136.5, 132.0, 128.8, 126.9, 126.2, 125.5, 123.3, 38.2, 21.6 ppm.
^{19}F NMR ($CDCl_3$, 471 MHz): δ = -59.61 ppm (s, 3F).
HRMS (ESI-TOF): m/z calculated for $C_{13}H_{12}F_3N_2$ $[M+H]^+$: 253.0874. Found 253.0865.

*tert-Butyl 4-[5-[2-(1,3-dioxolan-2-yl) ethyl]-2-pyridyl] piperazine-1-carboxylate (**18**)*

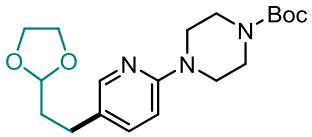

18

Prepared following the general procedure 2 on 0.5 mmol scale with tert-butyl 4-(5-bromo-2-pyridyl) piperazine-1-carboxylate (1 eq., 0.5 mmol); 2-(1,3-dioxolan-2-yl)]ethyl]zinc bromide (2 eq., 1 mmol); $NiCl_2$ glyme (0.05 eq., 0.025 mmol); dtbbpy (0.075 eq., 0.0375 mmol). Purification by flash chromatography ethyl acetate/heptane: 25/85 to afford the product as an amorphous solid. Yield: 80 mg, 44%.

^{1}H NMR ($CDCl_3$, 400 MHz): δ = 8.06 (d, J = 1.8 Hz, 1H), 7.37 (dd, J = 8.7, 2.4 Hz, 1H), 6.61 (d, J = 8.6 Hz, 1H), 4.88 (t, J = 4.6 Hz, 1H), 3.96-4.03 (m, 2H), 3.82-3.90 (m, 2H), 3.51-3.58 (m, 4H), 3.44-3.50 (m, 4H), 2.60-2.69 (m, 2H), 2.05 (s, 1H), 1.84-1.98 (m, 2H), 1.48 ppm (s, 9H).
^{13}C NMR ($CDCl_3$, 101 MHz): δ = 158.1, 154.9, 147.5, 137.8, 126.5, 107.2, 103.7, 79.9, 65.0, 45.5, 35.4, 28.4, 26.3 ppm.
HRMS (ESI-TOF): m/z calculated for $C_{19}H_{30}N_3O_4$ $[M+H]^+$: 364.2158. Found 364.2160.

*4-[[3-(Trifluoromethyl) phenyl] methyl] benzonitrile (**19**)*

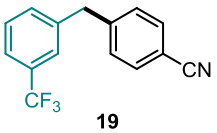

19

Prepared following the general procedure 2 on 0.5 mmol scale with 4-bromobenzonitrile (1 eq., 0.5 mmol); 3-trifluoromethylbenzylzinc bromide (**8**) (2 eq., 1 mmol); $NiCl_2$ glyme (0.05 eq., 0.025 mmol); dtbbpy (0.075 eq., 0.0375 mmol). Purification by flash chromatography ethyl acetate/heptane: 10/90 to afford the product as a white solid. Yield: 110 mg, 80%.

^{1}H NMR ($CDCl_3$, 400 MHz): δ = 7.60 (d, J = 8.1 Hz, 2H), 7.48-7.55 (m, 1H), 7.40-7.46 (m, 2H), 7.33 (d, J= 7.4 Hz, 1H), 7.28 (d, J = 8.1 Hz, 2H), 4.09 ppm (s, 2H).
^{13}C NMR ($CDCl_3$, 101 MHz): δ = 145.5, 140.2, 132.5, 132.3, 131.2 (q, J_{CF} = 32.3 Hz), 129.6, 129.3, 125.6 (q, J_{CF} = 3.8 Hz), 125.36, 123.7 (q, J_{CF} = 3.9 Hz), 122.7, 118.8, 110.6, 41.7 ppm.
^{19}F NMR ($CDCl_3$, 471 MHz): δ = -55.79 ppm (s, 3F).
GC-MS (ESI): m/z calculated for $C_{15}H_{10}F_3N$: 261.0765. Found 261.1.
Melting Point: 147.76 °C.

2-Methyl-6-tetrahydropyran-4-yl-pyrazine (**20**)

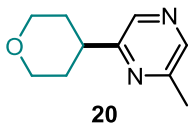

20

Prepared following the general procedure 2 on 0.5 mmol scale with 2-bromo-6-methyl-pyrazine (1 eq., 0.5 mmol); iodo(tetrahydropyran-4-yl) zinc (**12**) (2 eq., 1 mmol); $NiCl_2$ glyme (0.05 eq., 0.025 mmol); dtbbpy (0.075 eq., 0.0375 mmol). Purification by flash chromatography ethyl acetate/heptane: 10/90 to afford the product as a transparent oil. Yield: 80 mg, 90%.

^{1}H NMR ($CDCl_3$, 400 MHz): δ = 8.29 (d, J = 8.1 Hz, 2H), 4.04-4.22 (m, 2H), 3.55 (td, J = 11.7, 2.4 Hz, 2H), 2.86-3.05 (m, 1H), 2.54 (s, 3H), 1.80-2.01 ppm (m, 4H).
^{13}C NMR ($CDCl_3$, 101 MHz): δ = 158.4, 153.0, 142.3, 139.7, 67.9, 41.2, 32.0, 21.9 ppm.
HRMS (ESI-TOF): m/z calculated for $C_{10}H_{15}N_{2O}$ $[M+H]^+$: 179.1106. Found 179.1095.

*Methyl 3-benzylbenzoate (**21**)*

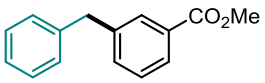

21

Prepared following the general procedure 2 on 0.5 mmol scale with methyl 3-bromobenzoate (1 eq., 0.5 mmol); benzylzinc bromide (**5**) (2 eq., 1 mmol); $NiCl_2$ glyme (0.02 eq., 0.01 mmol); dtbbpy (0.03 eq., 0.015 mmol). Purification by flash chromatography ethyl acetate/heptane: 20/80 to afford the product as a transparent liquid. Yield: 81 mg, 89%.

^{1}H NMR ($CDCl_3$, 500 MHz): δ = 7.86-7.92 (m, 2H), 7.32-7.41 (m, 2H), 7.25-7.31 (m, 2H), 7.15-7.22 (m, 3H), 4.02 (s, 1H), 3.96-4.05 (m, 1H), 3.89 ppm (s, 3H).
^{13}C NMR ($CDCl_3$, 126 MHz): δ = 167.2, 141.5, 140.5, 133.6, 130.4, 130.1, 128.9, 128.6, 127.5, 126.3, 52.1, 41.7 ppm.
HRMS (ESI-TOF): m/z calculated for $C_{15}H_{15}O_2$ $[M+H]^+$: 227.0993. Found 227.0904.

*Methyl 2-benzylbenzoate (**22**)*

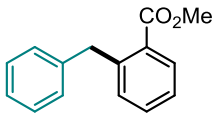

22

Prepared following General procedure 2 on 0.5 mmol scale with methyl 2-bromobenzoate (1 eq., 0.5 mmol); benzylzinc bromide (**5**) (2 eq., 1 mmol); NiCl2 glyme (0.02 eq., 0.01 mmol); dtbbpy (0.03 eq., 0.015 mmol). Purification by flash chromatography ethyl acetate/heptane: 20/80 to afford the product as a transparent liquid. Yield: 72 mg, 80%.

^{1}H NMR ($CDCl_3$, 400 MHz): δ = 7.89 (dd, J = 7.9, 1.4 Hz, 1H), 7.42 (d, J = 1.4 Hz, 1H), 7.21-7.33 (m, 4H), 7.09-7.21 (m, 3H), 4.38 (s, 2H), 3.82 ppm (s, 3H).
^{13}C NMR ($CDCl_3$, 101 MHz): δ = 168.1, 142.2, 140.9, 132.0, 131.6, 130.7, 130.0, 128.9, 128.3, 126.2, 125.9, 51.9, 39.6 ppm.
HRMS (ESI-TOF): m/z calculated for $C_{15}H_{15}O_2$ $[M+H]^+$: 227.0993. Found 227.0904.

*4-Benzylbenzonitrile (**23**)*

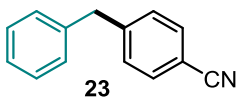

23

Prepared following the general procedure 2 on 0.5 mmol scale with 4-bromobenzonitrile (1 eq., 0.5 mmol); benzylzinc bromide (**5**) (2 eq., 1 mmol); $NiCl_2$ glyme (0.02 eq., 0.01

mmol); dtbbpy (0.03 eq., 0.015 mmol). Purification by flash chromatography ethyl acetate/heptane: 20/80 to afford the product as a transparent liquid. Yield: 64 mg, 83%.

^{1}H NMR ($CDCl_3$, 500 MHz): δ = 7.56 (d, J = 8.1 Hz, 2H), 7.21-7.34 (m, 5H), 7.15 (d, J = 7.5 Hz, 2H), 4.03 ppm (s, 2H).
^{13}C NMR ($CDCl_3$, 101 MHz): δ = 146.7, 139.3, 132.3, 129.7, 129.0, 128.8, 126.7, 119.0, 110.1, 42.0 ppm.
GC-MS (ESI): m/z calculated for $C_{14}H_{11}N$: 193.0891. Found 193.0.

*Methyl 4-(p-tolylmethyl) benzoate (**24**)*

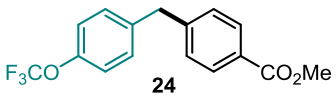

24

Prepared following the general procedure 2 on 0.5 mmol scale with methyl 4-bromobenzoate (1 eq., 0.5 mmol); 4-trifluoromethoxybenzylzinc bromide (**10**) (2 eq., 1 mmol); $NiCl_2$ glyme (0.02 eq., 0.01 mmol); dtbbpy (0.03 eq., 0.015 mmol). Purification by flash chromatography ethyl acetate/heptane: 15/85 to afford the product as a transparent liquid. Yield: 140 mg, 90%.

^{1}H NMR ($CDCl_3$, 500 MHz): δ = 7.97 (d, J = 8.4 Hz, 2H), 7.22-7.27 (m, 2H), 7.09-7.21 (m, 4H), 4.03 (s, 2H), 3.90 ppm (s, 3H).
^{13}C NMR ($CDCl_3$, 126 MHz): δ = 166.9, 147.8, 145.7, 138.9, 130.2, 130.0, 128.9, 128.4, 121.5, 121.0, 52.1, 41.2 ppm.
^{19}F NMR ($CDCl_3$, 471 MHz): δ = -57.93 ppm (br s, 3F).
HRMS (ESI-TOF): m/z calculated for $C_{16}H_{16}O_2$ $[M+H]^+$: 241.1150. Found 241.1151.

*2-[[5-(Trifluoromethyl)-3-pyridyl] methyl] benzonitrile (**25**)*

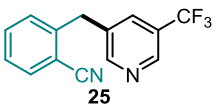

25

Prepared following the general procedure 2 on 0.5 mmol scale with 3-bromo-5-(trifluoromethyl) pyridine (1 eq., 0.5 mmol); 2-cianobenzylzinc bromide (**11**) (2 eq., 1 mmol); $NiCl_2$ glyme (0.02 eq., 0.01 mmol); dtbbpy (0.03 eq., 0.015 mmol). Purification by flash chromatography ethyl acetate/heptane: 15/85 to afford the product as an orange oil. Yield: 118 mg, 90%.

^{1}H NMR ($CDCl_3$, 400 MHz): δ = 8.71-8.80 (m, 2H), 7.76 (s, 1H), 7.70 (dd, J = 7.6, 1.2 Hz, 1H), 7.58 (td, J = 7.7, 1.4 Hz, 1H), 7.40 (td, J = 7.7, 0.9 Hz, 1H), 7.30 (d, J = 7.9 Hz, 1H), 4.30 ppm (s, 2H).
^{13}C NMR ($CDCl_3$, 101 MHz): δ = 153.3, 145.2 (q, J_{CF} = 4.0 Hz), 142.3, 134.6, 133.4 (q, J_{CF} = 3.6 Hz), 133.4, 133.2, 130.0, 127.8, 117.6, 112.8, 37.1 ppm.
^{19}F NMR ($CDCl_3$, 471 MHz): δ = -62.45 ppm (s, 3F).
HRMS (ESI-TOF): m/z calculated for $C_{14}H_{10}F_3N_2$ $[M+H]^+$: 263.0717. Found 263.0711.

*5-Benzylpyrimidin-2-amine (**26**)*

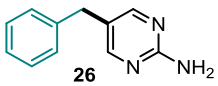

26

Prepared following the general procedure 2 on 0.5 mmol scale with 5-iodopyrimidin-2-amine (1 eq., 0.5 mmol); benzylzinc bromide (**5**) (3 eq., 1.5 mmol); $NiCl_2$ glyme (0.02 eq., 0.01 mmol); dtbbpy (0.03 eq., 0.015 mmol). Purification by flash chromatography ethyl acetate/heptane: 50/50 to afford the product as a white solid. Yield: 86 mg, 93%.

^{1}H NMR ($CDCl_3$, 400 MHz): δ = 8.15 (s, 2H), 7.27-7.36 (m, 2H), 7.22 (s, 1H), 7.17 (s, 2H), 4.96 (br s, 2H), 3.80 ppm (s, 2H).
^{13}C NMR ($CDCl_3$, 101 MHz): δ = 158.4, 139.8, 128.7, 128.6, 126.5, 123.9, 103.6, 35.7 ppm.
HRMS (ESI-TOF): m/z calculated for $C_{11}H_{10}N_3Na$ $[M+Na]^+$: 207.0772. Found 207.0689.
Melting point: 121.86 °C.

*1-Cyclobutyl-4-(trifluoromethyl) benzene (**27**)*

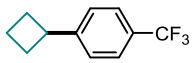

27

Prepared following the general procedure 2 on 0.5 mmol scale with 1-chloro-4-(trifluoromethyl) benzene (1 eq., 0.5 mmol); cyclobutylzinc bromide (3 eq., 1.5 mmol); $NiCl_2$ glyme (0.05 eq., 0.025 mmol); dtbbpy (0.075 eq., 0.0375 mmol). Purification by flash chromatography pentane 100% to afford the product as a transparent liquid. Yield: 70 mg, 70%.

^{1}H NMR ($CDCl_3$, 400 MHz): δ = 7.53 (d, J = 8.1 Hz, 2H), 7.27-7.33 (m, 2H), 3.59 (quint, J = 8.7 Hz, 1H), 2.31-2.44 (m, 2H), 2.09-2.21 (m, 2H), 1.98-2.09 (m, 1H), 1.81-1.94 ppm (m, 1H).

^{13}C NMR ($CDCl_3$, 101 MHz): δ = 127.7, 126.6, 125.9, 125.5, 125.2 (q, J_{CF} = 3.8 Hz), 40.0, 30.3, 29.6, 18.3 ppm.
GC-MS (ESI): m/z calculated for $C_{11}H_{11}F_3$: 200.0812. Found 200.0.

*1-(4-Cyclobutylphenyl) ethenone (**28**)*

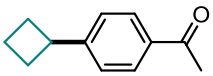

28

Prepared following the general procedure 2 on 0.5 mmol scale with 1-(4-chlorophenyl) ethanone (1 eq., 0.5 mmol); cyclobutylzinc bromide (2 eq., 1 mmol); NiCl2 glyme (0.05 eq., 0.025 mmol); dtbbpy (0.075 eq., 0.0375 mmol). Purification by flash chromatography ethyl acetate/pentane: 15/85 to afford the product as a transparent liquid. Yield: 85 mg, 98%.

^{1}H NMR ($CDCl_3$, 400 MHz): δ = 7.89 (d, J = 8.3 Hz, 2H), 7.29 (d, J = 8.3 Hz, 2H), 3.48-3.70 (m, 1H), 2.58 (s, 3H), 2.31-2.43 (m, 2H), 2.09-2.24 (m, 2H), 2.00-2.11 (m, 1H), 1.81-1.95 ppm (m, 1H).
^{13}C NMR ($CDCl_3$, 101 MHz): δ = 197.8, 152.0, 134.9, 128.4, 126.4, 40.2, 29.5, 26.5, 18.3 ppm.
GC-MS (ESI): m/z calculated for $C_{12}H_{14}O$: 174.1044. Found 174.1.

*2-Cyclobutyl-4-fluoro-pyridine (**29**)*

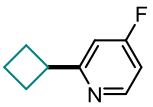

29

Prepared following the general procedure 2 on 0.5 mmol scale with 2-chloro-4-fluoropyridine (1 eq., 0.5 mmol); cyclobutylzinc bromide (2 eq., 1 mmol); $NiCl_2$ glyme (0.05 eq., 0.025 mmol); dtbbpy (0.075 eq., 0.0375 mmol). Purification by flash chromatography ethyl acetate/pentane: 30/70 to afford the product as an orange oil. Yield: 70 mg, 93%.

^{1}H NMR ($CDCl_3$, 400 MHz): δ = 8.51 (dd, J = 8.8, 5.5 Hz, 1H), 6.89 (dd, J = 10.1, 2.4 Hz, 1H), 6.84 (ddd, J = 8.4, 5.7, 2.5 Hz, 1H), 3.67 (quint, J = 8.7 Hz, 1H), 2.25-2.43 (m, 4H), 2.00-2.14 (m, 1H), 1.92 ppm (s, 1H).

^{13}C NMR ($CDCl_3$, 101 MHz): δ = 170.3, 168.4 (d, J_{CF} = 6.24 Hz), 167.7, 151.5 (d, J_{CF} = 7.0 Hz), 108.9 (d, J_{CF} = 16.5 Hz), 108.5 (d, J_{CF} = 16.1 Hz), 42.0 (d, J_{CF} = 2.6 Hz), 28.3, 18.1 ppm.
^{19}F NMR ($CDCl_3$, 471 MHz): δ = -55.79 ppm (s, 1F).
HRMS (ESI-TOF): m/z calculated for $C_9H_{11}FN$ $[M+H]^+$: 152.0797. Found 152.0792.

*Ethyl 4-benzylbenzoate (**30**)*

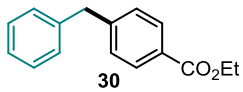

30

Prepared following the general procedure 2 on 0.5 mmol scale with ethyl 4-bromobenzoate (1 eq., 0.5 mmol); benzylzinc bromide (**5**) (2 eq., 1 mmol); $NiCl_2$ glyme (0.05 eq., 0.025 mmol); dtbbpy (0.075 eq., 0.0375 mmol). Purification by flash chromatography ethyl acetate/heptane: 30/70 to afford the product as a transparent liquid. Yield: 72 mg, 60%.

^{1}H NMR ($CDCl_3$, 400 MHz): δ = 7.96 (d, J = 8.3 Hz, 2H), 7.26 (dd, J = 12.8, 8.0 Hz, 4H), 7.14-7.21 (m, 2H), 4.35 (q, J = 7.2 Hz, 2H), 4.03 (s, 2H), 1.37 ppm (t, J = 7.2 Hz, 3H).
^{13}C NMR ($CDCl_3$, 101 MHz): δ = 166.6, 146.4, 140.2, 129.8, 128.9, 128.9, 128.6, 128.5, 126.4, 60.8, 41.9, 14.4 ppm.
HRMS (ESI-TOF): m/z calculated for $C_{16}H_{17}O_2$ $[M+H]^+$: 241.1150. Found 241.1148.

*Methyl 4-[[6-(trifluoromethyl)-3-pyridyl] methyl] benzoate (**31**)*

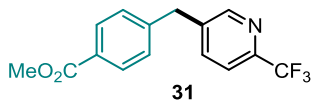

31

Prepared following the general procedure 2 on 0.5 mmol scale with 5-chloro-2-(trifluoromethyl) pyridine (1 eq., 0.5 mmol); [(4-methoxycarbonylphenyl) methyl] zinc bromide (**7**) (2 eq., 1 mmol); $NiCl_2$ glyme (0.05 eq., 0.025 mmol); dtbbpy (0.075 eq., 0.0375 mmol). Purification by flash chromatography ethyl acetate/heptane: 30/70 to afford the product as a white solid. Yield: 80 mg, 54%.

^{1}H NMR ($CDCl_3$, 400 MHz): δ = 8.61 (s, 1H), 8.00 (d, J = 8.3 Hz, 2H), 7.62 (d, J = 1.2 Hz, 2H), 7.24 (s, 1H), 4.12 (s, 2H), 3.91 ppm (s, 3H).
^{13}C NMR ($CDCl_3$, 101 MHz): δ = 166.7, 150.3, 146.6 (q, J_{CF} = 23 Hz), 143.8, 139.0, 137.5, 130.2, 128.9, 122.9, 120.4 (q, J_{CF} = 3.03 Hz), 52.2, 38.8 ppm.
^{19}F NMR ($CDCl_3$, 471 MHz): δ = -67.80 ppm (s, 3F).
HRMS (ESI-TOF): m/z calculated for $C_{15}H_{13}F_3NO_2$ $[M+H]^+$: 296.0820. Found 296.0809.
Melting Point: 63.2 °C.

*Ethyl 4-(cyclopentylmethyl) benzoate (**32**)*

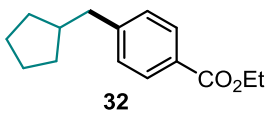

32

Prepared following General procedure 2 on 0.5 mmol scale with ethyl 4-bromobenzoate (1 eq., 0.5 mmol); cyclopentylmethylzinc iodide (**13**) (2 eq., 1 mmol); $NiCl_2$ glyme (0.05 eq., 0.025mmol); dtbbpy (0.075 eq., 0.0375 mmol). Purification by flash chromatography ethyl acetate/heptane: 20/80 to afford the product as a transparent liquid. Yield: 70 mg, 60%.

^{1}H NMR ($CDCl_3$, 400 MHz): δ = 7.95 (d, J = 8.3 Hz, 2H), 7.23 (d, J = 8.3 Hz, 2H), 4.36 (q, J = 7.2 Hz, 2H), 2.66 (d, J = 7.4 Hz, 2H), 1.98-2.22 (m, 1H), 1.57-1.80 (m, 4H), 1.44-1.56 (m, 2H), 1.38 (t, J = 7.2 Hz, 3H), 1.21 ppm (br s, 2H).
^{13}C NMR ($CDCl_3$, 101 MHz): δ = 166.8, 147.8, 129.5, 128.8, 128.0, 60.7, 42.1, 41.7, 32.4, 24.9, 14.4 ppm.
GCMS (ESI): m/z calculated for $C_{15}H_{20}O_2$: 232.1463. Found 232.0.

*3-Butyl-7-cyclopropyl-8-(trifluoromethyl)-[1,2,4] triazolo[4,3-a]pyridine (**33**)*

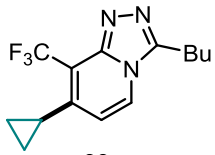

33

Prepared following the general procedure 2 on 0.5 mmol scale with 3-butyl-7-chloro-8-(trifluoromethyl)- [1,2,4] triazolo[4,3-a] pyridine (1 eq., 0.5 mmol); cyclopropyl zinc bromide (2 eq., 1 mmol); $NiCl_2$ glyme (0.05 eq., 0.025 mmol); dtbbpy (0.075 eq., 0.0375 mmol). Purification by flash chromatography ethyl acetate/heptane: 40/60 to afford the product as a white solid. Yield: 87 mg, 85%.

^{1}H NMR ($CDCl_3$, 400 MHz): δ = 7.88 (d, J = 7.4 Hz, 1H), 6.36 (d, J = 7.4 Hz, 1H), 3.00-3.14 (m, 2H), 2.36-2.52 (m, 1H), 1.83 (t, J = 7.7 Hz, 2H), 1.41-1.59 (m, 2H), 1.21-1.34 (m, 2H), 0.97 (t, J = 7.4 Hz, 3H), 0.88-0.93 ppm (m, 2H).
^{13}C NMR ($CDCl_3$, 126 MHz): δ = 147.0, 146.6, 144.7, 123.4 (q, J_{CF} = 277,2 Hz), 125.5, 124.6, 124.3, 116.0 (q, J_{CF} = 32,9 Hz), 112.0, 111.0, 28.8, 24.1, 22.4, 13.7, 12.6-12.5 (q, J_{CF}= 3.5 Hz), 9.8 ppm.

^{19}F NMR ($CDCl_3$, 471 MHz): δ = -54.91 ppm (s, 3F).
HRMS (ESI-TOF): m/z calculated for $C_{14}H_{17}F_3N_3$ $[M+H]^+$: 284.1296. Found 284.1290.
Melting Point: 165.03 °C.

*3-Butyl-7-[2-(1,3-dioxolan-2-yl) ethyl]-8-(trifluoromethyl)-[1,2,4] triazolo[4,3-a]pyridine (**34**)*

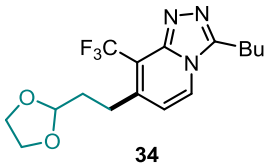

34

Prepared following the general procedure 2 on 0.5 mmol scale with 3-butyl-7-chloro-8-(trifluoromethyl)-[1,2,4] triazolo[4,3-a]pyridine (1 eq., 0.5 mmol); 2-(1,3-dioxolan-2-yl)]ethyl]zinc bromide (2 eq., 1 mmol); $NiCl_2$ glyme (0.05 eq., 0.025 mmol); dtbbpy (0.075 eq., 0.0375 mmol). Purification by flash chromatography ethyl acetate/heptane: 40/60 to afford the product as a transparent liquid. Yield: 50 mg, 56%.

^{1}H NMR ($CDCl_3$, 400 MHz): δ = 7.92 (d, J = 7.2 Hz, 1H), 6.78 (d, J = 7.2 Hz, 1H), 4.97 (t, J = 4.3 Hz, 1H), 3.97-4.12 (m, 2H), 3.86-3.95 (m, 2H), 3.04-3.16 (m, 2H), 2.99 (td, J = 8.1, 1.4 Hz, 2H), 1.95-2.10 (m, 2H), 1.79-1.91 (m, 2H), 1.37-1.55 (m, 2H), 0.98 ppm (t, J = 7.4 Hz, 3H).
^{13}C NMR ($CDCl_3$, 101 MHz): δ = 147.2, 146.6, 142.6, 124.6, 123.9, 116.9, 116.1, 115.8, 103.0, 65.1, 34.5, 28.8, 27.3, 24.2, 22.4, 13.7 ppm.
^{19}F NMR ($CDCl_3$, 471 MHz): δ = -55.79 ppm (s, 3F).
HRMS (ESI-TOF): m/z calculated for $C_{16}H_{21}F_3N_3O_2$ $[M+H]^+$: 344.1507. Found 344.1501.
Melting Point: 170.12 °C.

Bibliography

[1] (a) Metal-Catalyzed Cross-Coupling Reactions, 2nd ed. (Eds.: A. de Meijere, F. Diederich), **2004**, Wiley-VCH, Weinheim; (b) Johansson Seechurn, C. C. C.; Kitching, M. O.; Colacot, T. J.; Snieckus, V. Palladium-Catalyzed Cross-Coupling: A Historical Contextual Perspective to the 2010 Nobel Prize. *Angew. Chem. Int. Ed*. **2012**, 51 (21), 5062–5085; (c) Cantillo, D.; Kappe, C. O. Immobilized Transition Metals as Catalysts for Cross-Couplings in Continuous Flow - A Critical Assessment of the Reaction Mechanism and Metal Leaching. *ChemCatChem* **2015**, *6* (12), 3286–3305; (d) Noël, T.; Buchwald, S. L. Cross-Coupling in Flow. *Chem. Soc. Rev.* **2011**, *40* (10), 5010.

[2] Nicolaou, K. C.; Bulger, P. G.; Sarlah, D. Palladium-Catalyzed Cross-Coupling Reactions in Total Synthesis. *Angew Chem. Int. Ed*. **2005**, *44* (29), 4442–4489.

[3] Rosen, B. M.; Quasdorf, K. W.; Wilson, D. A.; Zhang, N.; Resmerita, A. M.; Garg, N. K.; Percec, V. Nickel-Catalyzed Cross-Couplings Involving Carbon-Oxygen Bonds. *Chem. Rev*. **2011**, *111* (3), 1346–1416.

[4] Wu, J.; Yang, Z. Nickel-Catalyzed Cross-Couplings of 4-Diethylphosphonooxycoumarins with Organozinc Reagents: An Efficient New Methodology for the Synthesis of 4-Substituted Coumarins. *J. Org. Chem.* **2001**, *66* (23), 7875–7878.

[5] Melzig, L.; Dennenwaldt, T.; Gavryushin, A.; Knochel, P. Direct Aminoalkylation of Arenes, Heteroarenes, and Alkenes via Ni-Catalyzed Negishi Cross-Coupling Reactions. *J. Org. Chem.* **2011**, *76* (21), 8891–8906.

[6] Terao, J.; Bando, F.; Kambe, N. Ni-Catalyzed Regioselective Three-Component Coupling of Alkyl Halides, Arylalkynes, or Enynes with R-M (M = MgX', ZnX'). *Chem. Commun. (Camb).* **2009**, No. 47, 7336–7338.

[7] (a) Shaw, M. H.; Twilton, J.; MacMillan, D. W. C. Photoredox Catalysis in Organic Chemistry. *J. Org. Chem.* **2016**, *81* (16), 6898–6926; (b) Zeitler, K. Photoredox Catalysis with Visible Light. *Angew. Chem. Int. Ed.* **2009**, *48*, 9785–9789.

[8] (a) Cavalcanti L.N., Molander G.A. Photoredox Catalysis in Nickel-Catalyzed Cross-Coupling. In: Correa A. (eds) Ni- and Fe-Based Cross-Coupling Reactions. Topics in Current Chemistry Collections. **2017**, Springer, Cham.; (b) Murphy, J. J.; Melchiorre, P. Organic Chemistry: Light Opens Pathways for Nickel Catalysis. *Nature*. **2015**, 524, 297–298.

[9] Osawa, M.; Nagai, H.; Akita, M. Photo-Activation of Pd-Catalyzed Sonogashira Coupling Using a Ru/Bipyridine Complex as Energy Transfer Agent. *Dalt. Trans.* **2007**, 8, 827.

[10] Neufeldt, S. R.; Sanford, M. S. Combining Transition Metal Catalysis with Radical Chemistry: Dramatic Acceleration of Palladium-Catalyzed C-H Arylation with Diaryliodonium Salts. *Adv. Synth. Catal.* **2012**, *354* (18), 3517–3522.

[11] (a) Yamashita, Y.; Tellis, J. C.; Molander, G. A. Protecting Group-Free, Selective Cross-Coupling of Alkyltrifluoroborates with Borylated Aryl Bromides via Photoredox/Nickel Dual Catalysis. *Proc. Natl. Acad. Sci.* **2015**, *112* (39), 12026–12029; (b) Ryu, D.; Primer, D. N.; Tellis, J. C.; Molander, G. A. Single-Electron Transmetalation: Synthesis of 1,1-Diaryl-2,2,2-Trifluoroethanes by Photoredox/Nickel Dual Catalytic Cross-Coupling. *Chem. Eur. J.* **2016**, *22* (1), 120–123.

[12] Primer, D. N.; Karakaya, I.; Tellis, J. C.; Molander, G. A. Single-Electron Transmetalation: An Enabling Technology for Secondary Alkylboron Cross-Coupling. *J. Am. Chem. Soc.* **2015**, *137* (6), 2195–2198.

[13] (a) Karakaya, I.; Primer, D. N.; Molander, G. A. Photoredox Cross-Coupling: Ir/Ni Dual Catalysis for the Synthesis of Benzylic Ethers. *Org. Lett.* **2015**, *17* (13), 3294–3297; (b) Amani, J.; Sodagar, E.; Molander, G. A. Visible Light Photoredox Cross-Coupling of Acyl Chlorides with Potassium Alkoxymethyltrifluoroborates: Synthesis of α-Alkoxyketones. *Org. Lett.* **2016**, *18* (4), 732–735.

[14] El Khatib, M.; Serafim, R. A. M.; Molander, G. A. α-Arylation/Heteroarylation of Chiral α-Aminomethyltrifluoroborates by Synergistic Iridium Photoredox/Nickel Cross-Coupling Catalysis. *Angew. Chem. Int. Ed.* **2016**, *55* (1), 254–258.

[15] (a) Jouffroy, M.; Primer, D. N.; Molander, G. A. Base-Free Photoredox/Nickel Dual-Catalytic Cross-Coupling of Ammonium Alkylsilicates. *J. Am. Chem. Soc.* **2016**, *138* (2), 475–478; (b) Patel, N. R.; Kelly, C. B.; Jouffroy, M.; Molander, G. A. Engaging Alkenyl Halides with Alkylsilicates via Photoredox Dual Catalysis. *Org. Lett.* **2016**, *18* (4), 764–767.

[16] Zuo, Z.; Ahneman, D. T.; Chu, L.; Terrett, J. A.; Doyle, A. G.; MacMillan, D. W. C. Merging Photoredox with Nickel Catalysis: Coupling of α-Carboxyl Sp3-Carbons with Aryl Halides. *Science.* **2014**, *345* (6195), 437–440.

[17] Shaw, M. H.; Shurtleff, V. W.; Terrett, J. A.; Cuthbertson, J. D.; MacMillan, D. W. C. Native Functionality in Triple Catalytic Cross-Coupling: Sp3C-H Bonds as Latent Nucleophiles. *Science* **2016**, *352* (6291), 1304–1308.

[18] Cornella, J.; Edwards, J. T.; Qin, T.; Kawamura, S.; Wang, J.; Pan, C. M.; Gianatassio, R.; Schmidt, M.; Eastgate, M. D.; Baran, P. S. Practical Ni-Catalyzed Aryl-Alkyl Cross-Coupling of Secondary Redox-Active Esters. *J. Am. Chem. Soc.* **2016**, *138* (7), 2174–2177.

[19] (a) Huck, L.; Berton, M.; de la Hoz, A.; Díaz-Ortiz, A.; Alcázar, J. Reformatsky and Blaise Reactions in Flow as a Tool for Drug Discovery. One Pot Diversity Oriented Synthesis of Valuable Intermediates and Heterocycles. *Green Chem.* **2017**, *19* (6), 1420–1424; (b) Berton, M.; Huck, L.; Alcázar, J. On-Demand Synthesis of Organozinc Halides under Continuous Flow Conditions. *Nat. Protoc.* **2018**, *13* (1), 324–334; (c) Alonso, N.; Miller, L. Z.; De M. Muñoz, J.; Alcázar, J.; McQuade, D. T. Continuous Synthesis of Organozinc Halides Coupled to Negishi Reactions. *Adv. Synth. Catal.* **2014**, *356* (18), 3737–3741.

[20] (a) Tellis, J. C.; Primer, D. N.; Molander, G. A. Single-Electron Transmetalation in Organoboron Cross-Coupling by Photoredox/Nickel Dual Catalysis. *Science.* **2014**, *345* (6195), 433–436; (b) Lima, F.; Kabeshov, M. A.; Tran, D. N.; Battilocchio, C.; Sedelmeier, J.; Sedelmeier, G.; Schenkel, B.; Ley, S. V. Visible Light Activation of Boronic Esters Enables Efficient Photoredox C(Sp2)–C(Sp3) Cross-Couplings in Flow. *Angew. Chemie Int. Ed.* **2016**, *55* (45), 14085–14089; (c) Heitz, D. R.; Tellis, J. C.; Molander, G. A. Photochemical Nickel-Catalyzed C-H Arylation: Synthetic Scope and Mechanistic Investigations. *J. Am. Chem. Soc.* **2016**, *138* (39), 12715–12718.

[21] (a) Cambié, D.; Bottecchia, C.; Straathof, N. J. W.; Hessel, V.; Noël, T. Applications of Continuous-Flow Photochemistry in Organic Synthesis, Material Science, and Water Treatment. *Chem. Rev*. **2016**, 117, 10276–10341; (b) Abdiaj, I.; Alcázar, J. Improving the Throughput of Batch Photochemical Reactions Using Flow: Dual Photoredox and Nickel Catalysis in Flow for C(Sp2)C(Sp3) Cross-Coupling. *Bioorganic Med. Chem.* **2017**, *25* (23), 6190–6196.

[22] Phapale, V. B.; Guisán-Ceinos, M.; Buñuel, E.; Cárdenas, D. J. Nickel-Catalyzed Cross-Coupling of Alkyl Zinc Halides for the Formation of C(Sp2)-C(Sp3) Bonds: Scope and Mechanism. *Chem. Eur. J.* **2009**, *15* (46), 12681–12688.

[23] Phapale, V. B.; Cárdenas, D. J. Nickel-CatalyzedNegishi Cross-Coupling Reactions: Scope and Mechanisms. *Chem. Soc. Rev.* **2009**, *38* (6), 1598.

[24] (a) Doornbos, M. L. J.; Cid, J. M.; Haubrich, J.; Nunes, A.; Van De Sande, J. W.; Vermond, S. C.; Mulder-Krieger, T.; Trabanco, A. A.; Ahnaou, A.; Drinkenburg, W. H.; et al. Discovery and Kinetic Profiling of 7-Aryl-1,2,4-Triazolo[4,3-a]Pyridines: Positive Allosteric Modulators of the Metabotropic Glutamate Receptor 2. *J. Med. Chem.* **2017**, *60* (15), 6704–6720; (b) Cid, J. M.; Tresadern, G.; Vega, J. A.; De Lucas, A. I.; Del Cerro, A.; Matesanz, E.; Linares, M. L.; García, A.; Iturrino, L.; Pérez-Benito, L.; et al. Discovery of 8-Trifluoromethyl-3-Cyclopropylmethyl-7-[(4-(2,4-Difluorophenyl)-1- Piperazinyl)Methyl]-1,2,4-Triazolo[4,3-a]Pyridine (JNJ-46356479), a Selective and Orally Bioavailable MGlu2 Receptor Positive Allosteric Modulator (PAM). *J. Med. Chem.* **2016**, *59* (18), 8495–8507; (c) Cid, J. M.; Tresadern, G.; Vega, J. A.; de Lucas, A. I.; Matesanz, E.; Iturrino, L.; Linares, M. L.; Garcia, A.; Andrés, J. I.; Macdonald, G. J.; et al. Discovery of 3-Cyclopropylmethyl-7-(4-Phenylpiperidin-1-Yl)-8-Trifluoromethyl[1,2,4]Triazolo[4,3-a]Pyridine (JNJ-42153605): A Positive Allosteric Modulator of the Metabotropic Glutamate 2 Receptor. *J. Med. Chem.* **2012**, *55* (20), 8770–8789; (d) Andrés, J.-I.; Alcázar, J.; Cid, J. M.; De Angelis, M.; Iturrino, L.; Langlois, X.; Lavreysen, H.; Trabanco, A. A.; Celen, S.; Bormans, G. Synthesis, Evaluation, and Radiolabeling of New Potent Positive Allosteric Modulators of the Metabotropic Glutamate Receptor 2 as Potential Tracers for Positron Emission Tomography Imaging. *J. Med. Chem.* **2012**, *55* (20), 8685–8699; (e) Fan, Y.; Hanai, J.; Le, P. T.; Bi, R.; Maridas, D.; DeMambro, V.; Figueroa, C. A.; Kir, S.; Zhou, X.; Mannstadt, M.; et al. Parathyroid Hormone Directs Bone Marrow Mesenchymal Cell Fate. *Cell Metab.* **2017**, *25* (3), 661–672.

[25] (a) Tsukamoto, T. Tough Times for Medicinal Chemists: Are We to Blame? *ACS Med. Chem. Lett*. **2013**, *4* (4), 369–370; (b) Walters, W. P.; Green, J.; Weiss, J. R.; Murcko, M. A. What Do Medicinal Chemists Actually Make? A 50-Year Retrospective. *J. Med. Chem.*. **2011**, *54* (19), 6405–6416.

[26] (a) Newman, S. G.; Jensen, K. F. The Role of Flow in Green Chemistry and Engineering. *Green Chem.* **2013**, *15* (6), 1456; (b) Löwe, H.; Hessel, V.; Löb, P.; Hubbard, S. Addition of Secondary Amines to α,β-Unsaturated Carbonyl Compounds and Nitriles by Using Microstructured Reactors. *Org. Process Res. Dev.* **2006**, *10* (6), 1144–1152.

[27] Parasram, M.; Gevorgyan, V. Visible Light-Induced Transition Metal-Catalyzed Transformations: Beyond Conventional Photosensitizers. *Chem. Soc. Rev.* **2017**, 46, 6227-6240.

[28] Guijarro, A.; Rosenberg, D. M.; Rieke, R. D. The Reaction of Active Zinc with Organic Bromides. *J. Am. Chem. Soc.* **1999**, *121* (17), 4155–4167.

[29] Mompeán, M.; Sánchez-Donoso, R. M.; De La Hoz, A.; Saggiomo, V.; Velders, A. H.; Gomez, M. V. Pushing Nuclear Magnetic Resonance Sensitivity Limits with Microfluidics and Photo-Chemically Induced Dynamic Nuclear Polarization. *Nat. Commun.* **2018**, *9* (1).

[30] Giannopoulou, G.; Stoimenov, N.; Huang, P.; Thiele, L.; de Dinechin, B. D. Mixed-Criticality Scheduling on Cluster-Based Manycores with Shared Communication and Storage Resources. *Real-Time Syst.* **2016**, *52* (4), 399–449.

[31] Klement, I.; Lütjens, H.; Knochel, P. Oxidation of Zinc Organometallics Prepared by Hydrozincation or Carbozincation Using Oxygen. *Tetrahedron Lett.* **1995**, *36* (18), 3161–3164.

[32] Chakraborty, S.; Piszel, P. E.; Brennessel, W. W.; Jones, W. D. A Single Nickel Catalyst for the Acceptorless Dehydrogenation of Alcohols and Hydrogenation of Carbonyl Compounds. *Organometallics* **2015**, *34* (21), 5203–5206.

[33] Soler-Yanes, R.; Arribas-Alvarez, I.; Guison-Ceinos, M.; Buï¿½uel, E.; Cardenas, D. J. NiICatalyzes the Regioselective Cross-Coupling of Alkylzinc Halides and Propargyl Bromides to Allenes. *Chem. Eur. J.* **2017**, *23* (7), 1584–1590.

[34] (a) Kurandina, D.; Parasram, M.; Gevorgyan, V. Visible Light-Induced Room-Temperature Heck Reaction of Functionalized Alkyl Halides with Vinyl Arenes/Heteroarenes. *Angew. Chem. Int. Ed.* **2017**, *56* (45), 14212–14216; (b) Fredricks, M. A.; Drees, M.; Köhler, K. Acceleration of the Rate of the Heck Reaction through UV- and Visible-Light-Induced Palladium(II) Reduction. *ChemCatChem* **2010**, *2* (11), 1467–1476.

Chapter 5

Photoinduced Palladium Negishi Cross-Coupling Through Visible Light Absorption of Palladium-Organozinc complexes.

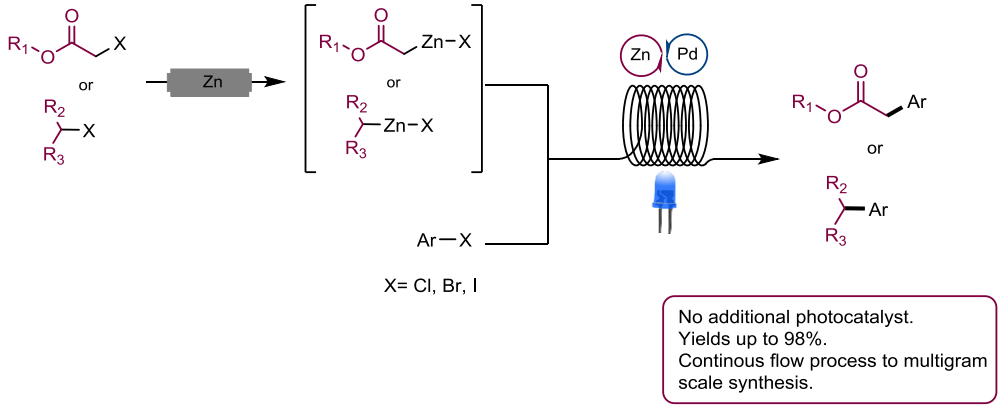

5.1 Introduction

The synthesis of α-aryl esters and their derivatives is of high interest in medicinal chemistry. The α-aryl ester functionality is present in many pharmaceuticals used in inflammatory diseases such as Naproxen, Ibuprofen, Flurbiprofen and Tolmetin. More recently, Allegra (fexofenadine hydrochloride), which contains the α-aryl isobutyric acid moiety, has been developed as a second-generation antihistaminic drug (Figure 0.1).[1] Beside these molecules, α-aryl esters are valuable building blocks as precursors of aryl alcohols, amines and nitriles. The ester functionality can be used to further build carbon skeleton and enrich the core with (sp^3) moieties.[2]

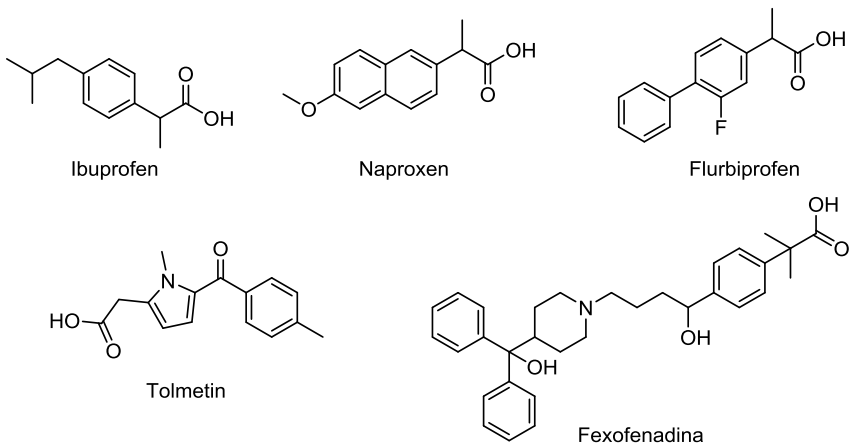

Figure 0.1: Commercial drugs containing α-aryl esters functionalities

Nowadays, the synthesis of α-arylated ester enolates is based on four major catalytic strategies (Figure 0.2): 1) Buchwald-Hartwig arylation of ester enolates[3]; 2) coupling of α-halo esters with arylmetallic species such as silanes[4], Grignard reagents[5], or boron compounds[6] catalyzed by nickel, iron or palladium; 3) nickel catalyzed coupling of aryl halides and α-halo esters[7]; 4) cross-coupling of Reformatsky reagent with aryl halides[8]. These methods are the bases for the insertion of an ester functionality. Nevertheless, they have their own limitation mostly on the limited scope of the reaction, low group tolerability due to drastic reaction conditions or equimolecular amounts of metals.

Metal-mediated coupling of enolates had been achieved initially with stoichiometric quantities of nickel complexes. In 1973, Semmelhack et al. reported the nickel-mediated intramolecular arylation of an ester[9], and afterwards Millard and Rathke discovered the nickel-mediated intermolecular arylation of lithium enolates[10]. Subsequently, Fauvarque and Jutand reported the nickel-catalyzed coupling of a few aryl halides with a Reformatsky reagent, but the scope of the reaction was narrow.[11]

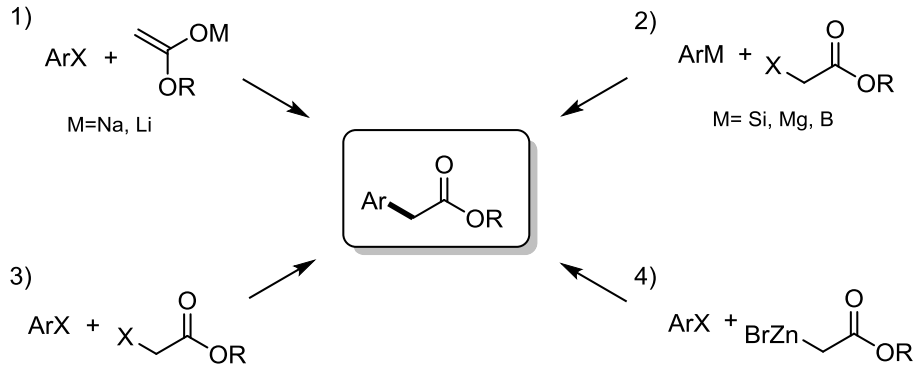

Figure 0.2: Synthesis of α-arylated ester enolates

In 1982, Kuwajima and Urabe discovered that tin enolates, generated in situ from silyl enol ethers in the presence of tributyltin fluoride, undergo palladium-catalyzed cross-coupling with aryl bromides to provide R-aryl ketones.[12] Based on this report, Sulikowski extended Kuwajima and Urabe's results to the synthesis of aryl acetates by palladium-catalyzed cross-coupling of aryl bromides and copper(II) enolates.[13] In this case, yields were good, but the reaction was limited to the synthesis of R-aryl acetates. In 1991-1992, the palladium coupling of trimethylsilylketene acetals with aryl triflates or halides in the presence of toxic thallium acetate to obtain alkyl 2-arylalkanoates was reported by Musco and Santi.[14] In the following year, Yamanaka published the palladium-catalyzed synthesis of ethyl aryl acetates using aryl halides and ethoxy (trialkylstannyl) acetylenes to afford ethoxy (ethynylalkylstannyl) acetylenes that, after solvolysis, provided ethylaryl acetates.[15] These methodologies, sometimes, require the use of highly reactive toxic reagents and the substrate scope in most cases is very narrow.

Reformatsky reagents, by the other hand, are milder bases and nucleophiles than alkali metal enolates. The coupling of zinc enolates could improve the functional group tolerance of the arylation of esters. The palladium catalyzed *α*-arylation of ester enolates was reported using the isolated Reformatsky reagents of tert butyl acetate and propionate.[11,16] These arylation reactions in general occurred in low yields with high palladium loading (10 mol %) using tri-arylphosphine ligands.

A plausible catalytic cycle for the palladium-catalyzed addition of enolates to aryl halides is shown Figure 0.3. Oxidative addition of an aryl halide to a Pd(0) complex would form an arylpalladium(II) halide complex (b). Substitution of the coordinated halide by an enolate nucleophile and reductive elimination from the resulting palladium enolate complex (c) or (d) would form the R-aryl ketone, ester, or amide and regenerate the Pd(0) complex (a) that started the cycle.

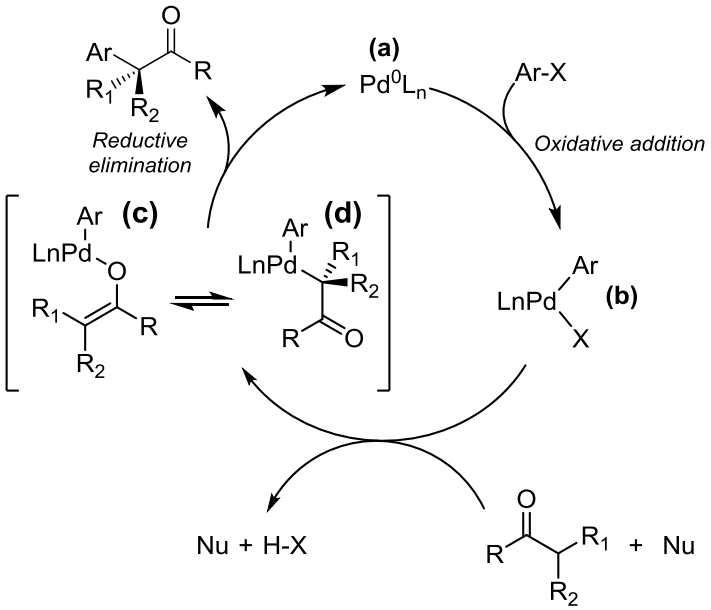

Figure 0.3: Catalytic cycle for the palladium-catalyzed addition of enolates to aryl halides

There are several challenges to be considered in the cross coupling of enolates with aryl halides by this mechanism. For instance, the pKa values of mono- and dicarbonyl compounds in organic solvents vary from 12 to 35.[17] Therefore, electronic effects may have a large influence on the reaction chemistry. Moreover, alkali metal enolates are typically generated and allowed to react at low temperatures. Cross-coupling reactions are usually conducted at elevated temperatures. Thus, uncatalyzed condensation chemistry of the enolate could occur before the desired catalytic coupling.

The structures of the arylpalladium enolates could also vary from substrate to substrate. The structures of transition metal enolates include C-bound[18] and O-bound[19] enolates of monocarbonyl compounds. These structures are in equilibrium between them and they may all interconvert and allow access to the one that undergoes reductive elimination with consecutive product formation. But, depending on the structure of the enolate, stable intermediates, that do not undergo reductive elimination, can be formed and therefore block the reaction.

Moreover, C-bound enolates of transition metals, despite those from methyl carbonyl compounds, have β-hydrogens. Therefore, β-hydrogen elimination could compete with reductive elimination to form the desired coupled product.

To alleviate such complications, the research groups of Hartwig and Buchwald worked in parallel to optimize the palladium catalyzed arylation of enolates. Both groups,

observed that the choice of the palladium ligand is crucial for the outcome of the reaction. While Hartwig focused their attention in the combination of $Pd(dba)_2$ with 1,1'-bis(di-o-tolylphosphino) ferrocene and its derivatives, Buchwald obtained better results with palladium and binap or tol-binap systems. It was speculated that the use of these bulky chelating ligands forces the palladium complex to be in a four-coordinate state which stabilizes the Pd, prevents the *β*-hydrogen elimination and push the catalytic cycle towards the reductive elimination and product formation. Moreover, the Buchwald group hypothesized that the use of bulky phosphines could suppress diarylation.[18c] Subsequently, they investigated the effects of the substituents in a wide series of biaryl electrone-rich phosphine ligands synthetized by them.[20]

As in the studies of Hartwig and coworkers, Buchwald group confirmed that both steric and electronic properties of the ligand are very important in the palladium catalyzed α-arylation reactions. They can be varied readily and independently permitting the fine-tuning of the coordinated species and thus allowing the desired properties to enhance different steps of a catalytic cycle.

As a result in 2003, Hartwig and coworkers reported the α-arylation of esters and amides in less basic conditions using Reformatsky reagents and Pd(I) complex $\{Pd(t\text{-}Bu)_3]PdBr\}_2$ or $Pd(dba)_2$ and Q-phos.[8a] In 2004, Moloney reported microwave assisted palladium catalyzed α-arylation of zinc enolate with stoichiometric quantities of $Pd(Ph_3)_4$.[21] Knochel in 2012, reported 3 other examples of Palladium catalyzed α-arylation reaction with zinc enolates by changing the phosphine ligand of the palladium.[8d]

In the last 10 years, visible light is used as a new tool to accelerate transition metal catalysis. More recently, there are several reports from Gevorgyan[22], Fu[23] and Yu[24] where they use visible light irradiation to accelerate palladium catalytic cycle by direct absorption of the palladium catalyst. The light energy excites the Pd (0) in $Pd(0)^*$ facilitating the single electron transfer process during the oxidative addition and therefore enabling the Heck reaction for unactivated substrates.

5.2 Results and discussion

Considering these precedents and importance of the arylated esters in medicinal chemistry, we decided to develop a mild and broadly applicable methodology to insert alfa aryl esters into disactivated aromatic cores. To maintain group tolerability and mild reaction conditions, fundamental for drug discovery substrates, we chose the coupling of zinc- enolates with aryl halides, as more group tolerant and milder nucleophiles than alkali metals. We started the exploration with *p*-benzyloxy bromobenzene, a substrate not described in similar transformation. In our last article, we reported photoinduced conditions for Negishi reaction.[25] The light had a direct effect in the acceleration of well-

known nickel-catalyzed Negishi cross-coupling broadening the scope to bromo and chloro aryles. Therefore, we tested the photo-induced Nickel Negishi reaction for the cross-coupling of the Reformatksy reagent but no reaction was observed (Figure 0.4).

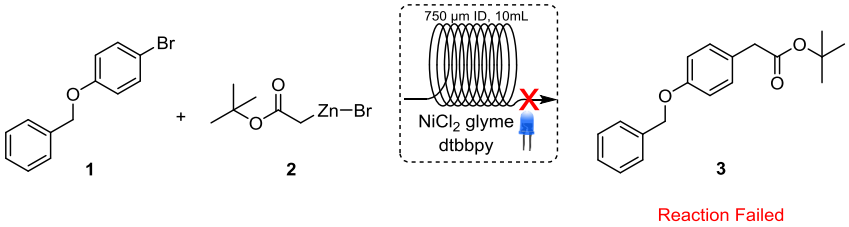

Figure 0.4: Photoinduced Ni Negishi reaction

Considering this result, we stepped back into traditional Negishi reaction opting that the selection of the phosphine would improve the reaction. As shown in Table 0.1 different combination of Pd catalyst with previously described phosphines and others of our own experience were tried.

Table 0.1: Traditional Pd-Negishi conditions

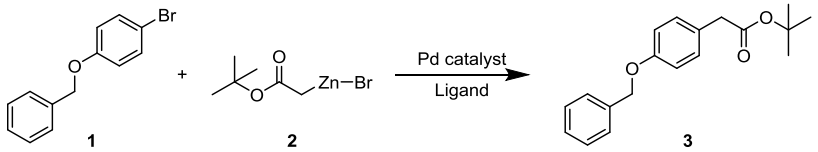

Entry	Catalyst	Conv. (%) 1h	Conv. (%) 16h
1	QPhos $Pd(dba)_2$	12	28
2	$Pd(^tBu_3P)_2$	3	7
3	SPhos, $Pd(dba)_2$	2	2
4	XPhos $Pd_2(dba)_3$	31	39
5	XantPhos $Pd(dba)_2$	0	0
6	JohnPhos $Pd(dba)_2$	3	4
7	Tetrakis	0	0

Reaction conditions: The reactions were run in parallel in batch; benzyloxy 4-bromobenzoate (1 eq., 0.5 mmol); (2-(tert-butoxy)-2-oxoethyl) zinc(II) bromide (1) (2 eq., 1 mmol); Pd catalyst (0.1 eq., 0.05 mmol).

We selected to test the Hartwig phophines Q-Phos and the direct complex $Pd(tBu_3P)_2$, the most described complexes for this kind of transformation.[8a,c] Then we opted for some of the biarylic Buchwald phosphines such as SPhos[8d,26], XPhos[27], XantPhos[8g] and JohnPhos. The three first ones are described in similar chemistry but Johnphos is not. We selected it because of its simplicity and the lack of substitution in the second aryl ring. At the end the traditional Tetrakis[28] complex was tested as well. The conversion was monitored in time in for 16 hours but, as expected in Negishi reactions, there was

no big difference between the first hour and the final hour. Combination of $Pd(dba)_2$ with XPhos and QPhos provided the best result, respectively 39% and 28% of product in 16 h (Table 0.1, Entry 1 and 4). With XantPhos the reaction failed (Table 0.1, Entry 5) and with SPhos only 2% of product was obtained (Table 0.1, Entry 3). Changing the $Pd(dba)_2$ with $Pd[(Ph_3)]_4$ did not provide conversion in product (Table 0.1, entry 7), and $Pd(tBu_3P)_2$ gave only traces of product (Table 0.1, Entry 2). To our surprise, even if it was not described before in literature, the less bulky phosphine, JohnPhos gave some traces of product (Table 0.1, Entry 6). However, unfortunately, none of these reaction conditions were efficient for us.

Taking into account, the work of Gevorgyan[22a] and our own experience in Photo-induced Negishi reaction we tried to irradiate the reaction mixture and see the outcome. The combination of $Pd(dba)_2$ and JohnPhos was selected to be tested with light irradiation because, between the tried phosphines, JohnPhos is the only one that has not been reported before in literature in this kind of transformations. Moreover, it is a cheap phosphine and has no substituents in the second aryl ring offering further opportunities for functionalization in more complicated substrates.

Table 0.2: Optimization of the Light Induced Pd- Negishi reaction

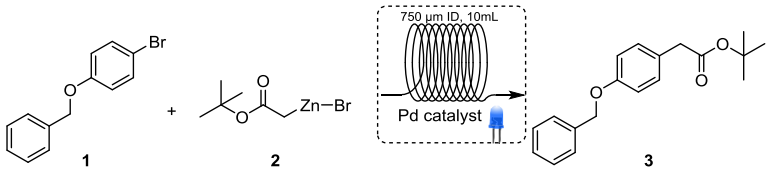

Entry	Time (min)	Temp. (°C)	Irradiation (nm)	Palladium catalyst*	Conv. (%)
1	30	40	450	(1) 10 mol%.	100
2	30	40	450	(1) 5 mol%	100(85%)[a]
3	30	40	450	(1) 2.5 mol%	31
4	20	40	450	(1) 5 mol%.	90
5	30	40	450	-	0
6	30	40	off	(1) 5 mol%	5
7	30	40	450	(2) 5 mol%	28

*(1) = $Pd(dba)_2$; (2) = $Pd(OAc)_2$
Reaction conditions: benzyloxy 4-bromobenzoate (1 eq., 0.2 mmol); (2-(tert-butoxy)-2-oxoethyl) zinc(II) bromide (1) (2 eq., 0.4 mmol); (a) isolated yield.

To our surprise light irradiation of $Pd(dba)_2$ with JohnPhos ligand provided full conversion in product (Table 0.2, Entry 1). The reaction proceeded in flow, only 30 minutes of residence time in 40 °C. The organozinc of the Reformatsky reagent was prepared using

our protocol for the preparation of the organozinc reagents in flow.[29] The protocol provided a solution of 0.35 M Reformatsky reagent. Reducing the time in 20 minutes was not necessary to provide full conversion in product (Table 0.2, Entry 4). The optimal palladium loading was 5 mol% (Table 0.2, Entry 2). Reducing it to 2.5 mol% reduced the conversion to 31% of product (Table 0.2, Entry 3). Control experiments indicated that both light and Pd-catalyst are essential for this transformation (Table 0.2, Entry 5, 6). Changing the palladium source from $Pd^0(dba)_2$ to $Pd^{II}(OAc)_2$ decreases the conversion to 28% (Table 0.2, Entry 7) suggesting that the catalytic cycle starts with Pd^0 complex.

5.3 Exploration of the scope of the reaction

With the optimized condition in our hands we explored the substrate scope of the reaction (Figure 0.5). First of all, the corresponding organozinc reagents were prepared. Tert-butyl bromoacetate, benzyloxy bromoacetate and ethyl bromoacetate provided their organozinc enolates **2**, **4** and **5** in concentrations that go from 0.3 M to 0.35 M. The zincate of the boc protected iodo-azetidine was prepared in LiCl/THF solution due to its instability. The iodo-zinc boc-azetidine **6** was obtained in 0.25 M solution. The 3-iodo-1,1,1-trifluoropropane provided the corresponding organozinc solution **7** in 0.34 M molarity. The cyclic ester and cyclic amide were slightly less reactive than the previous ones affording 0.2-0.22 M solutions respectively (Compound **8** and **9**).

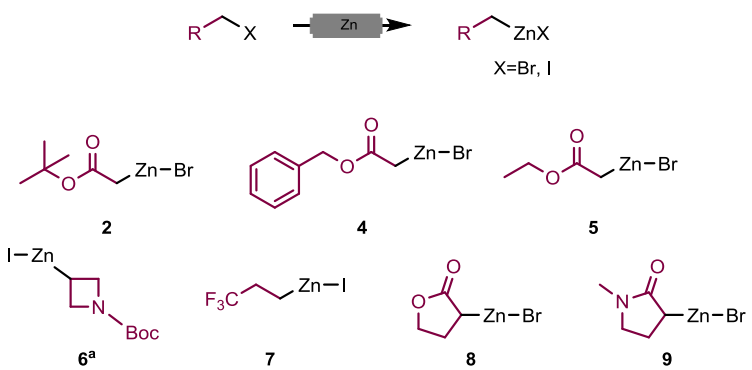

Figure 0.5: Organozinc reagents synthetized in flow; (a) Solution prepared in LiCl/THF

A broad variety of bromo derivatives were used as cross-coupling partners of Reformatsky reagents (Figure 0.6). The reaction showed to be chemoselective towards bromo substitution, example **10**. The scope of reformatsky reagents included tert-butyl bromo acetates, ethyl bromo acetates and benzyl bromoacetates. In all cases light irradiation was essential to obtain high conversions, from 40-100% and there was always a big gap between light and no light reaction. The use of visible light irradiation provides mild reaction conditions assuring wide group tolerability. The nitro group is well tolerated providing the product **11** in 91 % of isolated yield. 4-ciano bromo benzene

behaved similar providing the product **12** in 84% of isolated yield. Both ciano and nitro group can be used as precursors of amide derivatization for further functionalization for med-chem purposes. Not only aryl halides but even bromo heterocycles showed to be good coupling partners. 2-bromo-5-trifluoromethyl pyridine gave only 12% of conversion without light irradiation. The conversion was busted to 69% when the reaction mixture was irradiated (Compound **22**). Considering these results, we decided to further broad the scope with more variety of zincates. Azetidine has shown to be an important core in medicinal chemistry.[30] The organozinc reagent of the boc protected iodo azetidine was prepared and it was coupled with methyl 4 bromo benzoate. The reaction without light did not provide the expected product while, when light was on, 65% of isolated product was obtained (Compound **13**). The boc protection group was well tolerated. This is a big step for drug discovery projects because in one step we could functionalize the azetidine and leave the aminic group opened for further transformation.

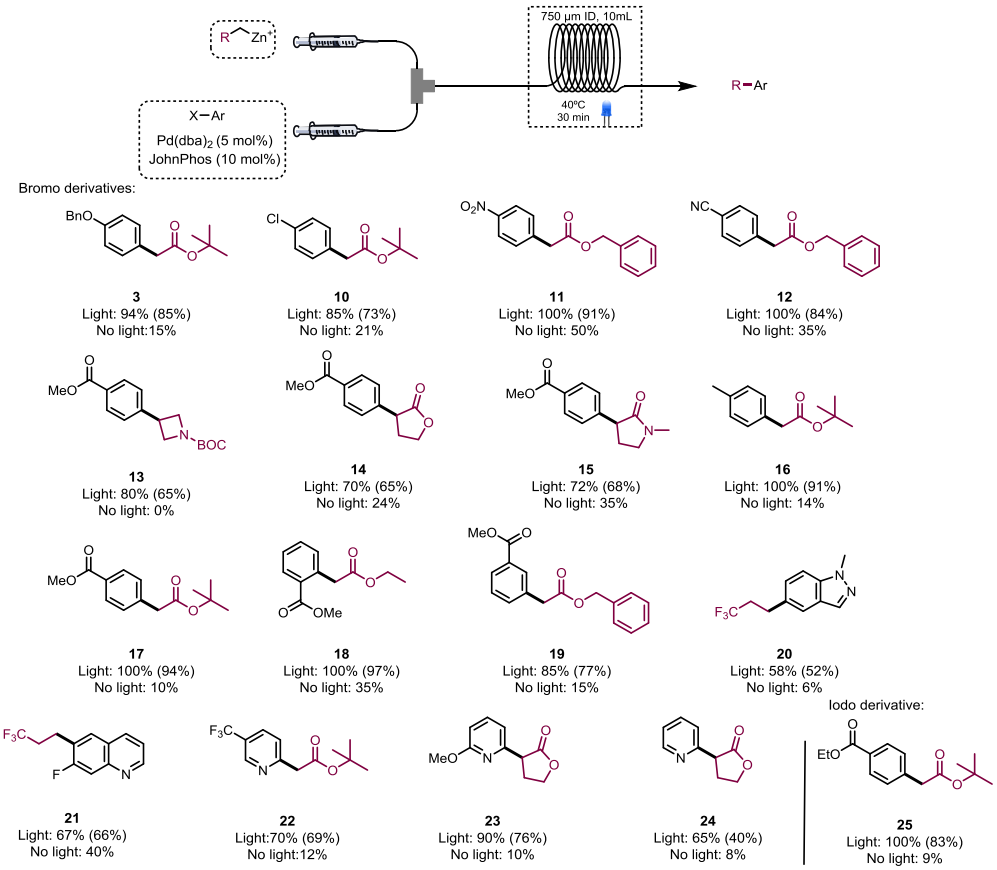

Figure 0.6: Substrate scope Light Promoted Pd-Negishi

Other examples of coupling of secondary carbons are the coupling of the cyclic amide and the α-butyro-lactone. The α-butyro lactone provided high conversion in product not only with methyl 4 bromo benzoate; 65% of product **14**, but as well with pyridines such as 2-bromo-pyridine and 2-methoxy-2-bromo-pyridine yielding the product in 40% and 76% respectively (Compounds **24** and **23**). In both cases, without light, we observe only traces of product. Alkylic chains are suitable zincate precursors that can functionalize complex bicyclic heterocycles increasing the three dimensionality of drug like molecules. As an example, the trifluoro propionate zinc bromide was coupled with the 5-bromo-1-methyl-1H-indazole and 6-bromo-7-fluoro-quinoleine yielding the products **20** and **21** in 52% and 67% each. Ethyl 4-iodo-benzoate showed to be good coupling partner as well providing the product **25** in 83% yield with light irradiation, and only 9 % no light irradiation.

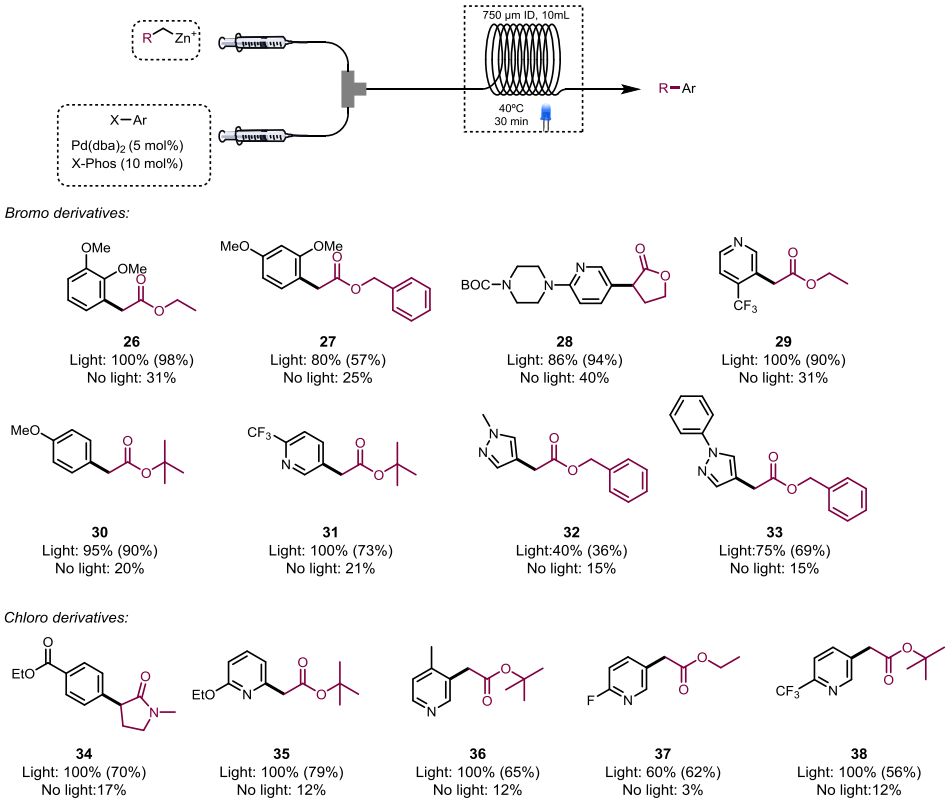

Figure 0.7: Substrate scope 2 Light Promoted Pd- Negishi

Changing the phosphine from JohnPhos to a bulkier phosphine with substituents in the second aryl ring such as XPhos allowed us to further broad the scope to more disactivated bromo derivatives and as well chloroderivatives (Figure 0.7). The catalytic reactivity of the complex $Pd(dba)_2$–XPhos was clearly enhanced by light irradiation. The

1-bromo-2,3-dimethoxy benzene and 1-bromo-2,4-dimethoxy benzene bypassed their steric hinderance problems and provided the products **26** and **27** in 98% and 57% each. The use of XPhos as phosphine allowed the functionalization of pyridines in meta position in excellent yields, 94%, 90% and 73% respectively (Compounds **28**,**29**,**31**). Not only bromo but even 3-chloro pyridines behaved in the same way yielding products **36**,**37** and **38** in 80%, 62% and 56% each. The 4-halogen-pyrazoles have never been described in literature as coupling partners in Pd-Negishi reactions due to their high electron density in position 4 that hinders the oxidative addition. Nevertheless, this protocol resulted effective to couple the methyl pyrazole and phenyl pyrazole with benzyl bromoacetate in moderate to good yield respectively (Compounds **32** and **33**).

Considering the difference in conversion between the purely thermal Negishi and the light induced one, kinetics studies were performed with compound **18** following its formation in flow at different timepoints in presence and absence of light. The results are presented in Figure 0.8. The light enhancement is notable since the initial moments of the reaction and we observe the same slope between the light and no light kinetics. The two curves are almost parallel between them. While the irradiated reaction goes on full conversion in 30 minutes, the maximum conversion reached without light irradiation is of 45% in 40 minutes. In the nickel catalysis both curves are different as shown in Figure 4.5 Chapter 4. This suggests that light absorption may occur in different steps of the catalytic cycle.

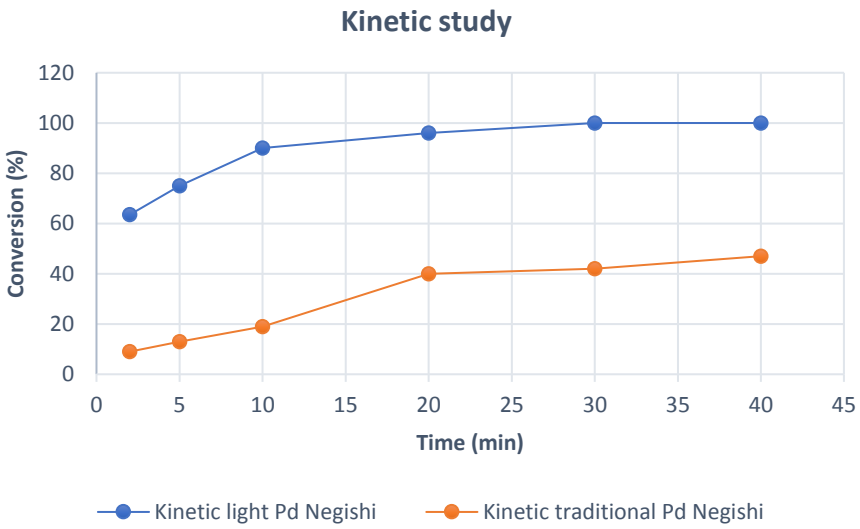

Figure 0.8: Kinetic study Pd- Negishi reaction

5.4 Scale up

The preparation of compound **19** was selected to demonstrate the scalability of this methodology. The organozinc reagent was prepared in flow, and the exiting stream was connected to a second solution stream containing the haloarene and the catalytic complex before entering the photoreactor). This process was run continuously for 5 h and compared with the same reaction in batch by sampling at different timepoints (Figure 0.10A).

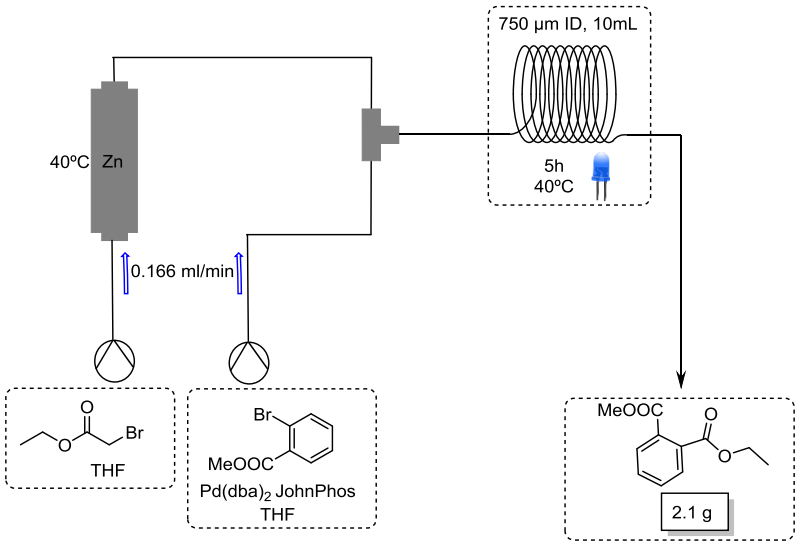

*Figure 0.9: Scale up of the reaction: Compound **18***

The flow protocol provided 2.1 g of the desired product upon isolation (97% yield), with a productivity of 520 mg/h. In contrast, in the traditional Negishi batch protocol, the product was only isolated in 36% yield. Considering the reaction times and reaction volumes, the space/time yields were calculated; these clearly support the new flow process (Figure 0.10B).

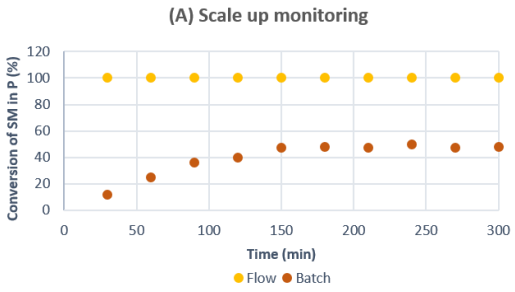

(B) Flow/Batch Comparison	Flow	Batch
Yield	97	36
Time	30 min	5 h
Throughput	420 mg/h	8 mg/h
Space-time Yield	42.0 mg/h·ml	1.6 mg/h·ml

Figure 0.10:(A) Scale up monitoring; (B) Comparison Flow/Batch

5.5 Mechanistic investigation

5.5.1 Absorbance studies

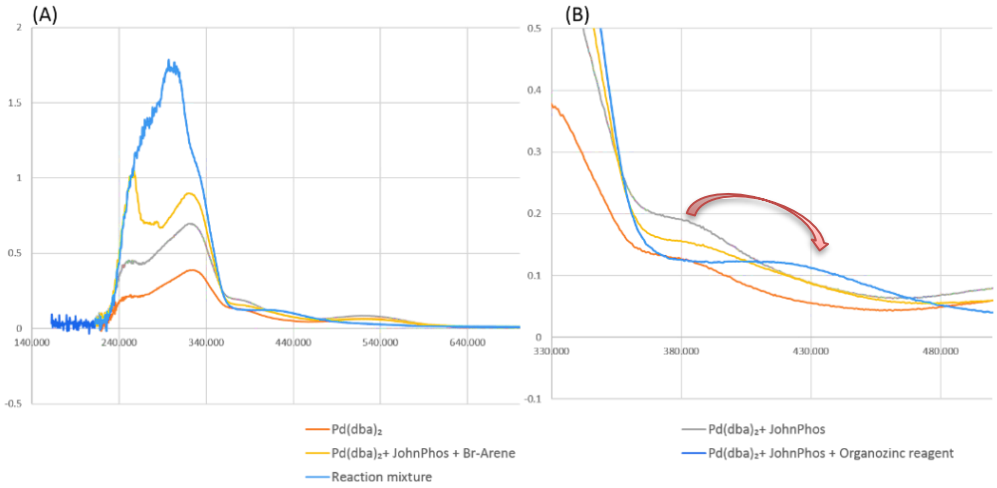

Figure 0.11: Absorbance spectra of different components of the reaction mixture; left: entire spectra; right: zoom on the area of interest; the arrow indicates the shift in absorbance spectra.

To identify is the photoabsorbing species, absorption spectra of different components of the reaction were recorded (Figure 0.11). Previous reports showed that Pd^0Ln can be photoactivated into Pd^{0*} with visible light irradiation due to tailing absorption into visible spectra. We could confirm that $Pd(dba)_2$ solution in THF has an absorbance tailing at 380 nm. Similar profile was observed when the complex between $Pd(dba)_2$ and JohnPhos is formed. When the organozinc reagent is added to the mixture a clear absorption band appears at 430 nm, shifting the absorption to completely visible light irradiation. Even the reaction mixture with all its components has similar absorption. These data suggest that the photoabsorbing species in this reaction requires the presence of the two metals Pd and Zn.

Considering the absorption spectra, we studied the formation of compound **3** under irradiation at different wavelengths to determine the effect of light in the reaction outcome. In concordance with the absorption spectra, blue light irradiation (450 nm) gave the best results providing full conversion in product.

Table 0.3: Effect of the light irradiation

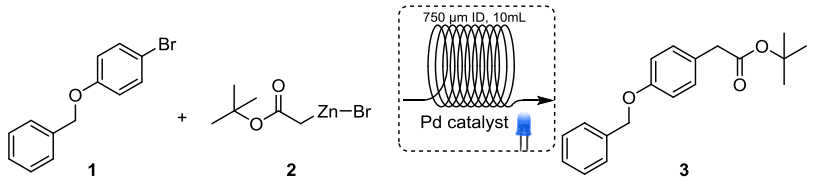

λ (nm)	dark	365	450	525
Conv. (%)	5	89	100	61

Reaction conditions: benzyloxy 4-bromobenzoate (1 eq., 0.2 mmol); (2-(tert-butoxy)-2-oxoethyl) zinc(II) bromide (1) (2 eq., 0.4 mmol); $Pd(dba)_2$ (0.05 eq.; 0.01 mmol); JohnPhos (0.1eq, 0.02 mmol).

5.5.2 Radical trap reactions

Single electron transfer (SET) processes has shown to be crucial in Palladium photoinduced reactions. We conducted radical trap experiments to probe the radical reactivity of metal alkyl species. Compound **38** was selected to test the presence of radicals in the reaction media. Considering our previous experience in the reactivity of the zincates with radical trap reagents described in Chapter 4 we chose the diphenylethylene and dibutylhydroxytoluene (BHT) as trapping reagents (Figure 0.12). None of them showed reactivity and the conversion of starting material in product **38** remained 100%. These results suggest the absence of the radicals in the reaction but as in the previous chapter their presence cannot be ruled out.

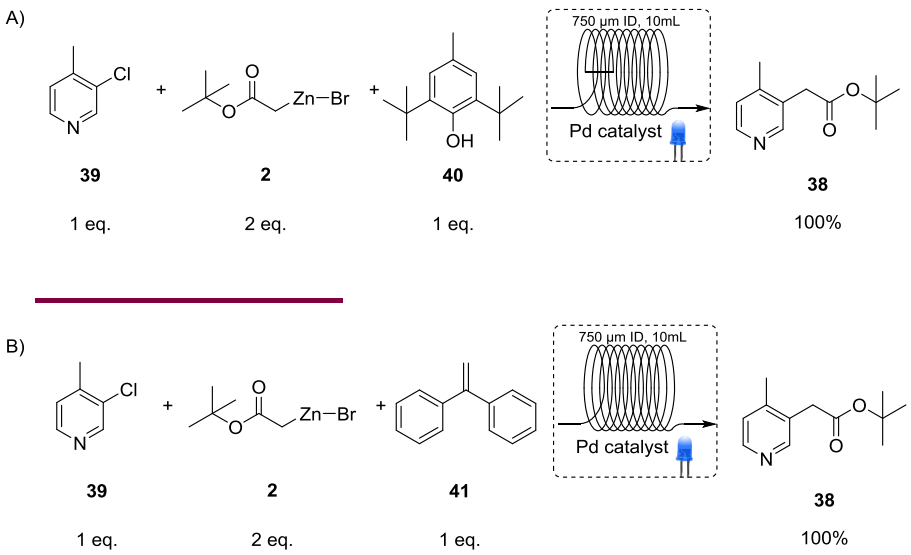

Figure 0.12: Radical trapping reactions

5.5.3 NMR investigation

In collaboration with the group of Dr. Maria Victoria Gomez and Prof. Antonio de la Hoz in the University of Castilla La Mancha, NMR spectroscopy was used as an analytical tool to elucidate the mechanism of the reaction. As described in the previous chapter, the collaboration with the UCLM gives access to a device that they have developed that allows to register NMR spectra irradiating with *in situ* light irradiation. The subsequent experiments were performed by Jose Miguel Mateo Gonzales at the UCLM and we are using them to provide insight about the mechanism of the reaction.

We selected 6-bromo-7-fluoroquinoline and CF_3-CH_2-CH_2-ZnI as cross-coupling partners since both reagents and the product present ^{19}F nuclei. Considering that we have JohnPhos as the Pd ligand, ^{31}P NMR gives direct information on the catalytic complexes that are formed in the reaction. In this way, we could monitor not only the consumption of the cross-coupling partners to form the reaction product but also the involvement of the catalytic complex in the reaction.

The first step was to observe the changes produced when forming the catalytic complex by ^{31}P NMR. Addition of $Pd(dba)_2$ to a solution of JohnPhos produces the appearance of a new small signal at 58.97 ppm that was assigned to the catalytic complex (Figure 0.13b). Addition of 6-bromo-7-fluoroquinoline to the catalytic complex does not produce appreciable changes in the chemical shift but an increase in its intensity and no evolution with time (Figure 0.13c). On the contrary, addition of the organozinc derivative to the catalytic complex produces downfield shift of this signal to 60.33 ppm and an increase in its intensity (Figure 0.13d).

These experiments clearly show an interaction between the organozinc reagent and Pd(0) (Figure 0.13). This may imply that the first step in the catalytic cycle is the coordination of the zincate to Pd in the catalytic complex and not the coordination of the bromoderivative as usually assumed. In order to determine whether the signal at 60.33 ppm corresponds either Pd(0) or Pd(II) complexes, some control experiments were performed. For that purpose, $Pd(OAc)_2$ was added to a solution of JohnPhos and analyzed by ^{31}P NMR (Figure 0.14c). The signal observed for the catalytic complex coordinated to Pd(II) was 69.70 ppm, chemical shift usually observed for this oxidation state of palladium.[31] This allows us to assign the signal at 60.33 ppm to Pd(0) complex. This fact is in agreement with the UV analysis, where the absorption band corresponding to Pd(0) at 380 nm is shifted to 430 nm upon addition of the zincate.

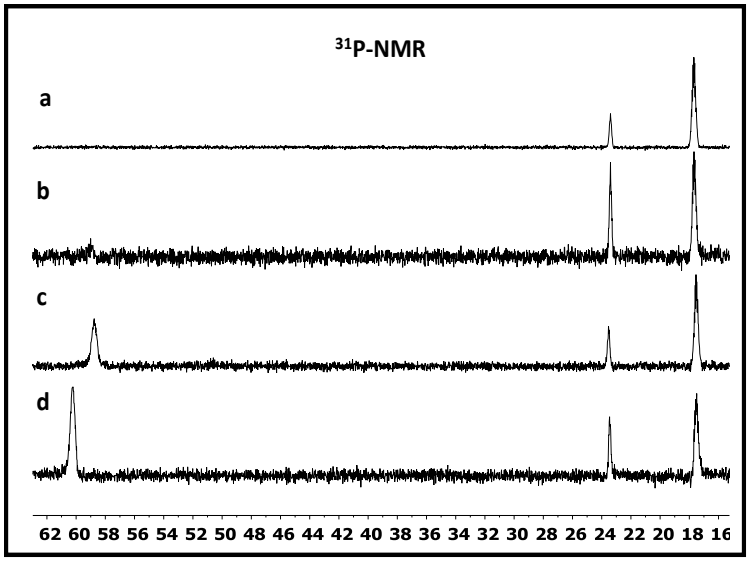

Figure 0.13: Figure 1. ^{31}P NMR spectra: a) JohnPhos (17.57 ppm); b) JohnPhos + $Pd(dba)_2$; c) JohnPhos + $Pd(dba)_2$ + 6-bromo-7-fluoroquinoline; d) JohnPhos + $Pd(dba)_2$ + (3,3,3-trifluoropropyl) zinc(II) bromide.

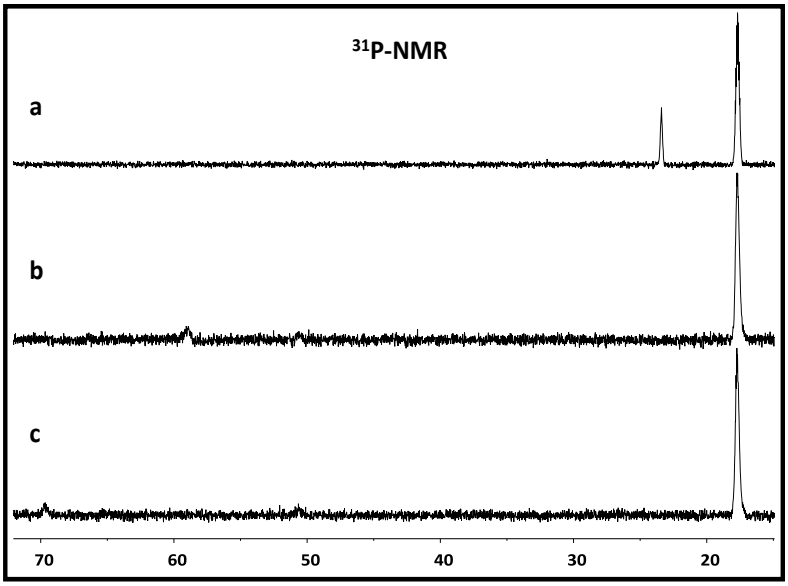

Figure 0.14: ^{31}P NMR spectra of a) JohnPhos solution (17.57 ppm), b) JohnPhos + $Pd(dba)_2$ (58.97 ppm) and c) JohnPhos + $Pd(OAc)_2$ (69.70 ppm)

The next step was to monitor the reaction with the aim of obtaining the cross-coupling reaction product. For that purpose, the zincate was added to the reaction mixture containing the catalyst, the ligand and the bromo derivative (Figure 0.15). As mentioned

above, the signal corresponding to the catalytic complex in the ^{31}P NMR spectra is downfield shifted because of its activation (Figure 0.15a). The reaction proceeds very slowly, since it requires up to two days for the complete consumption of the complex. In the case of ^{19}F NMR spectra, the cross-coupling product NMR signal starts to appear from 2 h on (Figure 0.15b). This experiment clearly shows the slow rate of this reaction. For that reason, we wondered if the presence of light would improve the outcome of this reaction.

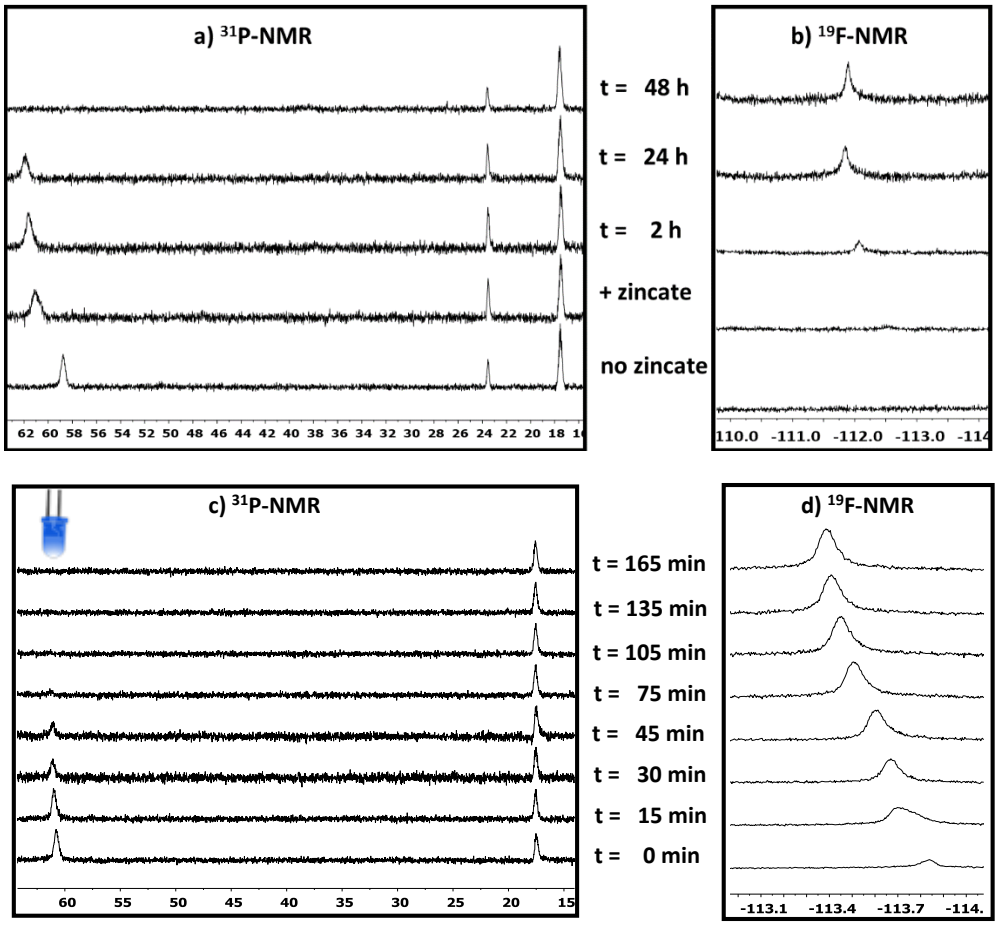

Figure 0.15: Reaction monitoring of JohnPhos + $Pd(dba)_2$ + 6-bromo-7-fluoroquinoline + (3,3,3-trifluoropropyl) zinc(II) bromide with equimolecular amounts of catalyst;. Reaction in the absence of light: a) ^{31}P NMR, b) ^{19}F NMR. Reaction in the presence of light: c) ^{31}P NMR, d) ^{19}F NMR.

As previously observed by us,[8] light plays an important role during this kind of reactions, since the reaction yields are considerably increased and reaction times reduced. In this approach some kinetic experiments were performed in the presence of light with both

catalytic and equimolecular amounts of the catalyst, and *off-line* irradiation was carried out. The reaction mixture was transferred to a 5 mm-NMR tube and placed inside the LED-illumination device previously reported by the group of UCLM to activate the reaction,[32] and ^{31}P and ^{19}F NMR spectra were recorded with time. In Figure 0.15c, two ^{31}P NMR signals are observed, corresponding to the ligand and the activated catalytic complex. The presence of both cross-coupling partners in the reaction mixture carries the reaction to completion, so that the NMR peak corresponding to the activated catalytic complex decreases with time and at 75 min is completely consumed. The evolution of the F-atom from the cross-coupling product (-113.94 ppm) was followed by ^{19}F NMR (Figure 0.15d). Importantly, the intensity of this peak increases up to 75 min, matching to the disappearance of the activated catalytic complex in the ^{31}P NMR spectra (Figure 0.15c), and then remains constant. It is important to remark that the catalytic complex does not evolve when the 6-bromo-7-fluoroquinoline is not present in the reaction mixture and remains constant with time even in the presence of light (Figure 0.16).

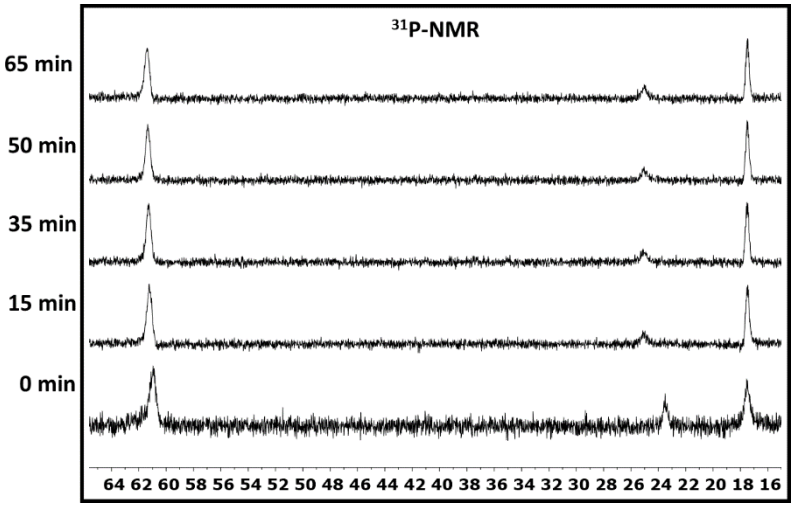

Figure 0.16: ^{31}P NMR spectra of JohnPhos + $Pd(dba)_2$ + (3,3,3-trifluoropropyl) zinc(II) bromide in the presence of light.

To further corroborate the role of light during this reaction, we used catalytic amounts of the reagents. In these conditions, the formation of the cross-coupling product is more favoured. As observed in Figure 0.17a, the organozinc derivative decreases very rapidly in the presence of light (orange line), while in the absence of light the consumption is much lower (orange triangles). At the same time, 6-bromo-7-fluoroquinoline behaves likewise, but in the presence of light is completely consumed at 45 min (green line). In the case of the formation of the organozinc derivative dimer (Figure 0.17b), no appreciable differences are observed both in the presence and in the absence of light

(yellow line *vs.* yellow triangles). However, formation of the cross-coupling product considerably increases when light is present (blue line), especially at the very beginning of the reaction. These experiments clearly show the role of light during the reaction, favouring the formation of the cross-coupling product while dimerization of the zincate is not affected at all.

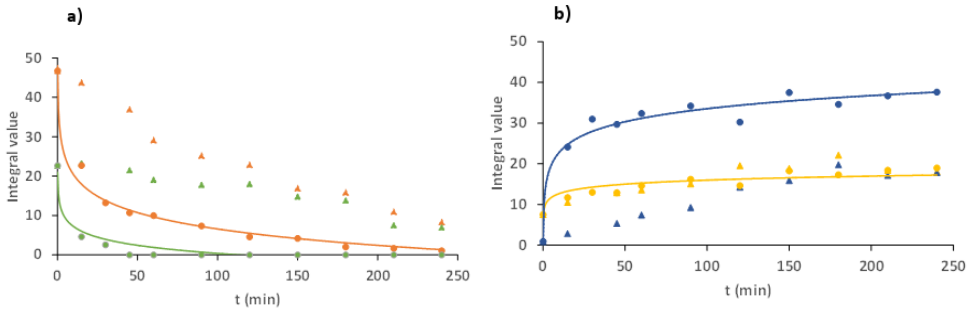

Figure 0.17: Reaction monitoring with catalytic amounts. a) Consumption of the zincate in the presence (▬) and in the absence (▲) of light, and 6-bromo-7-fluoroquinoline in the presence (▬) and in the absence (▲) of light. b) Formation of the organozinc derivative in the presence (▬) and in the absence (▲) of light, and the cross-coupling product in the presence (▬) and in the absence (▲) of light.

5.6 Plausible mechanism of the reaction

With this data in our hands, we proposed a plausible mechanism for the reaction (Figure 0.18). We hypothesize that before going into the oxidative addition step there is an interaction between the Pd-ligand complex and the organozinc reagent to form a new intermediate complex. This new complex is the one who absorbs blue light irradiation and brings Pd(0) to Pd(0)* excited state favoring the oxidative addition and accelerating the overall mechanism. This is based on the fact the complex Pd(0)-zincate only evolve into product when the haloarene is present in the reaction mixture. NMR experiments and absorbance studies demonstrated the formation of this complex between Pd(0) and the organozinc derivative that absorbs at 430 nm and appears 2 ppm higher than Pd + Johnphos complex in ^{31}P NMR due to the reduced electron density at the phosphorus nuclei. It is not clear if the oxidative addition is done directly on complex (c) or we have to undergo through (d) and then ordinary transmetalation and reductive elimination provides the product. Further experiments will be required to fully confirm the structures of the intermediates formed and fully elucidate the mechanism.

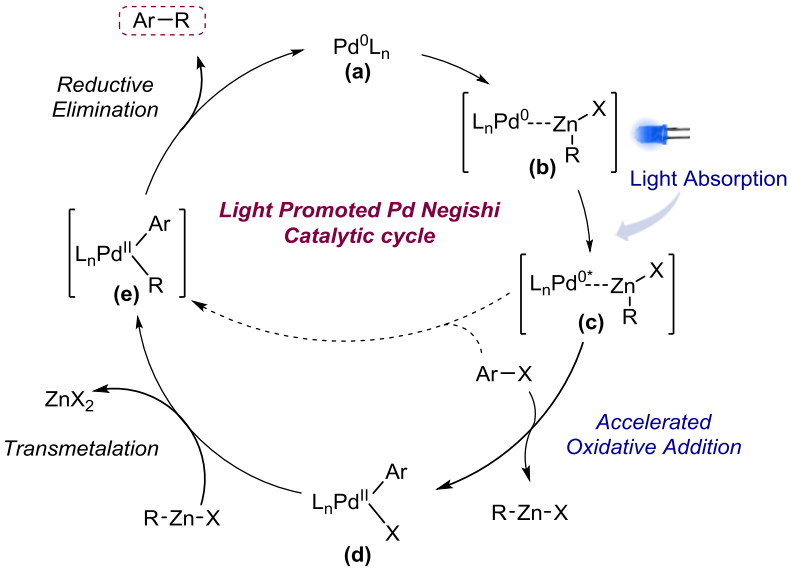

Figure 0.18: Plausible reaction mechanism

5.7 Conclusions

In summary, palladium catalyzed Negishi reactions are accelerated in the presence of visible blue light. This finding has a clear synthetic application as the scope of the coupling for Reformatsky reagents is clearly expanded to electron rich and chloro heterocycles. The protocol is easily scalable and clearly superior to the traditional batch. Kinetic, spectroscopic and NMR studies demonstrated the formation of a Pd(0)-zincate complex that allows the absorption of the visible light and accelerates the oxidative addition step of the catalytic cycle. This work provides new insights into Pd-driven photocatalysis and open new avenues within this field.

5.8 Experimental part

General information

GC measurements were performed using a 6890 Series Gas Chromatograph (Agilent Technologies) system comprising a 7683 Series injector and auto sampler, J&W HP-5MS column (20 m x 0.18 mm, 0.18 µm) from Agilent Technologies coupled to a 5973N MSD Mass Selective Detector (single quadrupole, Agilent Technologies). The MS detector was configured with an electronic impact ionization source/chemical ionization source (EI/CI). EI low-resolution mass spectra were acquired by scanning from 50 to 550 at a rate of 14.29 scan/s. The source temperature was maintained at 230 °C. Helium was used as the nebulizer gas. Data acquisition was performed with Chemstation-Open Action software. Thin layer chromatography (TLC) was carried out on silica gel 60 F254 plates (Merck) using reagent grade solvents. Unless otherwise specified, reagents were obtained from commercial sources and used without further purification. The reactions were carried out in a Vapourtec photoreactor UV-150 fixed on an E-series Vapourtec equipment. ^{1}H NMR spectra were recorded on Bruker DPX-400 or Bruker AV-500 spectrometers with standard pulse sequences, operating at 400 MHz and 500 MHz respectively. Chemical shifts are reported in parts per million (ppm) downfield from tetramethylsilane (TMS), which was used as an internal standard. All microfluidic fittings were purchased from IDEX Health and Science. The syringes were connected to the capillary using ¼-28 flat-bottom flangeless fittings. The peristaltic pumps of the Vapourtec system were used to feed liquid reagents through a high purity perfluoroalkoxyalkane (PFA) capillary tubing (I.D. = 0.75 mm) to a Tefzel® tee mixer (ID = 500 µm). The UV-visible measurement was performed using an UV/Vis spectrometer (Avantes, AvaSpec 2048).

General procedure for batch screening of Pd catalysts for traditional Negishi reaction

To a solution of benzyloxy 4-bromobenzoate (1 eq. 1 mmol), Pd catalyst (0.05 eq., 0.05 mmol); Ligand (when necessary) (0.1 eq., 0.1 mmol) in 1 mL of THF was added *(2-(tert-butoxy)-2-oxoethyl) zinc(II) bromide* (0.35 M; 2 eq., 2 mmol) and was reacted in batch in 16 h 40 °C without light irradiation. The solution was analysed by GC-MS every in 30 minutes, 1 hour and 16 hours.

Preparation of the organozinc compounds in flow:

Activation of the Zn column:

A solution 1.0 M trimethylchlorosilane (TMSCl) and 0.24 M 1-bromo-2-chloroethane was prepared under nitrogen (N_2) atmosphere in a dried flask by dissolving 1.25 mL of TMSCl

and 0.2 mL of 1-bromo-2-chloroethane in 10 mL of dried tetrahydrofuran (THF). 5 mL of this solution were passed through the 10 mm I.D. Omni-fit column containing Zn (12 g) using the Vapourtec E-series system at 40 °C and 1 mL/min flow rate.

General Procedure (1):

A solution of the correspondent halo derivative (1 mmol) 0.5 M in THF was passed through the column containing activated Zn using the Vapourtec E-series system at 40 °C and flow rate of 0.5 mL/min. The outcoming solution of the organozinc compound was collected in a closed flask under nitrogen (N_2) atmosphere.

Titration:

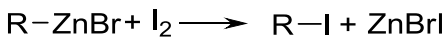

Figure 0.19: Titration reaction

Titration with I_2 was used to determine approximatively the concentration of the organozinc solution obtained. A known quantity (25 mg-30 mg approx.) of I_2 is weighted and dissolved in 0.5ml of dry THF in a closed vial under N_2 atmosphere. The solution of the organozinc compound was added dropwise until the I_2 solution became transparent. The volume of organozinc used to titrate the I_2 was used to calculate the molarity (Equation 0.1).

$$[RZnBr](M) = \frac{W\ iodine\ (mg)}{MW\ iodine\left(\frac{mg}{mmol}\right) * V\ RZnBr\ (ml)}$$

Equation 0.1:Calculation of the molarity of the organozinc compound (W ≡ weight; MW ≡ molecular weight; V ≡ volume).

General procedure (2) for Photo Induced Palladium Negishi cross-coupling

A solution of Bromoarene (1 eq. 0.5 mmol), $Pd(dba)_2$ (0.05 eq., 0.025 mmol); JohnPhos(0.1 eq., 0.05 mmol) in THF was mixed using a T-mixer with the corresponding solution of R-Zn prepared following General Procedure 1 in a Vapourtec UV-150 Photoreactor at 0.166 mL/min each line (t_R = 30 min; coil volume = 10 mL) at 40 °C irradiating with 450 nm blue LEDs. The out coming solution was diluted with ethyl acetate and added to a separatory funnel containing 15 mL of ammonium chloride saturated aqueous solution.* The layers were separated and the aqueous layer was extracted with ethyl acetate (3 x 15 mL). The combined organic extracts were washed

with brine, dried ($MgSO_4$) and concentrated in vacuo. Purification was carried out using flash column chromatography (silica, Ethyl acetate in Heptane) to obtain the product.

General procedure (3) for Photo Induced Palladium Negishi cross-coupling

A solution of Bromoarene (1 eq. 0.5 mmol), $Pd(dba)_2$ (0.05 eq., 0.025 mmol); XPhos(0.1 eq., 0.05 mmol) in THF was mixed using a T-mixer with the corresponding solution of R-Zn prepared following General Procedure 1 in a Vapourtec UV-150 Photoreactor at 0.166mL/min each line (t_R = 30 min; coil volume = 10 mL) at 40 °C irradiating with 450 nm blue LEDs. The out coming solution was diluted with ethyl acetate and added to a separatory funnel containing 15 mL of ammonium chloride saturated aqueous solution.* The layers were separated and the aqueous layer was extracted with ethyl acetate (3 x 15 mL). The combined organic extracts were washed with brine, dried ($MgSO_4$) and concentrated in vacuo. Purification was carried out using flash column chromatography (silica, Ethyl acetate in Heptane) to obtain the product.

*For low boiling point compounds extraction was done with diethyl ether instead of ethyl acetate and the purification in pentane/ethyl acetate instead of heptane/ethyl acetate.

Influence of the light irradiation

Two solutions: the first one of methyl 2-bromobenzoate, $Pd(dba)_2$ and JohnPhos in THF; the second one of benzyl ethyl bromo acetate zincate were prepared and flowed through a Vapourtec photoreactor UV-150 irradiating with 450 nm LEDs in a 10 mL coil using different flow rates and analyzing the sample at the stationary state by LC-MS:

- Flow rate 2.5 ml/min residence time 2 min: 63.5% P
- Flow rate 1 ml/min residence time 5 min: 75% P
- Flow rate 0.5 ml/min residence time 10 min: 90% P
- Flow rate 0.25 ml/min residence time 20 min: 96% P
- Flow rate 0.166 ml/min residence time 30 min: 100% P
- Flow rate 0.125 ml/min residence time 40 min: 100% P

The same experiment was repeated without light irradiation:

- Flow rate 2.5 ml/min residence time 2 min: 9% P
- Flow rate 1 ml/min residence time 5 min: 13% P
- Flow rate 0.5 ml/min residence time 10 min: 19% P
- Flow rate 0.25 ml/min residence time 20 min: 40% P
- Flow rate 0.166 ml/min residence time 30 min: 42% P
- Flow rate 0.165 ml/min residence time 40 min: 47% P

^{19}F-NMR experiments

NMR measurements:

NMR spectra were recorded in THF at 298 K on a Bruker Avance Neo 11.7 T (500.16 MHz ^{1}H resonance frequency) spectrometer with a broadband I-Probe indirect detection probe. Chemical shifts were referenced to triphenylphosphine oxide (23.39 ppm) and ethyl trifluoroacetate (-76.48 ppm) for ^{31}P (202.47 MHz) and ^{19}F (470.62 MHz) NMR experiments, respectively, as internal standards. The spectra were manually phased and baseline corrected. All spectra were Fourier transformed with MestReNova 10.1 software.

Flow-irradiation setup:

The irradiation source is a home-made design which consists of a 7x6 cm printed circuit board (PCB) formed by 18 LED bulbs of 10 mm diameter LEDs. The output power per blue LED unit (465 nm) is 250 kmcd (0.5 W). The PCB is placed inside a custom-built set-up for fixing the light source and the sample container, equipped with a fan to dissipate the excess of heating. A mirror is placed in front of the PCB of LEDs to maximize the light that irradiates the sample.

Sample preparation:

For equimolecular reactions, 0.0075 mmol of 6-bromo-7-fluoroquinoline, 0.0075 mmol of $Pd(dba)_2$ and 0.015 mmol of JohnPhos were solved in in 500 mL of THF. For the beginning of the reaction, 0.0075 mmol of (3,3,3-trifluoropropyl)zinc(II) bromide was added to the reaction mixture.

For catalytic reactions, 0.15 mmol of 6-bromo-7-fluoroquinoline, 0.0075 mmol of $Pd(dba)_2$ and 0.015 mmol of JohnPhos were solved in 500 mL of THF. For the beginning of the reaction, 0.3 mmol of (3,3,3-trifluoropropyl) zinc(II) bromide was added to the reaction mixture.

General procedure for the *off-line* NMR analysis:

The reaction mixture was transferred to a 5 mm-NMR tube and analyzed by ^{31}P and ^{19}F NMR to record t = 0 min. The reaction was monitored every 15 min until t = 60 min, and then every 30 min. In the case of dark experiments, the NMR tube was maintained in dark conditions between acquisitions. In the case of light experiments, the NMR tube was placed inside the custom-built set-up between the PCB of LEDs and the mirror during 15 min before acquisitions.

NMR assignments:

The signals corresponding to the starting zincate (-70.66 ppm), the cross-coupling product (CF_3: -67.32 ppm, F: -113.94 ppm) and the zincate dimer (CF_3: -69.59 ppm) can be identified in the ^{19}F NMR spectra. The signals corresponding to JohnPhos (17.57 ppm), JohnPhos + $Pd(dba)_2$ (58.97 ppm), JohnPhos + $Pd(dba)_2$ + quinoline (58.97 ppm) and JohnPhos + $Pd(dba)_2$ + zincate (60.33 ppm), can be identified in the ^{31}P NMR spectra.

Scale up procedure

Flow procedure: A solution (A) of ethyl bromoacetate (22.5 mmol; 2.5 eq.) in 45 mL of THF was pumped through a column containing activated zinc at 0.166 ml/min T= 40 °C. The outcome solution was combined with a solution (B) of methyl 2-bromobenzoate (1 eq. 9 mmol), $Pd(dba)_2$ (0.05 eq., 0.45 mmol); JohnPhos (0.1 eq., 0.9 mmol) in 45 mL of THF in a Vapourtec UV-150 Photoreactor at 0.250 mL/min each line (t_R = 30 min; coil volume= 10 mL) at 40 °C irradiating with 450 nm blue LEDs. The reaction was diluted with ethyl acetate and added to a separatory funnel containing 100 mL of ammonium chloride saturated aqueous solution.

The layers were separated and the aqueous layer was extracted with ethyl acetate (3 x 100 mL). The combined organic extracts were washed with brine, dried ($MgSO_4$) and concentrated in vacuo.

Purification by flash column chromatography (silica, Ethyl acetane:Heptane 0:100 to 10:90) to obtain the product as a transparent liquid (2.1 g, 97% of isolated yield).

Batch procedure: The same reaction was run in batch and the conversion was monitored in time during 8 h. To a solution of methyl 2-bromobenzoate (1 eq. 1 mmol), $Pd(dba)_2$ (0.05 eq., 0.05 mmol); JohnPhos (0.1 eq., 0.1 mmol) in 7.57 mL of THF the zincate solution of ethyl bromo acetate (0.33 M; 2.5 eq., 2.5 mmol) was added and was reacted in batch in 5 h 40 °C without light irradiation. The solution was analysed by GCMS every 30 minutes. The reaction was diluted with ethyl acetate and added to a separatory funnel containing 25 mL of water. The layers were separated and the aqueous layer was extracted with ethyl acetate (3 x 25 mL). The combined organic extracts were washed with brine, dried ($MgSO_4$) and concentrated in vacuo. Purification by flash column chromatography (silica, Ethyl acetate:Heptane 0:100 to10:90) to obtain the product as a transparent liquid (36% of isolated yield).

Product's characterization

*(2-(tert-butoxy)-2-oxoethyl) zinc(II) bromide (**2**)*

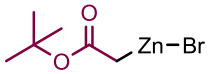

2

Prepared following General procedure 1; **Titration**: 0.35 M.

*(2-(benzyloxy)-2-oxoethyl) zinc(II) bromide (**4**)*

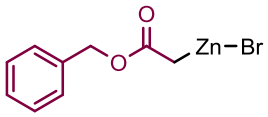

4

Prepared following General procedure 1; **Titration**: 0.33 M.

*(2-ethoxy-2-oxoethyl) zinc(II) bromide (**5**)*

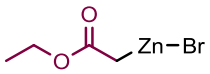

5

Prepared following General procedure 1; **Titration**: 0.3 M.

*(1-(tert-butoxycarbonyl) azetidin-3-yl) zinc(II) iodide (**6**)*

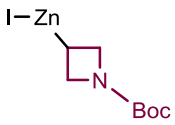

6

Prepared following General procedure 1; **Titration**: 0.25 M.

*(3,3,3-trifluoropropyl) zinc(II) iodide (**7**)*

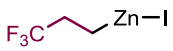

7

Prepared following General procedure 1; **Titration**: 0.34 M.

*(2-oxotetrahydrofuran-3-yl) zinc(II) bromide (**8**)*

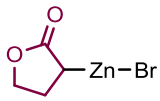

8

Prepared following General procedure 1; **Titration**: 0.2 M.

*(1-methyl-2-oxopyrrolidin-3-yl) zinc(II) bromide (**9**)*

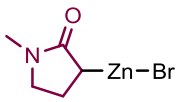

9

Prepared following General procedure 1; **Titration**: 0.2 M.

*tert-butyl 2-(4-benzyloxyphenyl) acetate (**3**):*

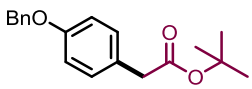

3

Prepared following the general procedure 3 on 0.5 mmol scale with benzyloxy 4-bromobenzoate (1 eq., 0.5 mmol); (2-(tert-butoxy)-2-oxoethyl)zinc(II) bromide (**2**) (2 eq., 1 mmol); $Pd(dba)_2$ (0.05 eq., 0.025 mmol); JohnPhos (0.1 eq., 0.05 mmol). Purification by flash chromatography ethyl acetate/heptane afforded the product as a transparent liquid. Yield: 126 mg, 85%.

^{1}H NMR ($CDCl_3$, 400MHz): δ = 7.29-7.45 (m, 5H), 7.18 (d, *J*=8.6 Hz, 2H), 6.92 (d, *J*=8.6 Hz, 2H), 5.04 (s, 2H), 3.46 (s, 2H), 1.43 ppm (s, 9H).
^{13}C NMR ($CDCl_3$, 101MHz): δ = 171.3, 157.8, 137.1, 130.3, 128.6, 127.9, 127.5, 127.2, 114.9, 80.7, 70.1, 41.8, 28.1 ppm.
GC-MS (EI): mass calcd. for $C_{19}H_{22}O_3$, 298.2; m/z found, 298.1 $[M+H]^+$.

*tert-butyl 2-(4-chlorophenyl) acetate (**10**)*

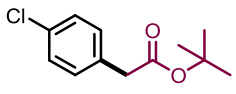

10

Prepared following the general procedure 2 on 0.5 mmol scale with 1-bromo-4-chlorobenzene (1 eq., 0.5 mmol); (2-(tert-butoxy)-2-oxoethyl) zinc(II) bromide (**2**) (2 eq., 1 mmol); $Pd(dba)_2$ (0.05 eq., 0.025 mmol); JohnPhos (0.1 eq., 0.05 mmol). Purification by flash chromatography ethyl acetate/heptane afforded the product as a as colorless oil. Yield: 86 mg, 73%.

^{1}H NMR ($CDCl_3$, 500MHz): δ = 7.28 (d, *J* = 7.21 Hz, 2H), 7.21 (d, *J* = 7.21 Hz, 2H), 3.49 (s, 2H), 1.43 ppm (s, 9H).
^{13}C NMR ($CDCl_3$ 101MHz): δ = 170.5, 133.2, 132.8, 130.6, 128.6, 81.1, 42.0, 28.0 ppm.
GC-MS (EI): mass calcd. for $C_{12}H_{15}ClO_2$, 226.7; m/z found, 226.9.

*benzyl 2-(4-nitrophenyl) acetate (**11**):*

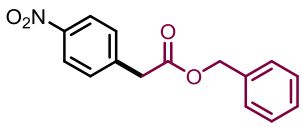

11

Prepared following the general procedure 2 on 0.5 mmol scale with 1-bromo-4-nitrobenzene (1 eq., 0.5 mmol); (2-(benzyloxy)-2-oxoethyl) zinc(II) bromide (**4**) (2 eq., 1 mmol); $Pd(dba)_2$ (0.05 eq., 0.025 mmol); JohnPhos (0.1 eq., 0.05 mmol). Purification by flash chromatography ethyl acetate/heptane afforded the product as a as colorless oil. Yield: 122 mg, 91%.

^{1}H NMR (CHLOROFORM-d, 500MHz): δ = 8.18 (d, *J*=7.8 Hz, 2H), 7.45 (d, *J*=7.8 Hz, 2H), 7.30-7.39 (m, 5H), 5.15 (s, 2H), 3.78 ppm (s, 2H).

^{13}C NMR (CHLOROFORM-d, 101MHz): δ = 170.0, 141.2, 135.4, 130.3, 128.7, 128.5, 128.3, 123.8, 67.2, 41.0 ppm.
GC-MS (EI): mass calcd. for $C_{15}H_{13}NO_4$, 271.1; m/z found, 271.0.

*benzyl 2-(4-cyanophenyl) acetate (**12**)*

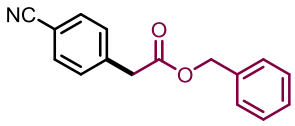

12

Prepared following the general procedure 2 on 0.5 mmol scale with 4-bromobenzonitrile (1 eq., 0.5 mmol); (2-(benzyloxy)-2-oxoethyl) zinc(II) bromide (**4**) (2 eq., 1 mmol); $Pd(dba)_2$ (0.05 eq., 0.025 mmol); JohnPhos (0.1 eq., 0.05 mmol). Purification by flash chromatography ethyl acetate/heptane afforded the product as a as colorless oil. Yield: 115 mg, 84%.

^{1}H NMR ($CDCl_3$, 500MHz): δ = 7.61 (d, *J*=8.7 Hz, 2H), 7.40 (d, *J*=8.7 Hz, 2H), 7.29-7.37 (m, 5H), 5.14 (s, 2H), 3.73 ppm (s, 2H).
^{13}C NMR ($CDCl_3$, 126MHz): δ = 170.1, 139.2, 135.4, 132.4, 130.2, 128.7, 128.5, 128.3, 118.7, 111.3, 67.1, 41.3 ppm.
GC-MS (EI): mass calcd. for $C_{16}H_{13}NO_2$, 251.1; m/z found, 250.1.

*tert-butyl 3-(4-methoxycarbonylphenyl) azetidine-1-carboxylate (**13**)*

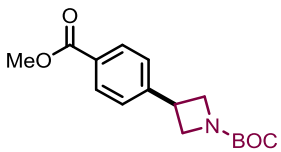

13

Prepared following the general procedure 2 on 0.5 mmol scale with 4-methyl bromobenzoate (1 eq., 0.5 mmol); (1-(tert-butoxycarbonyl)azetidin-3-yl)zinc(II) iodide (**6**) (2 eq., 1 mmol); $Pd(dba)_2$ (0.05 eq., 0.025 mmol); JohnPhos (0.1 eq., 0.05 mmol). Purification by flash chromatography ethyl acetate/heptane afforded the product as a as colorless oil. Yield: 89 mg, 61%.

^{1}H NMR ($CDCl_3$, 400MHz): δ = 8.02 (d, *J*=8.1 Hz, 2H), 7.38 (d, *J*=8.1 Hz, 2H), 4.35 (t, *J*=8.7 Hz, 2H), 3.98 (dd, *J*=8.7, 5.9 Hz, 2H), 3.92 (s, 3H), 3.73-3.83 (m, 1H), 1.47 ppm (s, 9H).

^{13}C NMR ($CDCl_3$, 101MHz): δ = 166.8, 156.4, 147.5, 130.1, 129.0, 126.8, 103.7, 79.7, 52.1, 33.5, 28.4 ppm.
GC-MS (EI): mass calcd. for $C_{16}H_{21}NO_4$, 291.3; m/z found, 291.4.

*methyl 4-(2-oxotetrahydrofuran-3-yl) benzoate (**14**)*

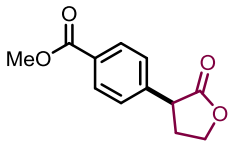

14

Prepared following the general procedure 2 on 0.5 mmol scale with 4-methyl bromobenzoate (1 eq., 0.5 mmol); (2-oxotetrahydrofuran-3-yl) zinc(II) bromide (**8**) (2 eq., 1 mmol); $Pd(dba)_2$ (0.05 eq., 0.025 mmol); JohnPhos (0.1 eq., 0.05 mmol). Purification by flash chromatography ethyl acetate/heptane afforded the product as a as colorless oil. Yield: 72 mg, 65%.

^{1}H NMR ($CDCl_3$, 500MHz): δ = 8.04 (d, *J*=8.1 Hz, 2H), 7.37 (d, *J*=8.1 Hz, 2H), 4.50 (td, *J*=8.7, 3.2 Hz, 1H), 4.34-4.41 (m, 1H), 3.92 (s, 3H), 3.88 (dd, *J*=10.4, 9.0 Hz, 1H), 2.75 (ddt, *J*=15.8, 9.2, 3.3 Hz, 1H), 2.42-2.52 ppm (m, 1H).
^{13}C NMR ($CDCl_3$, 101MHz): δ = 176.6, 166.7, 141.6, 130.2, 129.6, 128.0, 66.5, 52.2, 45.4, 31.4 ppm.
GC-MS (EI): mass calcd. for $C_{12}H_{12}O_4$, 220.2; m/z found, 220.2.

*methyl 4-(1-methyl-2-oxo-pyrrolidin-3-yl) benzoate (**15**):*

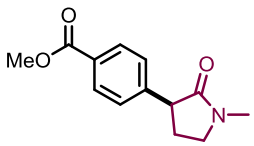

15

Prepared following the general procedure 2 on 0.5 mmol scale with 4-methyl bromobenzoate (1 eq., 0.5 mmol); (1-methyl-2-oxopyrrolidin-3-yl)zinc(II) bromide (**9**) (2 eq., 1 mmol); $Pd(dba)_2$ (0.05 eq., 0.025 mmol); JohnPhos (0.1 eq., 0.05 mmol). Purification by flash chromatography ethyl acetate/heptane afforded the product as a as colorless oil. Yield: 79 mg, 68%.

^{1}H NMR ($CDCl_3$, 400MHz): δ = 8.01 (d, *J*=7.9 Hz, 2H), 7.33 (d, *J*=7.9 Hz, 2H), 3.90 (s, 3H), 3.72 (t, *J*=8.9 Hz, 1H), 3.41-3.52 (m, 2H), 2.95 (s, 3H), 2.49-2.63 (m, 1H), 2.08-2.18 ppm (m, 1H).
^{13}C NMR ($CDCl_3$, 101MHz): δ = 174.1, 166.9, 145.2, 130.0, 128.9, 128.0, 52.1, 47.9, 47.7, 30.2, 27.8 ppm.
HRMS (ESI): mass calcd. for $C_{13}H_{15}NO_3$, 233.105; m/z found, 234.113 $[M+H]^+$.

*tert-butyl 2-(p-tolyl) acetate (**16**):*

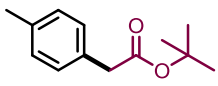

16

Prepared following the general procedure 2 on 0.5 mmol scale with 1-bromo-4-methylbenzene (1 eq., 0.5 mmol); (2-(tert-butoxy)-2-oxoethyl) zinc(II) bromide (**2**) (2 eq., 1 mmol); $Pd(dba)_2$ (0.05 eq., 0.025 mmol); JohnPhos (0.1 eq., 0.05 mmol). Purification by flash chromatography ethyl acetate/heptane afforded the product as a as colorless oil. Yield: 94 mg, 91%.

^{1}H NMR ($CDCl_3$, 400MHz): δ = 7.16 (d, *J* = 7.14 Hz, 2H), 7.11 (d, *J* = 7.14 Hz, 2H), 3.48 (s, 2H), 2.32 (s, 3H), 1.43 ppm (s, 9H).
^{13}C NMR ($CDCl_3$, 101MHz): δ = 171.2, 136.4, 131.7, 129.1, 103.7, 80.7, 42.2, 28.1, 21.1 ppm.
GC-MS (EI): mass calcd. for $C_{13}H_{18}O_2$, 206.2; m/z found, 206.0.

*methyl 4-(2-tert-butoxy-2-oxo-ethyl) benzoate (**17**):*

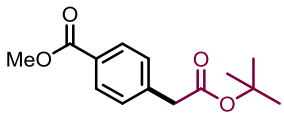

17

Prepared following the general procedure 2 on 0.5 mmol scale with 4-methyl bromobenzoate (1 eq., 0.5 mmol); (2-(tert-butoxy)-2-oxoethyl) zinc(II) bromide (**2**) (2 eq., 1 mmol); $Pd(dba)_2$ (0.05 eq., 0.025 mmol); JohnPhos (0.1 eq., 0.05 mmol). Purification by flash chromatography ethyl acetate/heptane afforded the product as a as colorless oil. Yield: 112 mg, 94%.

^{1}H NMR ($CDCl_3$, 400MHz): δ = 7.99 (d, *J*=8.1 Hz, 2H), 7.34 (d, *J*=8.1 Hz, 2H), 3.91 (s, 3H), 3.58 (s, 2H), 1.43 ppm (m, 9H)
^{13}C NMR ($CDCl_3$, 126MHz): δ = 170.1, 166.9, 139.9, 132.7, 129.8, 129.3, 126.6, 81.2, 52.1, 42.7, 28.0 ppm.
GC-MS (EI): mass calcd. for $C_{14}H_{18}O_4$, 250.3; m/z found, 250.4

*methyl 3-(2-benzyloxy-2-oxo-ethyl) benzoate (**18**):*

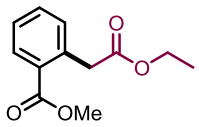

18

Prepared following the general procedure 2 on 0.5 mmol scale with 2-methyl bromobenzoate (1 eq., 0.5 mmol); (2-ethoxy-2-oxoethyl) zinc(II) bromide (**5**) (2 eq., 1 mmol); $Pd(dba)_2$ (0.05 eq., 0.025 mmol); JohnPhos (0.1 eq., 0.05 mmol). Purification by flash chromatography ethyl acetate/heptane afforded the product as a as colorless oil. Yield: 84 mg, 76%.

^{1}H NMR ($CDCl_3$, 400MHz): δ = 7.93-7.99 (m, 2H), 7.47-7.51 (m, 1H), 7.41 (d, *J*=7.4 Hz, 1H), 7.28-7.37 (m, 5H), 5.10-5.18 (m, 2H), 3.87-3.95 (m, 3H), 3.72 ppm (s, 2H).
^{13}C NMR ($CDCl_3$, 101MHz): δ = 170.9, 166.9, 135.7, 134.2, 133.9, 130.5, 128.7, 128.6, 128.5, 128.3, 128.2, 103.6, 66.8, 52.2, 41.0 ppm.
GC-MS (EI): mass calcd. for $C_{17}H_{16}O_4$, 284.3; m/z found, 284.2.

*methyl 2-(2-ethoxy-2-oxo-ethyl) benzoate (**19**):*

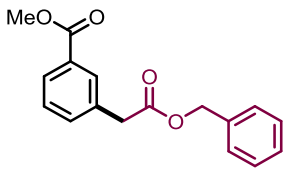

19

Prepared following the general procedure 2 on 0.5 mmol scale with 3-methyl bromobenzoate (1 eq., 0.5 mmol); (2-(benzyloxy)-2-oxoethyl) zinc(II) bromide (**4**) (2 eq., 1 mmol); $Pd(dba)_2$ (0.05 eq., 0.025 mmol); JohnPhos (0.1 eq., 0.05 mmol). Purification

by flash chromatography ethyl acetate/heptane afforded the product as a as colorless oil. Yield: 105 mg, 97%.

^{1}H NMR ($CDCl_3$, 400MHz): δ = 8.00 (dd, *J*=7.7, 1.3 Hz, 1H), 7.44-7.50 (m, 1H), 7.32-7.39 (m, 1H), 7.23-7.26 (m, 1H), 4.15 (q, *J*=7.2 Hz, 2H), 4.00 (s, 2H), 3.86 (s, 3H), 1.24 ppm (t, *J*=7.2 Hz, 4H).
^{13}C NMR ($CDCl_3$, 101MHz): δ = 172.8, 168.9, 137.4, 133.7, 133.6, 132.4, 128.7, 62.1, 53.3, 42.1, 15.6 ppm.
GC-MS (EI): mass calcd. for $C_{12}H_{14}O_4$, 222.2; m/z found, 222.1.

*1-methyl-5-(3,3,3-trifluoropropyl) indazole (**20**):*

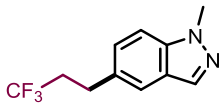

20

Prepared following the general procedure 2 on 0.5 mmol scale with 5-bromo-1-methyl-1H-indazole (1 eq., 0.5 mmol); (3,3,3-trifluoropropyl) zinc(II) iodide (**7**) (2 eq., 1 mmol); $Pd(dba)_2$ (0.05 eq., 0.025 mmol); JohnPhos (0.1 eq., 0.05 mmol). Purification by flash chromatography ethyl acetate/heptane afforded the product as a as colorless oil. Yield: 60 mg, 52%.

^{1}H NMR ($CDCl_3$, 500MHz): δ = 7.92 (d, *J*=0.9 Hz, 1H), 7.52-7.54 (m, 1H), 7.35 (d, *J*=8.7 Hz, 1H), 7.23 (dd, *J*=8.7, 1.4 Hz, 1H), 4.05-4.08 (m, 3H), 2.96-3.01 (m, 2H), 2.38-2.49 ppm (m, 2H).
^{13}C NMR ($CDCl_3$, 126MHz): δ = 139.0, 132.3, 131.1, 127.1, 124.4, 119.9, 109.3, 36.2 (q, *J*=28.2 Hz), 35.6, 28.1 (q, *J*=2.9 Hz) ppm.
GC-MS (EI): mass calcd. for $C_{11}H_{11}F_3N_2$, 228.2; m/z found, 228.23.

*tert-butyl 2-[5-(trifluoromethyl)-2-pyridyl] acetate (**21**):*

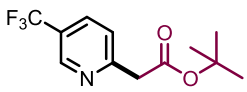

21

Prepared following the general procedure 2 on 0.5 mmol scale with 2-bromo-5-(trifluoromethyl) pyridine (1 eq., 0.5 mmol); (2-(tert-butoxy)-2-oxoethyl) zinc(II)

bromide (**2**) (2 eq., 1 mmol); $Pd(dba)_2$ (0.05 eq., 0.025 mmol); JohnPhos (0.1 eq., 0.05 mmol). Purification by flash chromatography ethyl acetate/heptane afforded the product as a as colorless oil. Yield: 90 mg, 69%.

^{1}H NMR ($CDCl_3$, 500MHz): δ = 8.83 (s, 1H), 7.90 (d, *J*=8.1 Hz, 1H), 7.44 (d, *J*=8.1 Hz, 1H), 3.85 (s, 2H), 1.46 ppm (s, 9H).
^{13}C NMR ($CDCl_3$, 126MHz): δ = 169.1, 158.9, 146.3 (d, *J*=4.4 Hz), 133.6 (d, *J*=3.5 Hz), 128.6, 126.6, 123.7, 81.8, 45.0, 28.0 ppm.
^{19}F NMR ($CDCl_3$, 471MHz): δ = -62.33 ppm (s, 3F).
GC-MS (EI): mass calcd. for $C_{12}H_{14}F_3NO_2$, 261.2; m/z found, 261.4.

*3-(6-methoxy-2-pyridyl) tetrahydrofuran-2-one (**22**):*

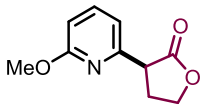

22

Prepared following the general procedure 2 on 0.5 mmol scale with 2-bromo-6-methoxypyridine (1 eq., 0.5 mmol); (2-oxotetrahydrofuran-3-yl) zinc(II) bromide (**8**) (2 eq., 1 mmol); $Pd(dba)_2$ (0.05 eq., 0.025 mmol); JohnPhos (0.1 eq., 0.05 mmol). Purification by flash chromatography ethyl acetate/heptane afforded the product as a as colorless oil. Yield: 78 mg, 76%.

^{1}H NMR ($CDCl_3$, 400MHz): δ = 7.55 (dd, *J*=8.3, 7.2 Hz, 1H), 6.91 (d, *J*=7.2 Hz, 1H), 6.66 (d, *J*=8.3 Hz, 1H), 4.62 (td, *J*=8.3, 5.8 Hz, 1H), 4.42 (ddd, *J*=8.3, 7.6, 6.7 Hz, 1H), 3.90 (s, 3H), 3.83 (dd, *J*=9.2, 7.6 Hz, 1H), 2.73-2.84 (m, 1H), 2.58-2.69 ppm (m, 1H).
^{13}C NMR ($CDCl_3$, 101MHz): δ = 177.0, 164.0, 153.9, 139.3, 116.0, 109.9, 67.7, 53.3, 47.3, 29.1 ppm.
GC-MS (EI): mass calcd. for $C_{10}H_{11}NO_3$, 193.2; m/z found, 193.0.

*3-(2-pyridyl) tetrahydrofuran-2-one (**23**):*

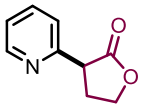

23

Prepared following the general procedure 2 on 0.5 mmol scale with 2-bromo-pyridine (1 eq., 0.5 mmol); (2-oxotetrahydrofuran-3-yl) zinc(II) bromide (**8**) (2 eq., 1 mmol); $Pd(dba)_2$ (0.05 eq., 0.025 mmol); JohnPhos (0.1 eq., 0.05 mmol). Purification by flash chromatography ethyl acetate/heptane afforded the product as a as colorless oil. Yield: 33 mg, 40%.

^{1}H NMR ($CDCl_3$, 400MHz): δ = 8.56-8.59 (m, 1H), 7.69 (td, *J*=7.7, 1.8 Hz, 1H), 7.37-7.40 (m, 1H), 7.22 (ddd, *J*=7.6, 4.9, 1.2 Hz, 1H), 4.59 (td, *J*=8.6, 4.9 Hz, 1H), 4.41 (dt, *J*=8.8, 7.6 Hz, 1H), 3.95 (dd, *J*=9.0, 8.3 Hz, 1H), 2.83 (dq, *J*=12.8, 8.0 Hz, 1H), 2.64-2.73 ppm (m, 1H)
^{13}C NMR ($CDCl_3$, 101MHz): δ = 149.7, 148.7, 137.5, 136.8, 123.6, 122.6, 118.7, 67.4, 47.0, 29.1 ppm
GC-MS (EI): mass calcd. for $C_9H_9NO_2$, 163.1; m/z found, 163.4.

*7-fluoro-6-(3,3,3-trifluoropropyl) quinoline (**24**):*

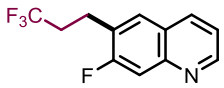

24

Prepared following the general procedure 2 on 0.5 mmol scale with 6-bromo-7-fluoroquinoline (1 eq., 0.5 mmol); (3,3,3-trifluoropropyl) zinc(II) iodide (**7**) (2 eq., 1 mmol); $Pd(dba)_2$ (0.05 eq., 0.025 mmol); JohnPhos (0.1 eq., 0.05 mmol). Purification by flash chromatography ethyl acetate/heptane afforded the product as a as colorless oil. Yield: 80 mg, 66%.

^{1}H NMR ($CDCl_3$, 400MHz): δ = 8.81 (dd, *J*=4.2, 1.6 Hz, 1H), 8.03 (dd, *J*=8.3, 1.2 Hz, 1H), 7.66 (d, *J*=11.3 Hz, 1H), 7.59 (d, *J*=8.1 Hz, 1H), 7.30 (dd, *J*=8.2, 4.3 Hz, 1H), 2.99-3.06 (m, 2H), 2.36-2.51 ppm (m, 2H).
^{13}C NMR ($CDCl_3$, 101MHz): δ = 161.7 (d, *J*=250.9 Hz), 151.1, 148.4 (d, *J*=12.8 Hz), 135.5, 129.0 (d, *J*=6.2 Hz), 127.9, 127.7, 125.4, 120.7 (d, *J*=2.2 Hz), 113.3 (d, *J*=21.3 Hz), 34.0 (dq, *J*= 28.3 and 2.0 Hz), 22.8 ppm.
^{19}F NMR ($CDCl_3$, 471MHz): δ = -67.75 (t, 3F); -113,94 ppm (s, 1F).
GC-MS (EI): mass calcd. for $C_{12}H_9F_4N$, 243.2; m/z found, 243.3.

*ethyl 4-(2-tert-butoxy-2-oxo-ethyl) benzoate (**25**):*

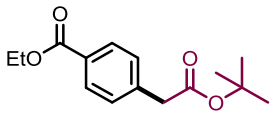

25

Prepared following the general procedure 2 on 0.5 mmol scale with 4-ethoxy bromobenzoate (1 eq., 0.5 mmol); (2-(tert-butoxy)-2-oxoethyl) zinc(II) bromide (**2**) (2 eq., 1 mmol); $Pd(dba)_2$ (0.05 eq., 0.025 mmol); JohnPhos (0.1 eq., 0.05 mmol). Purification by flash chromatography ethyl acetate/heptane afforded the product as a as colorless oil. Yield: 115 mg, 83%.

^{1}H NMR (CHLOROFORM-d, 500MHz): δ = 8.00 (d, *J*=8.4 Hz, 2H), 7.34 (d, *J*=8.4 Hz, 2H), 4.37 (q, *J*=7.0 Hz, 2H), 3.58 (s, 2H), 1.43 (s, 9H), 1.39 ppm (t, *J*=7.1 Hz, 3H).
^{13}C NMR ($CDCl_3$, 126MHz): δ = 170.1, 166.5, 139.8, 129.7, 129.2, 129.2, 81.2, 60.9, 42.7, 28.0, 14.4 ppm.
GC-MS (EI): mass calcd. for $C_{15}H_{20}O_4$, 264.3; m/z found, 264.2.

*ethyl 2-(2,3-dimethoxyphenyl) acetate (**26**):*

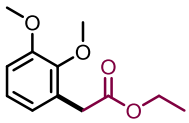

26

Prepared following the general procedure 3 on 0.5 mmol scale with 1-bromo-2,3-dimethoxybenzene (1 eq., 0.5 mmol); (2-ethoxy-2-oxoethyl) zinc(II) bromide (**5**) (2 eq., 1 mmol); $Pd(dba)_2$ (0.05 eq., 0.025 mmol); XPhos (0.1 eq., 0.05 mmol). Purification by flash chromatography ethyl acetate/heptane afforded the product as a as colorless oil. Yield: 106 mg, 95%.

^{1}H NMR ($CDCl_3$, 400MHz): δ = 6.97-7.03 (m, 1H), 6.84 (td, *J*=8.0, 1.4 Hz, 2H), 4.16 (q, *J*=7.2 Hz, 2H), 3.86 (s, 3H), 3.83 (s, 3H), 3.65 (s, 2H), 1.26 ppm (t, *J*=7.2 Hz, 4H).
^{13}C NMR ($CDCl_3$, 101MHz): δ = 171.8, 152.7, 147.4, 128.5, 123.8, 122.6, 111.7, 60.8, 60.6, 55.8, 35.7, 14.2 ppm.
GC-MS (EI): mass calcd. for $C_{12}H_{16}O_4$, 224.2; m/z found, 224.0.

*ethyl 2-[4-(trifluoromethyl)-3-pyridyl] acetate (**27**):*

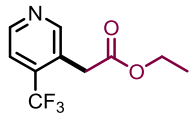

27

Prepared following the general procedure 3 on 0.5 mmol scale with 3-bromo-4-(trifluoromethyl) pyridine (1 eq., 0.5 mmol); (2-ethoxy-2-oxoethyl) zinc(II) bromide (**5**) (2 eq., 1 mmol); $Pd(dba)_2$ (0.05 eq., 0.025 mmol); XPhos (0.1 eq., 0.05 mmol). Purification by flash chromatography ethyl acetate/heptane afforded the product as a as colorless oil. Yield: 105 mg, 90%.

^{1}H NMR ($CDCl_3$, 400MHz): δ = 8.72 (d, *J*=5.1 Hz, 1H), 8.69 (s, 1H), 7.54 (d, *J*=5.1 Hz, 1H), 4.18 (q, *J*=7.1 Hz, 2H), 3.84 (s, 2H), 1.25 ppm (t, *J*=7.2 Hz, 3H)
^{13}C NMR ($CDCl_3$, 101MHz): δ = 169.6, 153.7, 149.5, 125.7 (q, *J*=263.3 Hz), 119.5 (q, *J*=4.6 Hz), 61.5, 35.8, 14.1 ppm
^{19}F NMR ($CDCl_3$, 471MHz): δ = -64.90 ppm, (s, 3F).
GC-MS (EI): mass calcd. for $C_{10}H_{10}F_3NO_2$, 233.19; m/z found, 233.2

*tert-butyl 4-[4-(2-oxotetrahydrofuran-3-yl) phenyl] piperazine-1-carboxylate (**28**):*

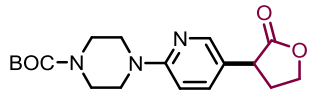

28

Prepared following the general procedure 3 on 0.5 mmol scale with tert-butyl 4-(5-bromopyridin-2-yl) piperazine-1-carboxylate (1 eq., 0.5 mmol); (2-oxotetrahydrofuran-3-yl)zinc(II) bromide (**8**) (2 eq., 1 mmol); $Pd(dba)_2$ (0.05 eq., 0.025 mmol); XPhos (0.1 eq., 0.05 mmol). Purification by flash chromatography ethyl acetate/heptane afforded the product as a as colorless oil; Yield: 163 mg, 94%.

^{1}H NMR ($CDCl_3$, 400MHz): δ = 8.10 (d, *J*=2.5 Hz, 1H), 7.45 (dd, *J*=8.8, 2.5 Hz, 1H), 6.66 (d, *J*=8.8 Hz, 1H), 4.48 (td, *J*=8.7, 2.8 Hz, 1H), 4.30-4.38 (m, 1H), 3.72 (dd, *J*=10.9, 8.8 Hz, 1H), 3.53 (s, 8H), 2.68 (dddd, *J*=11.0, 8.8, 6.4, 2.9 Hz, 1H), 2.32-2.45 (m, 1H), 2.05 (s, 1H), 1.49 ppm (m, 19H)
^{13}C NMR ($CDCl_3$, 101MHz): δ = 177.3, 158.7, 154.8, 147.3, 137.0, 121.4, 107.4, 80.0, 66.5, 45.1, 42.4, 31.3, 28.4 ppm
GC-MS (EI): mass calcd. for $C_{18}H_{25}N_3O_4$, 347.414; m/z found, 347.3.

*benzyl 2-(2,4-dimethoxyphenyl) acetate (**29**):*

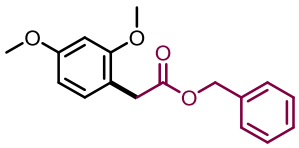

29

Prepared following the general procedure 3 on 0.5 mmol scale with 1-bromo-2,4-dimethoxybenzene (1 eq., 0.5 mmol); (2-(benzyloxy)-2-oxoethyl) zinc(II) bromide (**4**) (2 eq., 1 mmol); $Pd(dba)_2$ (0.05 eq., 0.025 mmol); XPhos (0.1 eq., 0.05 mmol). Purification by flash chromatography ethyl acetate/heptane afforded the product as a as colorless oil; Yield: 80 mg, 57%.

^{1}H NMR ($CDCl_3$, 500MHz): δ = 7.27-7.37 (m, 5H), 7.08 (d, *J*=9.0 Hz, 1H), 6.42-6.46 (m, 2H), 5.14 (s, 2H), 3.77-3.83 (m, 3H), 3.72 (s, 3H), 3.60 ppm (s, 2H)
^{13}C NMR ($CDCl_3$, 101MHz): δ = 172.0, 160.3, 158.5, 136.3, 131.2, 128.5, 128.1, 128.0, 115.5, 104.1, 98.6, 66.2, 55.4, 55.4, 35.4 ppm
GC-MS (EI): mass calcd. for $C_{17}H_{18}O_4$, 286.3; m/z found, 286.0

*benzyl 2-(1-methylpyrazol-4-yl) acetate (**30**):*

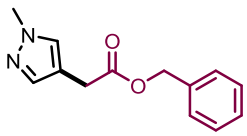

30

Prepared following the general procedure 3 on 0.5 mmol scale with 4-bromo-1-methyl-1H-pyrazole (1 eq., 0.5 mmol); (2-(benzyloxy)-2-oxoethyl) zinc(II) bromide (**4**) (2 eq., 1 mmol); $Pd(dba)_2$ (0.05 eq., 0.025 mmol); XPhos (0.1 eq., 0.05 mmol). Purification by flash chromatography ethyl acetate/heptane afforded the product as a as colorless oil. Yield: 42 mg, 36%.

^{1}H NMR (CHLOROFORM-d, 500MHz): δ = 7.40 (s, 1H), 7.32-7.37 (m, 6H), 5.14 (s, 2H), 3.86 (s, 3H), 3.54 ppm (s, 2H).
^{13}C NMR (CHLOROFORM-d, 101MHz): δ = 171.5, 139.3, 135.8, 129.5, 128.6, 128.3, 128.3, 66.7, 38.9, 30.3 ppm.
GC-MS (EI): mass calcd. for $C_{13}H_{14}N_2O_2$, 230.3; m/z found, 230.4.

*benzyl 2-(1-phenylpyrazol-4-yl) acetate (**31**):*

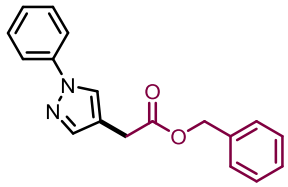

31

Prepared following the general procedure 3 on 0.5 mmol scale with 4-bromo-1-phenyl-1H-pyrazole (1 eq., 0.5 mmol); (2-(benzyloxy)-2-oxoethyl) zinc(II) bromide (**4**) (2 eq., 1 mmol); $Pd(dba)_2$ (0.05 eq., 0.025 mmol); XPhos (0.1 eq., 0.05 mmol). Purification by flash chromatography ethyl acetate/heptane afforded the product as a as colorless oil; Yield: 95 mg, 69%.

^{1}H NMR (CHLOROFORM-d, 500MHz): δ = 7.90 (s, 1H), 7.63-7.67 (m, 3H), 7.41-7.46 (m, 3H), 7.34-7.39 (m, 4H), 7.25-7.29 (m, 1H), 5.17 (s, 2H), 3.63 ppm (s, 2H)
^{13}C NMR (CHLOROFORM-d, 101MHz): δ = 171.1, 141.2, 140.1, 135.7, 129.4, 128.6, 128.4, 128.3, 126.4, 126.2, 119.0, 115.1, 66.9, 30.4 ppm
GC-MS (EI): mass calcd. for $C_{18}H_{16}N_2O_2$, 292.337; m/z found, 292.348.

*tert-butyl 2-(4-methoxyphenyl) acetate (**32**):*

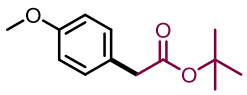

32

Prepared following the general procedure 3 on 0.5 mmol scale with 4-bromoanisole (1 eq., 0.5 mmol); (2-(tert-butoxy)-2-oxoethyl) zinc(II) bromide (**2**) (2 eq., 1 mmol); $Pd(dba)_2$ (0.05 eq., 0.025 mmol); XPhos (0.1 eq., 0.05 mmol). Purification by flash chromatography ethyl acetate/heptane afforded the product as a as colorless oil. Yield: 104 mg, 90%.

^{1}H NMR ($CDCl_3$, 500MHz): δ = 7.18 (d, *J*=8.7 Hz, 2H), 6.85 (d, *J*=8.7 Hz, 2H), 3.79 (s, 3H), 3.46 (s, 2H), 1.43 ppm (s, 9H).
^{13}C NMR ($CDCl_3$, 101MHz): δ = 171.3, 158.5, 130.2, 126.9, 113.9, 80.7, 55.3, 41.8, 28.1 ppm.
GC-MS (EI): mass calcd. for $C_{13}H_{18}O_3$, 222.2; m/z found, 222.0.

*tert-butyl 2-[6-(trifluoromethyl)-3-pyridyl] acetate (**33**):*

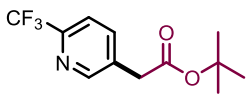

33

Prepared following the general procedure 3 on 0.5 mmol scale with 5-bromo-2-(trifluoromethyl) pyridine (1 eq., 0.5 mmol); (2-(tert-butoxy)-2-oxoethyl) zinc(II) bromide (**2**) (2 eq., 1 mmol); $Pd(dba)_2$ (0.05 eq., 0.025 mmol); XPhos (0.1 eq., 0.05 mmol). Purification by flash chromatography ethyl acetate/heptane afforded the product as a as colorless oil. Yield: 95 mg, 73%.

^{1}H NMR ($CDCl_3$, 400MHz): δ = 8.62 (d, *J*=1.8 Hz, 1H), 7.81-7.85 (dd, *J*= 8.1 and 1.8 Hz, 1H), 7.66 (d, *J*=8.1 Hz, 1H), 3.63 (s, 2H), 1.45 ppm (s, 9H)
^{13}C NMR ($CDCl_3$, 101MHz): δ = 169.1, 150.6, 138.1, 133.6, 120.2 (q, *J*=2.5 Hz), 82.1, 39.5, 28.0 ppm
^{19}F NMR ($CDCl_3$, 471MHz): δ = -62.33 ppm, (s, 3F)
GC-MS (EI): mass calcd. for $C_{12}H_{14}F_3NO_2$, 261.2; m/z found, 261.1

*ethyl 4-(1-methyl-2-oxo-pyrrolidin-3-yl) benzoate (**34**):*

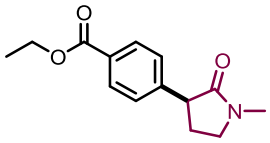

34

Prepared following the general procedure 3 on 0.5 mmol scale with 4-ethyl chlorobenzoate (1 eq., 0.5 mmol); (1-methyl-2-oxopyrrolidin-3-yl)zinc(II) bromide (**9**) (2 eq., 1 mmol); $Pd(dba)_2$ (0.05 eq., 0.025 mmol); XPhos (0.1 eq., 0.05 mmol). Purification by flash chromatography ethyl acetate/heptane afforded the product as a as colorless oil. Yield: 86 mg, 70%.

^{1}H NMR ($CDCl_3$, 400MHz): δ = 8.01 (d, *J*=8.6 Hz, 2H), 7.33 (d, *J*=8.6 Hz, 2H), 4.36 (q, *J*=7.2 Hz, 2H), 3.72 (t, *J*=8.9 Hz, 1H), 3.41-3.53 (m, 2H), 2.95 (s, 3H), 2.50-2.60 (m, 1H), 2.07-2.19 (m, 1H), 1.38 ppm (t, *J*=7.2 Hz, 3H).
^{13}C NMR ($CDCl_3$, 101MHz): δ = 174.1, 166.4, 145.0, 130.0, 129.2, 127.9, 60.9, 48.0, 47.7, 30.2, 27.8, 14.3 ppm.
GC-MS (EI): mass calcd. for $C_{14}H_{17}NO_3$, 247.294; m/z found, 247.217.

*tert-butyl 2-(6-methoxy-2-pyridyl) acetate (**35**):*

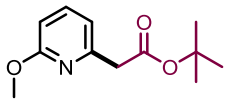

35

Prepared following the general procedure 3 on 0.5 mmol scale with 2-bromo-6-methoxypyridine (1 eq., 0.5 mmol); *(2-(tert-butoxy)-2-oxoethyl) zinc(II) bromide* (**2**) (2 eq., 1 mmol); $Pd(dba)_2$ (0.05 eq., 0.025 mmol); XPhos (0.1 eq., 0.05 mmol). Purification by flash chromatography ethyl acetate/heptane afforded the product as a as colorless oil; isolated yield: 87 mg, 78%.

^{1}H NMR ($CDCl_3$, 400MHz): δ = 7.44 (dd, *J*=8.2, 7.3 Hz, 1H), 6.74 (d, *J*=7.3 Hz, 1H), 6.54 (d, *J*=8.2 Hz, 1H), 3.84 (s, 3H), 3.57 (s, 2H), 1.39 ppm (s, 9H).
^{13}C NMR ($CDCl_3$, 101MHz): δ = 170.1, 163.7, 152.7, 138.9, 116.1, 108.6, 80.9, 53.3, 44.9, 28.1 ppm.
GC-MS (EI): mass calcd. for $C_{12}H_{17}NO_3$, 223.2; m/z found, 223.0.

*tert-butyl 2-(4-methylpyridin-3-yl) acetate (**36**)*

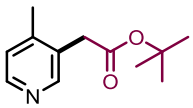

36

Prepared following the general procedure 3 on 0.5 mmol scale with 3-chloro-6-methylpyridine (1 eq., 0.5 mmol); *(2-(tert-butoxy)-2-oxoethyl) zinc(II) bromide* (**2**) (2 eq., 1 mmol); $Pd(dba)_2$ (0.05 eq., 0.025 mmol); XPhos (0.1 eq., 0.05 mmol). Purification by flash chromatography ethyl acetate/heptane afforded the product as a as colorless oil. Yield: 83 mg, 80%.

^{1}H NMR ($CDCl_3$, 500 MHz): δ = 8.31-8.43 (m, 2H), 7.09 (d, J = 5.2 Hz, 1H), 3.55 (s, 2H), 2.31 (s, 3H), 1.43 ppm (s, 9H)
^{13}C NMR ($CDCl_3$, 101 MHz): δ = 169.9, 150.7, 148.5, 146.1, 129.6, 125.2, 81.4, 37.8, 28.0, 19.0 ppm
GC-MS (EI): mass calcd. for $C_{12}H_{17}NO_2$, 207.1; m/z found, 207.2

*ethyl 2-(6-fluoropyridin-3-yl) acetate (**37**)*

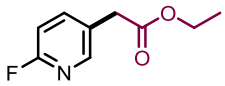

37

Prepared following the general procedure 3 on 0.5 mmol scale with 3-chloro-6-fluoro-pyridine (1 eq., 0.5 mmol); (2-ethoxy-2-oxoethyl) zinc(II) bromide (**5**) (2 eq., 1 mmol); $Pd(dba)_2$ (0.05 eq., 0.025 mmol); XPhos (0.1 eq., 0.05 mmol). Purification by flash chromatography ethyl acetate/heptane afforded the product as a as yellow oil; isolated yield: 57 mg, 62%.

^{1}H NMR ($CDCl_3$, 400 MHz): δ = 8.11 (d, *J* = 1.4 Hz, 1H), 7.76 (td, *J* = 8.0, 2.5 Hz, 1H), 6.92 (dd, *J* = 8.3, 3.0 Hz, 1H), 4.17 (q, *J* = 7.2 Hz, 2H), 3.62 (s, 2H), 1.27 ppm (t, *J* = 7.2 Hz, 3H)
^{13}C NMR ($CDCl_3$, 101 MHz): δ = 170.5, 164.1, 161.7, 147.9, 142.1, 127.5, 109.6, 109.2, 61.3, 37.4, 14.1 ppm
^{19}F NMR ($CDCl_3$, 471MHz): δ = -69.45 ppm (s, 1F)
GC-MS (EI): mass calcd. for $C_9H_{10}FNO_2$, 183.0; m/z found, 183.2

*tert-butyl 2-[6-(trifluoromethyl)-3-pyridyl] acetate (**38**):*

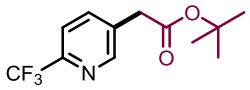

38

Prepared following the general procedure 3 on 0.5 mmol scale with 5-chloro-2-(trifluoromethyl) pyridine (1 eq., 0.5 mmol); (2-(tert-butoxy)-2-oxoethyl)zinc(II) bromide (**2**) (2 eq., 1 mmol); $Pd(dba)_2$ (0.05 eq., 0.025 mmol); XPhos (0.1 eq., 0.05 mmol). Purification by flash chromatography ethyl acetate/heptane afforded the product as a as colorless oil. Yield: 73 mg, 56%.

^{1}H NMR ($CDCl_3$, 400MHz): δ = 8.62 (d, *J*=1.8 Hz, 1H), 7.81-7.85 (dd, *J*= 8.1 and 1.8 Hz, 1H), 7.66 (d, *J*=8.1 Hz, 1H), 3.63 (s, 2H), 1.45 ppm (s, 9H).
^{13}C NMR ($CDCl_3$, 101MHz): δ = 169.1, 150.6, 138.1, 133.6, 120.2 (q, *J*=2.5 Hz), 82.1, 39.5, 28.0 ppm.
^{19}F NMR ($CDCl_3$, 471MHz): δ = -67.86 ppm (s, 3F)
GC-MS (EI): mass calcd. for $C_{12}H_{14}F_3NO_2$, 261.2; m/z found, 261.1.

Bibliography

[1] Kaplan, N. M. *Drugs*, 50th ed.; Simpson, K.; Jarvis, B., Ed.; **2000**, Springer,.
[2] Lloyd-Jones, G. C. Palladium-Catalyzed α-Arylation of Esters: Ideal New Methodology for Discovery Chemistry. *Angew. Chem. Int. Ed*. **2002**, *42* (6), 953–956.
[3] (a) Moradi, W. A.; Buchwald, S. L. Palladium-Catalyzed α-Arylation of Esters. *J. Am. Chem. Soc.* **2001**, *123* (33), 7996–8002; (b) Jørgensen, M.; Lee, S.; Liu, X.; Wolkowski, J. P.; Hartwig, J. F. Efficient Synthesis of α-Aryl Esters by Room-Temperature Palladium-Catalyzed Coupling of Aryl Halides with Ester Enolates. *J. Am. Chem. Soc.* **2002**, *124* (42), 12557–12565.
[4] Dai, X.; Strotman, N. A.; Fu, G. C. Catalytic Asymmetric Hiyama Cross-Couplings of Racemic α-Bromo Esters. *J. Am. Chem. Soc.* **2008**, *130* (11), 3302–3303.
[5] Jin, M.; Nakamura, M. Iron-Catalyzed Chemoselective Cross-Coupling of α-Bromocarboxylic Acid Derivatives with Aryl Grignard Reagents. *Chem. Lett.* **2011**, *40* (9), 1012–1014.
[6] Molander, G. A.; Traister, K. M.; Barcellos, T. Palladium-Catalyzed α-Arylation of 2-Chloroacetates and 2-Chloroacetamides. *J. Org. Chem.* **2013**, *78* (8), 4123–4131.
[7] Durandetti, M.; Gosmini, C.; Périchon, J. Ni-Catalyzed Activation of α-Chloroesters: A Simple Method for the Synthesis of α-Arylesters and β-Hydroxyesters. *Tetrahedron* **2007**, *63* (5), 1146–1153.
[8] (a) Hama, T.; Liu, X.; Culkin, D. A.; Hartwig, J. F. Palladium-Catalyzed α-Arylation of Esters and Amides under More Neutral Conditions. *J. Am. Chem. Soc.* **2003**, *125* (37), 11176–11177; (b) Hama, T.; Hartwig, J. F. Palladium-Catalyzed α-Arylation of Esters with Chloroarenes. *Org. Lett.* **2008**, *10* (8), 1549–1552; (c) Hama, T.; Ge, S.; Hartwig, J. F. Palladium-Catalyzed α-Arylation of Zinc Enolates of Esters: Reaction Conditions and Substrate Scope. *J. Org. Chem.* **2013**, *78* (17), 8250–8266; (d) Duez, S.; Bernhardt, S.; Heppekausen, J.; Fleming, F. F.; Knochel, P. Pd-Catalyzed α-Arylation of Nitriles and Esters and γ-Arylation of Unsaturated Nitriles with TMPZnCl•LiCl. *Org. Lett.* **2011**, *13* (7), 1690–1693; (e) Hlavinka, M. L.; Hagadorn, J. R. Zn(Tmp) 2 : A Versatile Base for the Selective Functionalization of C−H Bonds. *Organometallics* **2007**, *26* (17), 4105–4108; (f) Orsini, F.; Pelizzoni, F.; Vallarino, L. M. Influence of the Catalyst on the Pd0-Mediated Reactions of BrZnCH(CH3) COOtBu with Vinyl and Aryl Triflates. *J. Organomet. Chem.* **1989**, *367* (3), 375–382; (g) Wong, B.; Linghu, X.; Crawford, J. J.; Drobnick, J.; Lee, W.; Zhang, H. A Chemoselective Reformatsky-Negishi Approach to α-Haloaryl Esters. *Tetrahedron* **2014**, *70* (7), 1508–1515.
[9] Semmelhack, M. F.; Stauffer, R. D.; Rogerson, T. D. Nucleophilic Aromatic Substitution via a New Nickel-Catalyzed Process and via the SRN1 Reaction. Improved Synthesis of Cephalotaxinone. *Tetrahedron Lett.* **1973**, *14* (45), 4519–4522.
[10] Millard, A. A.; Rathke, M. W. A Nickel Catalyst for the Arylation and Vinylation of Lithium Ester Enolates. *J. Am. Chem. Soc.* **1977**, *99* (14), 4833–4835.
[11] Fauvarque, J. F.; Jutand, A. Catalysis of the Arylation of the Reformatsky Reagent by Palladium or Nickel Complexes. Synthesis of Aryl Acid Esters. *J. Organomet. Chem.* **1979**, *177* (1), 273–281.
[12] Kuwajima, I.; Urabe, H. Regioselective Arylation of Silyl Enol Ethers of Methyl Ketones with Aryl Bromides. *J. Am. Chem. Soc.* **1982**, *104* (24), 6831–6833.
[13] Agnelli, F.; Sulikowski, G. A. Synthesis of Arylacetates by the Palladium-Catalyzed Cross-Coupling of Aryl Bromides and Copper(II) Enolates. *Tetrahedron Lett.* **1998**, *39* (48), 8807–8810.

[14] (a) Carfagna, C.; Musco, A.; Sallese, G.; Santi, R.; Fiorani, T. Palladium-Catalyzed Coupling Reactions of Aryl Triflates or Halides with Ketene Trimethylsilyl Acetals. A New Route to Alkyl 2-Arylalkanoates. *J. Org. Chem.* **1991**, *56* (1), 261–263; (b) Galarini, R.; Musco, A.; Pontellini, R.; Santi, R. Asymmetric Synthesis of Alkyl 2-Arylalkanoates by Cross-Coupling Reactions Cabled by Pd Complexes. *J. Mol. Catal.* **1992**, *72* (3).

[15] Sakamoto, T.; Kondo, Y.; Masumoto, K.; Yamanaka, H. Synthesis of Methyl 2-(Heteroaryl)Propanoates via Palladium-Catalyzed Reaction. *Heterocycles* **1993**, *36* (11), 2509–2512.

[16] Fauvarque, J. F.; Jutand, A. Arylation of the Reformatsky Reagent Catalyzed by Zerovalent Complexes of Palladium and Nickel. *J. Organomet. Chem.* **1977**, *132* (2).

[17] Bordwell, F. G. Equilibrium Acidities in Dimethyl Sulfoxide Solution. *Acc. Chem. Res.* **1988**, *21* (12), 456–463.

[18] (a) Tamao, Kohei; Zembayashi,Michio; Kumada, M. α-alkylation and α-arylation of carbonyl groups: nickel-phosphine complex-catalyzed Grignard coupling of Vic-Bromotrimethylsiloxyalkenes. *Chem. Lett.* **1976**, *5* (11), 1239–1242; (b) Kosugi, M.; Hagiwara, I.; Sumiya, T.; Migita, T. Arylation and 1-Alkenylation on α-Position of Ketones via Tributyltin Enolates Catalyzed by Palladium Complex. *Bull. Chem. Soc. Jpn*. **1984**, 57, 242– 246; (c) Palucki, M.; Buchwald, S. L. Palladium-Catalyzed Alpha-Arylation of Ketones. *J. Am. Chem. Soc.* **1997**, *119* (97), 11108–11109; (d) Hamann, B. C.; Hartwig, J. F. Palladium-Catalyzed Direct α-Arylation of Ketones. Rate Acceleration by Sterically Hindered Chelating Ligands and Reductive Elimination from a Transition Metal Enolate Complex. *J. Am. Chem. Soc.* **1997**, *119* (50), 12382–12383; (e) Shaughnessy, K. H.; Hamann, B. C.; Hartwig, J. F. Palladium-Catalyzed Inter- and Intramolecular α-Arylation of Amides. Application of Intramolecular Amide Arylation to the Synthesis of Oxindoles. *J. Org. Chem.* **1998**, *63* (19), 6546–6553; (f) Kawatsura, M.; Hartwig, J. F. Simple, Highly Active Palladium Catalysts for Ketone and Malonate Arylation: Dissecting the Importance of Chelation and Steric Hindrance. *J. Am. Chem. Soc.* **1999**, *121* (7), 1473–1478; (g) Satoh, T.; Kawamura, Y.; Miura, M.; Nomura, M. Palladium-Catalyzed Regioselective Mono- and Diarylation Reactions of 2-Phenylphenols and Naphthols with Aryl Halides. *Angew. Chem. Int. Ed.* **1997**, *36* (16), 1740–1742; (h) Satoh, T.; Inoh, J. I.; Kawamura, Y.; Kawamura, Y.; Miura, M.; Nomura, M. Regioselective Arylation Reactions of Biphenyl-2-Ols, Naphthols, and Benzylic Compounds with Aryl Halides under Palladium Catalysis. *Bull. Chem. Soc. Jpn.* **1998**, *71* (9), 2239–2246.

[19] Ahman, J.; Wolfe, J. P.; Troutman, M. V.; Palucki, M.; Buchwald, S. L. Asymmetric Arylation of Ketone Enolates. *J. Am. Chem. Soc.* **1998**, *120* (8), 1918–1919.

[20] Surry, D. S.; Buchwald, S. L. Biaryl Phosphane Ligands in Palladium-Catalyzed Amination. *Angew. Chem. Int. Ed*. **2008**, *47* (34), 6338–6361.

[21] Bentz, E.; Moloney, M. G.; Westaway, S. M. Palladium-Catalysed α-Arylation of Esters and Amides under Microwave Conditions. *Tetrahedron Lett.* **2004**, *45* (40), 7395–7397.

[22] (a) Kurandina, D.; Parasram, M.; Gevorgyan, V. Visible Light-Induced Room-Temperature Heck Reaction of Functionalized Alkyl Halides with Vinyl Arenes/Heteroarenes. *Angew. Chem. Int. Ed.* **2017**, *56* (45), 14212–14216; (b) Ratushnyy, M.; Parasram, M.; Wang, Y.; Gevorgyan, V. Palladium-Catalyzed Atom-Transfer Radical Cyclization at Remote Unactivated C(Sp3)−H Sites: Hydrogen-Atom Transfer of Hybrid Vinyl Palladium Radical Intermediates. *Angew. Chem. Int. Ed.* **2018**, *57* (10), 2712–2715; (c) Parasram, Marvin; Chuentragool, Padon; Sarkar, Dhruba; Gevorgyan, V. Photoinduced Formation of Hybrid Aryl Pd-Radical Species

Capable of 1,5-HAT: Selective Catalytic Oxidation of Silyl Ethers into Silyl Enol Ethers. *J. Am. Chem. Soc.* **2016**, *138* (20).

[23] Zhou, W. J.; Cao, G. M.; Shen, G.; Zhu, X. Y.; Gui, Y. Y.; Ye, J. H.; Sun, L.; Liao, L. L.; Li, J.; Yu, D. G. Visible-Light-Driven Palladium-Catalyzed Radical Alkylation of C-H Bonds with Unactivated Alkyl Bromides. *Angew. Chem. Int. Ed*. **2017**, 56 (49), 15683-15687.

[24] Wang, G. Z.; Shang, R.; Cheng, W. M.; Fu, Y. Irradiation-Induced Heck Reaction of Unactivated Alkyl Halides at Room Temperature. *J. Am. Chem. Soc.* **2017**, *139* (50), 18307–18312.

[25] Abdiaj, I.; Fontana, A.; Gomez, M. V.; De la Hoz, A.; Alcazar, J. Visible-Light-Induced Nickel-Catalyzed Negishi Cross-Couplings by Exogenous-Photosensitizer-Free Photocatalysis. *Angew. Chem. Int. Ed. Engl.* **2018**, *57,* doi.org/10.1002/anie.201802656.

[26] Barl, N. M.; Malakhov, V.; Mathes, C.; Lustenberger, P.; Knochel, P. Palladium-Catalyzed Cross-Coupling between 7-Azaindoles and Reformatsky Reagents. *Synth.* **2015**, *47* (5), 692–700.

[27] Wu, Y.; Fu, W. C.; Chiang, C.-W.; Choy, P. Y.; Kwong, F. Y.; Lei, A.; Sivanandan, S. T.; Shaji, A.; Ibnusaud, I.; Seechurn, C. C.; et al. Palladium-Catalysed Mono-α-Alkenylation of Ketones with Alkenyl Tosylates. *Chem. Commun.* **2017**, *49*, 38.

[28] (a) De Vos, E.; Esmans, E. L.; Alderweireldt, F. C.; Balzarini, J.; De Clercq, E. Synthesis of 2-carbamoylmethyl-6-β-D-ribofuranosylpyridine with the Aid of a Pd(0) -catalyzed Reaction. *J. Heterocycl. Chem.* **1993**, *30* (5), 1245–1252; (b) Boldrini, G. P.; Mengoli, M.; Tagliavini, E.; Trombini, C.; Umani-Ronchi, A. Palladium Catalyzed Allylation of Reformatsky Reagents. Synthesis of γ,δ-Unsaturated Esters. *Tetrahedron Lett.* **1986**, *27* (35), 4223–4226.

[29] Berton, M.; Huck, L.; Alcázar, J. On-Demand Synthesis of Organozinc Halides under Continuous Flow Conditions. *Nat. Protoc.* **2018**, *13* (1), 324–334.

[30] (a) Pizzonero, M.; Dupont, S.; Babel, M.; Beaumont, S.; Bienvenu, N.; Blanqué, R.; Cherel, L.; Christophe, T.; Crescenzi, B.; De Lemos, E.; et al. Discovery and Optimization of an Azetidine Chemical Series as a Free Fatty Acid Receptor 2 (FFA2) Antagonist: From Hit to Clinic. *J. Med. Chem.* **2014**, *57* (23), 10044–10057; (b) Antermite, D.; Degennaro, L.; Luisi, R. Recent Advances in the Chemistry of Metallated Azetidines. *Org. Biomol. Chem.* **2017**, *15* (1), 34–50.

[31] Pratap, R.; Parrish, D.; Gunda, P.; Venkataraman, D.; Lakshman, M. K., Influence of biaryl phosphine structure on C-N and C-C bond formation. *J Am Chem Soc* **2009,** *131* (34), 12240-9.

[32] (a) Serrano, E.; Juan, A.; García-Montero, A.; Soler, T.; Jiménez-Márquez, F.; Cativiela, C.; Gomez, M. V.; Urriolabeitia, E. P., Stereoselective Synthesis of 1,3-Diaminotruxillic Acid Derivatives: An Advantageous Combination of C□H-ortho-Palladation and On-Flow [2+2]-Photocycloaddition in Microreactors. *Chemistry – A European Journal* **2016,** *22* (1), 144-152; (b) García-Montero, A.; Rodriguez, A. M.; Juan, A.; Velders, A. H.; Denisi, A.; Jiménez-Osés, G.; Gómez-Bengoa, E.; Cativiela, C.; Gómez, M. V.; Urriolabeitia, E. P., Metal-Free [2 + 2]-Photocycloaddition of (Z)-4-Aryliden-5(4H)-Oxazolones as Straightforward Synthesis of 1,3-Diaminotruxillic Acid Precursors: Synthetic Scope and Mechanistic Studies. *ACS Sustainable Chemistry & Engineering* **2017,** *5* (9), 8370-8381.

Chapter 6

Scalability of photochemical reactions: Visible light induced Nickel Negishi reaction one step closer to pharmaceutical manufacturing

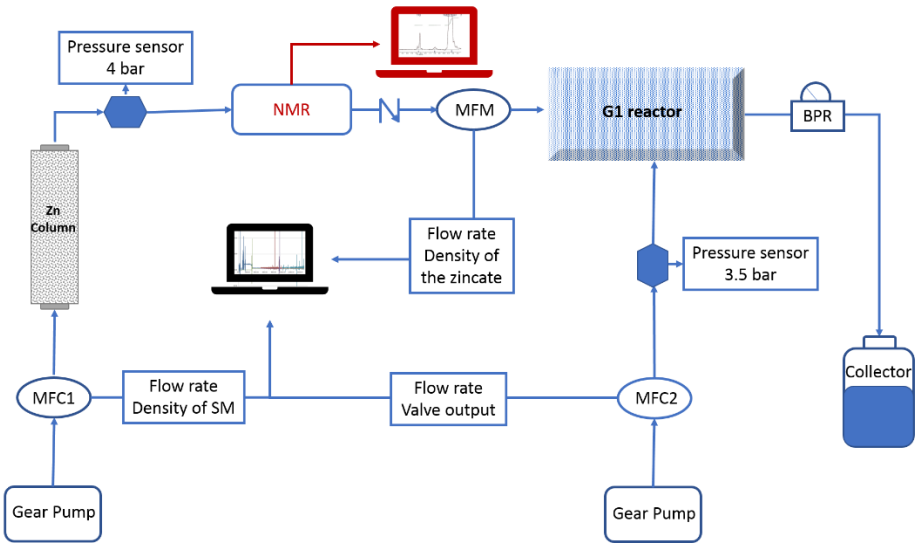

6.1 Introduction

Using light to accelerate a chemical reaction is one of the most promising opportunities to access new chemical transformation in a more effective and sustainable way. However, a serious problem limits the photochemical transformation on larger scales. The logarithmic decrease of the transmition of light is a function of the pathlength of the liquid medium (Lambert-Beer Law). Therefore, in large batch reaction vessels, the reaction mixture is inefficiently irradiated and low reaction rates may be obtained. These limitations can be avoided by changing from traditional batch processes to continuous flow approaches.[1] The large surface to volume ratio assures efficient irradiation of the entire reaction mixture. This results in significantly intensified protocols and allows scaling up of these novel chemistries.

106 years ago, Giacomo Ciamician already predicted that the future of synthetic chemistry would be based on the use of powerful and sustainable light energy under continuous flow processes. In his science report,[2] 'The photochemistry of the future', in 1912, he narrated his vision about the future of industrial synthetic chemistry describing lands full of transparent glass tubes where chemicals were flowing under the sun irradiation to produce new compounds, just like plants do.

A very important step towards this vision was the discovery of a simple and applicable flow photoreactor in 2005 from Booker-Milburn and his coworkers.[3] The photoreactor consisted in fluoropolymer tubing around a UV lamp and they could produce up to 658 gr of the desired product flowing the starting materials for 24 h. Flow photochemistry proved to intensify significantly the synthetic protocol and allowed to scale up the chemistry to synthetically useful quantities (Figure 6.1).

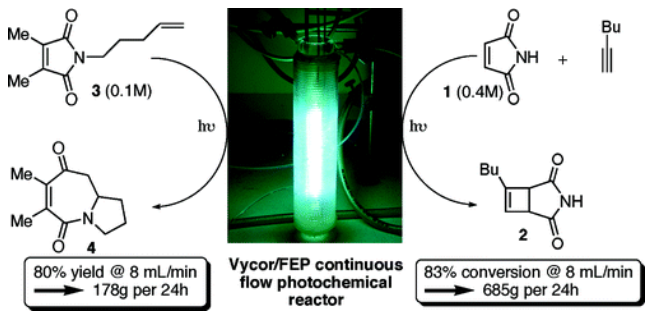

Figure 6.1: Booker-Milburn flow photoreactor for organic photosynthesis

In 2012, Lévesque and Seeberger reported a technically simple, efficient, and inexpensive scalable synthesis of artemisinin, one of the first line drugs for the treatment of malaria (Figure 6.2).[4] The photoinduced singlet oxygen generation in continuous flow process was key step to increase the productivity of artemisinin to 200

g/day. Estimating, that roughly 225 million doses of antimalarial medication are needed per year, approximately 1500 efficient, simple and productive photoreactors could meet this demand.[45] Later on, in 2015, Stephenson reported a direct comparison batch scale up and flow scale up. In batch, a reaction on 18 gram of *n-boc*-pyrrole provided similar yield as in small scale (57%), but when you go to 100g of starting material the yield decreased to 35 % and the reaction time was notably longer (62 h versus 15 h).[6] This can be attributed to a reduction of effective irradiation in the larger vessel. As expected in the flow reactor, the process was intensified and the reaction time reduced to 10 minutes with isolated yield of 71%. Recently, Monbaliu in collaboration with Corning SAS reported a scalable photocatalytic protocol for the oxidation of methionine under flow conditions.[7] They used the Corning lab reactor for initial reaction optimization and then transferred the reaction into the Corning G1 photoreactor obtaining a productivity of 31.1 mol/day.

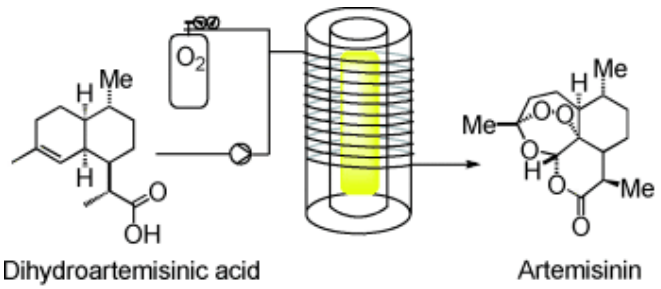

Figure 6.2: Continuous-Flow Synthesis of the Anti-Malaria Drug Artemisinin

However, developing photochemistry, especially at pilot/industrial scale where significant productivity is required, nowadays still remains challenging. In general, photochemical processes are not used in industry because the process chemists consider more economically and technically affordable conventional thermic driven reactions carried out in batch.

Lately, we published a new visible light induced photosensitizer free nickel catalyzed Negishi reaction for C(sp^3)-C(sp^2) cross coupling with a broader scope than traditional Negishi reaction.[8] In view of the need of the medicinal chemists nowadays for new methodologies to enrich drug candidates with (sp^3) motifs[9], we consider it a very important reaction and therefore we aimed to test its scalability in pilot scale. In collaboration with CORNING SAS, we chose Corning G1 photoreactor for the scale up of the reaction.[10]

6.2 Experiment 1: Set up optimization

The photoindinduced Negishi cross-coupling is a two step reaction that requires the formation of the organozinc reagent in flow and afterwards the coupling with the halide

derivative. The investigation started with an example that was already scaled up with our Vapourtec reactor[11] using a 10 mL coil of fluorinated ethylene propylene (FEP). The process was run continuously for 8 hours providing 6.7 grams of purified product.[8] This is enough quantity for drug-discovery processes however due to size limitation of the reactor we cannot reach higher productivities. Therefore, an appropriate pilot scale designed reactor, was selected to increase productivity.

Corning G1 photoreactor is a glass reactor with a complex design called Heat Exchange and Advanced Reaction technology (HEART) ensuring heat and mass transfer.[10] The light source consists in LED arrays placed on both sides of the glass fluidic modules and adjustable in terms of wavelength and light intensity. The wavelength available are 365 nm and 405 nm. Each LED array contains 20 LEDs and a heat exchanger. The irradiated volume of the fluidic module V_r is 8.2 mL and the channel depth is 1.2 mm. For each fluidic module the irradiated channel surface, S_{irrad} is equal to 78 cm^2. The 5 fluidic modules can be thermoregulated by the use of thermostats.[10]

One of the challenges we had to deal with was to build up a system where G1 photoreactor was connected with the SolventPlus™ Omnifit column used for the organozinc preparation. PFA tubing and gear pumps controlled from mass flow controllers were used to pump the reagents into the system.

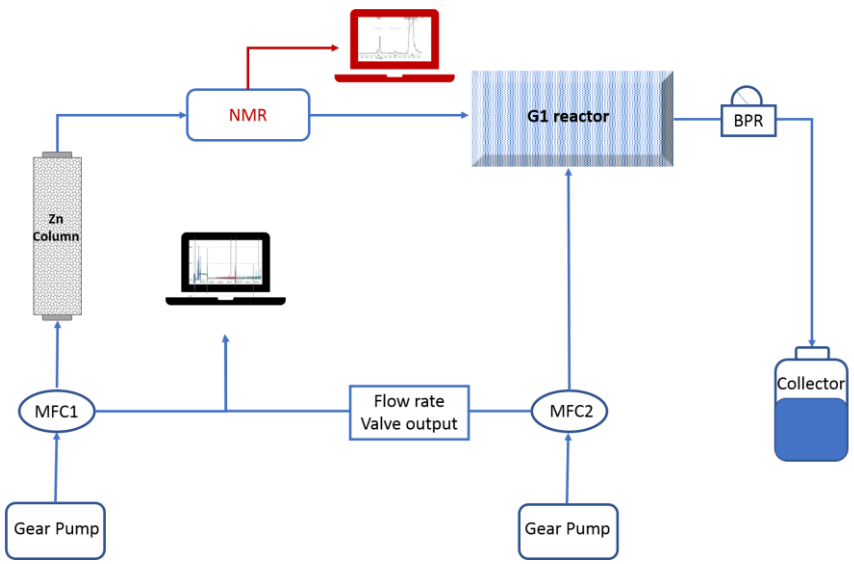

Figure 6.3: Schematic overview of the flow set up

In the initial system, the zinc column was alimented from gear pump 1 controlled from MFC1. At the exit of the zinc column a Magritek benchtop NMR was connected for inline

monitoring of the organozinc formation. At the exit of the NMR a valve was controlling the entrance of the organozinc solution into the photoreactor that was alimented directly from a second gear pump controlled from MFC2, once the organozinc reagent was formed. In order to predict possible clogging of the reactor the power of the valve out of the MFC1 and 2 was activated. It measures the power used from the gear pump to push the liquid into the reactors. To assure a stable flow rate the entire system was used under pressure controlled from a back-pressure regulator (BPR; setpoint 3.5-4 bars) at the exit of the photoreactor (Figure 6.3).

Table 6.1: Optimization of the conditions Experiment 1

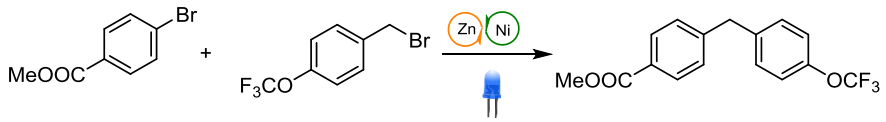

1 **2** **3**

Entry	RT(min)	T. (°C)	Conv. %
1	20	60	100
2	20[a]	60	79
3	20	40	90
4	12	60	70
5	15	60	100

a) No pressure in the system.

Reaction conditions: Methyl 4-bromobenzoate (1 eq., 15 mmol); 4-(trifluoromethoxy)benzyl bromide (2 eq., 30 mmol); Nickel catalyst (0.02 eq., 0.3 mmol); dtbbpy (0.03 eq., 0.45 mmol).

6.2.1 Optimization of the conditions

Preliminary experiments were performed with this initial set up to reach the ideal conditions for the scale up. The LED panels were set to 405 nm slightly lower wavelength that the one used in our lab reactor. With the initial reported lab-reactor conditions, we obtained full conversion (Table 6.1, entry 1). Decreasing the temperature to 40 °C was not beneficial to the reaction reducing the conversion in 90% (Table 6.1, entry 3). Furthermore, the pressurized system proved to be essential to maintain a stable flowrate and therefore on a stable residence time. Without a pressure regulator, in 20 minutes and 60 °C gas bubbles are formed in the reactor, probably THF evaporating (boiling point 68 °C) and the conversion obtained was just 79% (Table 6.1, entry 2). Maintaining the temperature 60 °C and the pressurized system the residence time was reduced to 15 minutes providing full conversion in product (Table 6.1, entry 5).

With the optimized conditions we ran the reaction for 6.5h in continuous flow. Samples were analysed every 30 minutes and conversion was checked by GCMS (Figure 6.4).

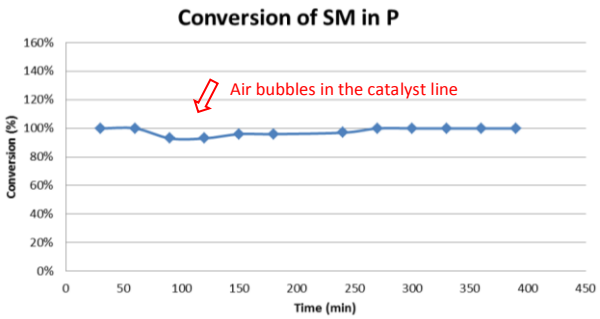

Figure 6.4: Conversion of starting material in product

The presence of some nitrogen bubbles in the catalyst line influenced the conversion of the corresponding fraction and reduced it into 93%. Yet, the overall conversion remained 98% and the final isolated yield was 93% providing 36.6g of pure product and increasing the productivity of the protocol from 0.8g/h to 5.63 g/h (Table 6.2).

Table 6.2: Comparison of productivity Experiment 1

	Vapourtec	**Corning G1**
Yield	93%	93%
Time	20 min	15 min
Reactor size	10 mL	40 mL
Throughput	0.8 g/h	**5.63g/h**

6.2.2 NMR monitoring

NMR spectroscopy is a great technique for monitoring organic reactions due to its high degree of functional group specificity.[12] Despite being one of the most powerful analytical techniques the use of the NMR integrated into processes has been scarcely reported and mainly used in by-pass configurations, flow cells in high field NMR machines or micro coils for microfluidic applications.[13]

Nowadays, apart from our work[8], there are no organozinc's NMR spectra. This is due to their instability in open air. However, with the use of NMR-inline monitoring, we expected that we could directly monitor the conversion of the starting material in organozinc reagent before flowing into the photoreactor. Effectually, we observed that the singlet of the CH_2 in alfa al bromo del trifluoromethoxy benzyl bromide is shifted at lower ppm when we form the organozinc reagent (Figure 6.5).

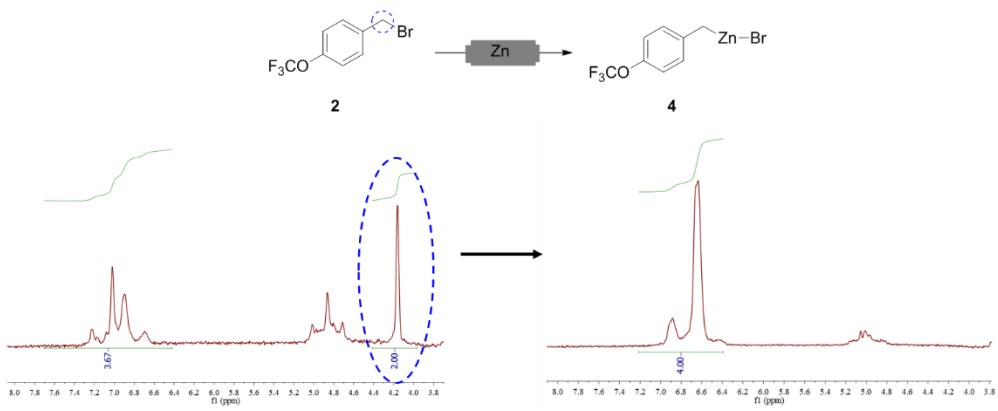

Figure 6.5: NMR monitoring of 4-(trifluoromethoxy) benzyl zinc bromide formation; Left: NMR spectra of 4-(trifluoromethoxy) benzyl bromide in THF; Right: NMR spectra of 4-(trifluoromethoxy)benzyl zinc bromide in THF

The protons corresponding the CH_2 signal are shielded due to the higher electron density at the carbon bonded the less nucleophilic zinc atom.[8] The same effect is observed even in ^{19}F NMR but the difference between **1** and **2** in ppm is lower (-57,04 and -57.27 ppm). Thus, we selected ^{1}H NMR analysis to monitor the reaction. We calculated the concentration of the outcoming organozinc reagent by the integration of the aromatic protons taking as benchmark the tetrahydrofuran (THF) protons. Our flow NMR cell was made from PTFE tube connected with Teflon connectors in the extremities. In this way we could support the 4 bars of pressure inside the NMR. The concentration of organozinc solution remained stable with slight variation between 4 to 5% in 6.5 h run (Figure 6.6). There were no traces of SM in the NMR spectra.

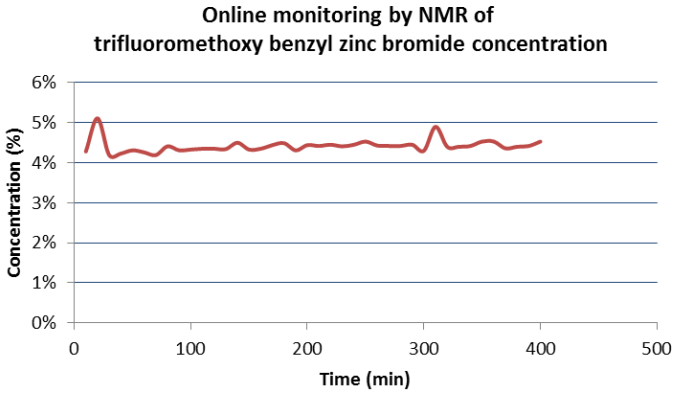

Figure 6.6:Inline NMR monitoring of the organozinc formation

6.2.3 Mass flow controllers

We used mass flow controllers to control the gear pumps to push the liquid into the system and also to directly monitor the flow rates, thereby giving indirect information about what is happening in both reactors, Zn column reactor and the photoreactor. After the run we observed that while in the catalyst feed (MFC2) the report showed a stable and linear graph in time, the benzyl bromide feed presented various instabilities. Over the first hour, both feeds presented stable flow rates without important fluctuations (Figure 6.7). It is in the course of time that fluctuations became more frequent, however only in the benzyl bromide feed (MFC1). This suggested to us that it probably is correlated with the instabilities of the zinc column due to the zinc consumption over time. Despite this, the instabilities did not affect our productivity. The mass flow controller gives a very sensitive measurement of the flow rates in time; one every 1/10 of a second. Thus, even though we had small spikes every tenth of a second the effect produced in conversion is insignificant. At minute 90 some nitrogen bubbles entered in the catalyst feed (MFC2) because the inlet tubing was not fully connected to the solution. As a result of this, the system was unstable for several seconds producing a clear effect in the conversion of the starting material in product (Figure 6.4). Eventually, in the corresponding fraction of collection the conversion decreased to 93%. This incident showed us that the system needed further optimization but even though it was not perfect thanks to the monitoring over time, in a hypothetic production plant we can select which fractions to collect and which not depending on the trend of monitoring. Further work was needed to optimize the system for stable continuous production.

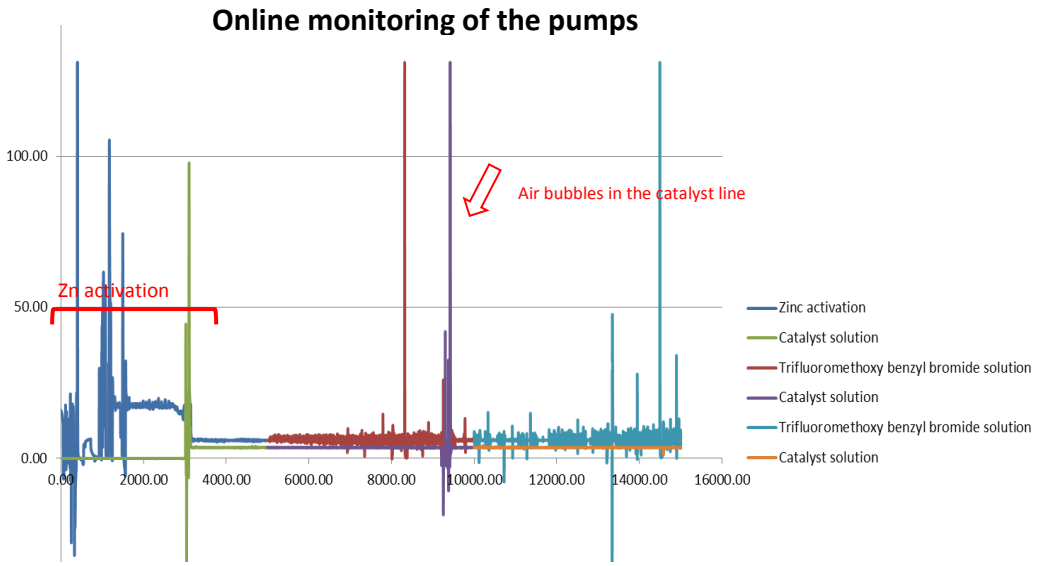

Figure 6.7: Online monitoring of the mass flow controllers

6.3 Experiment 2: Set up optimization

Therefore, we hypothesized that if the pressure in the zinc reactor would be higher than the pressure in the photoreactor, the flow would be always positive toward the photoreactor avoiding the backflow generated from the zinc consumption. With this idea in our mind we added parameters to the system to produce this difference of pressure that would assure stability. A valve needle was placed just after the NMR in order to generate 4 bars of pressure in the zinc column measured by a pressure sensor. To monitor the exact flow rate entering the photoreactor after the zinc column, a mass flow meter (MFM) was added. Moreover, in order to assure the lower pressure, the two (3.5 bars) in the photoreactor, a new pressure sensor was added at its entrance which was controlled from the BPR at the exit of the photoreactor (Figure 6.8). Two additional parameters of control were added to the system. The CORE-FLOW™ MFC/MFM have a density sensor which when activated measures the density of the liquid passing in the flowing channel. Therefore, we activated the density sensor of MFC1, flowing the starting material solution, and MFM, flowing the organozinc reagent solution. As expected, the density of the organozinc solution was higher than the starting material solution. This additional parameter of control can be used in cases of starting materials where the NMR monitoring does not give clear information about the organozinc formation. In Figure 6.9 is showed how the flow set up looks in the lab.

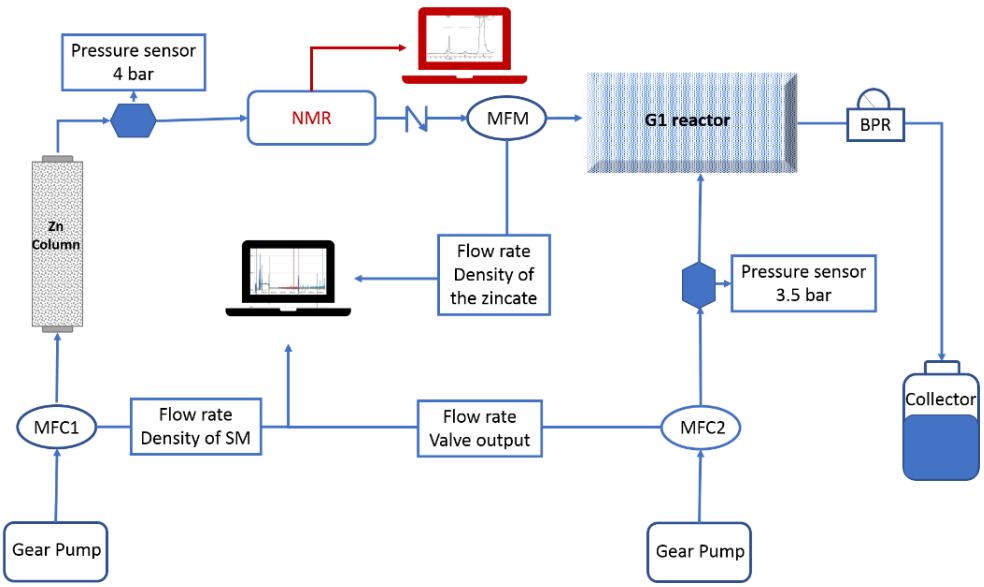

Figure 6.8: Schematic overview of the optimized flow set up

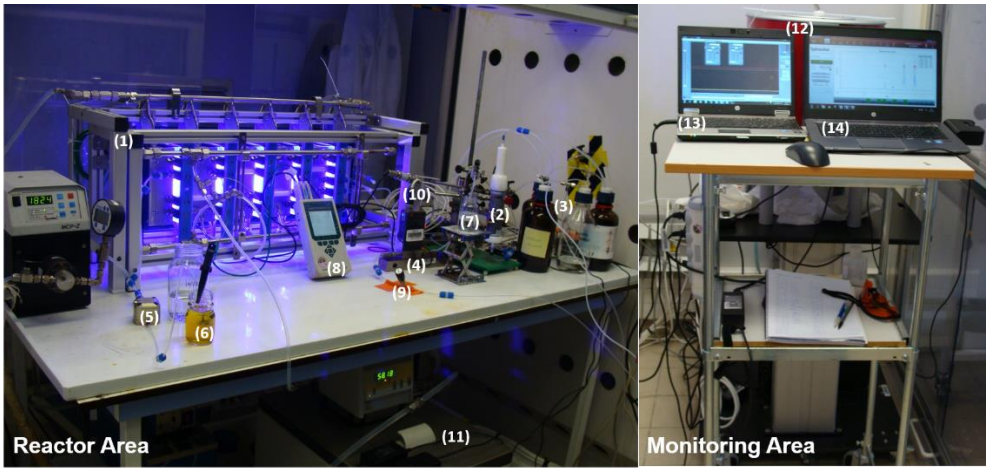

Figure 6.9: Set up of system: 1. G1-photoreactor; 2. Zinc column; 3. Reagents; 4. Mass flow controller; 5. Back pressure regulator; 6. Collecting fraction; 7. Waste of zinc activation; 8. Monitoring of pressure and temperature; 9. Needle valve; 10. Pressure sensor; 11. Chiller; 12. Magritek NMR spectrometer; 13. MFC monitoring computer; 14. NMR monitoring computer.

6.3.1 Optimization of the reaction conditions

The new optimized system was tested with another example consisting of a more medicinal chemistry like substrate. We selected 2-amino-5 iodo pyrimidine as a coupling partner with benzyl bromide. This product is already reported in small scale in our previous article and we find it especially interesting due to its heterocyclic nature[9a] and the free amine group opened to further derivatization of the core.

Table 6.3: Optimization of the conditions Experiment 2

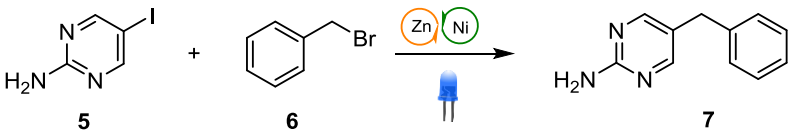

5 **6** **7**

Entry	RT(min)	T. (°C)	Eq. of B	Light irradiation	Conc. of (6)	Conv. %
1	20	60	3	On	0.5M	100
2	15	60	3	On	0.5M	100
3	12	60	3	On	0.5M	Traces of SM
4	15	60	2	On	0.5M	Traces of SM
5	15	60	2.5	On	0.5M	Traces of SM
6	15	60	3	On	1M	100 (94)[a]
7	15	60	3	Off	1M	34[a]

a) Isolated yield

b) ***Reaction conditions:*** 2-amino-5-iodopyrimidine (1 eq., 15 mmol); benzyl bromide (3 eq., 45 mmol); Nickel catalyst (0.02 eq., 0.3 mmol); dtbbpy (0.03 eq., 0.45 mmol).

Even in this case with the original conditions full conversion was obtained (Table 6.3, entry 1). Applying the optimized conditions of the first reactions 15 minutes residence time, 60 °C also provided full conversion (Table 6.3, entry 2). Reduction of time in 12 minutes resulted insufficient to convert all the starting material in product (Table 6.3, entry 3). Increasing the concentration of benzyl bromide to 1 M solution produced the same effect as 0.5 M but due to solubility issues of the 2-amino-5-iodo-pyrimidine we had to use pure DMF to dissolve the catalyst feed reagents (Table 6.3, entry 6). 3 equivalents of benzyl bromide were necessary for full conversion (Table 6.3, entry 5). No light reaction provided only 34% of isolated product (Table 6.3, entry 7).

Table 6.4: Comparison of productivity Experiment 2

	Vapourtec	**Corning G1-**
Yield	93%	94%
Time	20 min	15 min
Reactor size	10 mL	40 mL
Conc. RM	0.375M	0.75M
Throughput	0.3 g/h	3.4g/h

The scale up of the reaction was performed in 6 hours run. Increasing the concentration increased significantly the productivity of the reaction. The conversion of the starting material in product remained stable over time (Figure 6.10) yielding 20.68g of pure crystalline product (94%) (Table 6.4). Considering that chromatographic purification is complicated particularly for large-scale production, we envisioned it was necessary to find an alternative for the purification of the product.[14] Crystallization is a natural occurring process but also a process abundantly used in the industry.[15] After some literature research on similar products[16] we found out that our product could be re-crystallized in water. Therefore, the work-up procedure was modified in order to perform a purification by crystallization. Zn salts form water soluble complexes with ammonium salts, that is the reason why we normally use ammonium chloride solution to quench the reaction. However, in larger scale, the acidity of the ammonium chloride solution increases the solubility of our product in water thereby demanding huge amounts of organic solvent to extract it, increasing the quantity of zinc salts dissolved in the organic solvent. Thus, in the crystallization, traces of Zn salts can be found. An elegant solution to this problem is the use aqueous ammonia solution. In basic ammonia solution (pH=9) the zinc salts form water soluble complexes and furthermore the basic aqueous phase increases the solubility of the product in organic solvents. The organic phase was evaporated, the rests solubilized in a minimum quantity of dichloromethane

and then recrystallization in water afforded the desired product as a white crystalline solid (Figure 6.10A).

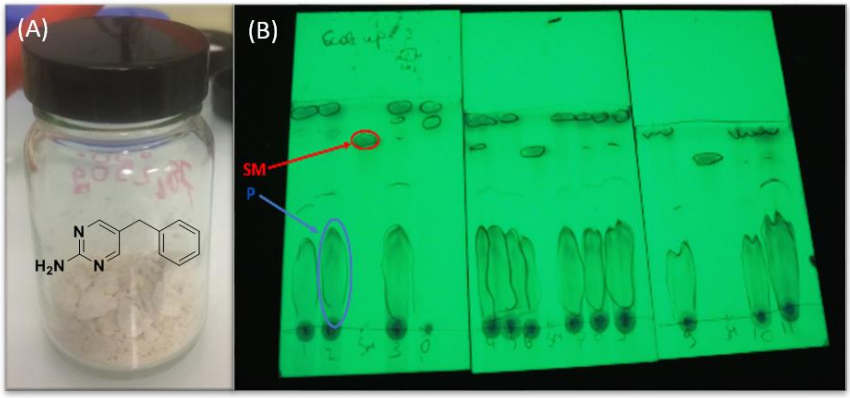

Figure 6.10: (A) Isolated product Experiment 2; (B) TLC monitoring of the conversion of starting material in product

6.3.2 NMR monitoring

Even in this second experiment NMR monitoring provided clear information about the concentration of the benzyl zinc bromide solution. The singlet corresponding to the CH_2 in alfa to the bromide was shifted in lower ppm when benzyl zinc bromide is formed. The integration of aromatic protons provided information about the concentration of the outcoming organozinc reagent. In this case we started the experiment with higher concentration. 1M benzyl bromide solution provided concentrations varying between 8.5%-9.8% of benzyl zinc bromide solution (Figure 6.11). The concentration remained stable in time without important variations.

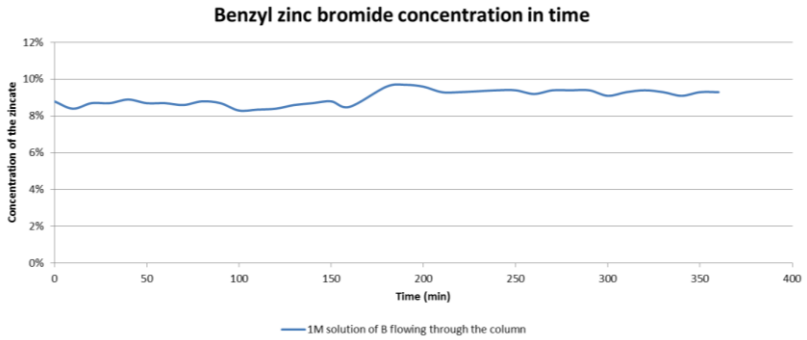

Figure 6.11: NMR monitoring online of the formation of benzyl zinc bromide

6.3.3 MFC/MFM

Under the new reaction conditions, the report showed stable flow rates in both feeds (Figure 6.12A). Some nitrogen bubbles were intentionally introduced into the Feed in order to see how this instability would be reflected in the other two flow rates (MFM and the MFC). As predicted, even though we had a big spike in the MFC1 measurement due to the nitrogen bubbles, the difference in pressure between the two reactors managed to maintain controlled flow rates in MFM and MFC2, thereby assuring stability of the system (Figure 6.12B). If the nitrogen bubbles are introduced in Feed 2, the effect in the other Feed is minimum and it has no impact in the conversion of the starting material in product (Figure 6.12C). Moreover, the system seems to get more and more stable over time. The density sensors showed the same results as the NMR monitoring. There was a clear difference between the density of the benzyl bromide solution (0.959 gr/mL) and the benzyl zinc bromide solution (1.022 gr/mL) and this difference remained stable over the 6 hours of the run.

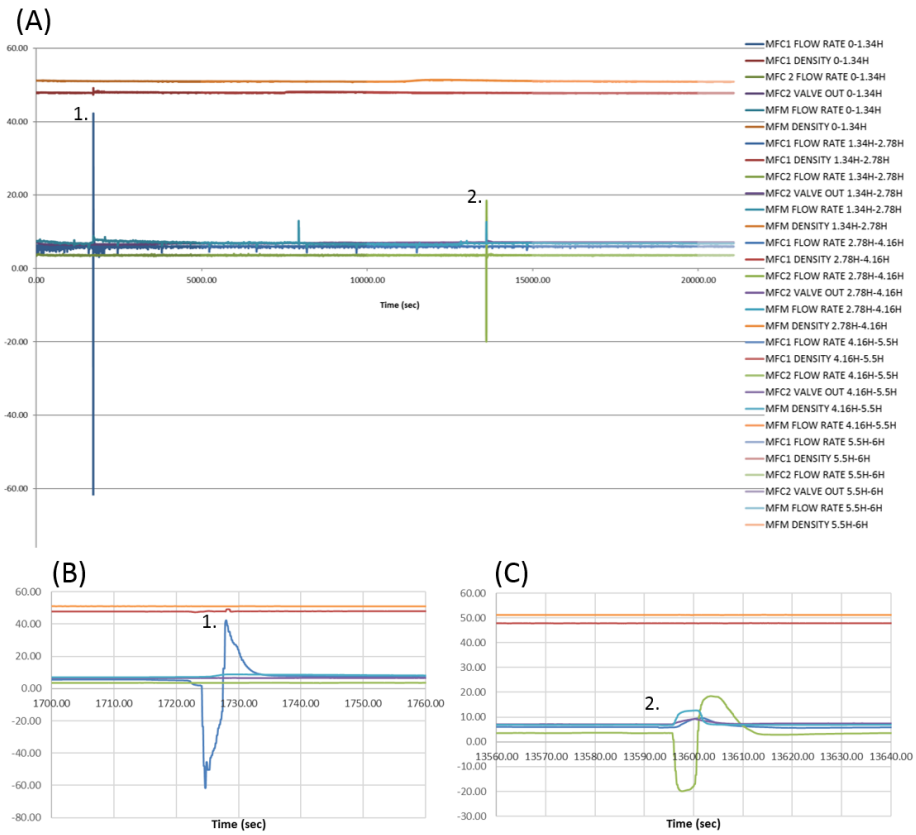

Figure 6.12: MFC/MFM monitoring Experiment 2; (A) Entire report from the mixing of benzyl zinc bromide solution with catalyst solution in the photoreactor; (B) Zoom of the 1st spike; (C) Zoom of the 2nd spike.

6.4 Experiment 3: The effect of the diffusion in the Zn column

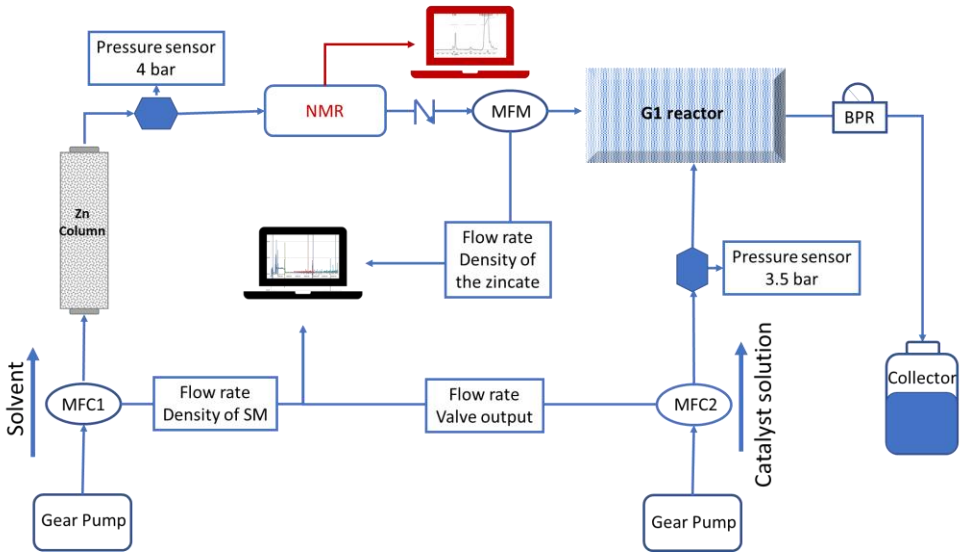

Figure 6.13:Set up for Experiment 3

In a third experiment the effect of the diffusion in the zinc column was studied. The experiment consisted in switching the injection valve from reagent to solvent once the zinc column had achieved different stationary phases and analyzed the effect of diffusion of the solvent in the concentration of the outcoming organozinc solution, reflected as well in the density and the conversion of starting material in product. Since the initial moments of the change the effect of diffusion was clearly visible. Moreover, this effect was directly transferred in the conversion of starting material in product. While benzyl bromide was flowing to the column no presence of starting material in the reaction mixture was observed by TLC. Nevertheless, when solvent started to flow the intensity of the spot corresponding to the starting material increased in time (Figure 6.6.14).

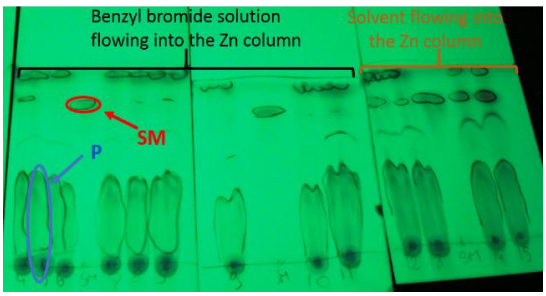

Figure 6.6.14: TLC monitoring

After just 10 minutes (13 mL of solvent flowing through the Zn column) the concentration of the zincate was reduced from 8.4% to 6.2%. Hereafter, the concentration decreased rapidly and in less than 1 hour only traces of organozinc solutions remained in the column (2.5% of concentration) (Figure 6.15).

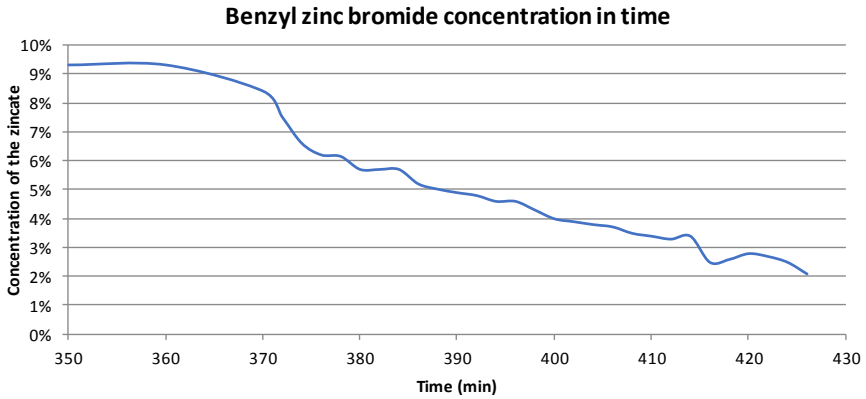

Figure 6.15: Inline-NMR monitoring of benzyl zinc bromide formation

The same behavior was followed even by the density sensor (Figure 6.16). In the first 10 minutes the decrease in concentration is smooth and afterwards it becomes more and more evident until the density of the pure solvent is reached after less than 1 hour of run.

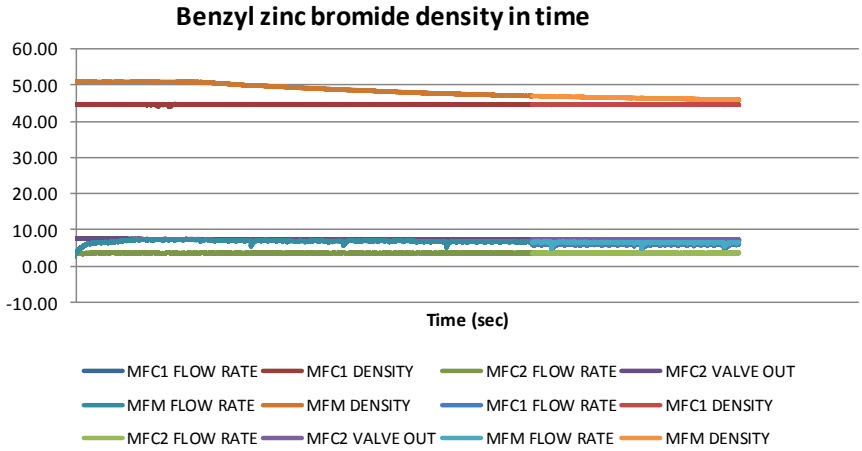

Figure 6.16: Online monitoring of the density

In conclusion, we must say that it is very important to prepare two extra column volumes of the initial starting material solution for the organozinc reagent. One column volume

is important in the beginning of the reaction, after zinc activation, to stabilize the flow rate in the zinc reactor. Ethene gas bubbles formed in the activation should be removed completely, before starting to flow the organozinc solution into the photoreactor. The second column volume is important because due to the diffusion of the solvent in the zinc column, it is important to aliment the column continuously with starting material solution. In this way, we will be left with a controlled system and stable conversion of starting material in product.

6.5 Conclusions

In conclusion, visible light induced nickel catalysed Negishi reaction can be scaled up for industrial application. Herein we proved that with the needed system optimization, this two step reaction works in gram scale with a productivity that goes from 82 to 270g/day. The reaction time was reduced to 15 minutes, 20% less than the original reported conditions and the nickel loading was 2 mol%. To increase the productivity, the organozinc compound can be prepared in double concentration of initial starting material solution. NMR online monitoring proved to be essential in tracking the first step of the reaction, formation of the organozinc reagents. The optimized system and the controlled parameters give autonomy to the chemist and reproduce a similar situation as in a production plant. A Corning advanced flow G3 reactor with similar process conditions would increase the productivity up to 800g/day. Future work for a completely automated system can bring the process to direct industrial production.

6.6 Experimental part

General information

The reactions were conducted in the Corning G1 photoreactor equipped with 5 glass fluidic modules connected in series (8.2 mL volume each). The light source consists in LED arrays placed on both sides of the glass fluidic modules and adjustable in terms of wavelength and light intensity. The wavelength available are 365nm and 405nm. Each LED array contains 20 LEDs and a heat exchanger. For each fluidic module the irradiated channel surface, S_{irrad} is equal to 78 cm^2. The thermoregulation of both the glass fluidic module and the LED panels was carried out with LAUDA® Proline RP 845 thermostats. Ethylene glycol, which is transparent, was utilized as thermofluid.

The reagents flow rates were controlled with two Bronkhorst® F210CTM mass flow controllers (MFC). A Zaiput Flow Technologies® dome-type back-pressure regulator (BPR) was inserted downstream and connected to a cylinder of compressed Argon (set point: 8 barg). LAUDA® Proline RP 845TM thermostats were used for the thermoregulation of the mesofluidic reaction glass modules and the LED illumination setup (Corning® Advanced-Flow G1 Photo Reactor). In-line NMR analysis was carried out with a 43 MHz SpinsolveTM NMR spectrometer from Magritek® equipped with the flow-through module.

For the preparation of the organozinc reagent SolventPlus™ Omnifit column (bore: 35 mm, length: 150 mm, AF (1× adjustable & 1× fixed endpiece); Omnifit, cat. no. 006SCC-35-15-AF. The needed parts are the glass tube, two 30 µm × 35 mm polytetrafluoroethylene (PTFE) frits, one fixed end piece as a bed support and one adjustable end piece (plunger) to adjust the bed height. (https://www.dibaind.com/wpcontent/uploads/2015/01/201501_1_OFLW_CAT.pdf).

GC measurements were performed using a 6890 Series Gas Chromatograph (Agilent Technologies) system comprising a 7683 Series injector and auto sampler, J&W HP-5MS column (20 m x 0.18 mm, 0.18 µm) from Agilent Technologies coupled to a 5973N FID Flame Ionization Detector. Thin layer chromatography (TLC) was carried out on silica gel 60 F254 plates (Merck) using reagent grade solvents. Unless otherwise specified, reagents were obtained from commercial sources and used without further purification.

Activation of the Zn column:

A solution 1.0 M trimethylchlorosilane (TMSCl) and 0.24 M 1-bromo-2-chloroethane was prepared under nitrogen (N_2) atmosphere in a dried flask by dissolving 6.25 mL of TMSCl and 1.25 mL of 1-bromo-2-chloroethane in 50 mL of dried tetrahydrofuran (THF). 5 mL

of this solution were passed through the 35 mm internal diameter Omnifit column containing Zn (150 g) using the MFC1 at room temperature and 4 mL /min flow rate.

Experiment 1

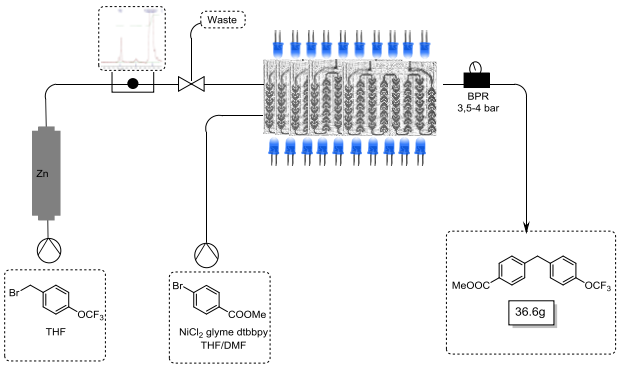

A solution of 4-(trifluoromethoxy) benzyl bromide (254 mmol; 2 eq.+50 mmol) in 608 mL of THF was pumped through a column containing activated zinc at room temperature at 1.35 mL /min using the MFC1. The outcoming solution of the organozinc compound was analysed by in line NMR monitoring and once the organozinc reagent started to flow, inserted into the photoreactor. The outcoming solution was combined with a solution (B) of methyl 4-bromobenzoate (1 eq. 127 mmol), $NiCl_2$ glyme (0.02 eq., 2.54 mmol); dtbbpy (0.03 eq., 3.81 mmol) in 407 mL of THF and 101 mL of DMF in Corning G1 Photoreactor at 1.35 mL /min each line (RT= 15 min; coil volume= 40 mL) at 60 °C irradiating with 405nm blue LEDs. The system was maintained under 3.5-4 bars of pressure with a back-pressure regulator. The out coming of the reactor was collected in fractions of 80mL each. The collected fractions were concentrated by evaporating the THF and then diluted with ethyl acetate and added to a separatory funnel containing 1 L of ammonium chloride saturated aqueous solution. The organic layer was separated, dried with $MgSO_4$, filtered and then the solvents evaporated. Purification by flash chromatography using Heptane: Ethyl acetate from 100:0 to 75:25 afforded the desired product as a transparent liquid in 36.6 grams, isolated yield 93%.

*Methyl 4-(p-tolylmethyl) benzoate (**3**)*

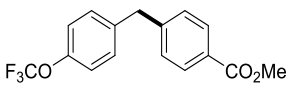

3

^{1}H NMR ($CDCl_3$, 500 MHz): δ = 7.97 (d, J = 8.4 Hz, 2H), 7.22-7.27 (m, 2H), 7.09-7.21 (m, 4H), 4.03 (s, 2H), 3.90 ppm (s, 3H).

^{13}C NMR ($CDCl_3$, 126 MHz): δ = 166.9, 147.8, 145.7, 138.9, 130.2, 130.0, 128.9, 128.4, 121.5, 121.0, 52.1, 41.2 ppm.
^{19}F NMR ($CDCl_3$, 471 MHz): δ = -57.93 ppm (br s, 1F).
HRMS (ESI-TOF): m/z calculated for $C_{16}H_{16}O_2$ $[M+H]^+$: 241.1150. Found 241.1151.

Experiment 2

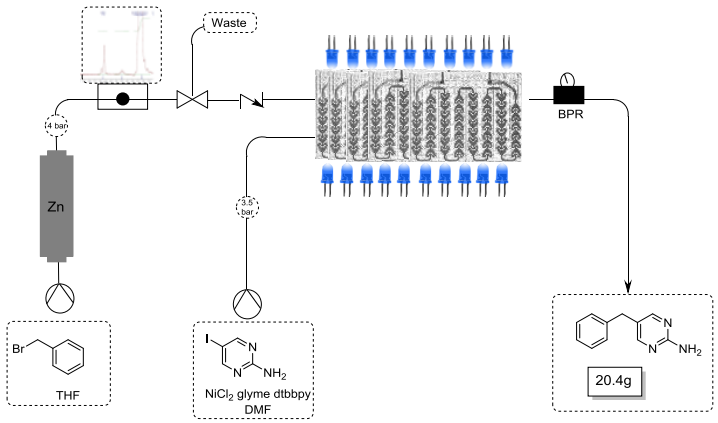

A solution of benzyl bromide (351 mmol; 3 eq.+ 100 mmol) in 451 mL of THF was pumped through a column containing activated zinc at room temperature at 1.35 mL /min using the MFC1. The outcoming solution of the organozinc compound was analysed by NMR in line monitoring and once the organozinc reagent started to flow, inserted into the photoreactor. The outcoming solution was combined with a solution (B) of 2-amino-5-iodopyrimidine (1 eq. 117 mmol), $NiCl_2$ glyme (0.02 eq., 2.34 mmol); dtbbpy (0.03 eq., 3.51 mmol) in 351 mL of DMF in Corning G1 Photoreactor at 1.35 mL ·min-1 each line (RT= 15 min; coil volume= 40 mL) at 60 °C irradiating with 405nm blue LEDs. The zinc reactor was maintained under 4 bars of pressure controlled from the needle valve and the photoreactor was maintained at 3.5 bars of pressure from the BPR. The out coming of the reactor was collected in fractions of 80mL each. The collected fractions were concentrated by evaporating the THF and then diluted with dichloromethane and added to a separatory funnel containing 1 L of aqueous ammonium solution (pH=9). The organic layer was separated, dried with $MgSO_4$, filtered and then the solvents evaporated. The rests were dissolved in minimum quantity of dichloromethane and the product was crystallized in water as 20.4 grams of a white crystalline solid, 94% of isolated yield

*5-Benzylpyrimidin-2-amine (**7**)*

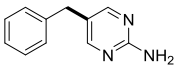

7

^{1}H NMR ($CDCl_3$, 400 MHz): δ = 8.15 (s, 2H), 7.27-7.36 (m, 2H), 7.22 (s, 1H), 7.17 (s, 2H), 4.96 (br s, 2H), 3.80 ppm (s, 2H).
^{13}C NMR ($CDCl_3$, 101 MHz): δ = 158.4, 139.8, 128.7, 128.6, 126.5, 123.9, 103.6, 35.7 ppm.
HRMS (ESI-TOF): m/z calculated for $C_{11}H_{10}N_3Na$ $[M+Na]^+$: 207.0772. Found 207.0689.
Melting point: 121.86 °C.

Experiment 3

A solution of benzyl bromide (150 mmol; 3 eq.) in 150 mL of THF was pumped through a column containing activated zinc at room temperature at 1.35 mL /min using the MFC1. The outcoming solution of the organozinc compound was analysed by NMR in line monitoring and once the organozinc reagent started to flow, inserted into the photoreactor. The outcoming solution was combined with a solution (B) of methyl 4-bromobenzoate (1 eq. 50 mmol), $NiCl_2$ glyme (0.02 eq., 1 mmol); dtbbpy (0.03 eq., 1.5 mmol) in 150 mL of DMF in Corning G1 Photoreactor at 1.35 mL ·min-1 each line (RT= 15 min; coil volume= 40 mL) at 60 °C irradiating with 405nm blue LEDs. The zinc reactor was maintained under 4 bars of pressure controlled from the needle valve and the photoreactor was maintained at 3.5 bars of pressure from the BPR. When the benzylbromide solution was all inside the zinc column, solvent was flowed into the column for 50 mL more. The organozinc reagent was analyzed by NMR and the outcome of the reactor was analyzed by TLC to see the conversion of the starting material in product.

Bibliography

[1] (a) Plutschack, M. B.; Pieber, B.; Gilmore, K.; Seeberger, P. H. The Hitchhiker's Guide to Flow Chemistry *Chem. Rev*. **2017**, *117*(18), 11796–11893; (b) Gilmore, K.; Seeberger, P. H. Continuous Flow Photochemistry. *Chem. Rec.* **2014**, *14* (3), 410–418.

[2] Ciamician, G. The photochemistry of the future. *Science.* **1912**, *36* (926), 385–394.

[3] Hook, B. D. A.; Dohle, W.; Hirst, P. R.; Pickworth, M.; Berry, M. B.; Booker-Milburn, K. I. A Practical Flow Reactor for Continuous Organic Photochemistry. *J. Org. Chem.* **2005**, *70* (19), 7558–7564.

[4] (a) Lévesque, F.; Seeberger, P. H. Continuous-Flow Synthesis of the Anti-Malaria Drug Artemisinin. *Angew. Chem. Int. Ed.* **2012**, *51* (7), 1706–1709; (b) Kopetzki, D.; Lévesque, F.; Seeberger, P. H. A Continuous-Flow Process for the Synthesis of Artemisinin. *Chem. Eur. J.* **2013**, *19* (17), 5450–5456.

[5] *World Malaria Report 2010*; Geneve, **2010**.

[6] Beatty, J. W.; Douglas, J. J.; Cole, K. P.; Stephenson, C. R. J. A Scalable and Operationally Simple Radical Trifluoromethylation. *Nat. Commun.* **2015**, *6*, 7919.

[7] Emmanuel, N.; Mendoza, C.; Winter, M.; Horn, C. R.; Vizza, A.; Dreesen, L.; Heinrichs, B.; Monbaliu, J. C. M. Scalable Photocatalytic Oxidation of Methionine under Continuous-Flow Conditions. *Org. Process Res. Dev.* **2017**, *21* (9), 1435–1438.

[8] Abdiaj, I.; Fontana, A.; Gomez, M. V.; De la Hoz, A.; Alcazar, J. Visible-Light-Induced Nickel-Catalyzed Negishi Cross-Couplings by Exogenous-Photosensitizer-Free Photocatalysis. *Angew. Chem. Int. Ed. Engl.* **2018**, *57*, doi.org/10.1002/anie.201802656.

[9] (a) Dua1, R.; Dua, R.; Shrivastava, S.; Sonwane, S. K.; Srivastava, S. K. Pharmacological Significance of Synthetic Heterocycles Scaffold: A Review. *Adv. Biol. Res. (Rennes).* **2011**, *5* (3), 120–144; (b) Walters, W. P.; Green, J.; Weiss, J. R.; Murcko, M. A. What Do Medicinal Chemists Actually Make? A 50-Year Retrospective. *J. Med. Chem*. **2011**, 54 (19), 6405–6416; (c) Tsukamoto, T. Tough Times for Medicinal Chemists: Are We to Blame? *ACS Med. Chem. Lett.* , **2013**, *4* (4), 369–370.

[10] Elgue, S.; Aillet, T.; Loubiere, K.; Conté, A.; Dechy-Cabaret, O.; Prat, L.; Horn, C. R.; Lobet, O.; Vallon, S. Flow Photochemistry: A Meso-Scale Reactor for Industrial Applications. *Chim. Oggi* **2015**, *33* (5), 58–61.

[11] For Further Information about Instrument Used Visit the Web: <www.Vapourtec.Com>.

[12] (a) Nordon, A.; McGill, C. A.; Littlejohn, D. Process NMR Spectrometry. *Analyst* **2001**, *126* (2), 260–272; (b) Sans, V.; Porwol, L.; Dragone, V.; Cronin, L. A Self Optimizing Synthetic Organic Reactor System Using Real-Time in-Line NMR Spectroscopy. *Chem. Sci.* **2015**, *6* (2), 1258–1264; (c) Jones, C. J.; Larive, C. K. Could Smaller Really Be Better? Current and Future Trends in High-Resolution Microcoil NMR Spectroscopy. *Anal. Bioanal. Chem.* **2012**, *402* (1), 61–68.

[13] (a) Bart, J.; Kolkman, A. J.; Vries, A. J. O. De; Koch, K.; Nieuwland, P. J.; Janssen, H. J. W. G.; Van Bentum, J. P. J. M.; Ampt, K. A. M.; Rutjes, F. P. J. T.; Wijmenga, S. S.; et al. A Microfluidic High-Resolution NMR Flow Probe. *J. Am. Chem. Soc.* **2009**, *131* (14), 5014–5015; (b) Fratila, R. M.; Gomez, M. V.; Sýkora, S.; Velders, A. H. Multinuclear Nanoliter One-Dimensional and Two-Dimensional NMR Spectroscopy with a Single Non-Resonant Microcoil. *Nat. Commun.* **2014**, *5; (c)* Nordon, A.; Diez-Lazaro, A.; Wong, C. W. L.; McGill, C. a; Littlejohn, D.; Weerasinghe, M.; Mamman, D. a; Hitchman, M. L.; Wilkie, J. Consideration of Some Sampling Problems in the On-Line Analysis of Batch Processes by Low-Field NMR Spectrometry.

Analyst **2008**, *133* (3), 339–347; (d) Buser, J. Y.; McFarland, A. D. Reaction Characterization by Flow NMR: Quantitation and Monitoring of Dissolved H_2 via Flow NMR at High Pressure. *Chem. Commun.* **2014**, *50* (32), 4234–4237; (e) Gomez, M. V.; Verputten, H. H. J.; Díaz-Ortíz, A.; Moreno, A.; de la Hoz, A.; Velders, A. H. On-Line Monitoring of a Microwave-Assisted Chemical Reaction by Nanolitre NMR-Spectroscopy. *Chem. Commun.* **2010**, *46* (25), 4514; (f) Gökay, O.; Albert, K. From Single to Multiple Microcoil Flow Probe NMR and Related Capillary Techniques: A Review. *Analytical and Bioanalytical Chemistry* **2012**, *402* (2), 647-669; (g) Dalitz, F.; Cudaj, M.; Maiwald, M.; Guthausen, G. Process and Reaction Monitoring by Low-Field NMR Spectroscopy. *Prog. Nucl. Magn. Reson. Spectrosc.* **2012**, *60*, 52–70; (h) Vargas, M. A.; Cudaj, M.; Hailu, K.; Sachsenheimer, K.; Guthausen, G. Online Low-Field 1H NMR Spectroscopy: Monitoring of Emulsion Polymerization of Butyl Acrylate. *Macromolecules* **2010**, *43* (13), 5561–5568; (i) Maiwald, M.; Fischer, H. H.; Kim, Y. K.; Albert, K.; Hasse, H. Quantitative High-Resolution on-Line NMR Spectroscopy in Reaction and Process Monitoring. *J. Magn. Reson.* **2004**, *166* (2), 135–146.

[14] (a) Schoenmakers, P. Chromatography in Industry. *Annu. Rev. Anal. Chem.* **2009**, *2* (1), 333–357; (b) Brown, P. R.; Grushk, E. *Advances in Chromatography*, (2nd ed.); Miller, J. M., Ed.; **1994**, Wiley-VCH: New York.; (c) Heftmann, E. *Chromatography*, (3rd ed).; **1974**, New York.; (d) Braithwaite, A.; Smith, F. J. *Chromatographic Methods*, (4th ed.); **1985**, London; (e) Mandík, L. Applications of Gel Permeation Chromatography in the Paint Industry. *Prog. Org. Coatings* **1977**, *5* (2), 131–198.

[15] (a) Joachim Ulrich. *The Crystallization Technology Handbook*, 2nd ed.; A. Marsmann, Ed.; American Chemical Society: **2001**, New York.; (b) *Crystallization: Basic Concepts and Industrial Applications*, 1st ed.; Beckmann, W., Ed.; **2013**, Wiley-VCH.

[16] (a) Walters, I. A. S. A Convenient One-Pot Negishi Coupling of Amino-Heteroaryl Chlorides and Alkyl Bromides. *Tetrahedron Lett.* **2006**, *47* (3), 341–344; (b) Otzen, T.; Wempe, E. G.; Kunz, B.; Bartels, R.; Lehwark-Yvetot, G.; Hänsel, W.; Schaper, K. J.; Seydel, J. K. Folate-Synthesizing Enzyme System as Target for Development of Inhibitors and Inhibitor Combinations against Candida Albicans - Synthesis and Biological Activity of New 2,4-Diaminopyrimidines and 4'-Substituted 4-Aminodiphenyl Sulfones. *J. Med. Chem.* **2004**, *47* (1), 240–253.

Conclusions and future perspective

The competitive nature of the pharmaceutical industry brings the medicinal chemists to aim always to innovation and introduction of new technologies into the field, in order to speed up the drug discovery and drug development process. Molecular complexity and presence of (sp^3) motifs in targeted drug molecules that have been marketed, has shown to be crucial for the success of the molecule. But, historically the availability of methodologies for C(sp^3)-C(sp^2) and C(sp^3)-C(sp^3) cross-coupling has been limited and challenging.

The aim of this thesis was to develop new methodologies for C(sp^3)-C(sp^2) bond construction in molecules with high interest in medicinal chemistry using photocatalysis in flow. Flow chemistry enables the use of photocatalysis in drug discovery because currently is the only technology which allows its scalability and improves the reactivity pattern of the light activated reactions.

We started our investigation with purely radical reactions such as trifluoromethylation reactions. The introduction of a fluorine into the molecule can improve physicochemical properties of the molecule such as acidity and lipophilicity. The challenge present in the already reported protocols was the use of gaseous or unstable reagents such as CF_3I, CF_3SO_2Cl, ect. as CF_3 source or the use strong oxidants such as tBuOOH to form the radical. We aimed to obtain a methodology for trifluoromethylation of highly functionalized heterocycle and selected $Na_2CF_3SO_2$ (Langlois Reagent) as an air stable and readily available CF_3 source. Iridium catalyst was the radical generator. Quenching experiments demonstrated that [Ir{dF(CF_3)ppy}$_2$]-(dtbpy)]PF_6 was better quenched from $Na_SO_2CF_3$ that fac-Ir(ppy)$_3$. The protocol required only 30 minutes of residence time and was applied to a wide range of complex heterocycles with moderate to good yields.

Next, we studied a stepwise procedure to transfer in flow, batch photochemical reactions with insoluble reagents. The combination of Iridium catalysis with Nickel catalysis through decarboxylative cross-coupling offers mild reaction conditions for C(sp^3)-C(sp^2) cross-coupling. This reaction increases the prevalence of C(sp^3) in drug compounds allowing medicinal chemists to access new chemical space and a scalable protocol is key for its application drug discovery. Flow chemistry was identified as a solution for this problem. Therefore, we developed homogeneous conditions to transfer this light mediated coupling protocol to continuous flow. An organic base, such as DBU combined with [Ir(dtbbpy)(ppy)$_2$][PF_6] were crucial to obtain productivity. The residence time was reduced from 72 h in 20-40 min. This optimized protocol increases significantly the space-time yield and productivity of the reaction. The substrate scope is broad and fits perfectly the requirements pf drug discovery.

Transition metal cross-coupling reagents have emerged as a powerful synthetic tool for C-C bond construction. Since its discovery, medicinal chemists have broadly used it to build complex new drug molecules otherwise not easily achievable. Negishi reaction is one of the most tolerant functional group transition metal catalysis reaction described so far, but its use is limited due to the instability and difficulties in preparation of the organozinc reagents. With our previous experience in preparing organozinc reagents in flow, we studied the behavior of the latter compounds in photocatalytic reactions. We observed that Ni-catalyzed Negishi reactions can be accelerated under visible light irradiation. The presence of both metals Ni and Zn is crucial for the absorption into the visible region. This method provides access to new derivatives with potential value in medicinal chemistry in only 20 minutes of reaction time and 2-5 mol% of nickel loading. As the reaction is carried out in flow direct scalability is easy achieved and the overall approach is superior to the batch protocols.

With this new insight in hand for the combination of transition metal catalysis with visible light, we further busted the scope of Negishi reaction but this time using Pd catalyst. When the reaction mixture was irradiated with blue light palladium catalyst behaved similarly as the nickel catalyst increasing significantly the difference between light and no light reaction. This new photocatalytic process allows the expansion of the scope of zinc enolates in Negishi coupling with deactivated aryl halides. Kinetic, spectroscopic and NMR studies demonstrated the formation of a Pd(0)-zincate complex that allows the absorption of the visible light and accelerates the oxidative addition step of the catalytic cycle.

In the final project of this thesis we wanted to extend the applicability of the latest methodologies to drug development process. The visible light induced nickel catalyzed Negishi reaction could be scaled up with a productivity that goes from 82 to 270 g/day. We used a Corning G1 5-modules Photoreactor to perform the scale up. The reaction time was reduced to 15 minutes. Inline NMR monitoring proved to be essential in analyzing the the formation of organozinc reagent. The controlled parameters open the path for a fully automated system that brings the process to direct industrial production. A Corning Advanced G3 flow reactor with similar process conditions would increase the productivity up to 800g/ day.

These new straightforward methodologies to insert aliphatic motifs into organic molecules provide new tools for synthetic chemists. The methodologies are simple to execute and flow chemistry allows easy reproducibility and scalability. Photocatalysis offers mild reaction conditions with broad group tolerance for different heterocyclic compounds, key compounds in medicinal chemistry. Moreover, combination of photocatalysis with transition metal catalysis without the use of exogenous

photosensitizer opens new avenues within this field. These findings not only enable new reactivity patterns for low reactivity molecules of interests, but also have created new insights about metal interaction and visible light absorption. As reported in the previous chapters of this thesis, there are clear proofs that the reactivity of two transition metals such as Ni and Pd can be enhanced by the interaction with Zn under visible light irradiation. Although, future mechanistic investigations are required to elucidate and characterize all the intermediates of these bimetallic interactions, the potential of this approach is obvious. It changes the way how synthetic chemists use the transition metal catalysts and enables new chemistry patterns through light irradiation. We really believe that there are still more bimetallic interaction to be explored and discovered that may open to the synthetic chemist new doors to access challenging chemistry.

List of abbreviations

ADMET	Absorption, Distribution, Metabolism, Excretion and Toxicity in pharmacokinetics
API	Active Principle Ingredient
BEH	Ethylene Bridged Hybrid
BHT	Dibutylhydroxytoluene
Boc	*tert*-butyloxycarbonyl
Boc-Pro-OH	N-(tert-Butoxycarbonyl)-L-proline, Boc-L-proline
BPR	Back pressure regulator
$CDCl_3$	Deuterated chloroform
CF_3I	Trifluoromethyl iodide
CF_3SO_2Na	Sodium triflinate
CF_3SO_2Cl	Trifluoromethanesulfonyl chloride
CFL	Compact Fluorescent Lamp
CH_2Cl_2	Dichloromethane
CO	Carbon monoxide
CO_2	Carbon dioxide
COSY	Correlation Spetroscopy
Cs_2CO_3	Cesium carbonate
2D	Two Dimensional
DAD	Diode Array Detector
DBU	1,8-Diazabicyclo[5.4.0]undec-7-ene
DIBAL-H	Diisobutylaluminium hydride
DMA	Dimethylacetamide
DMF	Dimethylformamide
DMSO	Dimethylsulfoxide
DPEPhos	(Oxydi-2,1-phenylene)bis(diphenylphosphine)
DSC	Differential scanning calorimetry
Dtbbpy	4,4'-Di-tert-butyl-2,2'-dipyridyl
ED_{50}	Dose required to yield maximum therapeutic effect in 50% of test animals
EI/CI	Electronic impact ionization/ Chemical ionization source
ESCi	Multi-Mode Ionization Source; Electrospray ionization and chemical ionization
ESI	Electro spray ionization
ESI-TOF	Electrospray ionization time-of-flight mass spectrometry
Et_2O	Diethyl ether
Et_3N	Triethylamine
Fac-$Ir(ppy)_3$	Tris[2-phenylpyridinato-C2,N]iridium(III)
FDA	U.S. Food and Drug Administration
FEP	Fluorinated ethylene propylene
FID	Flame Ionization Detector
GC	Gas chromatography
GCMS	Gas chromatography – Mass Spectrometry
H_2O	Water
HAT	Hydrogen Atom Transfer

HEART	Heat Exchange and Advanced Reactor Technology
HSQC	Heteronuclear single-quantum correlation spectroscopy
I.D	Internal Diameter
$[Ir(dtbbpy)(ppy)_2][PF_6]$	(4,4'-Di-tert-butyl-2,2'-bipyridine)bis[(2-pyridinyl)phenyl]iridium(III) hexafluorophosphate
$[Ir\{dF(CF_3)ppy\}_2(dtbpy)]PF_6$	[4,4'-Bis(tert-butyl)-2,2'-bipyridine]bis[3,5-difluoro-2-[5-(trifluoromethyl)-2-pyridinyl]phenyl]iridium(III) hexafluorophosphate,
LC-MS	Liquid Chromatography - Mass Spetrometry
LED	Light Emitting Diode
LiCl	Lithium chloride
logP	Partition Coefficient; Log10 of the ratio of a compound's concentration in 1-octanol vs. water equilibrium
LSC	Luminescent Solar Concentrator
MeOH	Methanol
MFC	Mass Flow Controller
MFM	Mass Flow Meter
$MgSO_4$	Magnesium sulphate
MS	Mass Spectrometry
MSD	Mass Spectrometry Detector
MW	Molecular Weight
Na_2SO_4	Sodium sulphate
$NaHCO_3$	Sodium bicarbonate
$(NH_4)_2S_2O_8$	Ammonium persulphate
NH_4OH	Ammonium hydroxide
$Ni(acac)_2$	Nickel acetylacetonate
$Ni(cod)_2$	Nickel cyclooctadiene
$NiCl_2$	Nickel chloride
NMR	Nuclear Magnetic Resonance
NOESY	Nuclear Overhauser effect spectroscopy
$Pd(dba)_2$	Bis(dibenzylideneacetone)palladium
$Pd(OAc)_2$	Palladium acetate
$Pd(Ph_3)_4$	Palladium-tetrakis(triphenylphosphine)
$Pd(t\text{-}Bu_3P)_2$	Bis(tri-tert-butylphosphine) palladium
PFA	Perfluoroalkoxy alkanes
pKa	Acid dissociation constant
PTFE	Polytetrafluoroethylene
QTOF-MS	Quadrupole Time of Flight Mass Spectrometer
$[Ru(bpy)_3Cl_2]$	Tris(bipyridine)ruthenium(II) chloride
SAR	Structure Activity Relationshpi
SCE	Saturated Calomel Electrode
SET	Single Electron Transfer
S_{irrad}	Irradiated channel surface
SM	Starting Material
SQD	Single Quad Detector
t-BuOOH	*tert*- Butyl peroxide
TEMPO	2,2,6,6-Tetramethyl-1-piperidinyloxy, free radical

THF	Tetrahydrofuran
TLC	Thin Layer Chromatography
TMS	Trimethylsilyl
TMSCl	Trimethylsilyl chloride
t_R	Residence time
TU/e	Eindhoven University of Technology
UCLM	University of Castilla La Mancha
UPL	Ultraperformance liquid chromatography
$ZnBr_2$	Zinc bromide

List of publications

Peer reviewed articles

1. Abdiaj, I., Bottecchia, C., Alcazar, J. & Noël, T. Visible-Light-Induced Trifluoromethylation of Highly Functionalized Arenes and Heteroarenes in Continuous Flow. *Synth.* **49,** 4978–4985 (2017).
2. Abdiaj, I. & Alcázar, J. Improving the throughput of batch photochemical reactions using flow: Dual photoredox and nickel catalysis in flow for $C(sp^2)$-$C(sp^3)$ cross-coupling. *Bioorganic Med. Chem.* **25,** 6190–6196 (2017).
3. Abdiaj, I., Fontana, A., Gomez, M. V., De la Hoz, A., Alcazar, J. Visible Light-Induced Nickel-Catalyzed Negishi Cross-Coupling. By Exogenous-Photosensitizer-free Photocatalysis. Angew. Chem. Int. Ed. (2018). doi:10.1002/anie.201802656- *selected as back cover of the corresponding issue.*

Future publications

4. Abdiaj, I.; Huck, L.; Gonzalez, J. M. M.; Gomez, M. V., De La Hoz A.; Díaz-Ortiz, A.; Alcazar, J., Photoinduced Palladium Negishi Cross-Coupling Through Visible Light Absorption of Palladium-Organozinc complexes. **2018**, *manuscript in preparation*.
5. Abdiaj, I.; Horn, C.; Alcázar, J., Scalability of photochemical reactions: Visible light induced Nickel Negishi reaction one step closer to pharmaceutical manufacturing. **2018**, *manuscript in preparation*.

Poster Presentations

6. Rapid and practical trifluoromethylation and difluoromethylation of different scaffolds in flow *via* photoredox catalysis; 07th – 08th February 2017 **Flow Chemistry Europe 2017**; Cambridge, UK.
7. Dual Photoredox and Nickel Catalysis in flow to achieve Csp^3-Csp^2 decarboxylative cross-coupling; 25th – 28th April 2016 **4th Zing Continuous Flow Chemistry Conference**; Albufeira, Portugal.

Oral Presentations

8. Breaking the wall of photochemistry in Pharma-Industry; 25th September 2017 **1st MSCA Falling Walls Lab**; Brussels, Belgium.

9. MSCA fellow testimony; 5th December 2016 **Marie Skłodowska-Curie Actions MSCA: From Association to Participation**; Tirana, Albania.

Other pubblications:

10. Back-cover of Angewandte Chemie Volume 57; Abdiaj, I., Fontana, A., Gomez, M. V., De la Hoz, A., Alcazar, J. Visible Light-Induced Nickel-Catalyzed Negishi Cross-Coupling. By Exogenous-Photosensitizer-free Photocatalysis. Angew. Chem. Int. Ed. (**2018**); doi.org/10.1002/anie.201804573

Appendixes

Synthesis I. Abdiaj et al. Paper

Visible-Light-Induced Trifluoromethylation of Highly Functionalized Arenes and Heteroarenes in Continuous Flow

Irini Abdiaj[a]
Cecilia Bottecchia[b]
Jesus Alcazar*[a]
Timothy Noël*[b]

[a] Janssen Research & Development, Jarama 75A, 45007 Toledo, Spain
jalcazar@its.jnj.com
[b] Department of Chemical Engineering and Chemistry, Micro Flow Chemistry & Process Technology, Eindhoven University of Technology, Den Dolech 2, 5612 AZ Eindhoven, The Netherlands
t.noel@tue.nl

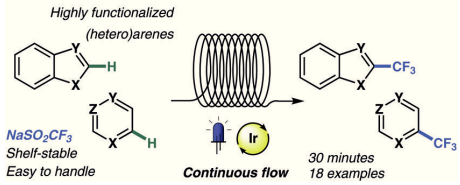

Received: 07.06.2017
Accepted after revision: 07.07.2017
Published online: 09.08.2017
DOI: 10.1055/s-0036-1588527; Art ID: ss-2017-e0382-op

Abstract We report a continuous-flow protocol for the trifluoromethylation of arenes, heteroarenes, and benzofused heterocycles. This photoredox methodology relies on the use of solid sodium trifluoromethanesulfinate (CF_3SO_2Na) as the trifluoromethylating agent and the iridium complex $[Ir\{dF(CF_3)ppy\}_2](dtbpy)]PF_6$ as the photoredox catalyst. A diverse set of highly functionalized heterocycles proved compatible with the methodology, and moderate to good yields were obtained within 30 minutes of residence time.

Key words trifluoromethylation, photoredox catalysis, continuous flow, Langlois reagent, visible light

Novel methodologies for the trifluoromethylation of arenes and heteroarenes are in high demand in the chemical and pharmaceutical industry.[1] In structure–activity relationship (SAR) studies, the introduction of fluorine atoms can greatly impact the electronic properties, acidity, and lipophilicity of drug candidates.[2] These effects are due to the high electronegativity of the fluorine atom, to its relatively small radius, and to the less polarizable nature of C–F bonds compared to C–H bonds.[1b] The replacement of methyl groups with their trifluoromethyl counterparts represents a conservative substitution in terms of steric hindrance, while constituting a valuable strategy to block potential metabolically labile sites in drug candidates, prolonging their half-life and metabolic stability.[1a]

The initially reported trifluoromethylation protocols relied on transition-metal-catalyzed cross-coupling methods, but suffered from the need for prefunctionalized substrates and stoichiometric amounts of metal salts.[3] More recently, several strategies reported in the literature demonstrated the utility of photocatalytic protocols for the trifluoromethylation of alkenes, thiols, heterocycles, and arenes.[4] The most commonly used trifluoromethyl sources include expensive Togni and Umemoto's reagents, unstable triflyl chloride (CF_3SO_2Cl), gaseous CF_3I, and readily available trifluoroacetic anhydride.[4e,5] In addition, the Langlois reagent (CF_3SO_2Na) can be regarded as an easy-to-handle, inexpensive, and solid trifluoromethylating agent, capable of generating CF_3 radicals in the presence of a strong oxidant (e.g., *t*-BuOOH).[6,7]

As part of our interest to develop efficient continuous-flow protocols as enabling tools for drug discovery, we envisioned a photocatalytic strategy for the trifluoromethylation of a variety of highly functionalized heteroarenes, which are of interest in medicinal chemistry.[4a,b,8] Such substrates are often ignored in many reports, since these compounds are known to be highly challenging and thus low yielding. In order to develop a practical and widely applicable methodology, we opted to use the stable, inexpensive, and solid Langlois reagent (CF_3SO_2Na) as trifluoromethyl source.

We commenced our investigations by performing luminescence quenching studies, which allowed us to rapidly select the optimal photocatalyst for our transformation (see Supporting Information).[9] Among the photocatalysts tested, the luminescence of both *fac*-$Ir(ppy)_3$ and $[Ir\{dF(CF_3)ppy\}_2](dtbpy)]PF_6$ was significantly quenched by increasing equivalents of CF_3SO_2Na, as depicted in Figure 1. This suggests that the excited state of both photocatalysts can be reductively quenched by the Langlois reagent, thus generating a CF_3 radical. In particular, a high luminescence quenching percentage of 58% was obtained for $[Ir\{dF(CF_3)ppy\}_2](dtbpy)]PF_6$ in the presence of 300 equivalents of the Langlois reagent, while 2500 equivalents of CF_3SO_2Na were needed to obtain a quenching percentage of only 44% in the case of *fac*-$Ir(ppy)_3$ (Figure 1). The higher quenching efficiency observed with $[Ir\{dF(CF_3)ppy\}_2](dtbpy)]PF_6$ is consistent with the higher excited state reduction potential reported for this catalyst compared to *fac*-$Ir(ppy)_3$ [1.21 V vs 0.31 V, re-

Downloaded by: Johnson & Johnson Pharmaceutical. Copyrighted material.

spectively; both values reported versus the saturated calomel electrode (SCE)].[10] As reported by Glorius and coworkers, a quenching percentage higher than 25% should be considered as significant and relevant for photocatalytic reaction purposes.[9b] Therefore, we selected [Ir{dF(CF$_3$)ppy}$_2$](dtbpy)]PF$_6$ as the photocatalyst for our further investigations.

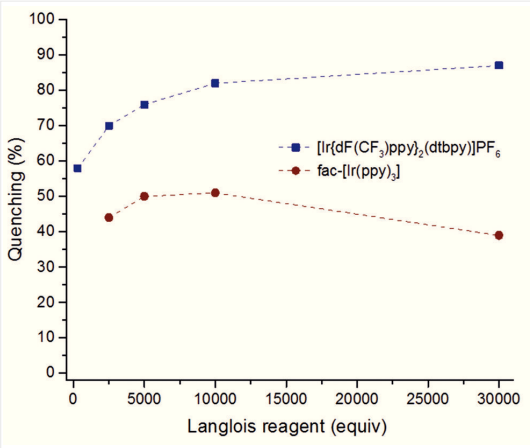

Figure 1 Luminescence quenching percentage of [Ir[dF(CF$_3$)ppy]$_2$](dtbpy)]PF$_6$ (squares) and *fac*-Ir(ppy)$_3$ (dots) in the presence of increasing amounts of Langlois reagent. *Experimental conditions*: The solutions of both photocatalysts were prepared in degassed acetonitrile with a 10 μM concentration. Solutions with increasing concentrations of quencher (CF_3SO_2Na) were prepared in degassed acetonitrile and tested. Compared to the amount of catalyst present, the concentrations and number of equivalents of CF_3SO_2Na employed were the following: 25 mM (2500 equiv), 50 mM (5000 equiv), 100 mM (10000 equiv), 300 mM (30000 equiv). For [Ir[dF(CF$_3$)ppy]$_2$](dtbpy)]PF$_6$, a concentration of 0.3 mM (300 equiv and corresponding to reaction conditions) was also tested. For more details on the procedure followed and for the calculation of the quenching percentages, see the Supporting Information.

The trifluoromethylation of caffeine was selected as the benchmark reaction for our optimization studies in flow (Table 1). The photoflow reactor consisted of a Vapourtec UV-150 photoreactor equipped with a 10 mL capillary reactor (i.d. 1.3 mm), which was subjected to 450 nm irradiation (54 blue LEDs; 24 W). DMSO was chosen as a suitable solvent, ensuring high solubility of the densely functionalized substrates and thus avoiding the occurrence of microreactor clogging. At 40 °C, unsatisfactory yields were observed in flow for the trifluoromethylated caffeine (Table 1, entries 1 and 2). We rationalized that the addition of an oxidant might assist the re-aromatization of the radical intermediate to the final product. Indeed, in the presence of $(NH_4)_2S_2O_8$ (1 equiv) as an oxidant, an improved LC-MS yield of 48% was obtained (entry 3). Next, diacetoxyiodobenzene was tested as the oxidant, but this resulted in a lower 32% isolated yield (entry 4). Increasing the amount of Langlois reagent to three equivalents further boosted the LC-MS yield to 54% (entry 5) (45% isolated yield). Notably, under the same reaction conditions, the reaction with *fac*-Ir(ppy)$_3$ gave 38% yield (entry 6), thus confirming the choice of the photocatalyst based on the luminescence quenching studies. Increasing the reaction temperature to 60 °C did not lead to a further improvement of the reaction yield (entry 7). Control experiments revealed the photocatalytic nature of our protocol, as little to no product was observed in the absence of either light or photocatalyst (entries 8 and 9). Finally, irradiation of the reaction mixture with a 365 nm UV lamp resulted in 46% of the target compound, which can be attributed to the UV-tailing absorption of the iridium photocatalyst (entry 10). Nevertheless, it should be noted that, especially for the synthesis of densely functionalized drug candidates, irradiation with low-energy blue light is preferred over higher-energy ultraviolet, to minimize the occurrence of side reactions and compound degradation.[11]

Table 1 Optimization of Reaction Conditions for the Trifluoromethylation of Caffeine in Continuous Flow[a]

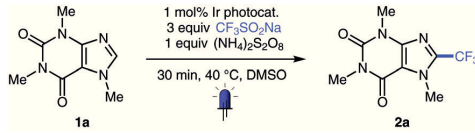

Entry	Changes from optimized conditions[a]	Yield by LC-MS (%)
1	20 min residence time, no oxidant	5
2	no oxidant, CF_3SO_2Na (1.5 equiv)	12
3	$(NH_4)_2S_2O_8$ (1 equiv), CF_3SO_2Na (1.5 equiv)	48
4	diacetoxyiodobenzene (1 equiv), CF_3SO_2Na (1.5 equiv)	32[b]
5	none	54 (45[b])
6	*fac*-Ir(ppy)$_3$ as photocatalyst	38
7	60 °C	50
8	no light	6
9	light, no [Ir[dFCF$_3$(ppy)]$_2$](dtbpy)]PF$_6$	–
10	365 nm LEDs	46

[a] Reaction conditions: caffeine (0.2 mmol), [Ir[dF(CF$_3$)ppy]$_2$](dtbpy)]PF$_6$ (1 mol%), CF_3SO_2Na (3 equiv), $(NH_4)_2S_2O_8$ (1 equiv), DMSO (2 mL; 0.1 M). Reactions performed in a commercially available Vapourtec UV-150 photoreactor, irradiation with 450 nm blue LEDs, 30 min residence time.
[b] Isolated yield.

With the optimized reaction conditions in hand, our photocatalytic trifluoromethylation strategy was evaluated on a wide range of heteroarenes and arenes, as well as benzofused heterocycles (Scheme 1). We focused our attention specifically on halogen-bearing substrates, which are of high value for drug discovery programs. In these programs, such functionalized substrates are key building blocks for

Downloaded by: Johnson & Johnson Pharmaceutical. Copyrighted material.

the very popular cross-coupling methods, which allow the construction of carbon–carbon or carbon–heteroatom bonds.[12]

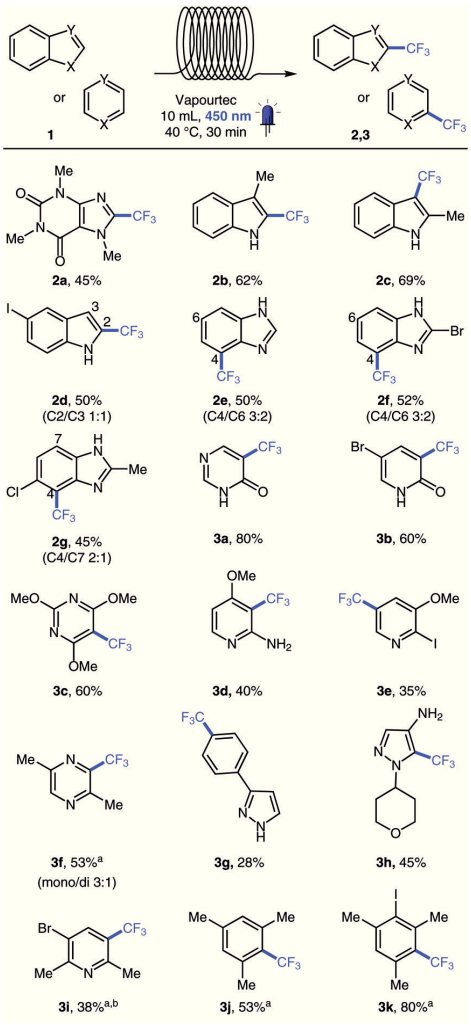

Scheme 1 Scope of the trifluoromethylation of heteroarenes, benzofused heterocycles, and arenes. *Reagents and conditions*: substrate (0.5 mmol), $[Ir[dF(CF_3)ppy]_2](dtbpy)]PF_6$ (1 mol%), CF_3SO_2Na (3 equiv), $(NH_4)_2S_2O_8$ (1 equiv), DMSO (2 mL, 0.1 M). Reactions performed in a Vapourtec UV-150 photoreactor, irradiation with 450 nm blue LEDs, 30 min residence time, isolated yields. [a] Yield determined by LC-MS. [b] Regioselectivity determined by ^1H NMR analysis of the crude reaction mixture.

3-Methyl and 2-methylindole derivatives **2b** and **2c** were obtained in satisfactory yields (62% and 69%, respectively; Scheme 1). Notably, the presence of an iodo substituent on the indole was well tolerated (**2d**; 50% isolated yield; C2/C3, 1:1). We then explored our transformation on a series of benzimidazole derivatives. Unlike indoles, benzimidazoles showed higher reactivity for the C4 and C6 positions on the aromatic ring.[13] For example, (trifluoromethyl)benzimidazole **2e** was obtained in 50% yield as a separable mixture of C4/C6 (3:2) isomers; the 2-bromo trifluoromethyl derivative **2f** was obtained in 52% yield (C4/C6, 3:2, separable mixture). Interestingly, 5-chlorobenzimidazole showed different selectivity, and was trifluoromethylated at positions C4 and C7 (**2g**, 45%; C4:C7 2:1), probably due to the electronic and steric effect of the chlorine atom. Notably, the possibility to easily separate the regioisomers obtained for compounds **2d** to **2g** renders our strategy advantageous for the simultaneous synthesis of fluorinated analogues relevant for medicinal chemistry SAR studies.

Next, we tested pyridone and pyrimidone, which are frequently used scaffolds in the synthesis of novel active pharmaceutical ingredients (APIs).[14] Trifluoromethylated pyrimidone **3a** and bromopyridone **3b** were obtained in good to excellent yields (80% and 60%, respectively; Scheme 1). We further investigated the reactivity of pyridine, obtaining trifluoromethylated pyridine derivatives **3d**, **3e**, and **3f** in modest yields (40%, 35%, and 53%, respectively). Furthermore, phenylpyrazole could be trifluoromethylated on the phenyl substituent and isolated in 28% yield (**3g**). Conversely, the tetrahydropyran-substituted 4-aminopyrazole derivative **3h** was trifluoromethylated at position C5 on the pyrazole ring and isolated in a reasonable 45% yield. 3-Bromo-2,5-dimethylpyridine was successfully trifluoromethylated, giving **3i** in 38% yield.

Finally, we explored the scope of our methodology with regard to unactivated arene substrates (Scheme 1). Trifluoromethylated mesitylene and iodomesitylene **3j** and **3k** were obtained in good to excellent yields (53% and 80%, respectively). Trifluoromethylation of unactivated arenes is a particularly challenging transformation, often requiring long reaction times (18–24 h), and has so far rarely been reported in photoredox-based protocols.[4h,15] Therefore, we were pleased to observe significant product formation in our system within only 30 minutes of reaction time. The main reason for the remarkable acceleration of the reaction rate observed in our protocol lies in the improved irradiation of the reaction mixture obtained in the microflow reactor.[11,16] Moreover, to showcase the potential of microreactors in terms of productivity, we performed a scale-up experiment on bromopyridone.[16c,17] The Vapourtec UV-150 photoreactor was continuously run for 3.5 hours without any intervention, affording 545 mg of trifluoromethylated derivative **3b** (56%).

In conclusion, we developed a continuous-flow trifluoromethylation strategy for arenes, heteroarenes, and benzofused heterocycles. Luminescence quenching studies were employed to accelerate initial protocol optimization and to select the best photocatalyst for the transformation.

Downloaded by: Johnson & Johnson Pharmaceutical. Copyrighted material.

Easy-to-handle CF_3SO_2Na (Langlois reagent) was successfully used as trifluoromethylating agent. A variety of substrates of high interest in drug discovery programs were trifluoromethylated in good to excellent yields. Moreover, bromo-, chloro-, and iodo-containing substrates were well tolerated, thus demonstrating the compatibility of our methodology with cross-coupling methods. Process intensification in a microflow reactor afforded reduced reaction times (30 minutes residence time) and high productivity. Therefore, we anticipate that our methodology will find application in the late-stage functionalization of pharmaceutical ingredients, as well as in the preparation of key intermediates in drug discovery programs.

The UPLC (Ultra Performance Liquid Chromatography) measurement was performed using an Acquity® IClass UPLC® (Waters) system comprising a sampler organizer, a binary pump with degasser, a column oven, a diode-array detector (DAD), and a column as specified below. The MS detector (Waters, SQD or QTOF) was configured with an ESCI dual ionization source (electrospray combined with atmospheric pressure chemical ionization). Nitrogen was used as the nebulizer gas. The source temperature was maintained at 140 °C. Data acquisition was performed with MassLynx-Openlynx software. For IClass-SQD, reversed phase UPLC was carried out on an RRHD Eclipse Plus-C18 (1.8 µm, 2.1 × 50 mm) from Agilent, with a flow rate of 1.0 mL/min, at 50 °C. The gradient conditions used were: 95% A (0.5 g/L ammonium acetate solution + 5% acetonitrile), 5% B (acetonitrile), to 40% A, 60% B in 1.2 min, to 5% A, 95% B in 0.6 min, held for 0.2 min. Injection volume 1.0 µL. Low-resolution ESI mass spectra (single quadrupole, SQD detector) were acquired by scanning from 100 to 1000 in 0.1 s using an interchannel delay of 0.08 s. The capillary needle voltage was 3 kV. The cone voltage was 25 V for positive ionization mode and 30 V for negative ionization mode. For IClass-QTOF, reversed phase UPLC was carried out on a BEH-C18 (1.7 µm, 2.1 × 50 mm) from Waters, with a flow rate of 1.0 mL/min, at 50 °C. The gradient conditions used are: 95% A (0.5 g/L ammonium acetate solution + 5% acetonitrile), 5% B (acetonitrile), to 40% A, 60% B in 1.2 min, to 5% A, 95% B in 0.6 min, held for 0.2 min. Injection volume 1.0 µL. High-resolution ESI mass spectra were recorded on a Xevo G2-S QTOF mass spectrometer (Waters) configured with an electrospray ionization source, maintained at 140 °C, using nitrogen as the nebulizer gas, argon as collision gas, and Lockmass device for mass calibration using leucine-enkephalin as standard substance. Spectra were acquired either in positive or in negative ionization mode, by scanning from 50 to 1200 Da in 0.1 s. In positive mode the capillary needle voltage was 0.25 kV and the cone voltage was 25 V. In negative mode the capillary needle voltage was 2.0 kV and the cone voltage was 25 V.

GC measurements were performed using a 6890 Series gas chromatograph (Agilent Technologies) system comprising a 7683 Series injector and auto sampler, J&W HP-5MS column (20 m × 0.18 mm, 0.18 µm) from Agilent Technologies coupled to a 5973N MSD mass selective detector (single quadrupole, Agilent Technologies). The MS detector was configured with an electronic impact ionization source/chemical ionization source (EI/CI). EI low-resolution mass spectra were acquired by scanning from 50 to 550 at a rate of 5.51 scans per second. The source temperature was maintained at 230 °C. Helium was used as the nebulizer gas. Data acquisition was performed with Chemstation-Open Action software. TLC was carried out on silica gel 60 F254 plates (Merck), using reagent grade solvents. Unless otherwise specified, reagents were obtained from commercial sources and used without further purification. The reactions were carried out in a Vapourtec photoreactor UV-150 fixed on an E-series Vapourtec equipment. ^{1}H NMR spectra were recorded on Bruker DPX-400 or Bruker AV-500 spectrometers with standard pulse sequences, operating at 400 MHz and 500 MHz, respectively. Chemical shifts (δ) are reported in parts per million (ppm) downfield from tetramethylsilane (TMS), which was used as an internal standard. ^{13}C NMR spectra were recorded on the same spectrometers operating at 101 MHz and 126 MHz, respectively. ^{19}F NMR spectra were recorded on the Bruker AV-500 spectrometer operating at 471 MHz. All microfluidic fittings were purchased from IDEX Health and Science. The syringes were connected to the capillary using ¼-28 flat-bottom flangeless fittings. A syringe pump (Fusion 200 Classic) equipped with 5 or 10 mL syringes was used to feed liquid reagents through a high purity perfluoroalkoxyalkane (PFA) capillary tubing (i.d. 1.3 mm) to a Tefzel® tee mixer (i.d. 1.25 mm). The melting points were measured on DSC equipment (Mettler 823 Toledo; method: 30–300 °C, 10 °C/min).

Trifluoromethylation; General Procedure:

In an oven-dried vial equipped with a magnetic stirrer and a PTFE septum, $[Ir\{dF(CF_3)ppy\}_2](dtbpy)]PF_6$ (5.6 mg, 1 mol%) was added to a mixture of the substrate (0.5 mmol, 1 equiv), CF_3SO_2Na (1.5 mmol, 3 equiv), and $(NH_4)_2S_2O_8$ (0.5 mmol, 1 equiv) in DMSO (5 mL). The solution was pumped into the Vapourtec photoreactor (fluoropolymer tube, 1.3 mm i.d., 10 mL) and the liquid flowrate was set at 0.33 mL/min (30 min residence time). The reactor was irradiated with 54 blue LEDs (450 nm, total power 24 W). The reaction mixture collected from the outlet was diluted with H_2O and extracted with Et_2O (3×). The combined organic layers were washed with brine, dried over $MgSO_4$, and concentrated in vacuo. The crude was then pre-adsorbed onto silica, dried in vacuo, and purified by flash chromatography to yield the trifluoromethylated product.

1,3,7-Trimethyl-8-(trifluoromethyl)-7*H*-purine-2,6-dione (2a)[6a]

The product was prepared according to the general procedure and was purified by flash chromatography (silica gel, heptane–EtOAc, 75:25); this afforded the desired product as a white solid.

Yield: 59 mg (45%); mp 130.9 °C.

^{1}H NMR (500 MHz, $CDCl_3$): δ = 4.14–4.19 (m, 3 H), 3.60 (s, 3 H), 3.42 (s, 3 H).

^{13}C NMR (101 MHz, $CDCl_3$): δ = 155.5, 151.3, 146.5, 138.9, 119.5, 109.6, 33.2, 29.9, 28.2.

^{19}F NMR (471 MHz, $CDCl_3$): δ = –62.37 (s).

HRMS (ESI): *m*/*z* [M + H]$^+$ calcd for $C_9H_9F_3N_4O_2$: 263.0749; found: 263.0742.

3-Methyl-2-(trifluoromethyl)-1*H*-indole (2b)[18]

The product was prepared according to the general procedure and was purified by flash chromatography (silica gel, heptane–EtOAc, 80:20); this afforded the desired product as a white amorphous solid.

Yield: 61.8 mg (62%).

^{1}H NMR (400 MHz, $CDCl_3$): δ = 8.18 (br s, 1 H), 7.64 (d, *J* = 8.1 Hz, 1 H), 7.37–7.41 (m, 1 H), 7.29–7.35 (m, 1 H), 7.15–7.23 (m, 1 H), 2.45 (q, *J* = 1.8 Hz, 3 H).

^{13}C NMR (101 MHz, $CDCl_3$): δ = 135.2, 128.1, 124.8, 124.6, 121.6, 122.2, 120.1, 114.1, 8.4.

^{19}F NMR (471 MHz, $CDCl_3$): δ = –58.65 (s).

Downloaded by: Johnson & Johnson Pharmaceutical. Copyrighted material.

HRMS (ESI): *m*/*z* [M + H]$^+$ calcd for $C_{10}H_8F_3N$: 200.0680; found: 200.0683.

2-Methyl-3-(trifluoromethyl)-1*H*-indole (2c)[4f]

The product was prepared according to the general procedure and was purified by flash chromatography (silica gel, heptane–EtOAc, 80:20); this afforded the desired product as a white solid.

Yield: 68.7 mg (69%); mp 147.5 °C.

^{1}H NMR (500 MHz, $CDCl_3$): δ = 8.18 (br s, 1 H), 7.67 (br d, *J* = 7.5 Hz, 1 H), 7.24–7.32 (m, 1 H), 7.09–7.22 (m, 2 H), 2.49 (s, 3 H).

^{13}C NMR (101 MHz, $CDCl_3$): δ = 133.9, 121.8, 121.3, 120.2, 119.1, 117.3, 113.7, 110.7, 99.3, 12.4.

^{19}F NMR (471 MHz, $CDCl_3$): δ = –54.63 (s).

HRMS (ESI): *m*/*z* [M + H]$^+$ calcd for $C_{10}H_8F_3N$: 200.0680; found: 200.0686.

5-Iodo-3-(trifluoromethyl)-1*H*-indole (2d-C3 isomer)

The product was prepared according to the general procedure and was purified by flash chromatography (silica gel, heptane–EtOAc, 90:10); this afforded the desired product as a transparent oil.

Yield: 39 mg (25%).

^{1}H NMR (400 MHz, $CDCl_3$): δ = 8.47 (br s, 1 H), 8.10 (s, 1 H), 7.56 (dd, *J* = 8.6, 1.6 Hz, 1 H), 7.51 (dd, *J* = 2.7, 1.3 Hz, 1 H), 7.23 (s, 1 H).

^{13}C NMR (101 MHz, $CDCl_3$): δ = 138.0, 134.9, 132.2, 128.4, 125.1, 125.0, 124.2, 113.5, 85.2.

^{19}F NMR (471 MHz, $CDCl_3$): δ = –57.37 (s).

HRMS (ESI): *m*/*z* [M – H]$^-$ calcd for $C_9H_5F_3IN$: 309.9345; found: 309.9368.

5-Iodo-2-(trifluoromethyl)-1*H*-indole (2d-C2 isomer)

The product was prepared according to the general procedure and was purified by flash chromatography (silica gel, heptane–EtOAc, 80:20); this afforded the desired product as a transparent oil.

Yield: 39 mg (25%).

^{1}H NMR (500 MHz, $CDCl_3$): δ = 8.52 (br s, 1 H), 8.03 (s, 1 H), 7.58 (d, *J* = 10.4 Hz, 1 H), 7.22 (d, *J* = 8.4 Hz, 1 H), 6.85 (s, 1 H).

^{13}C NMR (101 MHz, $CDCl_3$): δ = 135.2, 133.2, 130.9, 129.1, 126.7, 126.4, 121.9, 113.7, 103.4, 84.5.

^{19}F NMR (471 MHz, $CDCl_3$): δ = –60.73 (s).

HRMS (ESI): *m*/*z* [M – H]$^-$ calcd for $C_9H_5F_3IN$: 309.9345; found: 309.9368.

4-(Trifluoromethyl)benzimidazole (2e-C4 isomer)[13]

The product was prepared according to the general procedure and was purified by flash chromatography (silica gel, heptane–EtOAc, 80:20); this afforded the desired product as a white amorphous solid.

Yield: 27 mg (29%).

^{1}H NMR (500 MHz, CD_3OD): δ = 8.20 (s, 1 H), 7.63–7.88 (br s, 1 H), 7.48 (br d, *J* = 7.2 Hz, 1 H), 7.31 (t, *J* = 7.8 Hz, 1 H).

^{13}C NMR (126 MHz, CD_3OD): δ = 164.1, 143.0, 133.2, 125.2, 123.1, 100.0, 99.8.

^{19}F NMR (471 MHz, CD_3OD): δ = –64.21 (s).

HRMS (ESI): *m*/*z* [M – H]$^-$ calcd for $C_8H_5F_3N_2$: 185.0331; found: 185.0337.

6-(Trifluoromethyl)benzimidazole (2e-C6 isomer)

The product was prepared according to the general procedure and was purified by flash chromatography (silica gel, heptane–EtOAc, 80:20); this afforded the desired product as a yellow oil.

Yield: 19 mg (20%).

^{1}H NMR (400 MHz, $CDCl_3$): δ = 8.25 (s, 1 H), 7.99 (s, 1 H), 7.74 (d, *J* = 8.6 Hz, 1 H), 7.57 (d, *J* = 8.6 Hz, 1 H).

^{13}C NMR (101 MHz, $CDCl_3$): δ = 142.6, 128.7, 126.0, 125.7, 125.4, 123.3, 120.1.

^{19}F NMR (471 MHz, $CDCl_3$): δ = –62.20 (s).

HRMS (ESI): *m*/*z* [M – H]$^-$ calcd for $C_8H_5F_3N_2$: 185.0331; found: 185.0337.

2-Bromo-4-(trifluoromethyl)benzimidazole (2f-C4 isomer)

The product was prepared according to the general procedure and was purified by flash chromatography (silica gel, heptane–EtOAc, in gradient from 100/0 to 50:50); this afforded the desired product as a white solid.

Yield: 40.2 mg (30%); mp 214.7 °C.

^{1}H NMR (400 MHz, CD_3OD): δ = 7.85 (s, 1 H), 7.68 (d, *J* = 8.6 Hz, 1 H), 7.55 (d, *J* = 8.6 Hz, 1 H).

^{13}C NMR (101 MHz, CD_3OD): δ = 140.8, 131.2, 130.1, 126.2, 122.2, 120.8, 115.7, 113.7.

^{19}F NMR (471 MHz, CD_3OD): δ = –62.40 (s).

HRMS (ESI): *m*/*z* [M – H]$^-$ calcd for $C_8H_4BrF_3N_2$: 262.9436; found: 262.9434.

2-Bromo-6-(trifluoromethyl)-1*H*-benzimidazole (2f-C6 isomer)

The product was prepared according to the general procedure and was purified by flash chromatography (silica gel, heptane–EtOAc, gradient 100:0 to 50:50); this afforded the desired product as a white solid.

Yield: 26.7 mg (20%); mp 214.7 °C.

^{1}H NMR (400 MHz, $CDCl_3$): δ = 8.25 (s, 1 H), 7.99 (s, 1 H), 7.74 (d, *J* = 8.6 Hz, 1 H), 7.57 (d, *J* = 8.6 Hz, 1 H).

^{13}C NMR (101 MHz, $CDCl_3$): δ = 142.6, 128.7, 126.0, 125.7, 125.4, 123.3, 120.1.

^{19}F NMR (471 MHz, $CDCl_3$): δ = –62.20 (s).

HRMS (ESI): *m*/*z* [M – H]$^-$ calcd for $C_8H_4BrF_3N_2$: 262.9436; found: 262.9434.

5-Chloro-2-methyl-7-(trifluoromethyl)-1*H*-benzimidazole (2g-C7 isomer)

The product was prepared according to the general procedure and was purified by flash chromatography (silica gel, heptane–EtOAc, 80:20); this afforded the desired product as a white amorphous solid.

Yield: 23.8 mg (20%).

^{1}H NMR (400 MHz, $CDCl_3$): δ = 9.48 (br s, 1 H), 7.82 (br s, 1 H), 7.47 (s, 1 H), 2.68 (s, 3 H).

^{13}C NMR (101 MHz, CD_3OD): δ = 157.3, 128.1, 126.1, 123.4, 120.7, 105.2, 14.3.

^{19}F NMR (471 MHz, CD_3OD): δ = –62.87 (s).

HRMS (ESI): *m*/*z* [M – H]$^-$ calcd for $C_9H_6ClF_3N_2$: 233.0098; found: 233.0108.

Downloaded by: Johnson & Johnson Pharmaceutical. Copyrighted material.

5-Chloro-2-methyl-4-(trifluoromethyl)-1*H*-benzimidazole (2g-C4 isomer)

The product was prepared according to the general procedure and was purified by flash chromatography (silica gel, heptane–EtOAc, 80:20); this afforded the desired product as a white amorphous solid.

Yield: 35.2 mg (30%).

^{1}H NMR (500 MHz, $CDCl_3$): δ = 9.50 (br s, 1 H), 7.74 (d, *J* = 8.4 Hz, 1 H), 7.34 (d, *J* = 8.4 Hz, 1 H), 2.66 (s, 3 H).

^{13}C NMR (126 MHz, $CDCl_3$): δ = 153.3, 143.5, 131.9, 127.0, 125.1, 122.9, 15.3.

^{19}F NMR (471 MHz, $CDCl_3$): δ = –57.09 (s).

HRMS (ESI): *m*/*z* [M – H]$^-$ calcd for $C_9H_6ClF_3N_2$: 233.0098; found: 233.0108.

5-(Trifluoromethyl)pyrimidin-4(3*H*)-one (3a)

The product was prepared according to the general procedure, after which the solvent was evaporated in a Genevac turboevaporator overnight. The rests of the reaction mixture were washed with CH_2Cl_2 and the solvent was evaporated; the product was purified by flash chromatography (silica gel, MeOH–NH_4OH, 9:1/CH_2Cl_2, 0–10%); this afforded the desired product as a yellow oil.

Yield: 65.9 mg (80%).

^{1}H NMR (400 MHz, DMSO-d_6): δ = 8.44 (s, 1 H), 8.40 (s, 1 H)

^{13}C NMR (126 MHz, $CDCl_3$): δ = 154.7, 152.1, 129.7, 121.9

^{19}F NMR (471 MHz, $CDCl_3$): δ = –65.35 (s).

HRMS (ESI): *m*/*z* [M – H]$^-$ calcd for $C_5H_3F_3N_2O$: 163.0124; found: 163.0129.

5-Bromo-3-(trifluoromethyl)-1*H*-pyridin-2-one (3b)[19]

The product was prepared according to the general procedure and was purified by flash chromatography (silica gel, heptane–EtOAc, 50:50); this afforded the desired product as a yellow solid.

Yield: 72.6 mg (60%); mp 213.3 °C.

^{1}H NMR (500 MHz, $CDCl_3$): δ = 12.52–14.24 (m, 1 H), 7.92 (d, *J* = 2.0 Hz, 1 H), 7.76 (d, *J* = 2.3 Hz, 1 H).

^{13}C NMR (126 MHz, $CDCl_3$): δ = 160.0, 143.8, 139.4, 121.5, 121.9, 97.7.

^{19}F NMR (471 MHz, $CDCl_3$): δ = –65.98.

HRMS (ESI): *m*/*z* [M – H]$^-$ calcd for $C_6H_3BrF_3NO$: 239.9277; found: 239.9272.

2,4,6-Trimethoxy-5-(trifluoromethyl)pyrimidine (3c)

The product was prepared according to the general procedure and was purified by flash chromatography (silica gel, heptane–EtOAc, 80:20); this afforded the desired product as a pink solid.

Yield: 71.4 mg (60%); mp 123.6 °C.

^{1}H NMR (500 MHz, $CDCl_3$): δ = 4.03 (s, 6 H), 4.01 (s, 3 H).

^{13}C NMR (101 MHz, $CDCl_3$): δ = 169.8, 165.0, 123.5, 89.3, 55.1, 55.0.

^{19}F NMR (471 MHz, $CDCl_3$): δ = –55.97 (s).

4-Methoxy-3-(trifluoromethyl)pyridin-2-amine (3d)

The product was prepared according to the general procedure and was purified by flash chromatography (silica gel, heptane–EtOAc, 40:60); this afforded the desired product as a yellow solid.

Yield: 38.5 mg (40%); mp 213.4 °C.

^{1}H NMR (400 MHz, $CDCl_3$): δ = 8.07 (d, *J* = 5.8 Hz, 1 H), 6.31 (dd, *J* = 5.9, 0.8 Hz, 1 H), 5.00–5.20 (m, 2 H), 3.88 (s, 3 H).

^{13}C NMR (101 MHz, $CDCl_3$): δ = 166.3, 156.6, 152.8, 124.9, 98.3, 56.1.

^{19}F NMR (471 MHz, $CDCl_3$): δ = –55.42 (s).

HRMS (ESI): *m*/*z* [M – H]$^-$ calcd for $C_7H_7F_3N_2O$: 191.0437; found: 191.0423.

2-Iodo-3-methoxy-5-(trifluoromethyl)pyridine (3e)

The product was prepared according to the general procedure and was purified by flash chromatography (silica gel, pentane–Et_2O, 90:10); this afforded the desired product as a transparent oil.

Yield: 52.9 mg (35%).

^{1}H NMR (400 MHz, $CDCl_3$): δ = 7.59 (d, *J* = 8.6 Hz, 1 H), 7.05 (d, *J* = 8.6 Hz, 1 H), 3.98 (s, 3 H).

^{13}C NMR (101 MHz, $CDCl_3$): δ = 157.4, 140.4, 134.2, 121.0, 116.1, 111.7, 56.7.

^{19}F NMR (471 MHz, $CDCl_3$): δ = –66.70.

HRMS (ESI): *m*/*z* [M + H]$^+$ calcd for $C_7H_5F_3INO$: 303.9488; found: 303.9492.

2,5-Dimethyl-3-(trifluoromethyl)pyrazine (3f)

The product was prepared according to the general procedure. The organic layer was evaporated and the crude was analyzed by LC-MS and GC-MS; yield: 53%.

3-[4-(Trifluoromethyl)phenyl]-1*H*-pyrazole (3g)

The product was prepared according to the general procedure and was purified by flash chromatography (silica gel, heptane–EtOAc, 40:60); this afforded the desired product as a transparent oil.

Yield: 29.7 mg (28%).

^{1}H NMR (400 MHz, $CDCl_3$): δ = 7.90 (d, *J* = 8.1 Hz, 2 H), 7.65–7.70 (m, 1 H), 7.62–7.74 (m, 2 H), 6.70 (d, *J* = 2.3 Hz, 1 H).

^{13}C NMR (101 MHz, $CDCl_3$): δ = 136.0, 131.8, 129.5, 129.0, 128.8, 126.0, 125.7, 124.6, 122.6, 103.3.

^{19}F NMR (471 MHz, $CDCl_3$): δ = –62.58 (s).

HRMS (ESI): *m*/*z* [M – H]$^-$ calcd for $C_{10}H_7F_3N_2$: 211.0488; found: 211.0486.

1-Tetrahydropyran-4-yl-5-(trifluoromethyl)pyrazol-4-amine (3h)

The product was prepared according to the general procedure and was purified by flash chromatography (silica gel, heptane–EtOAc, 50:50); this afforded the desired product as a dark yellow oil.

Yield: 52.9 mg (45%).

^{1}H NMR (400 MHz, $CDCl_3$): δ = 7.16 (s, 1 H), 4.24 (tt, *J* = 11.5, 4.0 Hz, 1 H), 4.10 (dd, *J* = 11.8, 4.6 Hz, 2 H), 3.50 (td, *J* = 12.2, 2.0 Hz, 2 H), 3.28–3.42 (m, 2 H), 2.26 (qd, *J* = 12.4, 4.6 Hz, 2 H), 1.78–1.92 (m, 2 H).

^{13}C NMR (101 MHz, $CDCl_3$): δ = 130.8, 130.0, 121.8, 114.9, 67.1, 57.0, 32.9.

^{19}F NMR (471 MHz, $CDCl_3$): δ = –56.70 (s).

HRMS (ESI): *m*/*z* [M – H]$^-$ calcd for $C_9H_{12}F_3N_3O$: 234.2859; found: 234.2855.

Downloaded by: Johnson & Johnson Pharmaceutical. Copyrighted material.

3-Bromo-2,6-dimethyl-5-(trifluoromethyl)pyridine (3i)

The product was prepared according to the general procedure. The organic layer was evaporated and the crude was analyzed by LC-MS; yield: 38%.

^{1}H NMR (400 MHz, $CDCl_3$): δ = 7.97 (s, 1 H), 2.68 (s, 3 H), 2.62–2.64 (m, 3 H).

^{19}F NMR (471 MHz, $CDCl_3$): δ = –62.23.

1,3,5-Trimethyl-2-(trifluoromethyl)benzene (3j)

The product was prepared according to the general procedure. The organic layer was evaporated and the crude was analyzed by LC-MS; yield: 53%.

2-Iodo-1,3,5-trimethyl-4-(trifluoromethyl)benzene (3k)

The product was prepared according to the general procedure. The organic layer was evaporated and the crude was analyzed by LC-MS; yield: 80%.

Funding Information

The authors acknowledge the European Union for a Marie Curie ITN Grant (Photo4Future, Grant No. 641861). Further financial support for this work was provided by a VIDI grant (T.N., SensPhotoFlow, No. 14150).

Acknowledgment

The authors would like to thank Dr. José Manuel Alonso for the support with NMR analysis.

Supporting Information

Supporting information for this article is available online at https://doi.org/10.1055/s-0036-1588527.

References

(1) (a) Zhou, Y.; Wang, J.; Gu, Z.; Wang, S.; Zhu, W.; Aceña, J. L.; Soloshonok, V. A.; Izawa, K.; Liu, H. *Chem. Rev.* **2016**, *116*, 422. (b) Purser, S.; Moore, P. R.; Swallow, S.; Gouverneur, V. *Chem. Soc. Rev.* **2008**, *37*, 320. (c) Müller, K.; Faeh, C.; Diederich, F. *Science* **2007**, *317*, 1881.

(2) (a) Ilardi, E. A.; Vitaku, E.; Njardarson, J. T. *J. Med. Chem.* **2014**, *57*, 2832. (b) Huchet, Q. A.; Kuhn, B.; Wagner, B.; Kratochwil, N. A.; Fischer, H.; Kansy, M.; Zimmerli, D.; Carreira, E. M.; Müller, K. *J. Med. Chem.* **2015**, *58*, 9041.

(3) (a) Barata-Vallejo, S.; Postigo, A. *Coord. Chem. Rev.* **2013**, *257*, 3051. (b) Tomashenko, O. A.; Grushin, V. V. *Chem. Rev.* **2011**, *111*, 4475. (c) Huiban, M.; Tredwell, M.; Mizuta, S.; Wan, Z.; Zhang, X.; Collier, T. L.; Gouverneur, V.; Passchier, J. *Nat. Chem.* **2013**, *5*, 941.

(4) (a) Straathof, N. J. W.; Cramer, S. E.; Hessel, V.; Noël, T. *Angew. Chem. Int. Ed.* **2016**, *55*, 15549. (b) Bottecchia, C.; Wei, X. J.; Kuijpers, K. P.; Hessel, V.; Noel, T. *J. Org. Chem.* **2016**, *81*, 7301. (c) Lefebvre, Q.; Hoffmann, N.; Rueping, M. *Chem. Commun.* **2016**, *52*, 2493. (d) Chatterjee, T.; Iqbal, N.; You, Y.; Cho, E. J. *Acc. Chem. Res.* **2016**, *49*, 2284. (e) Beatty, J. W.; Douglas, J. J.; Cole, K. P.; Stephenson, C. R. J. *Nat. Commun.* **2015**, 6. (f) Straathof, N. J. W.; Gemoets, H. P. L.; Wang, X.; Schouten, J. C.; Hessel, V.; Noël, T. *ChemSusChem* **2014**, *7*, 1612. (g) Prier, C. K.; Rankic, D. A.; MacMillan, D. W. C. *Chem. Rev.* **2013**, *113*, 5322. (h) Nagib, D. A.; MacMillan, D. W. C. *Nature* **2011**, *480*, 224. (i) Iqbal, N.; Choi, S.; Kim, E.; Cho, E. J. *J. Org. Chem.* **2012**, *77*, 11383. (j) Cui, L.; Matusaki, Y.; Tada, N.; Miura, T.; Uno, B.; Itoh, A. *Adv. Synth. Catal.* **2013**, *355*, 2203.

(5) (a) Pan, X.; Xia, H.; Wu, J. *Org. Chem. Front.* **2016**, *3*, 1163. (b) Barata-Vallejo, S.; Lantaño, B.; Postigo, A. *Chem. Eur. J.* **2014**, *20*, 16806.

(6) (a) Ji, Y.; Brueckl, T.; Baxter, R. D.; Fujiwara, Y.; Seiple, I. B.; Su, S.; Blackmond, D. G.; Baran, P. S. *Proc. Natl. Acad. Sci. U.S.A.* **2011**, *108*, 14411. (b) Wang, D.; Deng, G.-J.; Chen, S.; Gong, H. *Green Chem.* **2016**, *18*, 5967. (c) Langlois, B. R.; Billard, T.; Mulatier, J.-C.; Yezeguelian, C. *J. Fluorine Chem.* **2007**, *128*, 851. (d) Langlois, B. R.; Laurent, E.; Roidot, N. *Tetrahedron Lett.* **1991**, *32*, 7525. (e) Tordeux, M.; Langlois, B.; Wakselman, C. *J. Org. Chem.* **1989**, *54*, 2452.

(7) (a) Lefebvre, Q. *Synlett* **2016**, *28*, 19. (b) Zhang, C. *Adv. Synth. Catal.* **2014**, *356*, 2895.

(8) (a) Huck, L.; Berton, M.; de la Hoz, A.; Diaz-Ortiz, A.; Alcazar, J. *Green Chem.* **2017**, *19*, 1420. (b) Wirth, T. *ChemSusChem* **2012**, *5*, 215. (c) Galloway, W. R. J. D.; Isidro-Llobet, A.; Spring, D. R. *Nat. Commun.* **2010**, *1*, 1.

(9) (a) Teders, M.; Gómez-Suárez, A.; Pitzer, L.; Hopkinson, M. N.; Glorius, F. *Angew. Chem. Int. Ed.* **2017**, *56*, 902. (b) Hopkinson, M. N.; Gómez-Suárez, A.; Teders, M.; Sahoo, B.; Glorius, F. *Angew. Chem. Int. Ed.* **2016**, *55*, 4361. (c) Demissie, T. B.; Hansen, J. H. *Dalton Trans.* **2016**, *45*, 10878.

(10) Teegardin, K.; Day, J. I.; Chan, J.; Weaver, J. *Org. Process Res. Dev.* **2016**, *20*, 1156.

(11) Cambié, D.; Bottecchia, C.; Straathof, N. J. W.; Hessel, V.; Noël, T. *Chem. Rev.* **2016**, *116*, 10276.

(12) (a) Brown, D. G.; Boström, J. *J. Med. Chem.* **2016**, *59*, 4443. (b) Alonso, N.; Miller, L. Z.; de M. Muñoz, J.; Alcázar, J.; McQuade, D. T. *Adv. Synth. Catal.* **2014**, *356*, 3737. (c) Egle, B.; Muñoz, J.; Alonso, N.; De Borggraeve, W.; de la Hoz, A.; Díaz-Ortiz, A.; Alcázar, J. *J. Flow Chem.* **2014**, *4*, 22. (d) de M. Muñoz, J.; Alcázar, J.; de la Hoz, A.; Díaz-Ortiz, A. *Adv. Synth. Catal.* **2012**, *354*, 3456. (e) Noël, T.; Musacchio, A. J. *Org. Lett.* **2011**, *13*, 5180. (f) Cooper, T. W. J.; Campbell, I. B.; Macdonald, S. J. F. *Angew. Chem. Int. Ed.* **2010**, *49*, 8082.

(13) Gao, G.-L.; Yang, C.; Xia, W. *Chem. Commun.* **2017**, *53*, 1041.

(14) (a) Linghu, X.; Wong, N.; Iding, H.; Jost, V.; Zhang, H.; Koenig, S. G.; Sowell, C. G.; Gosselin, F. *Org. Process Res. Dev.* **2017**, *21*, 387. (b) Peng, A.; Jiang, J.; Hu, P.; Luo, Y. *J. Chromatogr., B* **2010**, *878*, 2442.

(15) (a) Chang, B.; Shao, H.; Yan, P.; Qiu, W.; Weng, Z.; Yuan, R. *ACS Sustainable Chem. Eng.* **2017**, *5*, 334. (b) Li, L.; Mu, X.; Liu, W.; Wang, Y.; Mi, Z.; Li, C.-J. *J. Am. Chem. Soc.* **2016**, *138*, 5809.

(16) (a) Noël, T. *Photochemical Processes in Continuous-Flow Reactors*; World Scientific: New Jersey, **2017**. (b) Tucker, J. W.; Zhang, Y.; Jamison, T. F.; Stephenson, C. R. J. *Angew. Chem. Int. Ed.* **2012**, *51*, 4144. (c) Elliott, L. D.; Knowles, J. P.; Koovits, P. J.; Maskill, K. G.; Ralph, M. J.; Lejeune, G.; Edwards, L. J.; Robinson, R. I.; Clemens, I. R.; Cox, B.; Pascoe, D. D.; Koch, G.; Eberle, M.; Berry, M. B.; Booker-Milburn, K. I. *Chem. Eur. J.* **2014**, *20*, 15226. (d) Knowles, J. P.; Elliott, L. D.; Booker-Milburn, K. I. *Beilstein J. Org. Chem.* **2012**, *8*, 2025.

Downloaded by: Johnson & Johnson Pharmaceutical. Copyrighted material.

(17) (a) Elliott, L. D.; Berry, M.; Harji, B.; Klauber, D.; Leonard, J.; Booker-Milburn, K. I. *Org. Process Res. Dev.* **2016**, *20*, 1806. (b) Abdiaj, I.; Alcázar, J. *Bioorg. Med. Chem.* **2016**, in press; DOI: 10.1016/j.bmc.2016.12.041. (c) Su, Y.; Kuijpers, K.; Hessel, V.; Noël, T. *React. Chem. Eng.* **2016**, *1*, 73.

(18) Pitre, S. P.; McTiernan, C. D.; Ismaili, H.; Scaiano, J. C. *ACS Catal.* **2014**, *4*, 2530.

(19) Gleave, R. J.; Beswick, P. J.; Brown, A. J.; Giblin, G. M. P.; Haslam, C. P.; Livermore, D.; Moses, A.; Nicholson, N. H.; Page, L. W.; Slingsby, B.; Swarbrick, M. E. *Bioorg. Med. Chem.* **2009**, *19*, 6578.

Downloaded by: Johnson & Johnson Pharmaceutical. Copyrighted material.

Bioorganic & Medicinal Chemistry 25 (2017) 6190–6196

Contents lists available at ScienceDirect

Bioorganic & Medicinal Chemistry

journal homepage: www.elsevier.com/locate/bmc

Improving the throughput of batch photochemical reactions using flow: Dual photoredox and nickel catalysis in flow for C(sp^2)—C(sp^3) cross-coupling

Irini Abdiaj, Jesús Alcázar *

Janssen Research and Development, Janssen-Cilag, S.A., C/Jarama 75, 45007 Toledo, Spain

ARTICLE INFO

Article history:
Received 16 November 2016
Revised 16 December 2016
Accepted 23 December 2016
Available online 27 December 2016

Keywords:
Photoredox
Dual catalysis
Flow chemistry
C(sp^2)—C(sp^3) cross-coupling
Medicinal chemistry

ABSTRACT

We report herein the transfer of dual photoredox and nickel catalysis for C(sp^2)—C(sp^3) cross coupling form batch to flow. This new procedure clearly improves the scalability of the previous batch reaction by the reactor's size and operating time reduction, and allows the preparation of interesting compounds for drug discovery in multigram amounts.

© 2017 The Authors. Published by Elsevier Ltd. This is an open access article under the CC BY-NC-ND license (http://creativecommons.org/licenses/by-nc-nd/4.0/).

1. Introduction

Light has long been recognized as a valuable tool for performing efficient organic reactions. It allows access to complex molecules using photon as a traceless reagent that adds energy to a chemical system without generating waste in the process.[1] In recent years, visible light photoredox catalysis has emerged as a powerful strategy for organic synthesis, since organic or organometallic photoredox catalyst are able to transfer light into chemical energy.[2]

However, the scalability of photochemical processes is limited by the attenuation effect of photon transport (Bourguer-Lambert-Beer law). To overcome this issue, photoredox catalysis has been combined with continuous flow technology, in order to ensure a uniform irradiation of the narrow channels, where the reaction mixture is circulating within.[3] Additionally, the use of continuous flow reactors offers other advantages, such as very efficient heat transfer, good control of reaction temperature and enhanced mass transfer,[4] making procedures more reproducible and scalable. Furthermore, flow chemistry has been identified as a very interesting sustainable alternative in chemical research and production.[5]

From a medicinal chemistry point of view, a very interesting reaction is the synergistic combination of photoredox and nickel catalysis to achieve C(sp^2)—C(sp^3) cross-coupling, not straightaway possible by using either catalysis alone.[6] This approach will increase the prevalence of sp^3 carbons in drug discovery compounds allowing medicinal chemists to access new chemical space with improved phisicochemical properties.[7] Recently a first example of dual catalysis in flow has been reported by Ley and coworkers.[8] They reported a new activation mode for boronic esters to use these highly soluble reagents in flow avoiding the poor soluble trifluoroborate salts used in the corresponding batch protocols.[6d,6e] Following this approach a series of benzyboronates were coupled with several bromoarenes.

Considering the interest of cyclic amines in medicinal chemistry[9] and the advantages of flow photochemistry, we consider that the transfer of the decarboxylative coupling of amino acids with aryl halides described by MacMillan and coworkers in batch[10] to flow would help to achieve a fast and scalable C(sp^2)—C(sp^3) coupling process and make this procedure more suitable for drug discovery as productivity per time unit would be clearly increased (Fig. 1).

2. Results and discussion

2.1. Exploration of suitable reagents for flow

Recently Stephenson and co-workers have reported the translation of a photoredox trifluomethylation from batch to flow in order to get kilogram amounts of the desired product.[11] In this example,

* Corresponding author.
E-mail address: jalcazar@its.jnj.com (J. Alcázar).

http://dx.doi.org/10.1016/j.bmc.2016.12.041
0968-0896/© 2017 The Authors. Published by Elsevier Ltd.
This is an open access article under the CC BY-NC-ND license (http://creativecommons.org/licenses/by-nc-nd/4.0/).

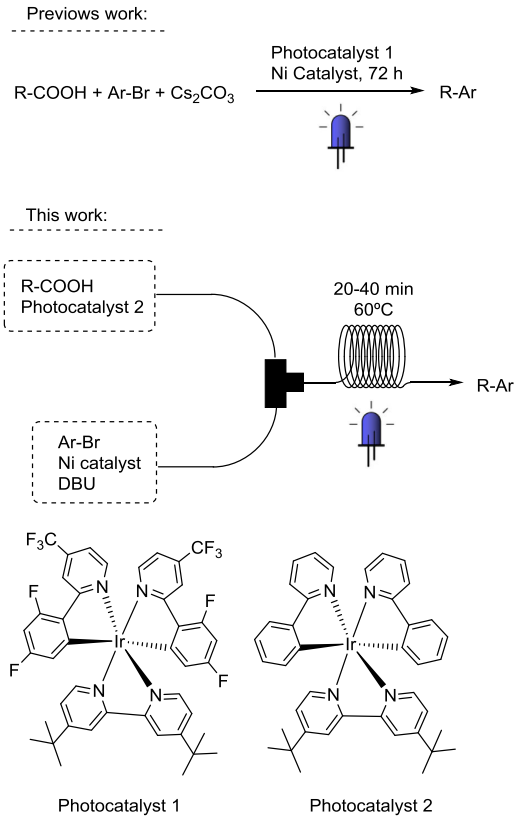

Fig. 1. Continuous flow process to obtain $C(sp)^3$—$C(sp)^2$ cross-coupling.

direct transfer to flow was possible as all components are soluble in the reaction solvent used. However, this is not suitable with McMillan's dual catalysis, as the base used was not soluble in the solvent reported. For this reason, the first challenge to develop a flow protocol was to identify a suitable combination base-solvent that would avoid a potential blockage of the reactor (Table 1). In order to speed up the finding of such combination, a parallel batch screening was performed under non optimal conditions using a handmade photoreactor irradiated with a CFL bulb (9 W). In this way differences of performance among all possible combinations would be more sensitive and would help the identification of the most promising one.[12] Control reactions using the base and solvent described in batch were also included in the set to provide appropriate comparison (Table 1, entries 1 and 2).

To begin with, a set of different organic bases of was tried in DMF (Table 1, entries 3–9). Among all of them, 1,5-diazabiciclo [5.4.0]undec-5-ene (DBU) was found as the most promising one (Table 1, entry 4). Conversion to product with this base was comparable to the one obtained with cesium carbonate, but a different photocatalyst (photocatalyst 2) was required. Once the appropriate base and photocatalyst were identified, solvent screening was performed (Table 1, entries 10–12). THF, acetone, toluene and ethyl acetate were found to provide good conversion to product (Table 1, entries 11, 14, 15 and 17), but precipitation of insoluble material was observed, most probably the corresponding HBr salt of the base, preventing their potential use in flow, as blockage of the reactor may take place. DMA provided the best conversion keeping all the material in solution (Table 1, entry 12).

In order to prove that the reaction required the combination of both catalytic cycles, several blind experiments were performed (Table 2, entries 7–10). Running the reaction in the dark provided just low conversion (entry 7). Similar outcome was achieved when the photocatalyst was removed (entry 8). In both examples, a dirty reaction crude was observed. Only when the reaction was run in the absence of nickel catalyst, no conversion of starting materials were observed (entry 9). For this reason, it was decided to run the reaction in two separated lines, so that no transformations would take place in the initial solution before entering the photochemical reactor. Finally, the presence of di*tert*buthylbipyridine (dtbbpy) ligand was also key for the reaction outcome (entry 10).

2.2. Optimization of reaction conditions in flow

The parallel batch screening provided the best combination of base (DBU), solvent (DMA) and photocatalyst (2) to be transferred in flow. The following step was to optimize reaction conditions in flow for the present reaction (Table 2). To perform these studies, the commercially available UV-150 photoreactor from Vapourtec was used.[13] This system is ideally suited for exploratory studies as it can be operated at various temperatures via active heating or cooling.

As the reaction in batch proceeded in 72 h, the initial attempt was to perform the reaction at 40 °C with a relatively long residence time for a flow reactor (Table 2, entry 1). The conversion achieved was a promising starting point as it was higher than the one observed in batch at the same temperature but after overnight reaction (Table 1, entry 12). Then, the temperature was increased to 60 °C to see its influence in the conversion. Full conversion was observed but a dirty crude reaction mixture was found and only 40% of isolated product was obtained (Table 2, entry 2). To control overreaction products, different reaction times and temperatures were attempted to improve the outcome. The best isolated yield was achieved at 60 °C and 20 min residence time (Table 2, entry 4).

2.3. Exploration of reaction scope

Substrate scope was then explored, focusing on aromatic substituents and heterocycles of potential interest for drug discovery (Table 3). The results shown in this table were the most optimal found after testing different conditions. In this way, it was observed that most of the compounds tried required 30 min to get products in good yields. Using these slightly modified conditions, a wide range of functionalized aryl bromides, with functional groups as diverse as ketones, esters, nitriles, trifluoromethyl groups, halides, and monocyclic or bicyclic heterocycles provided the desired products in good yields, demonstrating the value of the protocol for medicinal chemistry. It is important to highlight that π-exceeding heterocycles **2e** and **2f** also provided the target compounds **3ae** and **3af**, although in the latter example, 40 min of reaction time was required. For compounds **3ac** and **3ai**, best results were found using lower temperature.

Cyclic amines are important for medicinal chemistry and modulating their properties is a key element to finding good clinical candidates.[9] In this way, cyclic aminoacid **1b** was selected to check how substitution may affect the reaction. Both conformers were isolated from the reaction, being the compound **3bb** (trans) the mayor isomer. This result is interesting as stereochemistry can be modulated by such substitution. Not only aminoacids, but also oxycarboxylic acid **1c** worked as coupling partners, producing alfa arylated ether **3cb** in a single step.

Table 1
Screening suitable conditions in batch.

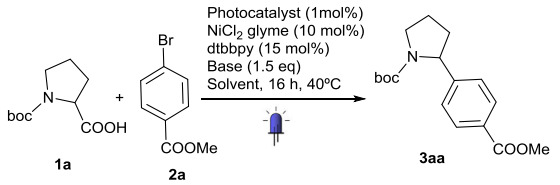

Entry	Base	Solvent	Photocatalyst	Conv.[a] (%)
1	Cs_2CO_3	DMF	1	8
2	Cs_2CO_3	DMF	2	4
3	DBU	DMF	1	Traces
4	DBU	DMF	2	6
5	DMAP	DMF	2	0
6	MTBD	DMF	2	3
7	TEA	DMF	2	0
8	Lutidine	DMF	2	Traces
9	BTPP	DMF	2	0
10	DBU	DMSO	2	Traces
11	DBU	THF	2	24[b]
12	DBU	DMA	2	12
13	DBU	ACN	2	2[b]
14	DBU	Acetone	2	12[b]
15	DBU	Toluene	2	13[b]
16	DBU	Isopropanol	2	0
17	DBU	EtOAc	2	22[b]
18	DBU	$(MeO)_2CO$	2	0

[a] % of product measured by LC-MS.
[b] Precipitation of side products.

Table 2
Optimization of the conditions in flow.

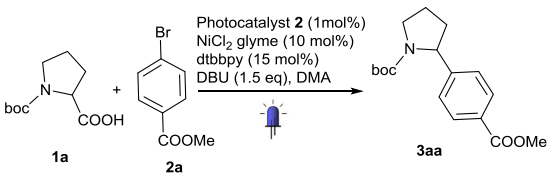

Entry	Temperature (°C)	Time (min)	Conversion[a] (%)
1	40	33	40
2	60	33	100 (40)[b]
3	60	10	42
4	60	20	100 (74)[b]
5	75	10	47
6	80	5	40
7	60	20	2[c]
8	60	20	4[d]
9	60	20	0[e]
10	60	20	4[f]

[a] Conversion of **2a** by LC-MS.
[b] Isolated yield.
[c] Test reaction without light irradiation.
[d] Test reaction without photocatalyst.
[e] Test reaction without nickel catalyst.
[f] Test reaction without 4,4′-di-*tert*-butyl-2,2′-dipyridyl (dtbbpy).

2.4. Scale up and comparison with batch

With all this information in our hands, the next step was scaling up the reaction to investigate if the flow approach adds value over the batch one (Table 4). Thus, the flow protocol was allowed to run for 1 h in continuously in the machine and the outcome compared with the best result reported in batch[10] Even though the isolated yield in flow was confirmed and still lower than the one described in batch, 644 mg of **3aa** as a white solid were isolated, enough material to support drug-discovery processes. The lower yield was balanced by the reduced time and increased concentration. These combined effects provided a 430 times better space-time yield[4d,14] than the reported batch method, clearly demonstrating the improved efficacy of the flow procedure.

3. Conclusion

Herein, a stepwise procedure to translate photochemical batch reactions with insoluble reagents in flow is described. This has allowed the development of a more sustainable flow protocol for challenging C(sp^2)—C(sp^3) cross-coupling by dual photoredox and nickel catalysis. The reaction has a broad scope that perfectly fits the requirements for drug discovery in terms of functionalized aryl groups and heterocycles as well as cyclic amines. The huge time reduction achieved in flow, from 3 days to 20–30 min allows its scalability to reach amounts of compound that could be difficult to achieve in batch and improve drastically the space-time yield, demonstrating at the same time its sustainability. Further applications of this protocol in drug discovery programs will be presented elsewhere.

Table 3
Scope of dual catalysis reaction in flow.

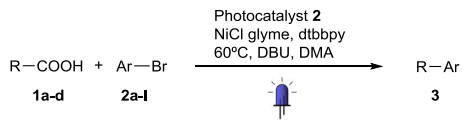

1	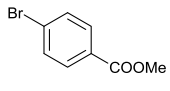	**2a**	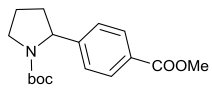	**3aa** (74%)[a]	
2	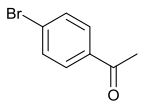	**2b**	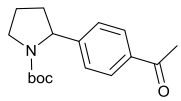	**3ab** (74%)	
3	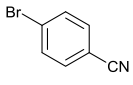	**2c**	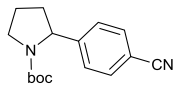	**3ac** (45%)[b]	
4	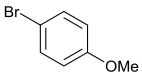	**2d**	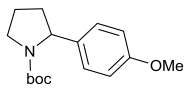	**3ad** (44%)	
5	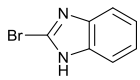	**2e**	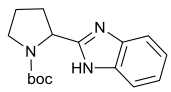	**3ae** (56%)[e]	
6	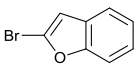	**2f**	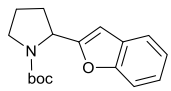	**3af** (37%)	
7	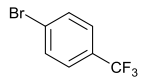	**2g**	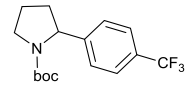	**3ag** (32%)	
8	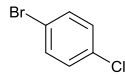	**2h**	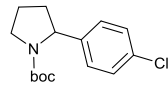	**3ah** (43%)	
9	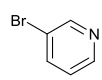	**2i**	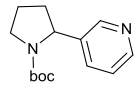	**3ai** (45%)[c]	
10		**2j**	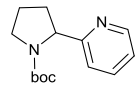	**3aj** (42%)	
11	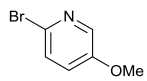	**2k**	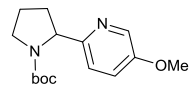	**3ak** (38%)	
12		**2l**	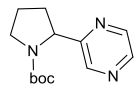	**3al** (30%)	
13	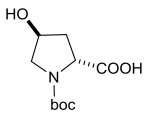	**1b**	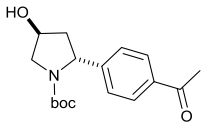	**3bb trans (30%)**[d]	
			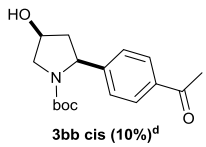	**3bb cis (10%)**[d]	
14	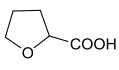	**1c**	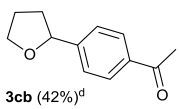	**3cb** (42%)[d]	
15	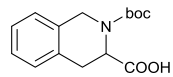	**1d**	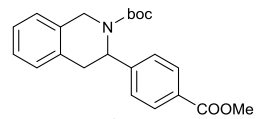	**3db** (71%)[d]	
16	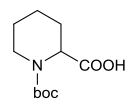	**1e**	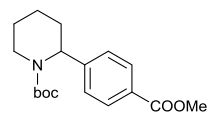	**3ea** (37%)[d]	

General conditions: Ar—X (0.2 mmol), R—COOH (1.5 eq.), DBU (1.5 eq.), Ir(ppy)2(dtbbpy)$^{3+}$ (1 mol%), $NiCl_2$ (10 mol%), dtbbpy (15 mol%), t_R = 30 min, T = 60 °C LED = 450 nm.
[a] t_R = 20 min, T = 60 °C.
[b] t_R = 20 min, T = 40 °C.
[c] t_R = 30 min, T = 40 °C.
[d] R—COOH (3 eq.), DBU (3 eq.).
[e] t_R = 40 min, T = 60 °C.

4. Experimental section

4.1. General information

GC measurements were performed using a 6890 Series Gas Chromatograph (Agilent Technologies) system comprising a 7683 Series injector and autosampler, J&W HP-5MS column (20 m × 0.18 mm, 0.18 μm) from Agilent Technologies coupled to a 5973N MSD Mass Selective Detector (single quadrupole, Agilent Technologies). The MS detector was configured with an electronic impact ionization source/chemical ionization source (EI/CI). EI low-resolution mass spectra were acquired by scanning from 50 to 550 at a rate of 5.5 scan/s. The source temperature was maintained at 230 °C. Helium was used as the nebulizer gas. Data acquisition was performed with Chemstation-Open Action software. Thin layer chromatography (TLC) was carried out on silica gel 60 F254 plates (Merck) using reagent grade solvents. Unless otherwise specified, reagents were obtained from commercial sources and used without further purification. The reactions were carried out in a Vapourtec photoreactor UV-150 fixed on a E-series Vapourtec equipment. ^{1}H NMR spectra were recorded on Bruker DPX-400 or Bruker AV-500 spectrometers with standard pulse sequences, operating at 400 MHz and 500 MHz respectively. Chemical shifts (δ) are reported in parts per million (ppm) downfield from tetramethylsilane (TMS), which was used as an internal standard.

4.2. Dual photoredox-nickel catalysis for decarboxylative arylation. General procedure A

Two different solutions for feeds A and B were separately prepared in 2 mL vial equipped with a Teflon septum and magnetic stir bar. Feed A: [Ir(dtbbpy)(ppy)$_2$][PF_6] (2.00 μmol, 0.01 equiv) and Boc-Pro-OH (0.3 mmol, 1.5 equiv) in 1 mL of DMA; Feed B: $NiCl_2$ glyme (0.02 mmol, 0.1 equiv), 4,4′-di-*tert*-butyl-2,2′-bipyridyl (0.03 mmol, 0.15 equiv), the corresponding aromatic halides (0.20 mmol, 1.0 equiv), DBU (0.3 mmol, 1.5 equiv) in 1 mL of DMA. The two solutions were degassed by bubbling nitrogen stream for 20 min. Feeds A and B were injected simultaneously into the photoreactor, mixed in a T-mixer, and passed through a 10 mL residence time coil (0.8 mm inner diameter, 4 m length, fluoropolymer tube) irradiated with blue LED 450 nm and heated at the indicated temperature. The reaction mixture collected from the output was diluted with saturated aqueous $NaHCO_3$ solution, extracted with Et_2O (3 × 10 mL). The combined organic extracts were washed with water and brine, dried over $MgSO_4$ and concentrated in vacuo. Purification of the crude product by flash chromatography on silica gel using as eluent heptane/ethyl acetate afforded the desired product.

4.3. Dual photoredox-nickel catalysis for decarboxylative arylation. General procedure B

Two different solutions for feeds A and B were separately prepared in 2 mL vial equipped with a Teflon septum and magnetic stir bar. Feed A: [Ir(dtbbpy)(ppy)$_2$][PF_6] (2.00 μmol, 0.01 equiv) and the correspondent carboxylic acid (0.6 mmol, 3 equiv) in 1 mL of DMA; Feed B: $NiCl_2$ glyme (0.02 mmol, 0.1 equiv), 4,4′-di-*tert*-butyl-2,2′-bipyridyl (0.03 mmol, 0.15 equiv), the corresponding aromatic halides (0.20 mmol, 1.0 equiv), DBU (0.6 mmol, 3 equiv) in 1 mL of DMA. The two solutions were degassed by bubbling nitrogen stream for 20 min. Feeds A and B were injected simultaneously into the photoreactor, mixed in a T-mixer, and passed through a 10 mL residence time coil (0.8 mm inner diameter, 4 m length, fluoropolymer tube) irradiated with blue LED 450 nm and heated at the indicated temperature. The reaction mixture collected from the output was diluted with saturated aqueous $NaHCO_3$ solution, extracted with Et_2O (3 × 10 mL). The combined organic extracts were washed with water and brine,

Table 4
Comparison batch-flow.

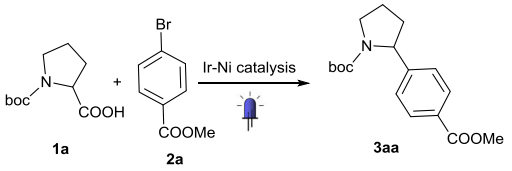

1a 2a 3aa

	Flow	Batch[a]
Yield	74%	90%
Reaction time	20 min	72 h
Product throughput	644 mg/h	109 mg/72 h
[**2a**]	0.1 M	0.02 M
Space-time yield[b]	64.4 mg/h mL	0.15 mg/h mL

[a] Results from Ref. 10.
[b] Calculated according to Refs. 4d,14.

dried over $MgSO_4$ and concentrated in vacuo. Purification of the crude product by flash chromatography on silica gel using as eluent heptane/ethyl acetate afforded the desired product.

*4.3.1. tert-Butyl 2-(4-methoxycarbonylphenyl)pyrrolidine-1-carboxylate (**3aa**)*

According to general procedure A r_T = 20 min, T = 60 °C, 45 mg (74%); ^{1}H NMR (500 MHz, $CDCl_3$) δ ppm 7.90 (d, *J* = 10.0 Hz, 2 H), 7.29 (d, *J* = 5.0 Hz, 2 H), 4.67 and 5.06 (2brs, 1 H rotamer) 3.91 (s, 3 H), 3.51–3.70 (m, 2 H), 2.37–2.34 (m, 1 H), 1.77–1.96 (m, 3 H), 1.46 (s, 3 H), 1.17 (br s, 6 H); ^{13}C NMR (126 MHz, $CDCl_3$) rotameric mixture, resonances for minor rotamer are enclosed in parenthesis (): δ ppm 166.9, 154.3, 150.6 (149.5), (129.7) 129.6, 128.5, 125.4, 79.4, 61.2 (60.6),51.9, (47.4) 47.1, 35.91 (34.7), (28.4) 28.1, (23.6) 23.2; MS (ESI) *m*/*z* calcd. for $C_{17}H_{23}NO_4$ 305.1627, found 328.1531 [(M+Na)$^+$].

*4.3.2. tert-Butyl 2-(4-acetylphenyl)pyrrolidine-1-carboxylate (**3ab**)*

According to general procedure A r_T = 30 min, T = 60 °C, 43 mg (74%); ^{1}H NMR (400 MHz, $CDCl_3$): δ ppm 7.91 (br d, *J* = 8.09 Hz, 2 H), 7.21 (d, *J* = 8.09 Hz, 2 H), 4.82 and 5.06 (2 br s, 1 H rotamer), 3.65–3.52 (m, 2 H), 2.60–2.58 (m, 3 H), 2.36–2.32 (m, 1 H), 1.75–1.98 (m, 2 H), 1.40–1.52 (m, 3 H), 1.18 (br s, 6 H); ^{13}C NMR (101 MHz, $CDCl_3$) rotameric mixture, resonances for minor rotamer are enclosed in parenthesis (): δ ppm 197.8, 154.4, 150.8, 135.7, (128.6) 128.4, 125.6 (125.2), 79.5, 61.2 (60.7), (47.5) 47.2, 35.9, (28.4) 28.2, 26.6, (23.7) 23.3; MS (ESI) *m*/*z* calcd. for $C_{17}H_{23}NO_3$ 289.1677, found 312.1579 [(M+Na)$^+$].

*4.3.3. tert-Butyl 2-(4-cyanophenyl)pyrrolidine-1-carboxylate (**3ac**)*

According to general procedure A r_T = 20 min, T = 40 °C, 24.5 mg (45%), ^{1}H NMR (500 MHz, $CDCl_3$) δ ppm 7.60 (d, *J* = 8.09 Hz, 2 H), 7.28 (d, *J* = 8.38 Hz, 2 H), 4.72–5.09 (m, 1 H), 3.52–3.73 (m, 2 H), 2.36 (br d, *J* = 6.65 Hz, 1 H), 1.89 (br d, *J* = 6.07 Hz, 2 H), 1.78 (br dd, *J* = 11.70, 5.64 Hz, 1 H), 1.41–1.53 (m, 3 H), 1.18 (br s, 6 H); ^{13}C NMR (126 MHz, $CDCl_3$) rotameric mixture, resonances for minor rotamer are enclosed in parenthesis (): δ ppm 150.8, 134.3, 132.2, 126.2, 118.9, 110.5, 79.8, 61.2 (60.7), (47.5) 47.2, 35.9 (34.7), (28.5) 28.2, (23.7) 23.3; MS (ESI) *m*/*z* calcd. for $C_{16}H_{20}N_2O_2$ 272.1524, found 295.1424 [(M+Na)$^+$].

*4.3.4. tert-Butyl 2-(4-methoxyphenyl)pyrrolidine-1-carboxylate (**3ad**)*

According to general procedure A r_T = 30 min, T = 60 °C, 49 mg (44%); ^{1}H NMR (500 MHz, $CDCl_3$) δ ppm 7.08 (d, *J* = 7.5 Hz, 2 H), 6.83 (d, *J* = 8.5 Hz, 2 H), 4.69 and 4.90 (2brs, 1 H rotamer), 3.79 (s, 3 H), 3.54–3.65 (m, 2 H), 2.28 (br, 1 H), 1.72–1.98 (m, 3 H), 1.46 (s, 3 H), 1.20 (br s, 6 H); ^{13}C NMR (126 MHz, $CDCl_3$) rotameric mixture, resonances for minor rotamer are enclosed in parenthesis (): δ ppm 158.2, 154.6, 137.3, 126.6, (113.8) 113.5, 79.1, 60.8, 55.3, (47.3) 47.0, 36.1 (34.9), (28.6) 28.2, (23.5) 23.5; MS (ESI) *m*/*z* calcd. for $C_{17}H_{23}NO_3$ 289.1677, found 312.1705 [(M+Na)$^+$].

*4.3.5. tert-Butyl 2-(1H-benzimidazol-2-yl)pyrrolidine-1-carboxylate (**3ae**)*

According to general procedure A r_T = 40 min, T = 60 °C, 21 mg (57%); ^{1}H NMR (400 MHz, $CDCl_3$) δ ppm 10.36–10.85 (m, 1 H), 7.60–7.87 (m, 1 H), 7.37–7.46 (m, 1 H), 7.19–7.25 (m, 2 H), 5.13 (br d, *J* = 5.78 Hz, 1 H), 3.41 (br s, 2 H), 3.08 (br s, 1 H) 2.20 (br s, 2 H), 2.01 (br s, 2 H), 1.51 (br s, 9 H); ^{13}C NMR (101 MHz, $CDCl_3$) δ ppm 156.6, (154.9), 133.9, 122.8 (121.8), 119.5, 110.9, 80.7, 54.7, 47.4, 28.1, 28.5 (31.9), 24.9; MS (ESI) *m*/*z* mass calcd. for $C_{16}H_{21}N_3O_2$ 287.1633, found 288.1713 [(M+H)$^+$].

*4.3.6. tert-Butyl 2-(benzofuran-2-yl)pyrrolidine-1-carboxylate (**3af**)*

According to general procedure A r_T = 30 min, T = 60 °C, 21 mg (36%), ^{1}H NMR (400 MHz, $CDCl_3$) δ ppm 7.45–7.53 (m, 1 H),7.41 (d, *J* = 7.63 Hz, 1 H),7.17–7.27 (m, 2 H) 6.41–6.53 (m, 1 H),4.97 (br s, 1 H),3.61 (br s, 1 H), 3.49 (br d, *J* = 5.55 Hz, 1 H), 2.09–2.28 (m, 2 H), 2.05 (br d, *J* = 6.01 Hz, 1 H),1.87–2.01 (m, 1 H), 1.51–1.62 (m, 1 H), 1.47 (br d, *J* = 6.94 Hz, 3 H), 1.32 (br s, 6 H); ^{13}C NMR ($CDCl_3$, 126 MHz) rotameric mixture, resonances for minor rotamer are enclosed in parenthesis (): δ ppm 154.4, 128.4, 123.7 (122.5), (120.6) 102.4, 79.7, 55.3 (54.9), (46.9) 46.2, 32.2 (31.2), 29.7, (28.6) 28.1, (24.1) 23.3; MS (ESI) *m*/*z* calcd. for $C_{17}H_{21}NO_3$ 287.1521, found 310.1420 [(M+Na)$^+$].

*4.3.7. tert-Butyl 2-[4-(trifluoromethyl)phenyl]pyrrolidine-1-carboxylate (**3ag**)*

According to general procedure A r_T = 30 min, T = 60 °C, 21 mg (32%); ^{1}H NMR ($CDCl_3$, 400 MHz): δ ppm 7.56 (d, *J* = 8.1 Hz, 2H), 7.28 (d, *J* = 8.1 Hz, 2H), 4.81 (br s, 1H), 3.64 (br s, 2H), 2.34 (br s, 1H), 1.86–1.93 (m, 2H), 1.80 (br dd, *J* = 11.4, 5.4 Hz, 1H), 1.46 (br s, 3H), 1.18 ppm (br s, 6H); ^{13}C NMR ($CDCl_3$, 126 MHz) rotameric mixture, resonances for minor rotamer are enclosed in parenthesis (): δ ppm 149.3, 128.9, 125.8, (125.4), 125.1, 79.6, 61.1 (60.5), (47.5) 47.2, 36.0 (34.8), 28.6, 28.1, (23.6) 23.2; MS (ESI) *m*/*z* calcd. for $C_{16}H_{20}F_3NO_2$ 315.3354, found 338.1324 [(M+Na)$^+$].

*4.3.8. tert-Butyl 2-(4-chlorophenyl)pyrrolidine-1-carboxylate (**3ah**)*

According to general procedure A r_T = 30 min, T = 60 °C, 24 mg (43%); ^{1}H NMR ($CDCl_3$, 400 MHz): δ ppm 7.24–7.27 (m, 2H), 7.10 (d, *J* = 8.3 Hz, 2H), 4.66 and 4.97 (2brs, 1H rotamer), 3.61 (br s, 2H), 2.18–2.38 (m, 1H), 1.82–1.94 (m, 2H), 1.70–1.81 (m, 1H), 1.45 (br s, 3H), 1.20 ppm (br s, 6H); ^{13}C NMR ($CDCl_3$, 126 MHz) rotameric mixture, resonances for minor rotamer are enclosed in parenthesis (): δ ppm 154.5, 143.8, 132.1, (128.5), 128.2, 126.9, 79.4, 60.8 (60.2), (47.4) 47.1, 36.0 (34.9), 29.7 (29.37), (28.5) 28.2, (23.6) 23.2 ppm; MS (ESI) *m*/*z* calcd. for $C_{15}H_{20}ClNO_2$ 281.1182, found 304.1081 [(M+Na)$^+$].

*4.3.9. tert-Butyl 2-(3-pyridyl)pyrrolidine-1-carboxylate (**3ai**)*

According to general procedure A r_T = 30 min, T = 40 °C, 24 mg (45%), ^{1}H NMR ($CDCl_3$, 400 MHz): δ ppm 8.47 (s, 2H), 7.49 (br d, *J* = 7.9 Hz, 1H), 7.23 (dd, *J* = 7.6, 5.1 Hz, 1H), 4.78 and 4.96 (2 br s, 1H rotamer), 3.63 (br s, 2H), 1.73–1.99 (m, 3H), 1.20 (br s, 6H); ^{13}C NMR ($CDCl_3$, 126 MHz) rotameric mixture, resonances for minor rotamer are enclosed in parenthesis (): δ ppm 154.3, 148.2 (147.7), 132.9 (133.1), 123.1, 100.1, 79.7, 59.0 (58.7), 47.2, 35.9 (34.5), (28.6) 28.3, (23.7) 23.3; MS (ESI) *m*/*z* calcd. for $C_{14}H_{20}N_2O_2$ 248.1524, found 249.1607 [(M+H)$^+$].

*4.3.10. tert-Butyl 2-(2-pyridyl)pyrrolidine-1-carboxylate (**3aj**)*

According to general procedure A r_T = 30 min, T = 60 °C, 21 mg (42%); ^{1}H NMR ($CDCl_3$, 400 MHz): δ ppm 8.53 (br d, *J* = 4.4 Hz, 1H), 7.63 (br t, *J* = 7.6 Hz, 1H), 7.09–7.20 (m, 2H), 4.87 (br d, *J* = 3.5 Hz, 1H), 3.54–3.69 (m, 2H), 2.30–2.45 (m, 1H), 1.98–2.10 (m, 1H), 1.84–1.93 (m, 2H), 1.42–1.50 (m, 3H), 1.20 ppm (s, 6H); ^{13}C NMR ($CDCl_3$, 126 MHz): δ ppm 163.8, 154.5, (149.3) 149.0, (136.4) 136.2, 121.4, (120.1) 119.7, 79.3, 63.0 (62.2), (47.4) 47.1, 34.3 (33.0), (28.5) 28.2, (23.8) 23.2; MS (ESI) *m*/*z* calcd. for $C_{14}H_{20}N_2O_2$ 248.1524, found 271.1432 [(M+Na)$^+$].

*4.3.11. tert-Butyl 2-(5-methoxy-2-pyridyl)pyrrolidine-1-carboxylate (**3ak**)*

According to general procedure A r_T = 30 min, T = 60 °C, 21 mg (38%); ^{1}H NMR ($CDCl_3$, 400 MHz): δ ppm 8.24 (s, 1H), 7.01–7.21 (m, 2H), 4.68–5.14 (m, 1H), 3.80–3.96 (m, 3H), 3.49–3.72 (m, 2H), 2.25–2.44 (m, 1H), 1.82–2.11 (m, 3H), 1.76 (br s, 1H), 1.39–1.56 (m, 3H), 1.15–1.31 ppm (m, 6H); ^{13}C NMR ($CDCl_3$, 126 MHz) rotameric mixture, resonances for minor rotamer are enclosed in parenthesis (): δ ppm 155.8, 154.7, 154.2, (136.9) 136.3, 121.0 (120.6), 120.0, 79.4, 62.0 (61.4), 55.6, (47.7) 47.0, 34.3 (33.0),

(28.7) 28.0, (24.0) 23.1 ppm; MS (ESI) *m*/*z* calcd. for $C_{14}H_{20}N_2O_2$ 278.1630, found 301.1538 [(M+Na)$^+$].

*4.3.12. tert-Butyl 2-pyrazin-2-ylpyrrolidine-1-carboxylate (**3al**)*

According to general procedure A r_T = 30 min, T = 40 °C, 15 mg (30%); ^{1}H NMR ($CDCl_3$, 400 MHz): δ ppm 8.50 (br s, 2H), 8.44 (br s, 1H), 4.84 and 5.08 (2 br s, 1H rotamer), 3.65 (br d, *J* = 5.1 Hz, 2H), 2.29–2.49 (m, 1H), 1.98–2.11 (m, 2H), 1.93 (br d, *J* = 6.0 Hz, 1H), 1.45 (br s, 3H), 1.21 ppm (s, 6H); ^{13}C NMR ($CDCl_3$, 126 MHz) rotameric mixture, resonances for minor rotamer are enclosed in parenthesis (): δ ppm 158.9 (158.0), (154.7) 154.1, (144.0) 143.8, (142.9) 142.8, 79.8, 60.9 (60.3), (47.4) 47.1, 34.1 (32.8), (28.5) 28.2, (24.0) 23.5; MS (ESI) *m*/*z* calcd. for $C_{13}H_{19}N_3O_2$ 249.1477, found 272.1378 [(M+Na)$^+$].

*4.3.13. tert-Butyl 2-(4-acetylphenyl)-4-hydroxy-pyrrolidine-1-carboxylate (**3bb** trans)*

According to general procedure B r_T = 30 min, T = 40 °C, 18 mg (30%); ^{1}H NMR ($CDCl_3$, 400 MHz): δ = 7.91 (d, *J* = 8.3 Hz, 2H), 7.37 (d, *J* = 8.1 Hz, 2H), 4.80–5.18 (m, 1H), 4.42–4.59 (m, 1H), 3.88 (br s, 1H), 3.60 (dd, *J* = 11.8, 3.2 Hz, 1H), 2.59 (s, 3H), 1.98 (dt, *J* = 13.3, 4.1 Hz, 1H), 1.47 (br s, 3H), 1.19 ppm (br s, 6H); ^{13}C NMR ($CDCl_3$, 101 MHz): δ = 197.7, 154.7, 150.4, 135.9, (128.8) 128.6, 125.7 (125.5), 80.0, 69.6, 60.1, 55.9, 45.1, (28.4) 28.1, 26.6 ppm; MS (ESI) *m*/*z* calcd. for $C_{14}H_{20}N_2O_2$ 305.1627, found 328.1527 [(M+Na)$^+$].

*4.3.14. tert-Butyl 2-(4-acetylphenyl)-4-hydroxy-pyrrolidine-1-carboxylate (**3bb** cis)*

According to general procedure B r_T = 30 min, T = 40 °C, 6 mg (10%); ^{1}H NMR ($CDCl_3$, 400 MHz): δ = 7.91 (d, *J* = 8.3 Hz, 2H), 7.29 (d, *J* = 8.1 Hz, 3H), 4.86–5.25 (m, 1H), 4.51 (br s, 1H), 3.66–4.09 (m, 2H), 2.60 (s, 3H), 2.42 (br dd, *J* = 12.7, 6.7 Hz, 1H), 1.93 (ddd, *J* = 13.4, 8.8, 4.4 Hz, 1H), 1.84 (br s, 1H), 1.44 (br s, 2H), 1.14 ppm (br s, 6H); ^{13}C NMR ($CDCl_3$, 101 MHz): δ = 197.7, 154.7, 150.4, 135.9, (128.8) 128.6, 125.7 (125.5), 79.9, 69.7, 60.0, 55.9, 45.1, (28.43) 28.1, 26.6 ppm; MS (ESI) *m*/*z* calcd. for $C_{14}H_{20}N_2O_2$ 305.1627, found 328.1527 [(M+Na)$^+$].

*4.3.15. 1-(4-Tetrahydrofuran-2-ylphenyl)ethanone (**3cb**)*

According to general procedure B r_T = 30 min, T = 60 °C, 13 mg (34%); ^{1}H NMR ($CDCl_3$, 400 MHz): δ ppm 7.93 (d, *J* = 8.3 Hz, 2H), 7.43 (s, 2H), 4.92–4.99 (m, 1H), 4.05–4.16 (m, 1H), 3.93–4.00 (m, 1H), 2.60 (s, 3H), 2.33–2.42 (m, 1H), 1.97–2.06 (m, 2H), 1.73–1.83 ppm (m, 1H); ^{13}C NMR ($CDCl_3$, 126 MHz): δ ppm 153.1, 150.3, 128.5, 128.3, 126.4, 125.6, 80.1, 69.5, 68.9, 37.5, 34.7, 26.9, 26.0, 25.0; MS (ESI) *m*/*z* calcd. for $C_{12}H_{14}O_2$ 190.0993, found 213.0965 [(M+Na)$^+$].

*4.3.16. tert-Butyl 3-(4-methoxycarbonylphenyl)-3,4-dihydro-1H-isoquinoline-2-carboxylate (**3da**)*

According to general procedure B r_T = 30 min, T = 60 °C, 59 mg (71%); ^{1}H NMR ($CDCl_3$, 400 MHz): δ ppm 8.60 (dd, *J* = 5.1, 0.7 Hz, 1H), 7.88 (d, *J* = 8.3 Hz, 2H), 7.17 (br d, *J* = 8.1 Hz, 4H), 7.13–7.20 (m, 1H), 7.09 (br d, *J* = 6.9 Hz, 1H), 4.81 (br d, *J* = 16.0 Hz, 1H), 4.41 (br s, 1H), 3.87 (s, 3H), 3.32 (br dd, *J* = 15.6, 5.4 Hz, 1H), 3.06 (br s, 1H), 1.29–1.48 ppm (m, 9H); ^{13}C NMR ($CDCl_3$, 126 MHz): δ ppm 183.9, 166.9, 155.1, 129.6, 128.7, (127.5) 126.7, 125.6, 100.0, 80.3, 52.0, 44.2, 28.4; MS (ESI) *m*/*z* calcd. for $C_{14}H_{20}N_2O_2$ 367.1783, found 390.1679 [(M+Na)$^+$].

*4.3.17. tert-Butyl 2-(4-methoxycarbonylphenyl)piperidine-1-carboxylate (**3ea**)*

According to general procedure B r_T = 30 min, T = 60 °C, 24 mg (37%); ^{1}H NMR (CHLOROFORM-*d*, 400 MHz): δ ppm 7.98–8.04 (m, 2H), 7.27–7.32 (m, 2H), 5.40–5.47 (m, 1H), 4.03–4.13 (m, 1H), 3.91 (s, 3H), 2.71–2.82 (m, 1H), 2.26–2.34 (m, 1H), 1.87–1.97 (m, 1H), 1.47–1.69 (m, 4H), 1.45 ppm (s, 9H); ^{13}C NMR (CHLOROFORM-*d*, 101 MHz): δ ppm 167.0, 155.6, 146.3, 129.9, 128.4, 126.5, 79.8, 53.5, 52.1, 40.3, 28.4, 28.3, 25.3 ppm; MS (ESI) *m*/*z* calcd. for $C_{14}H_{20}N_2O_2$ 367.1783, found 390.1679 [(M+Na)$^+$].

Acknowledgments

The authors thank Prof. Antonio de la Hoz and Prof. Ángel Díaz Ortiz for their assistance in the preparation of this manuscript and Dr. José Manuel Alonso for the NMR support. The project leading to this application has received funding from the European Union's Horizon 2020 research and innovation program under the Marie Sklodowska-Curie Grant Agreement No. 641861.

A. Supplementary material

Supplementary data associated with this article can be found, in the online version, at http://dx.doi.org/10.1016/j.bmc.2016.12.041.

References

1. Albini A. *Photochemistry: Past, Present and Future*. Heidelberg: Springer-Verlag GmbH; 2016. 285–298.
2. (a) Prier CK, Rankic DA, MacMillan DWC. *Chem Rev*. 2013;113:53225363;
(b) Romero NA, Nicewicz DA. *Chem Rev*. 2016;116:10075–10166.
3. (a) Knowles JP, Elliot LD, Brooker-Milburn KI. *Beilstein J Org Chem*. 2012;8:2025–2052;
(b) Plutschack MB, Correia CA, Seeberger PH, Gilmore K. *Organic Photoredox Chemistry in Flow*. Heidelberg: Springer-Verlag GmbH; 2015;
(c) Su Y, Straathof NJW, Hessel V, Noël T. *Chem Eur J*. 2014;20:10562–10589;
(d) Cambié D, Bottecchia C, Straathof NJW, Hessel V, Noël T. *Chem Rev*. 2016;116:10276–10341.
4. (a) Malet-Sanz L, Flavien S. *J Med Chem*. 2012;55:4062–4098;
(b) Rasheed M, Wirth T. *Angew Chem Int Ed*. 2011;50:357–358;
(c) Wegner J, Ceylan S, Kirschning A. *Chem Commun*. 2011;47:4583–4592;
(d) Newman SG, Jensen KF. *Green Chem*. 2013;15:2.
5. (a) Wiles C, Watts P. *Green Chem*. 2012;14:38–54;
(b) Ley SV. *Chem. Rec*.. 2012;12:378–390.
6. (a) Gui Y-Y, Sun L, Lu Z-P, Yu D-G. *Org. Chem. Front*.. 2016;3:522–526;
(b) Skubi KL, Blum TR, Yoon TP. *Chem Rev*. 2016;116:10035–10074;
(c) Hopkinson MN, Sahoo B, Li J-L, Glorious F. *Chem Eur J*. 2014;20:3874–3886;
(d) Primer DN, Karakaya I, Tellis JC, Molander GA. *J Am Chem Soc*. 2015;137:2195–2198;
(e) Karakaya I, Primer DN, Molander GA. *Org Lett*. 2015;17:3294–3297.
7. (a) Tsukamoto T. *ACS Med Chem Lett*. 2013;4:369–370;
(b) Walters WP, Green J, Weiss JR, Murcko MAJ. *J Med Chem*. 2011;54:6405–6416.
8. Lima F, Kabeshov MA, Tran DN, et al. *Angew Chem Int Ed*. 2016;55:14085–14089.
9. Morgenthaler M, Schweizer E, Hoffmann-Röder A, et al. *ChemMedChem*. 2007;2:1100–1115.
10. Zuo Z, Ahneman DT, Chu L, Terret JA, Doyle AG, MacMillan DWC. *Science*. 2014;345:437–440.
11. Beatty JW, Douglas JJ, Miller R, McAtee RC, Cole KP, Stephenson CRJ. *Chemistry*. 2016;1:456–472.
12. (a) Alcazar J, Diels G, Schoentjes B. *QSAR Comb Sci*. 2004;23:906–910;
(b) Alcazar J. *J Comb Chem*. 2005;7:353–356.
13. For further information about instrument used visit the web: <www.vapourtec.com>.
14. Löwe H, Hessel V, Löbe P, Hubbard S. *Org Process Res Dev*. 2006;10:1144–1152.

Photocatalysis

International Edition: DOI: 10.1002/anie.201802656
German Edition: DOI: 10.1002/ange.201802656

Visible-Light-Induced Nickel-Catalyzed Negishi Cross-Couplings by Exogenous-Photosensitizer-Free Photocatalysis

*Irini Abdiaj, Alberto Fontana, M. Victoria Gomez, Antonio de la Hoz, and Jesús Alcázar**

Abstract: *The merging of photoredox and transition-metal catalysis has become one of the most attractive approaches for carbon–carbon bond formation. Such reactions require the use of two organo-transition-metal species, one of which acts as a photosensitizer and the other one as a cross-coupling catalyst. We report herein an exogenous-photosensitizer-free photocatalytic process for the formation of carbon–carbon bonds by direct acceleration of the well-known nickel-catalyzed Negishi cross-coupling that is based on the use of two naturally abundant metals. This finding will open new avenues in cross-coupling chemistry that involve the direct visible-light absorption of organometallic catalytic complexes.*

The development of transition-metal-mediated cross-coupling chemistry for carbon–carbon bond formation has changed the way in which organic synthesis is carried out.[1,2] More recently, the advent of dual-catalysis approaches based on the combination of organometallic catalysts with a photosensitizer has opened new avenues in $C(sp^3)$–$C(sp^2)$ bond formation.[3–5] However, the photocatalysts used are based on rare metals, such as ruthenium or iridium, rendering these procedures less sustainable and less suitable in terms of scalability. Different alkyl boron reagents,[6,7] ammonium alkyl silicates,[8] *O*-benzyl xanthates,[9] and α-heteroatom-containing carboxylic acids[10] have been used to promote the formation of nucleophilic alkyl radicals. Baran and co-workers recently reported the use of organozinc derivatives in combination with light for $C(sp^3)$–$C(sp^2)$ couplings but, as reported by the authors, the reaction is a purely thermal process, and light did not add value to the reaction.[11] Beyond this article, there are no other reports on the use of organozinc reagents in a photochemical reaction to date. Considering the lack of knowledge on the behavior of these intermediates in photochemical processes and given our experience in organozinc chemistry,[12–14] we decided to explore the use of these reagents in dual catalysis as a replacement for other, previously reported organometallic reagents (Figure 1).[6–8]

[*] I. Abdiaj, A. Fontana, Dr. J. Alcázar
Oncology & Discovery Chemistry
Janssen Research and Development
Janssen-Cilag, S.A.
Jarama 75A, 45007 Toledo (Spain)
E-mail: jalcazar@its.jnj.com
Dr. M. V. Gomez, Prof. A. de la Hoz
Facultad de Ciencias Químicas
Universidad de Castilla-La Mancha
Av. Camilo José Cela 14, 13005 Ciudad Real (Spain)
Supporting information and the ORCID identification number(s) for the author(s) of this article can be found under: https://doi.org/10.1002/anie.201802656.

Initially, we selected methyl 4-bromobenzoate (**2**) and benzylzinc bromide (**1**) as coupling partners, and conducted the reaction in the presence of 1 mol% of an iridium photocatalyst and 2 mol% of a nickel cross-coupling catalyst in a batch setup. We obtained clear evidence for the formation of the expected product in the crude mixture (see the Supporting Information). Photochemical reactions are often enhanced by flow designs,[15,16] and we therefore decided to apply this technology (Table 1). As anticipated, a higher

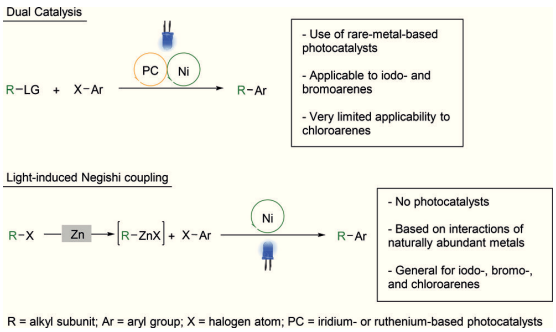

Figure 1. Comparison of dual catalysis with light-induced Negishi cross-couplings.

conversion was achieved in flow than in the batch process (entry 1). Control reactions were carried out in an effort to determine whether this process was driven by temperature or light. To our surprise, while irradiation was essential for the reaction (entry 3), the use of a photocatalyst was not (entry 2). A temperature of 60 °C was required to achieve full conversion (entry 4). The use of our flow procedure for the formation of the organozinc derivative,[12] instead of the commercially available reagent, also led to full conversion; however, in the absence of light, the conversion was still 78% (entry 5), implying that the thermally driven process is much more significant for our zincate reagent than for the commercial one.

To reduce the effect of the thermal component of the reaction, we selected 4-bromoanisole as the coupling partner, a substrate that has not been used in nickel-catalyzed Negishi couplings. With the commercially available reagent, no reaction was observed (see the Supporting Information). Nevertheless, by applying our flow process to generate the zincate, a conversion of 53% was achieved at a catalyst loading of 2% (entry 7), and full conversion was observed when the catalyst loading was increased to 5% (entry 8). The

 © 2018 Wiley-VCH Verlag GmbH & Co. KGaA, Weinheim

Table 1: Optimization of the flow reaction.

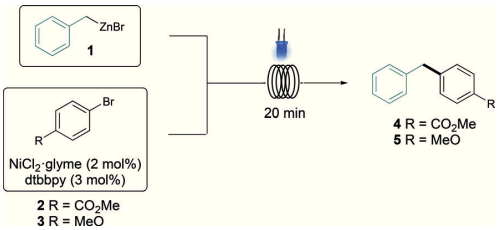

Entry	T [°C]	R	Irradiation	Photocatalyst	Conv. [%]
1	40	CO_2Me	450 nm	*fac*-Ir(ppy)$_3$	64
2	40	CO_2Me	450 nm	–	70
3	40	CO_2Me	–	–	4
4	60	CO_2Me	450 nm	–	100
5[a]	60	CO_2Me	–	–	78
6	60	MeO	450 nm	–	0
7[a]	60	MeO	450 nm	–	53
8[a,b]	60	MeO	450 nm	–	100
9[a,b]	60	MeO	–	–	55

[a] Organozinc reagent prepared in flow. [b] With 5 mol% of the nickel catalyst. dtbbpy = 4,4′-di-*tert*-butyl-2,2′-dipyridyl.

same reaction conditions in the absence of light provided the compound with 55% conversion (entry 9).

Even though the difference in conversion between the purely thermal Negishi coupling and the new light-driven reaction was only 45%, we considered it sufficient to follow the conversion in flow at different timepoints both in the presence and absence of light (see the Supporting Information, Figure S1). This experiment confirmed that the reaction is accelerated in the presence of light and that this acceleration is particularly marked at the beginning of the reaction.

Based on the findings outlined above, the scope of the reaction was further explored by varying both substrates (Figure 2). Our study was focused on bromo- and chloroarenes as they are rarely used in nickel-catalyzed Negishi cross-couplings.[17] To obtain comparable results, the reactions were performed under the same conditions either in the presence or absence of light.

Compounds with electron-withdrawing groups only required 2 mol% of the nickel catalyst. Light irradiation had a particularly strong effect on the reaction when strongly electron-donating groups were present in the molecule, such as in compounds **8** and **10**, where the conversion significantly increased in the presence of light. Iodine derivatives were also suitable substrates but a strongly electron-donating group, such as a free amino group, was required to observe significant differences between the light-irradiated and thermal reactions (e.g., compound **18**). This procedure is also applicable to different alkylzinc reagents beyond benzyl analogues, either freshly prepared or commercially available, to generate compounds such as **6**, **7**, and **12**.

It is important to highlight the fact that chloroarenes participate in this reaction as these coupling partners have only rarely been described in the literature in this context.[17] The synthesis of compound **19** clearly illustrates the value of the new method as irradiation with light was key to generated the desired product in good yield from the chloroarene. It is also important to highlight that compound **23** can only be obtained in the presence of light. To demonstrate the value of this method in a medicinal chemistry setting, compounds **25** and **26** were prepared, which are based on the chlorotriazolopyridine core that has previously been described in a series of compounds with activity as positive allosteric modulators of the metabotropic glutamate receptor 2, but has never been used in a Negishi cross-coupling.[18–22] Both reactions clearly

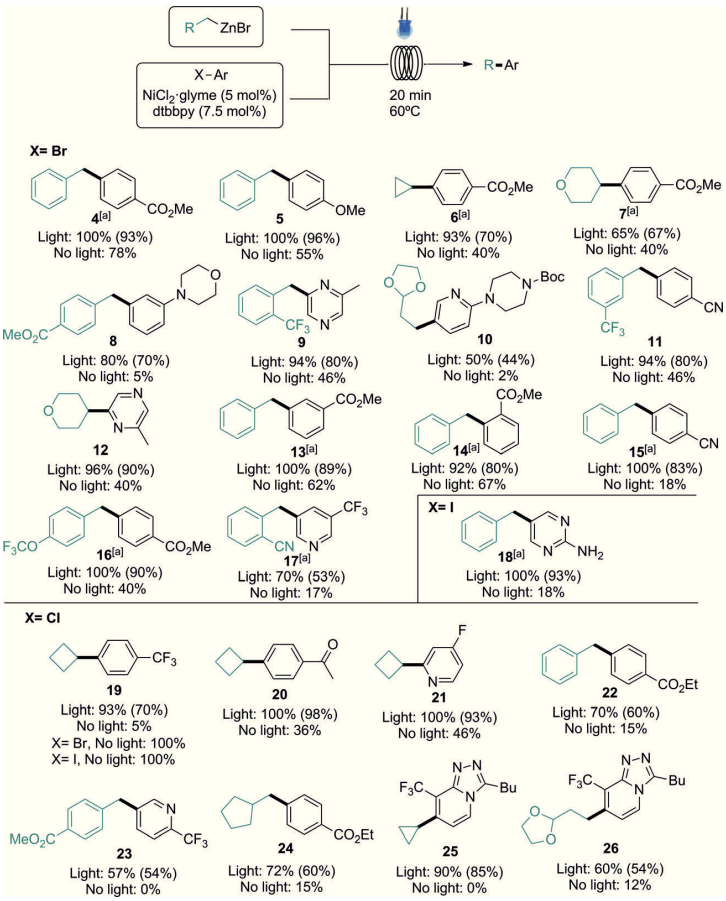

Figure 2. Scope of the light-induced nickel-catalyzed Negishi coupling with respect to the organozinc and haloarene coupling partners. Conversions determined by liquid chromatography. Yields of isolated products given in parentheses. [a] With 2 mol% of catalyst. See the Supporting Information for details.

© 2018 Wiley-VCH Verlag GmbH & Co. KGaA, Weinheim

These are not the final page numbers!

benefited from light irradiation, and the products were obtained in good to excellent yields, whereas little or no conversion was observed in the absence of light. This finding will be key to introduce C(sp^3)-enriched motifs, which could improve various physicochemical parameters such as the solubility.[23,24]

The preparation of compound **16** was selected to demonstrate the scalability of this method. The organozinc reagent was prepared in flow, and the exiting stream was connected to a second solution stream containing the haloarene and the catalytic complex before entering the photoreactor (Figure S9). This process was run continuously for 8 h and compared with the same reaction in batch by sampling at different timepoints (Figure S10). The flow protocol provided 6.7 g of the desired product upon isolation (93 % yield), with a productivity of 800 mg h^{-1}. In contrast, for the batch process, the product was only isolated in 39 % yield. Considering the reaction times and reaction volumes, the space/time yields[25,26] were calculated; these clearly favor the new flow process (Figure S10).

Regarding the mechanism of the reaction, it is important to note that visible-light-induced transition-metal-catalyzed transformations are known in the literature and have been recently reviewed.[27] Metals used for such reactions include cobalt, iron, copper, palladium, gold, and platinum. However, the use of nickel has not been described for this chemistry. To clarify the impact of light irradiation on the reaction, we initially recorded UV/Vis spectra for each component of the reaction and different mixtures. We only observed a broad band in the visible region when the catalytic complex was mixed with the organozinc reagent (Figure 3). When $NiCl_2$, that is, Ni^{II}, was replaced by Ni(COD), Ni^0, there was no absorption in the visible region, which demonstrates the need for nickel(II) species for light absorption.

Considering the spectra shown in Figure 3, we studied the generation of compound **1a** under irradiation at different wavelengths to determine the effect on the reaction outcome. The best conversion was achieved when the reaction mixture was irradiated at $\lambda = 450$ nm (blue light). Lower conversions were achieved when the reaction was irradiated at either $\lambda =$ 360 nm (black light) or $\lambda = 520$ nm (green light; see Table S8). These results are consistent with the absorption spectra.

Single electron transfer (SET) processes and radical formation play key roles in dual-catalytic light-induced reactions. In this respect, different reactions were carried out to detect such radicals. However, conclusive results were not obtained in these experiments (Table S7). The radical traps reacted with the organozinc derivative in the absence of catalyst or light so that the reaction was quenched because of the reactivity of the zincate, or no trapping was observed. Rearrangements of radical probes, also known as radical clocks, cannot be used in the reaction discussed here as radicals had been detected during the organozinc formation in batch.[28] The use of a flow process did not make any difference in this respect (see the Supporting Information). None of these assays provided suitable data to support the presence of radicals during the coupling process although the absence of radicals cannot be ruled out.

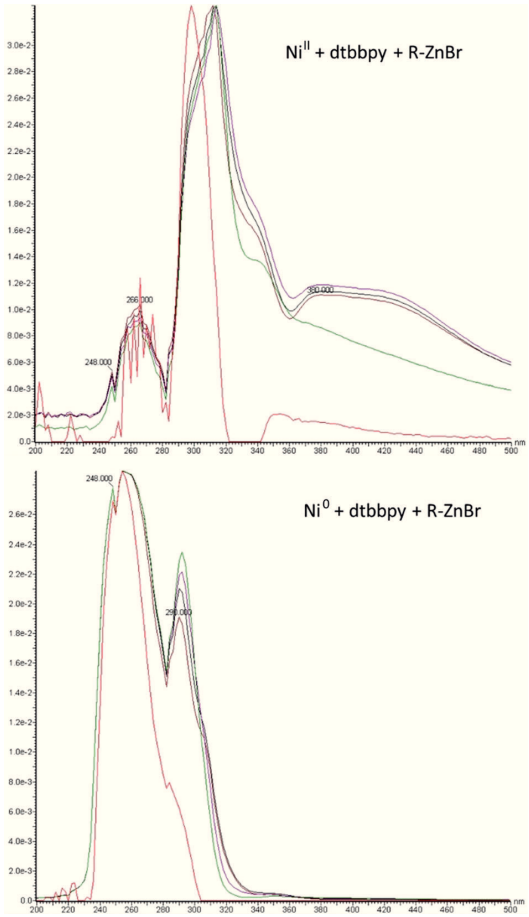

Figure 3. Absorption spectra of mixtures of nickel complexes with the organozinc reagent. Evolution of the absorption recorded over 20 min.

With the aim of shedding additional light on the mechanism of the reaction, NMR spectroscopy was employed as an analytical tool given its potential to elucidate molecular structures. The aim was to study the reaction generating compound **9** by following the signal of the trifluoromethyl group close to the reactive site by ^{19}F NMR spectroscopy. The laser-diode-based illumination device previously reported by us[29] was used to activate the reaction mixture in a 5 mm NMR tube for in situ NMR monitoring.[30] The reaction mixtures were freshly prepared and transferred quickly to the 5 mm NMR tube to record the ^{19}F NMR spectrum. Consecutive NMR spectra were recorded as a function of monitoring time, and the light was switched on or off at different monitoring times (see the Supporting Information for details).

To detect the intermediate that is absorbing in the blue region (Figure 3), we very rapidly added equimolar amounts of a zincate derivative and the nickel complex in an NMR tube, which allowed us to see a new resonance in the ^{19}F NMR spectrum at $\delta = -61.0$ ppm. It should be noted that the new

 © 2018 Wiley-VCH Verlag GmbH & Co. KGaA, Weinheim

signal is deshielded and appears approximately 2 ppm downfield from the signal of the original zincate, indicating a reduction in the electron density on this reagent. Consecutive NMR experiments with the light turned on or off showed that this signal decreases in intensity only in the presence of light (Figure 4, left). As this signal is decreasing in

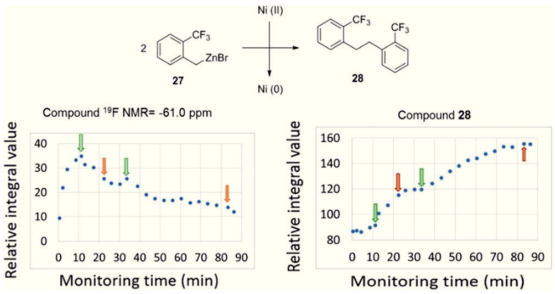

Figure 4. The effect of light irradiation on the degradation of an intermediate signal and the acceleration of the formation of dimer **28**. Green arrows indicated when the light was turned on, and orange arrows indicated when the light was turned off.

intensity, the signal corresponding to dimer **28** clearly increased, following the same pattern observed for the previous intermediate (Figure 4, right). It has been widely reported that the dimerization of organozinc reagents is linked to the reduction of a Ni^{II} precatalyst to Ni^0 as the first step to form the real catalytic complex.[17,31] The results from this experiment demonstrate that this step is clearly accelerated in the presence of light. Similar accelerated conversions of Pd^{II} into Pd^0 have been observed in light-induced Heck reactions.[32,33]

In a second experiment, the standard reaction was performed by adding all of the components at the required concentrations to an NMR tube. The evolution of the resonance of the product was then followed. At the beginning of the reaction, with the light turned off, product formation was slow, but this was clearly accelerated once the light had been switched on after approximately 5 min (Figure S8). The data obtained from these two experiments are consistent with light acceleration of the overall reaction at two distinct points in the catalytic cycle. First, light accelerates the reduction of the Ni^{II} to the Ni^0 complex with concomitant oxidation of the zincate to the dimer **28**. Then, product formation is also accelerated by light irradiation. MacMillan and co-workers have described the acceleration of the reductive elimination step of the catalytic cycle to an energy transfer from the iridium photocatalyst to a Ni^{II} intermediate.[34] Similarly, the UV/Vis spectra shown in Figure 3 may indicate that the direct light absorption of a complex between the two metals would accelerate the reductive elimination step of the catalytic cycle (Scheme S3). Nevertheless, further work will be required to unveil the species formed and to fully elucidate the mechanism.

In conclusion, nickel-catalyzed Negishi cross-couplings can be accelerated by visible-light irradiation. This can be considered as a new photocatalytic process involving two naturally abundant metals. The use of freshly prepared organozinc derivatives in a flow process is key for the success of the reaction. The scope of the reaction is broader than that of traditional batch Negishi and dual-catalytic reactions, especially with regard to aryl chlorides. The catalyst loading can be reduced to only 2 mol% nickel. This method provides access to new derivatives with potential value in medicinal chemistry. As the reaction is carried out in flow, direct scalability is easily achieved, and the overall approach is superior to batch protocols. Even though further work will be required to understand the mechanism in more detail, it seems that two steps of the reaction are accelerated upon light irradiation, namely the formation of the catalyst and the catalytic cycle itself. We believe that the current findings provide new insight into photocatalysis and open new avenues within this field. Further work to explore the potential of this approach in other bimetallic reactions is currently ongoing in our laboratories.

Acknowledgements

The project leading to this application has received funding from the European Union's Horizon 2020 research and innovation program under Marie Sklodowska-Curie grant agreement No. 641861. We also acknowledge financial support from the Spanish MINECO (CTQ2017-84825-R and CTQ2014-54987-P). M.V.G. thanks MINECO for participation in the Ramón y Cajal program (RYC2007-14768).

Conflict of interest

The authors declare no conflict of interest.

Keywords: $C(sp^3)$–$C(sp^2)$ coupling · flow chemistry · Negishi coupling · photocatalysis · visible light

[1] *Metal-catalyzed cross-coupling reactions*, 2nd ed. (Eds.: A. de Meijere, F. Diederich), Wiley-VCH, Weinheim, **2004**.
[2] a) C. C. C. Johansson-Seechurn, M. O. Kitching, T. J. Colacot, V. Snieckus, *Angew. Chem. Int. Ed.* **2012**, *51*, 5062–5085; *Angew. Chem.* **2012**, *124*, 5150–5174; b) D. Cantillo, C. O. Kappe, *ChemCatChem* **2014**, *6*, 3286–3305; c) T. Noël, S. L. Buchwald, *Chem. Soc. Rev.* **2011**, *40*, 5010–5029.
[3] a) K. L. Skubi, T. R. Blum, T. P. Yoon, *Chem. Rev.* **2016**, *116*, 10035–11074; b) U. K. Sharma, H. P. G. L. Gemoets, F. Schröder, T. Nöel, E. V. Van der Eycken, *ACS Catal.* **2017**, *7*, 3818–3823.
[4] J. Twilton, C. Le, P. Zhang, M. H. Shaw, R. W. Evans, D. W. C. MacMillan, *Nat. Rev. Chem.* **2017**, 0052.
[5] J. C. Tellis, C. B. Kelly, D. N. Primer, M. Jouffroy, N. R. Patel, G. A. Molander, *Acc. Chem. Res.* **2016**, *49*, 1429–1439.
[6] J. C. Tellis, D. N. Primer, G. A. Molander, *Science* **2014**, *345*, 433–436.
[7] F. Lima, M. A. Kabeshov, D. C. Tran, C. Battilocchio, J. Sedelmeier, G. Sedelmeier, B. Schenkel, S. V. Ley, *Angew. Chem. Int. Ed.* **2016**, *55*, 14085–14089; *Angew. Chem.* **2016**, *128*, 14291–14295.

 © 2018 Wiley-VCH Verlag GmbH & Co. KGaA, Weinheim

These are not the final page numbers!

[8] M. Jouffroy, D. N. Primer, G. A. Molander, *J. Am. Chem. Soc.* **2016**, *138*, 475 – 478.
[9] B. A. Vara, N. R. Patel, G. A. Molander, *ACS Catal.* **2017**, *7*, 3955 – 3959.
[10] Z. Zuo, D. T. Ahneman, L. Chu, J. A. Terret, A. G. Doyle, D. W. C. MacMillan, *Science* **2014**, *345*, 437 – 440.
[11] J. Cornella, J. T. Edwards, T. Qin, S. Kawamura, J. Wang, C.-M. Pan, R. Gianatassio, M. Schmidt, M. D. Eastgate, P. S. Baran, *J. Am. Chem. Soc.* **2016**, *138*, 2174 – 2177.
[12] M. Berton, L. Huck, J. Alcázar, *Nat. Protoc.* **2018**, *13*, 324 – 334.
[13] L. Huck, M. Berton, A. de la Hoz, A. Díaz-Ortiz, J. Alcázar, *Green Chem.* **2017**, *19*, 1420 – 1424.
[14] N. Alonso, L. Z. Miller, J. de M. Muñoz, J. Alcázar, D. T. McQuade, *Adv. Synth. Catal.* **2014**, *356*, 3737 – 3741.
[15] D. Cambié, C. Bottecchia, N. J. W. Straathof, V. Hessel, T. Nöel, *Chem. Rev.* **2016**, *116*, 10276 – 10341.
[16] I. Abdiaj, J. Alcázar, *Bioorg. Med. Chem.* **2017**, *25*, 6190 – 6196.
[17] V. B. Phapale, D. J. Cárdenas, *Chem. Soc. Rev.* **2009**, *38*, 1598 – 1607.
[18] M. L. J. Doornbos, J. M. Cid, J. Haubrich, A. Nunes, J. W. van de Sande, S. C. Vermond, T. Mulder-Krieger, A. A. Trabanco, A. Ahnaou, W. H. Drinkenburg, H. Lavreysen, L. H. Heitman, A. P. IJzerman, G. Tresadern, *J. Med. Chem.* **2017**, *60*, 6704 – 6720.
[19] M. A. Higgins, L. R. Marcin, F. C. Zusi, R. Gentles, M. Ding, B. C. Pearce, A. Easton, W. A. Kostich, M. A. Seager, C. Bourin, L. J. Bristow, K. A. Johnson, R. Miller, J. Hogan, V. Whiterock, M. Gulianello, M. Ferrante, Y. Huang, A. Hendrickson, A. Alt, J. E. Macor, J. J. Bronson, *Bioorg. Med. Chem.* **2017**, *25*, 496 – 513.
[20] J. M. Cid, G. Tresadern, J. A. Vega, A. I. de Lucas, A. del Cerro, E. Matesanz, M. L. Linares, A. García, L. Iturrino, L. Pérez-Benito, G. J. Macdonald, D. Oehlrich, H. Lavreysen, L. Peeters, M. Ceusters, A. Ahnaou, W. H. Drinkenburg, C. Mackie, M. Somers, A. A. Trabanco, *J. Med. Chem.* **2016**, *59*, 8495 – 8507.
[21] J. M. Cid, G. Tresadern, J. A. Vega, A. I. de Lucas, E. Matesanz, L. Iturrino, M. L. Linares, A. García, J. I. Andrés, G. J. Macdonald, D. Oehlrich, H. Lavreysen, A. Megens, A. Ahnaou, W. H. Drinkenburg, C. Mackie, S. Pype, D. Gallacher, A. A. Trabanco, *J. Med. Chem.* **2012**, *55*, 8770 – 8789.
[22] J. I. Andrés, J. Alcázar, J. M. Cid, M. De Angelis, L. Iturrino, X. Langlois, H. Lavreysen, A. A. Trabanco, S. Celen, G. Bormans, *J. Med. Chem.* **2012**, *55*, 8685 – 8699.
[23] T. Tsukamoto, *ACS Med. Chem. Lett.* **2013**, *4*, 369 – 370.
[24] W. P. Walters, J. Green, J. R. Weiss, M. A. Murcko, *J. Med. Chem.* **2011**, *54*, 6405 – 6416.
[25] S. G. Newman, K. F. Jensen, *Green Chem.* **2013**, *15*, 1456 – 1472.
[26] H. Löwe, V. Hessel, P. Löb, S. Hubbard, *Org. Process Res. Dev.* **2006**, *10*, 1144 – 1152.
[27] M. Parasram, V. Gevorgyan, *Chem. Soc. Rev.* **2017**, *46*, 6227 – 6240.
[28] A. Guijarro, D. M. Rosenberg, R. D. Rieke, *J. Am. Chem. Soc.* **1999**, *121*, 4155 – 4167.
[29] M. Mompeán, R. M. Sánchez-Donoso, A. de la Hoz, V. Saggiomo, A. H. Velders, M. V. Gomez, *Nat. Commun.* **2018**, *9*, 108.
[30] J. Kind, L. Kaltschnee, M. Leyendecker, C. M. Thiele, *Chem. Commun.* **2016**, *52*, 12506 – 12509.
[31] R. Soler-Yanes, I. Arribas-Álvarez, M. Guisán-Ceinos, E. Buñuel, D. J. Cárdenas, *Chem. Eur. J.* **2017**, *23*, 1584 – 1590.
[32] M. A. Fredricks, M. Drees, K. Köhler, *ChemCatChem* **2010**, *2*, 1467 – 1476.
[33] D. Kurandina, M. Parasram, V. Gevorgyan, *Angew. Chem. Int. Ed.* **2017**, *56*, 14212 – 14216; *Angew. Chem.* **2017**, *129*, 14400 – 14404.
[34] E. R. Welin, C. Le, D. M. Arias-Rotondo, J. K. McCusker, D. W. C. MacMillan, *Science* **2017**, *355*, 380 – 385.

Manuscript received: March 2, 2018
Accepted manuscript online: March 22, 2018
Version of record online: ■■ ■■, ■■■■

 © 2018 Wiley-VCH Verlag GmbH & Co. KGaA, Weinheim

Communications

Photocatalysis

I. Abdiaj, A. Fontana, M. V. Gomez, A. de la Hoz, J. Alcázar* ——

Visible-Light-Induced Nickel-Catalyzed Negishi Cross-Couplings by Exogenous-Photosensitizer-Free Photocatalysis

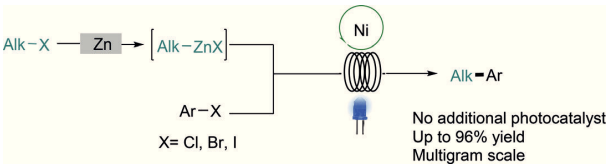

Visible acceleration: An exogenous-photosensitizer-free photocatalytic process enables the formation of carbon–carbon bonds by direct acceleration of the well-known nickel-catalyzed Negishi cross-coupling. This process is based on the use of two naturally abundant metals and is readily scalable.

 © 2018 Wiley-VCH Verlag GmbH & Co. KGaA, Weinheim

These are not the final page numbers!

A Journal of the Gesellschaft Deutscher Chemiker

Angewandte International Edition

GDCh

Chemie

www.angewandte.org

The two earth-abundant metals zinc and nickel enable the formation of new $C(sp^3)–C(sp^2)$ bonds under irradiation with visible light. In their Communication (DOI: 10.1002/anie.201802656), J. Alcázar and co-workers describe how these reaction conditions lead to a direct acceleration of the well-known nickel-catalyzed Negishi cross-coupling without requiring the addition of an exogenous photosensitizer.

WILEY-VCH

Cover design by Natalia Collado, Audiovisual MGR., MKT. Global Serv. at Jan-Cil, Spain.

Photos copyright © Created by Freepik